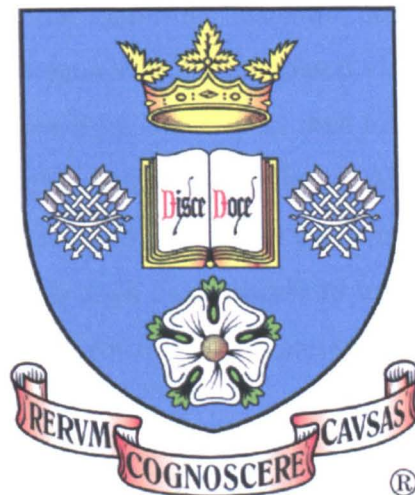


**Characterisation  
Of Human Bladder Urothelium Using  
Electrical Impedance Spectroscopy**

**By**

**Ahmad Keshtkar**

**(BSc in Applied physics and MSc in Medical Physics)**



**Thesis submitted for the degree of Doctor of Philosophy**

**Department of Medical Physics and Engineering**

**University of Sheffield**

**January 2004**

# **Characterisation of human bladder urothelium using electrical impedance spectroscopy**

Ahmad Keshtkar

## **Summary**

Bladder cancer is the most common malignancy in elderly people. In developed countries most bladder cancers are transitional cell carcinomas (TCC). This is a cancer of the urothelium (a transitional epithelium lining the bladder). In the UK there are approximately 13,000 new cases and 5400 deaths per annum (Black, Bray et al. 1997). Carcinoma *in situ* (CIS) is an early case of the invasive cancer, which is flat, non-papillary and difficult to detect precisely by using common methods. It is an aggressive form of TCC which may progress to muscle invasive cancer. Bladder pathology is usually investigated visually by cystoscopy. Erythematous areas of the urothelium are usually observed but these can represent different conditions ranging from simple inflammation to flat CIS. CIS cannot be differentiated visually from other erythematous tissues. Biopsies must be taken from the suspect area to obtain diagnostic information. The selection of biopsy sites depends on simple visual inspection thus is effectively random, and can be negative in up to 90% of the patients (van der Meijden, Oosterlinck et al. 1999). This is a relatively high cost procedure in terms of both time and money and is associated with discomfort for the patient and morbidity.

Electrical impedance spectroscopy (EIS) is a non-invasive screening technique to separate malignant areas from non-malignant areas in the urinary bladder. This is a result of the electrical impedance spectrum of the tissue being a function of tissue structure at the cellular level. The feasibility of adapting this minimally invasive technique to screen for bladder cancer, CIS during cystoscopy has been explored and compared with histopathological evaluation of urinary bladder lesions, both *ex vivo* and *in vivo*. Finite element modelling technique have been used to explore the relationship between urothelial morphology and the impedance spectrum. Both measured and modelled results showed that this technique is able to separate benign and malignant bladder tissue groups and the *in vivo* measurements suggest that classification of individual measurements should be possible.

## Acknowledgements

I would like to thank my supervisors Professor Rod Smallwood and Professor Freddie C Hamdy for their important guidance and patience in reading this thesis. I would like to thank Professor John Lee of the department of Histopathology for giving his time to help me in assessing biopsies and Dr. Bev Wilkinson and Dr. A. R. Azzouzi for their invaluable help in arranging practical work.

Thanks to Ron. Shepherd and his colleagues for preparing my probe tips and many thanks to Dr. Velazquez of the department of Engineering Materials, Sir Robert Hadfield Building, who helped the author to apply vacuum plasma method to treat these probes. The author thanks for the help of Mr. Christ Mody from fluorescent photography room in Ophthalmology department of the Royal Hallamshire Hospital to take photos from the probe in the probe treatment procedure.

Many thanks to Dr. Steven Wood, who kindly provided me with computer programmes and took the time to answer my many questions on this study. Thanks to Professor B H Brown, Dr. Andrew Leathard, Dr. Alan Waterworth and Dr. Carlos Gonzales-Correa who kindly allowed their experiences to be used for this work. The author thanks for the help of Dr. P. Lawford and Dr. Dawn Walker in preparing digital images and finite element analysis of the electrical properties procedure. I would like to thank all staffs of theatre 1,2 in the Royal Hallamshire Hospital for their help in the *in vivo* and *ex vivo* studies. Finally thanks to staffs of the sterilization unit, the out-patient of Urology Department for sterilizing my probes before any measurement. Thanks to all of the staff of the instrumentation laboratory and everybody from the Medical Physics and Engineering Department and Urology Department who helped me to do this PhD.

I gratefully acknowledge the contributions of the Tabriz University of Medical Sciences and Iranian Health and Medical Education Ministry who kindly provided me with financial support to do this study.

## Outline of thesis

The following chapter will discuss introduction and clinical background. Electrical impedance spectroscopy and its applications to tissue characterisation will be outlined in chapter 2. This chapter also deals with the relationship between bladder tissue morphology and electrical impedance spectra, including: morphological parameters of normal and pathological tissue; an estimation of expected morphological parameter changes of the bladder tissue with pathology. Chapter 3 will discuss existing equipment; methods and development of experimental protocol. The methods of transfer impedance measurements of the bladder (*in vivo* and *ex vivo*) will be presented in chapter 4. Data analysis of measured data will be discussed in chapter 5 and the effect of different parameters such as probe pressure, bladder volume changes, saline solutions and glycine on bio-impedance measurements is presented in chapter 6. The finite element analysis and its application on bladder structural modelling and the modelled data of the bladder will be outlined in chapter 7. This will include the comparison of electrical impedance measurements with the impedance resulting from modelling procedure. Conclusions and recommendations for future work are given in chapter 8. References, appendices and published papers follow.

# Table of contents

Summary .....	ii
Acknowledgements .....	iii
Outline of thesis .....	iv
<i>Table of contents</i> .....	v
<i>Table of Figures</i> .....	xvi
<i>Chapter 1</i> .....	1
<i>Introduction and clinical background</i> .....	1
<b>1.1 The aim of this study</b> .....	2
<b>1.2 Anatomy, histology and pathology of the human urinary bladder</b> .....	3
1.2.1 Introduction .....	3
1.2.2 Anatomy and physiology of the urinary bladder .....	3
1.2.3 Histology of the urinary bladder.....	5
1.2.3.1 Urothelium.....	5
1.2.3.2 Lamina propria and Detrusor muscle .....	8
1.2.3.3 Tight junctions of the bladder.....	10
1.2.4 Pathology of the human urinary bladder .....	11
1.2.4.1 Non-malignant diseases of the bladder.....	11
1.2.4.1.1 Inflammation and Oedema .....	11
1.2.4.1.2 Interstitial Cystitis (IC).....	12

1.2.4.1.3 Von Brunn's nests .....	12
1.2.4.2 Malignant disease of the bladder (Bladder cancer) .....	13
1.2.4.2.1 Staging (grading) of bladder cancer .....	13
1.2.4.2.2 Transitional Cell Carcinomas (TCC).....	15
1.2.4.2.3 Carcinoma <i>in situ</i> (CIS).....	15
<b>1.3 A review of existing bladder cancer detection techniques.....</b>	<b>18</b>
<b>1.4 Conclusions .....</b>	<b>21</b>
<b>Chapter 2.....</b>	<b>23</b>
<b><i>Electrical Impedance Spectroscopy (EIS) and its applications to tissue characterisation: Technical background.....</i></b>	<b>23</b>
<b>2.1 Introduction .....</b>	<b>23</b>
<b>2.2 4-electrode technique.....</b>	<b>23</b>
<b>2.3 Electrical properties of living tissue.....</b>	<b>25</b>
2.3.1 Conductive and displacement currents .....	27
2.3.2 Electrical parameters (Conductivity and Permittivity).....	28
2.3.3 Dielectric dispersion in biological tissues .....	33
2.3.4 Effects of physical and physiological changes on tissue dielectric properties .....	36
<b>2.4 Electrical impedance spectrum of living tissue.....</b>	<b>37</b>
<b>2.5 Morphological parameters of normal and pathological tissue.....</b>	<b>43</b>
2.5.1 Morphological parameters of normal bladder tissue .....	44

2.5.2 Estimation of expected changes in morphological parameters of bladder tissue with pathology .....	46
<b>2.6 Electrical impedance changes of malignant tissue and a new approach for detecting bladder cancer using EIS .....</b>	<b>48</b>
<b>2.7 Feasibility of the existing EIS equipment and methods to distinguish the normal and abnormal bladder tissue.....</b>	<b>52</b>
<b>2.8 Conclusions .....</b>	<b>53</b>
<i>Chapter 3.....</i>	<i>56</i>
<i>Equipment.....</i>	<i>56</i>
<b>3.1 Introduction .....</b>	<b>56</b>
<b>3.2 Existing equipment and development of experimental protocol.....</b>	<b>56</b>
3.2.1 Probe development .....	56
3.2.1.1 Introduction .....	56
3.2.1.2 Electrode impedance .....	57
3.2.1.3 Probe sensitivity distribution.....	61
3.2.1.4 Contact polarisation of probes.....	63
3.2.1.5 Probe construction, development and safety testing .....	64
3.2.1.6 Results and discussions .....	71
3.2.1.7 Conclusions .....	72
3.2.2 Electrical impedance spectroscopy systems.....	73
3.2.2.1 Introduction .....	73

3.2.2.2 Current source and generator.....	74
3.2.2.2.1 Supply-Sensing Current Source .....	74
3.2.2.2.2 The Howland circuit generator .....	76
3.2.2.3 Voltage measurement, differential amplifier and demodulator.....	79
3.2.2.4 Computer interface and data acquisition unit.....	80
3.2.2.5 Electrical safety in EIS .....	81
3.2.2.6 Mk3.a Sheffield System .....	81
3.2.2.6.1 General description.....	81
3.2.2.6.2 Current Generation .....	82
3.2.2.6.3 Voltage measurement .....	84
3.2.2.6.4 Computer interface .....	86
3.2.2.6.5 Electrical safety .....	86
3.2.2.7 Mk3.5 Sheffield System .....	86
3.2.2.7.1 General description.....	86
3.2.2.7.2 Current Generation .....	90
3.2.2.7.3 Voltage measurement .....	91
3.2.2.7.4 Computer interface .....	91
3.2.2.7.5 Electrical safety .....	91
3.2.2.8 Conclusions .....	91
<b>3.3 Conclusions .....</b>	<b>92</b>

<b>Chapter 4.....</b>	<b>94</b>
<b><i>Impedance measurement methods, data acquisition, storage and analysis.....</i></b>	<b>94</b>
<b>4.1 Introduction .....</b>	<b>94</b>
<b>4.2 Probe calibration .....</b>	<b>95</b>
4.2.1 Probe calibration using Mk3.a Sheffield System .....	95
4.2.2 Probe calibration using Mk3.5 Sheffield System .....	99
<b>4.3 Electrical impedance of resected bladder (<i>ex vivo</i> study) .....</b>	<b>101</b>
<b>4.4 Biopsy and tissue sampling procedure .....</b>	<b>105</b>
4.4.1 Histological classification .....	107
<b>4.5 Electrical impedance of living bladder tissue (<i>in vivo</i> study) .....</b>	<b>111</b>
<b>4.6 Data acquisition, storage and analysis.....</b>	<b>114</b>
4.6.1 Introduction .....	114
4.6.2 Data acquisition.....	115
4.6.3 Data storage.....	117
4.6.4 Data analysis.....	118
4.6.4.1 Data extraction and classification.....	118
4.6.4.2 Fitting a model to the measured data.....	119
4.6.4.3 Statistical method .....	121
<b>4.7 Conclusions .....</b>	<b>122</b>
<b>Chapter 5.....</b>	<b>123</b>

<i>Electrical impedance measurements in urinary bladders</i> .....	123
<b>5.1 Introduction</b> .....	123
<b>5.2 Electrical impedance measurement results and discussion</b> .....	123
5.2.1 <i>Ex vivo</i> study.....	123
5.2.1.1 Mk3.a Sheffield System results and discussion .....	123
5.2.1.1.1 Reproducibility of the impedance readings .....	124
5.2.1.1.2 Separation of malignant impedance from the benign.....	124
5.2.1.1.3 Evaluation of impedance spectrum linearity .....	127
5.2.1.1.4 The Cole equation fitting.....	129
5.2.1.1.5 The effect of inflammation and oedema on measured impedance	130
5.2.1.1.6 Evaluation of individual points of the malignant data in the benign area .....	131
5.2.1.1.7 Separation of Carcinoma <i>in situ</i> (CIS) from the inflammation area .....	132
5.2.1.2 Mk3.5 Sheffield System results and discussion .....	132
5.2.1.2.1 Reproducibility of the impedance readings.....	132
5.2.1.2.2 Separation of malignant impedance from the benign.....	132
5.2.1.2.3 The Cole equation fitting.....	135
5.2.1.2.4 The effect of inflammation and oedema on measured impedance	135
5.2.1.2.5 Evaluation of individual points of the malignant data in benign area .....	137
5.2.1.3 Results and discussion of the Combined Mk3.a and Mk3.5 Sheffield	

Systems.....	137
5.2.1.3.1 Separation of malignant impedance from the benign.....	138
5.2.1.3.2 The Cole equation fitting.....	141
5.2.1.3.3 The effect of inflammation and oedema on measured impedance	142
5.2.1.3.4 Separation of Carcinoma <i>in situ</i> (CIS) from the inflammation area .....	144
5.2.1.4 Conclusion.....	145
5.2.2 <i>In vivo</i> study .....	146
5.2.2.1 Measured transfer impedance of the bladder.....	146
5.2.2.2 Mk3.a Sheffield System results and discussion .....	146
5.2.2.2.1 Separation of malignant impedance from the benign.....	146
5.2.2.2.2 The Cole equation fitting.....	148
5.2.2.3 Mk3.5 Sheffield System results and discussion .....	149
5.2.2.3.1 Separation of malignant impedance from the benign.....	149
5.2.2.3.2 The Cole equation fitting.....	151
5.2.2.4 Results and discussion of the Combined Mk3.a and Mk3.5 Sheffield Systems.....	152
5.2.2.4.1 Separation of malignant impedance from the benign.....	152
5.2.2.4.1 The Cole equation fitting.....	154
5.2.2.5 Conclusion.....	156
5.2.3 Lower frequency study of the urothelium ( <i>In vivo</i> ).....	157

5.2.3.1 Separation of malignant impedance from the benign.....	158
5.2.3.2 The Cole equation fitting.....	161
5.2.3.3 Conclusion.....	163
5.2.4 Receiver Operating Characteristic curve (ROC) application on the combined <i>ex vivo</i> and <i>in vivo</i> results.....	163
<b>5.3 Conclusions .....</b>	<b>166</b>
<b>Chapter 6.....</b>	<b>168</b>
<b><i>The effects of experimental conditions on bio-impedance measurements.....</i></b>	<b>168</b>
<b>6.1 Introduction .....</b>	<b>168</b>
<b>6.2 The effect of applied pressure on measured results (<i>ex vivo</i>) .....</b>	<b>168</b>
6.2.1 Introduction .....	168
6.2.2 Measurement method .....	169
6.2.3 Measured results and discussions.....	175
6.2.4 Conclusion.....	183
<b>6.3 The effect of bladder volume changes on the measured results.....</b>	<b>183</b>
6.3.1 Introduction .....	183
6.3.2 Measurement method for <i>ex vivo</i> study.....	184
6.3.3 Results and discussion.....	185
6.3.4 Measurement method for <i>in vivo</i> study .....	186
6.3.5 Results and discussion.....	187
6.3.6 Conclusion.....	189

3.2.2.2 Current source and generator.....	74
3.2.2.2.1 Supply-Sensing Current Source .....	74
3.2.2.2.2 The Howland circuit generator .....	76
3.2.2.3 Voltage measurement, differential amplifier and demodulator.....	79
3.2.2.4 Computer interface and data acquisition unit.....	80
3.2.2.5 Electrical safety in EIS .....	81
3.2.2.6 Mk3.a Sheffield System .....	81
3.2.2.6.1 General description.....	81
3.2.2.6.2 Current Generation .....	82
3.2.2.6.3 Voltage measurement .....	84
3.2.2.6.4 Computer interface .....	86
3.2.2.6.5 Electrical safety .....	86
3.2.2.7 Mk3.5 Sheffield System .....	86
3.2.2.7.1 General description.....	86
3.2.2.7.2 Current Generation .....	90
3.2.2.7.3 Voltage measurement .....	91
3.2.2.7.4 Computer interface .....	91
3.2.2.7.5 Electrical safety .....	91
3.2.2.8 Conclusions .....	91
<b>3.3 Conclusions .....</b>	<b>92</b>

7.3.2 Macroscopic tissue level finite element models .....	209
<b>7.4 Results and discussions: Comparison of modelling and the experimental results.....</b>	<b>212</b>
<b>7.5 Conclusions .....</b>	<b>216</b>
<b>Chapter 8.....</b>	<b>217</b>
<b><i>Conclusions and recommendations for future work.....</i></b>	<b><i>217</i></b>
<b>8.1 Conclusions .....</b>	<b>217</b>
<b>8.2 Recommendations for future work.....</b>	<b>221</b>
<b><i>References</i></b>	<b>223</b>
<b><i>Appendices</i> .....</b>	<b><i>232</i></b>
Appendix (1): The dimensions of cable parts, structure and its electrical characteristics .....	232
Appendix (2): Tip structure .....	233
Appendix (3): Probe-Cable 9way Connector .....	234
Appendix (4): Mk3.a : Probe PCB Circuit (Sheet 1 of 2) .....	235
Appendix (5): Mk3.a: Main PCB Circuit (Sheet 2 of 2) .....	236
Appendix (6): Mk3.5: (Sheet 1 of 2) .....	237
Appendix (7): Mk3.5: (Sheet 2 of 2) .....	238
Appendix(8): Patient's consent form to sign: Electrical measurements of the bladder lining.....	239
Appendix(9): Patient information and impedance measurement form .....	240

Appendix (10): Instructions in Matlab programme to build the data base files...	241
Appendix (11): AppendRecord m.file .....	242
Appendix (12): The cellular morphological parameters of the human urinary bladder .....	244
<b><i>Publications</i></b> .....	<b>247</b>

# Table of Figures

Figure 1.1 Structure of the urinary bladder (Seeley, Stephens et al. 2000) with permission from McGraw-Hill Education .....	4
Figure 1.2 a) Transitional epithelium of the urinary bladder in relaxed and stretched states (a,b). Transitional epithelium in a relaxed state (c) (Tortora and Grabowski 2000). With permission from John Wiley & Sons .....	6
Figure 1.3 Plaques present on surface of the relaxed bladder epithelium .....	7
Figure 1.4 Lamina propria (a connective tissue) is under the transitional epithelium and the basement membrane (Eroschenko 2000). With permission from Lippincott Williams & Wilkins.....	8
Figure 1.5 Urinary Bladder Muscles, IL: Inner Long Muscle OC: Outer Circular Muscle OL: Outer Long Muscle. Modified from (Young 2000) .....	9
Figure 1.6 Conductivity in S/m and relative permittivity of the Muscle (Parallel Fiber) against frequency in Hz (Gabriel, Gabriel et al. 1996).....	9
Figure 1.7 Conductivity in S/m and relative permittivity of the Muscle (Transverse Fiber) against frequency in Hz (Gabriel, Gabriel et al. 1996).....	9
Figure 1.8 Transepithelial capacitance of the rabbit urinary bladder in fully stretched (A), moderately stretched (B) and the relaxed states (C). Modified from (Lewis and Diamond 1976) .....	10
Table 1.1 TNM grading system of bladder cancer. Modified from (UICC 1997) ..	14
Table 1.2 The staging of urinary bladder tumours. Modified from (UICC 1987).	14
Figure 1.9 Carcinoma <i>in situ</i> (CIS).....	16
Figure 1.10 Development of invasive cancer into either a high- grade papillary stage or by direct progression to flat or sessile invasive cancer. Modified from (Farrow and Utz 1982) .....	17
Figure 1.11 A flexible scope: A useful diagnostic tool for the diagnosis of bladder tumours under local anaesthetic in the out patient department. ....	20
Figure 2.1 4 Electrodes and their connections to both the current power supply and the voltage measurement system .....	24
Figure 2.2 Dependence of conduction and displacement currents on the frequency for a typical living tissue .....	28
Figure 2.3 The living tissue as capacitance and resistance equivalent .....	29
Figure 2.4 Distribution of permittivity and conductivity of a typical tissue as a function of frequency. Modified from (Pethig and Kell 1987; Foster and Schwan	

1989).....	34
Figure 2.5 Equivalent electrical circuits for biological tissue.....	35
Figure 2.6 Conductivity in S/m and relative permittivity of the urinary bladder against frequency in Hz (Gabriel, Gabriel et al. 1996). .....	36
Figure 2.7 Real and imaginary parts of impedance against the frequency for single dispersion (a). A parametric curve shows the imaginary part against the real part of impedance for $\alpha = 0$ (b) and $\alpha \neq 0$ (c). Modified from (Cole and Cole 1941)....	40
Figure 2.8 The electrical current passes through the normal and abnormal living tissue (in low and high frequencies).....	42
Figure 2.9 The structure of the normal urinary bladder tissue. Modified from (Lewis and Hanrahan 1990) .....	46
Figure 2.10 Cytological appearance of TCC of the bladder. a) Transitional cell carcinoma, grade 1 b) Transitional cell carcinoma, grade 2 c) Transitional cell carcinoma, grade 3 (Sonny and Samuel 1996), Modified from Anderson's Pathology.....	48
Table 2.1 <i>In vivo</i> electrical resistivity ( $\Omega.m$ ) measurements in the human oesophagus.....	51
Table 2.2 <i>In vitro</i> electrical resistivity ( $\Omega.m$ ) measurements in the human oesophagus.....	51
Figure 3.1 2-electrodes in contact with tissue (tissue is assumed to be both homogenous and semi-infinite in extent, $r \gg d$ ). Modified from (Brown, Smallwood et al. 1999).....	57
Figure 3.2 a) 4-electrodes in contact with living tissue (tissue is assumed to be both homogenous and semi-infinite in extent). b) 4-electrodes are in contact with living tissue and are demonstrating $R_1, R_2, R_3$ as tissue impedances, R as electrode contact impedance and V as a perfect voltmeter. Modified from (Brown, Smallwood et al. 1999).....	60
Figure 3.3 Computational modelling (Finite element analysis) results for the current sensitivity distribution of the urinary bladder with 30 $\mu m$ thickness of mucosa (a combined study by the author and Dr. D. C. Walker).....	62
Figure 3.4 a) PTFE tube was coiled to a diameter of about 10-15 cm (Cling film was wrapped around this tube except 2 cm of each tube end). b) PTFE tube was placed inside a vacuum plasma tube.....	65
Figure 3.5 Probe structure.....	67
Figure 3.6 Treatment of probe with ultraviolet: a) UV Source b) Equipment to treat the probe c) The probe treatment processing.....	68

<b>Figure 3.7 Connection of the probe to the bladder tissue (<i>ex vivo</i>).....</b>	<b>68</b>
<b>Figure 3.8 Liquid leakage test of the probe using water and positive air pressure</b>	<b>69</b>
<b>Figure 3.9 Liquid leakage test of the probe using fluorescent liquid and negative air pressure.....</b>	<b>70</b>
<b>b.....</b>	<b>71</b>
<b>Figure 3.10 a) Completed probe b) A ruler shows the probe small size.....</b>	<b>71</b>
<b>Figure 3.11 Supply-Sensing Current Source.....</b>	<b>75</b>
<b>Table 3.1 The number of researchers that used Supply-Sensing Current Source, Modified from (Boone and Holder 1996). ....</b>	<b>76</b>
<b>Figure 3.12 Howland basic circuit .....</b>	<b>77</b>
<b>Table 3.2 Researchers that used the Howland circuit for Current Source, modified from (Boone and Holder 1996).....</b>	<b>79</b>
<b>Figure 3.13 Instrumentation amplifier .....</b>	<b>80</b>
<b>Figure 3.14 Mk3.a Sheffield System .....</b>	<b>82</b>
<b>Table 3.3 Frequencies used in Mk3.a Sheffield System in Hz .....</b>	<b>82</b>
<b>Figure 3.15 Current driver of Mk3.a Sheffield System .....</b>	<b>83</b>
<b>Figure 3.16 Current generation of Mk3.a Sheffield System.....</b>	<b>83</b>
<b>Figure 3.17 Frequency controller and demodulator of Mk3.a Sheffield System....</b>	<b>84</b>
<b>Figure 3.18 Voltage measurement of Mk3.a Sheffield System.....</b>	<b>85</b>
<b>Figure 3.19 Gain controller circuit of Mk3.a Sheffield System.....</b>	<b>85</b>
<b>Figure 3.20 Low pass filter and demultiplexer of Mk3.a Sheffield System.....</b>	<b>86</b>
<b>Table 3.4 Frequencies (in Hz) used in MK3.5 Sheffield System .....</b>	<b>87</b>
<b>Figure 3.21 Mk3.5 Sheffield System (data acquisition system).....</b>	<b>87</b>
<b>Figure 3.22 Four Connectors were used to connect the probe to the measurement system of the Mk3.5 Sheffield System (Electrodes 1 and 2 are Current Drive, Electrodes 3 and 4 are Voltage Drive) and 4 Resistors (200 <math>\Omega</math>) were used to block another 4 Electrode Connections (Connections 5, 6, 7 and 8).....</b>	<b>89</b>
<b>Figure 3.23 Diagram of 4 electrodes connections to the data acquisition system in Mk3.5 Sheffield System (D/A is digital-to-analogue converter and A/D is analogue -to-digital converter and the numbers 1, 2, 3 and 4 are the contact point of</b>	

electrodes with tissue).....	90
Figure 4.1 Conductivity Meter .....	96
Table 4.1 Calibration Process for Mk3.a Sheffield System (Conductivity and Resistivity) Y1-Y21 are the impedance measurement system readings at Laptop screen (their values are shown in Table 4.2). .....	96
Table 4.2 Calibration Process, readings in volts at seven frequencies for Mk3.a Sheffield System.....	97
Table 4.3 Conversion Factor for Gain 4 and reading Y8 at 7 frequencies.....	97
Table 4.4 Conversion Factors for Gain 4 and for 7 readings at 7 frequencies ( $\frac{\Omega.m}{Volt}$ ) .....	98
Table 4.5 Conversion Factor for Gain 4 at 7 frequencies ( $\frac{\Omega.m}{Volt}$ ) .....	98
Table 4.6 Conversion Factor for Gain 8 at 7 frequencies ( $\frac{\Omega.m}{Volt}$ ) .....	98
Figure 4.2 Probe calibration (Mk3.5) .....	99
Table 4.7 Calibration Process for Mk3.5 Sheffield System (Conductivity and Resistivity).....	99
Figure 4.3 One of the calibration curves (the vertical axis is in arbitrary units).	100
Figure 4.4 Resected bladder sample under the probe (the bladder specimen was pinned to a corkboard).....	102
Table 4.8 Age (mostly in their 60's and 70's), sex and reason for cystectomy in 35 <i>ex vivo</i> patients .....	103
Figure 4.5 a) Mk3.a Sheffield System    b and c) Mk3.5 Sheffield System.....	105
Figure 4.6 A typical slide of histopathological sections.....	107
Figure 4.7 The Normal Epithelium                      Figure 4.8 Ragged Epithelium (R)	109
Figure 4.9 Denuded Epithelium (D)    Figure 4.10 Denuded Epithelium with Residual von Brunn's nests (DvB) .....	109
Figure 4.11 Full Coverage <i>Carcinoma in situ</i> (CISf)    Figure 4.12 Carcinoma (Ca) .....	109

**Figure 4.13 Oedema 1(Mild)      Figure 4.14 Oedema 2 (Moderate)..... 110**

**Figure 4.15 The Oedema 3 (Severe)      Figure 4.16 Inflammation 1 (Mild) 110**

**Figure 4.17 Inflammation 2 (Moderate)      Figure 4.18 Inflammation 3 (Severe) ..... 110**

**Table 4.9 Reasons for biopsies in 74 patients..... 111**

**Figure 4.19 a) Cystoscope including probe b) Cystoscope and whole measurement system..... 112**

**Figure 4.20 Indigo carmine (a) and Sclerosing endoscopy needle (b) used to mark inside of the bladder to choose the impedance measurement point and then taken the biopsies from this point..... 113**

**Figure 4.21 One of the cystoscopy photos of the inside of the bladder a) A blue mark has been made with the indigo carmine b) Probe contacts the bladder tissues near the blue area ..... 114**

**Figure 4.22 Data acquisition on laptop screen: Mk3.a Sheffield System ..... 115**

**Figure 4.23 Data acquisition on the laptop screen: Mk3.5 Sheffield System..... 116**

**Figure 4.24 Data acquisition on the laptop screen: Improved Mk3.5 Sheffield System for lower frequencies..... 116**

**Figure 5.1 Evaluation of reproducibility of the measured data using 3 independent readings per point..... 124**

**Figure 5.2 Median and 90% percentile ranges for malignant (a) and non-malignant (b) points of the bladder tissue separately and together (c). d) Real part of impedivity versus log of frequency for normal and malignant bladder tissue in the Mk3.a Sheffield System ..... 125**

**Figure 5.3 The distribution of measured impedance data in non-malignant (a) and malignant (b) areas of the urinary bladder using Mk3.a Sheffield System ..... 126**

**Figure 5.3c Structure of a box plot display ..... 127**

**Figure 5.4 The real part of permittivity against frequency using assumptions such as:  $\epsilon_{\infty}=8$ ,  $\epsilon_0=20$ , shows that for the different values of  $\alpha$ , the shape of this spectrum is changing from a sigmoid ( $\alpha = 0$ ) to a straight line ( $\alpha = 0.8$  or higher). Dashed lines demonstrated the shape changes using different values of  $\alpha$  ..... 128**

**Figure 5.5 The Cole equation fitting for benign and malignant bladder tissue in the Mk3.a Sheffield System (the numbers show the position of 22 malignant points exactly)..... 129**

**Figure 5.6 a) Effect of different degrees of oedema (0= no oedema and 3= severe**

oedema) and b) inflammation (0= no inflammation and 3= severe inflammation) on the impedance measurements of the bladder tissue in the Mk3.a Sheffield System ..... 131

**Table 5.1 The malignant points which are categorised in non-malignant area with the respective pathological reports ..... 132**

**Figure 5.7 Median and 90% percentile ranges for malignant and non-malignant points of the bladder tissue separately (a and b) and together (c). d) Real part of impedivity versus log of frequency for normal and malignant bladder tissue in the Mk3.5 Sheffield System..... 133**

**Figure 5.8 The distribution of measured impedance data in non-malignant (a) and malignant (b) areas of the urinary bladder using Mk3.5 Sheffield System ..... 134**

**Figure 5.9 The Cole equation fitting for normal and malignant bladder tissue in the Mk3.5 Sheffield System (the numbers show the position of 25 malignant points exactly)..... 135**

**Figure 5.10 a) Effect of different degrees of oedema (0= no oedema and 3= severe oedema) and b) inflammation (0= no inflammation and 3= severe inflammation) on the impedance measurements of the bladder tissue in the Mk3.5 Sheffield System ..... 136**

**Table 5.2 The malignant points which are categorised in non-malignant area with the respective pathological reports ..... 137**

**Figure 5.11 Comparison of the measured non-malignant impedance data using Mk3a and Mk3.5 Sheffield Systems with each other. .... 139**

**Figure 5.12 Median and 90% percentile ranges for malignant and non-malignant points of the bladder tissue separately (a and b) and together (c). d) Real part of impedivity versus log of frequency for normal and malignant bladder tissue in the combined form of Mk3.a and Mk3.5 Sheffield Systems ..... 140**

**Figure 5.13 The distribution of measured impedance data in non-malignant (a) and malignant (b) area of the urinary bladder using combined Mk3.a and Mk3.5 Sheffield Systems ..... 141**

**Figure 5.14 The Cole equation fitting for normal and malignant bladder tissue in the combined form of Mk3.a and Mk3.5 Sheffield Systems (the numbers show the position of 46 malignant points exactly) ..... 142**

**Figure 5.15 Effect of different degrees of oedema (a) and inflammation (b) on the electrical impedance measurements of the bladder tissue in the combined form of Mk3.a and Mk3.5 Sheffield Systems..... 143**

**Figure 5.16 Differentiating CIS from Inflammation grades 0 (a) and 1 (b) of the bladder tissue using the combined form of Mk3.a and Mk3.5 Sheffield Systems (error bars are mean  $\pm$ 1 standard error of mean) ..... 144**

<b>Figure 5.17 Differentiating CIS from Inflammation grades 2 (a) and 3 (b) of the bladder tissue using the combined form of Mk3.a and Mk3.5 Sheffield Systems (error bars are mean <math>\pm</math>1 standard error of mean) .....</b>	<b>144</b>
<b>Figure 5.18 Differentiating CIS- Inflammation grade 2 from Inflammation grade 2 of all non-malignant measured data of the bladder tissue in using the combined Mk3.a and Mk3.5 Sheffield Systems.....</b>	<b>145</b>
<b>Figure 5.19 Median and 90% percentile ranges for malignant (a) and non-malignant (b) points of the bladder tissue separately and together (c). d) Real part of impedivity versus log of frequency for normal and malignant bladder tissue in the Mk3.a Sheffield System .....</b>	<b>147</b>
<b>Figure 5.20 The distribution of measured impedance data in non-malignant (a) and malignant (b) areas of the urinary bladder using Mk3.a Sheffield System...</b>	<b>148</b>
<b>Figure 5.21 The Cole equation fitting for benign and malignant bladder tissue in the Mk3.a Sheffield System .....</b>	<b>149</b>
<b>Figure 5.22 Median and 90% percentile ranges for malignant (a) and non-malignant (b) points of the bladder tissue separately and together (c). d) Real part of impedivity versus log of frequency for normal and malignant bladder tissue in the Mk3.5 Sheffield System .....</b>	<b>150</b>
<b>Figure 5.23 The distribution of measured impedance data in non-malignant (a) and malignant (b) areas of the urinary bladder using Mk3.5 Sheffield System...</b>	<b>151</b>
<b>Figure 5.24 The Cole equation fitting for normal and malignant bladder tissue in the Mk3.5 Sheffield System (one malignant point is located at <math>R=65 \Omega m</math> and <math>\ln R/S=0.2</math>).....</b>	<b>152</b>
<b>Figure 5.25 The distribution of measured impedance data in non-malignant (a) and malignant (b) area of the urinary bladder using combined Mk3.a and Mk3.5 Sheffield Systems .....</b>	<b>153</b>
<b>Figure 5.26 Median and 90% percentile ranges for malignant and non-malignant points of the bladder tissue separately (a and b) and together (c). d) Real part of impedivity versus log of frequency for normal and malignant bladder tissue in the combined Mk3.a and Mk3.5 Sheffield Systems .....</b>	<b>154</b>
<b>Figure 5.27 The Cole equation fitting for benign and malignant bladder tissue in the combined Mk3.a and Mk3.5 Sheffield Systems (Malignanat:2 outlier at <math>65 \Omega m</math> and <math>120 \Omega m</math> and Non-malignant: 2 outlier at <math>36 \Omega m</math> and <math>60 \Omega m</math> ).....</b>	<b>155</b>
<b>Figure 5.28 Effect of different degrees of oedema (0= no oedema and 3= severe oedema) on the electrical impedance measurements of the bladder tissue in the combined Mk3.a and Mk3.5 Sheffield Systems .....</b>	<b>156</b>
<b>Figure 5.29 Effect of different degrees of inflammation (0= no inflammation and 3= severe inflammation) on the electrical impedance measurements of the bladder</b>	

tissue in the combined Mk3.a and Mk3.5 Sheffield Systems.....	156
Table 5.3 Frequencies (in Hz) used in the modified Mk3.5 Sheffield System.....	158
Table 5.4 The <i>p</i> values of statistical analysis of malignant and non-malignant bladder tissue using modified Mk3.5 System.....	158
Figure 5.30 Real part of impedivity versus log of frequency for benign and malignant bladder tissue in the modified Mk3.5 Sheffield System.....	159
Figure 5.31 The distribution of measured impedance data in non-malignant (a) and malignant (b) areas of the urinary bladder using modified Mk3.5 Sheffield System.....	160
Figure 5.32 The Cole equation fitting for benign and malignant areas of the bladder tissue using the modified Mk3.5 Sheffield System .....	161
Figure 5.33 The ROC curve for the parameter <i>R</i> (b) and parameter $\frac{R}{S}$ (b) using the modified Mk3.5 Sheffield System ( <i>in vivo</i> study) .....	162
Figure 5.34 The ROC curve for the parameters <i>R</i> and $\frac{R}{S}$ using the combined Mk3.a and Mk3.5 Sheffield Systems ( <i>Ex vivo</i> study): a) <i>R</i> b) $\frac{R}{S}$ .....	164
Figure 5.35 The ROC curve for the parameters <i>R</i> and $\frac{R}{S}$ using the combined Mk3.a and Mk3.5 Sheffield Systems ( <i>In vivo</i> study): a) <i>R</i> b) $\frac{R}{S}$ .....	165
Figure 6.1 Set-up of bladder sample, probe, digital balance and Mk3.5 Sheffield System to assess the effect of applied pressure on the measured electrical impedances .....	171
Table 6.1a The forces applied to the three resected bladder tissues to study the effect of different pressures on the bladder tissue impedivity (the reading of the balance in grams was proportional to the applied force, gf). .....	172
Table 6.1b 7 force groups were used to assess the effect of force on the measured impedance in three resected bladders (gf=gram force).....	172
Table 6.2 5 force groups were used to assess the effect of probe contact area on the measured impedance using two resected bladders (gf=gram force).....	173
Figure 6.2 Probe size affects electrical impedance measurements. a) Small size (1 mm radius) probe b) Large size (5 mm radius) probe c) Large size probe with cable (the probe was placed in the centre of the white plastic disc and then secured in its place using a screw).....	174

<b>Table 6.3 The variance for the measured impedance of 6 resected bladders (using small sized probe) .....</b>	<b>175</b>
<b>Figure 6.3 The reproducibility of the measurements resultant from the 6 resected bladders without pressure using small probe (each point is the average of 3 different measurements from that point). The calculated variance (<math>Var = \frac{SD}{Mean}</math>) for these plots are: Var 1 = 1.20, Var 2 = 0.46, Var 3 = 0.28, Var 4 = 0.69, Var 5 = 1.20, Var 6 = 0.27. ....</b>	<b>176</b>
<b>Figure 6.4a The reproducibility of the measurements resultant from the 6 resected bladders with pressure (each point is the average of 3 different measurements from that point). The calculated variance (<math>Var = \frac{SD}{Mean}</math>) for these plots are: Var 1 = 0.11, Var 2 = 0.33, Var 3 = 0.21, Var 4 = 0.20, Var 5 = 0.19, Var 6 = 0.29. ....</b>	<b>177</b>
<b>Figure 6.4b The reproducibility of the measurements resultant from the 6 resected bladders with pressure (each point is the average of 3 different measurements from that point). The calculated variance (<math>Var = \frac{SD}{Mean}</math>) for these plots are: Var 7 = 0.26, Var 8 = 0.44, Var 9 = 0.21, Var 10 = 0.52. (Left hand side: using large probe, Right hand side: using small probe) .....</b>	<b>178</b>
<b>Figure 6.5 Effect of applied pressure on the electrical impedance using small probe: a) Low force: 0-10 gf b) High force: 11-200 gf c) All forces .....</b>	<b>179</b>
<b>Figure 6.6 Effect of applied pressure on the electrical impedance using small probe: All forces .....</b>	<b>180</b>
<b>Figure 6.7 Effect of applied pressure (Low: 0-10gf and High: 11-200gf) on the electrical impedance using small probe.....</b>	<b>181</b>
<b>Figure 6.8 Effect of applied pressure on the electrical impedance using small (1mm radius) and large (5mm radius) probes over the resected bladders 1 and 2 in different forces: a) Large probe b) Small probe c) All of the measured points</b>	<b>182</b>
<b>Figure 6.9 The <i>ex vivo</i> training box to assess the effect of porcine bladder volume changes on the resulting impedance using a defined glycine solution. ....</b>	<b>184</b>
<b>Figure 6.10 Effect of volume changes of porcine urinary bladder on the measured impedance (<i>ex vivo</i>). There are three separated resected bladders. ....</b>	<b>185</b>
<b>Figure 6.11 Effect of volume changes of the porcine urinary bladder on the measured impedance (<i>ex vivo</i>) at 30 frequencies for the total number of points of three separated bladders.....</b>	<b>186</b>
<b>Table 6.4 The different values of glycine solution inside the five bladders (<i>in vivo</i>) at different points. The initial volume for minimum distension is the range 150-230 ml and the final volume for maximum distension will be about 450-740 ml. ....</b>	<b>187</b>

<b>Figure 6.12 Effect of volume changes of human urinary bladders on the measured impedance (<i>in vivo</i>) for all of five human patient's bladders. ....</b>	<b>188</b>
<b>Figure 6.13 Effect of the bladder volume changes on the measured electrical impedance (<i>in vivo</i>) in the forms of impedivity against increased volume with glycine solution (the straight line is an arbitrary line to show a possible decrease of impedance with the bladder extension). ....</b>	<b>189</b>
<b>Figure 6.14 Impedivity of saline and glycine solutions at 21 frequencies (2-192 KHz) The volume of these liquids was about 100 ml. Note that the system failed to obtain several readings at certain frequencies because these points are out of probe calibration range (see Figure 4.3). The data represent the mean of 3 readings per point for reason of reproducibility.....</b>	<b>192</b>
<b>Figure 6.15a Comparison of Malignant (n=4) and Non-malignant (n=26) points in air .....</b>	<b>193</b>
<b>Figure 6.15b Comparison of Malignant (n=4) and Non-malignant (n=26) points in saline solution (0.9 %) .....</b>	<b>193</b>
<b>Figure 6.15c Comparison of Malignant (n=4) and Non-malignant (n=26) points in glycine (1.5 %) .....</b>	<b>194</b>
<b>Figure 6.16a Comparison of non-malignant points (n=25) in air, saline (0.9 %) and glycine (1.5 %) (each point is the average of 3 separated readings because of reproducibility).....</b>	<b>195</b>
<b>Figure 6.16b Comparison of malignant points (n=4) in air, saline (0.9 %) and glycine (1.5 %) (each point is the average of 3 separated readings because of reproducibility).....</b>	<b>195</b>
<b>Figure 6.17 Comparison of the benign bladder impedance when it is submerged in saline and then glycine (<i>in vivo</i>).....</b>	<b>197</b>
<b>Table 7.1 Dimensions of cellular compartments used in model construction (N:C=nuclear – cytoplasmic ratio, ECS=extra-cellular space).(Walker, Brown et al. 2002).....</b>	<b>199</b>
<b>Figure 7.1 Three dimensional diagram of gland section finite element model. Dimensions A, B, C and D are given in Table 7.2 (Jones 2003).....</b>	<b>201</b>
<b>Table 7.2 Properties used in modelling procedure (Jones, Smallwood et al. 2003) .....</b>	<b>201</b>
<b>Figure 7.2 Finite element mesh of part of a single cell.....</b>	<b>204</b>
<b>Table 7.3 The cellular morphological parameters of the normal rabbit urinary bladder obtained from literature (Lewis and Hanrahan 1990; Lewis 2000). .....</b>	<b>205</b>
<b>Figure 7.3 A digital image of benign section of the urinary bladder .....</b>	<b>205</b>

<b>Table 7.4 The mean values of the cellular morphological parameters of the human urinary bladder obtained from analysis of the both malignant and normal bladder histology sections by the author .....</b>	<b>206</b>
<b>Table 7.5 Dimensions of cellular compartments of the human urinary bladder used in model construction (ECS=extra-cellular space). These data obtained from analysis of the both malignant and benign bladder histology sections by the author .....</b>	<b>207</b>
<b>Figure 7.4 Method of obtaining electrical transfer properties from cellular level finite element models.....</b>	<b>208</b>
<b>Figure 7.5 Macroscopic tissue model constructed from the literature using the morphological parameters of rabbit urothelium (ecs=extracellular space).....</b>	<b>210</b>
<b>Figure 7.6 (a) Central surface (x-y plane) of macroscopic tissue model showing electrodes highlighted in grey (b) Layering in macroscopic model (x-z plane). Mesh densities used in the model solution were approximately twice those illustrated above.....</b>	<b>211</b>
<b>Figure 7.7 The real part of the complex modelled impedance spectra for normal rabbit bladder tissue using the literature review.....</b>	<b>212</b>
<b>Figure 7.8 The real part of the complex modelled impedance spectra for normal and malignant urothelial tissue .....</b>	<b>213</b>
<b>Figure 7.9 Modelled current – depth distribution midway between drive electrodes for (a) normal tissue model, (b) Malignant tissue model at different frequencies and surface layer thicknesses (dm) Layer no. key: 1 – surface fluid, 2-superficial urothelium, 3-intermediate urothelium, 4-basal urothelium, 5- basement membrane, 6- connective tissue.....</b>	<b>215</b>
<b>Table A1 The cellular morphological parameters of the human urinary bladder obtained from analysis of the normal bladder histology sections (Superficial cell size) by the author (SD = Standard deviation).....</b>	<b>244</b>
<b>Table A2 The cellular morphological parameters of the human urinary bladder obtained from analysis of the normal bladder histology sections (Intermediate cell size) by the author (SD = Standard deviation).....</b>	<b>244</b>
<b>Table A3 The cellular morphological parameters of the human urinary bladder obtained from analysis of the normal bladder histology sections (Basal cell size) by the author (SD = Standard deviation) .....</b>	<b>245</b>
<b>Table A4 The cellular morphological parameters of the human urinary bladder obtained from analysis of the malignant bladder histology sections (Superficial cell size) by the author (SD = Standard deviation).....</b>	<b>245</b>
<b>Table A5 The cellular morphological parameters of the human urinary bladder obtained from analysis of the malignant bladder histology sections (Intermediate</b>	

**cell size) by the author (SD = Standard deviation)..... 246**

**Table A6 The cellular morphological parameters of the human urinary bladder obtained from analysis of the malignant bladder histology sections (Basal cell size) by the author (SD = Standard deviation) ..... 246**

# Chapter 1

## Introduction and clinical background

In developed countries, most bladder cancers are transitional cell carcinomas (TCC). TCC is one of the commonest cancers, with approximately 13,000 new cases and 5400 deaths per year in the UK (Black, Bray et al. 1997). The majority of patients present with haematuria and superficial papillary tumours, and although recurrence is common (50-70%), the disease can usually be controlled by local treatment. Nevertheless, 10-15% of patients with superficial TCC eventually progress to muscle-invasive and metastatic disease (Silverman, Rothman et al. 1999). At present, the accepted treatment strategy for patients presenting with superficial disease is transurethral resection, followed by adjuvant intra-vesical chemotherapy to combat recurrence. Patients are followed-up with regular check cystoscopies, placing a high load on clinical resources. Approximately 20% of patients have tumours which are muscle-invasive at presentation. These tumours are thought to develop from carcinoma in situ (CIS), have a poor prognosis (less than 40% 5-year survival compared with 80-90% for superficial disease) and require radical treatment. Cystourethroscopy remains the gold-standard for investigating these patients. The erythematous areas seen at cystoscopy can represent several different pathologies from simple inflammation through to flat carcinoma in situ, and significant pathology may be present in areas with no obvious visible abnormality.

This thesis investigates whether it is possible to diagnostically classify bladder mucosa using the minimally invasive technique of electrical impedance spectroscopy (EIS), which was developed initially to screen for cervical cancer (Brown, Tidy et al. 2000), and has subsequently been used in the assessment of Barrett's esophagus (Gonzales-Correa, Brown et al. 1999). The morphology of urothelium, and the natural history of pre-cancerous changes in urothelium, are significantly different from that found in the cervix and esophagus. The impedance spectrum generated by EIS is a function of the detailed structure of the tissue at the cellular level. Normal human urothelial mucosa consists of an epithelial layer 3 – 6 cells thick, a lamina propria of loose connective tissue and a variable, discontinuous band of submucosal muscle. Occasionally white blood cells are often present. The superficial epithelial cells are specialized known as "umbrella" cells. They have abundant eosinophilic cytoplasm and may contain and

secrete mucin. In CIS the umbrella cells usually disappear and are replaced by undifferentiated cells. Urothelial carcinoma *in situ* is characterized by flat, disordered proliferation of urothelial cells with marked cytological abnormalities including; nucleomegaly (increased nuclear size), nucleolomegaly (increased nucleoli size), pleomorphism (abnormally shaped cells), loss of cellular polarity and mitoses. The normal lamina propria can be divided into an inner and outer zone by a prominent collection of arteries and veins (Reuter 1992). In inflammatory conditions, the white cells, small vessels and fibrous tissue components of the lamina propria may all increase, sometimes dramatically.

EIS measurements have been made on both fresh excised human bladders and, following development of a suitably small probe that could be passed down the biopsy channel of a cystoscope, *in vivo* during cystoscopy. The effect of fluid volume in the bladder and pressure on the probe tip, both of which would be expected to alter the impedance spectrum as a result of morphological changes, have been explored. Finite element modelling of the current flow at a cellular and macroscopic level in a simple model of the urothelium has been used to explore the spectral characteristics that are peculiar to urothelium.

## 1.1 The aim of this study

The **primary aim** of this study is to develop a non-invasive screening technique to distinguish malignant and non-malignant areas in the urinary bladder. To achieve the primary aim, the **secondary aims** are to:

- 1) Use computational modelling at a cellular level to investigate the effect of morphological changes on the impedance spectrum, and inform the measurement regime.
- 2) Develop a probe which can be passed through the biopsy channel of a standard cystoscope to enable measurements to be taken *in vivo*.
- 3) Develop and validate techniques for comparing EIS measurements and histological sections in *ex vivo* bladders.
- 4) Develop and validate techniques for comparing EIS measurements and biopsies *in vivo*.
- 5) Determine the effect of bladder distension on the electrical impedance spectrum.

- 6) Determine the effect on the electrical impedance spectrum of varying the pressure on the probe tip.
- 7) Compare impedance spectra, measured in *ex vivo* bladders, for tissue varying from normal to frank malignancy.
- 8) Compare impedance spectra, measured *in vivo*, for tissue varying from normal to frank malignancy.

## **1.2 Anatomy, histology and pathology of the human urinary bladder**

### **1.2.1 Introduction**

It would be very useful if one could have a good understanding of human urinary bladder anatomy, physiology, histology and common pathologies especially bladder cancers. In the following chapters, the author will describe the electrical impedance technique, the measured data and then any changes in this data related to malignant or non-malignant areas of the bladder. Thus, first the function and fine structure of the urinary bladder will be discussed briefly then the bladder pathology will be reviewed.

### **1.2.2 Anatomy and physiology of the urinary bladder**

The urinary bladder is a smooth, collapsible and muscular sac, which provides a temporary store for urine. Urine is formed continuously by the kidneys then stored in the bladder until its release is convenient. Jequier and Rousseau in 1987 measured the thickness of the bladder wall sonographically in children and adults. They showed that the bladder wall thickness varied principally according to the degree of filling, age and gender. The mean thickness of the normal bladder wall was 2.76 mm when the bladder was almost empty and 1.55 mm when distended. They found a highly significant relation between the degree of bladder distension and wall thickness ( $p < 0.0001$ ) (Jequier and Rousseau 1987). Two long muscular tubes (ureters) extend from the kidneys to the urinary bladder. The ureter plays an active role in carrying urine. Muscles contract as urine comes in from the kidneys. Also due to the special arrangement of the ureters, the backflow of urine into them is prevented during bladder filling. The other tube that extends from the bladder to the sphincter is the urethra. This tube empties the bladder. The bladder varies in size, shape and position according to the degree of distension. It has the ability to distend and store up to 500 ml. of urine without

a change in intra-luminal pressure (Memmler, Cohen et al. 1996). Except for the bladder neck it lies relatively free within the fibrofatty tissues of the pelvis. Expulsion of urine from the urinary bladder is usually known as urination. When a person is ready to urinate, the bladder walls contract and the internal sphincter (a ring-like muscle that guards the entrance from the bladder to the urethra) relaxes. Contraction of the smooth muscle in the bladder wall, which is called the detrusor muscle, is mainly responsible for emptying this organ during urination. Urination takes place through the urethra, and the bladder empties. As shown in Figure 1.1, the interior of this organ has 3 openings for both ureters (urine coming into the bladder from kidneys) and the urethra (urine leaving the bladder). Together these are known as the trigone. This triangular region (trigone) has a different histological structure to the other parts of the bladder because its mucosa is firmly bound to the muscularis, thus the trigone has a smooth appearance and expands minimally during bladder filling (Marieb 1998). The neck is the lowest and most fixed point of the bladder. It is pierced by the internal urethral orifice and alters little in position with the varying conditions of the bladder or rectum. When the bladder is empty (or contains little urine), the wall collapses into its basic pyramidal shape. As urine fills the bladder, the wall expands and the bladder becomes pear-shaped rising upwards in the abdominal cavity thus stretching and thinning the bladder wall.

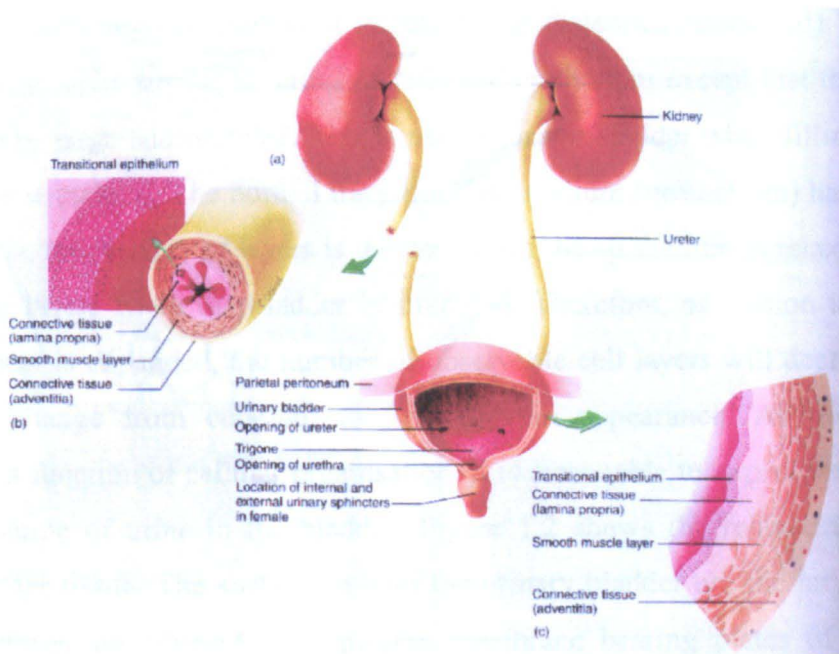


**Figure 1.1 Structure of the urinary bladder (Seeley, Stephens et al. 2000) with permission from McGraw-Hill Education**

### 1.2.3 Histology of the urinary bladder

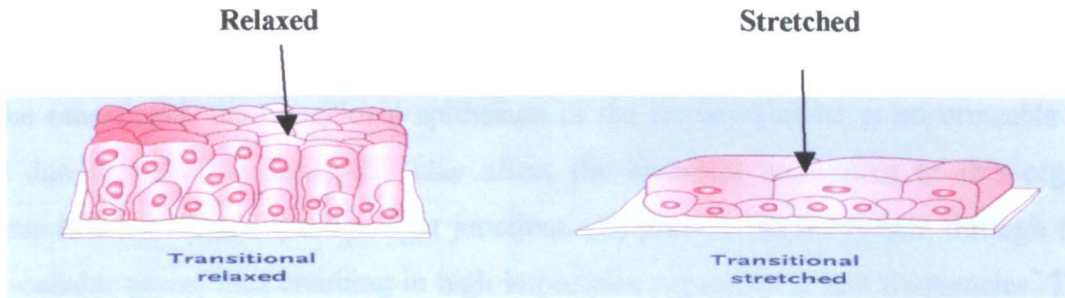
The electrical impedance of a tissue (bladder tissue in this case) depends on tissue composition, structure, fat and water content. It also varies considerably with the pathological state of the tissue such as inflammation, oedema, ischaemia and cell proliferation. Therefore, first of all, a section will explain the histology of the bladder and then the bladder pathology. We are primarily interested in the urothelium, but, for completeness, the whole structure will be described. The fine structure of the bladder consists of three important layers (Figure 1.1):

- 1) **Urothelium** including transitional epithelium
- 2) **Lamina propria** including connective tissue
- 3) **Detrusor muscle** layers

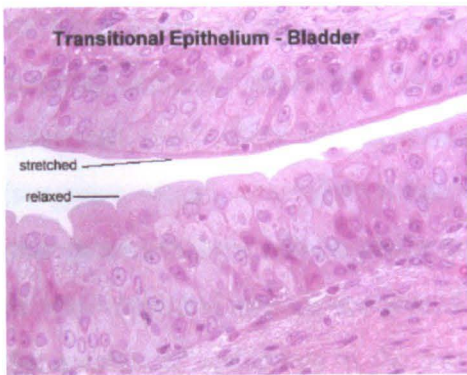
#### 1.2.3.1 Urothelium

The urothelium or epithelial tissues in the bladder are usually transitional thus the superficial shape changes from squamous (cells which are flat, attached to each other like tiles) to cuboidal (cells which are thicker and cube shaped) depending on the degree of stretch. This means that the transitional epithelium of the bladder is variable in appearance, depending on whether it is relaxed or distended (stretched). If it is in a relaxed state, it looks similar to stratified cuboidal epithelium except that the superficial cells tend to be large and rounded. This is useful for the bladder when filling with urine (distended or stretched). The normal transitional epithelium (urothelium) has three to six layers of cells, the number of layers is greatest when the epithelium is relaxed and it has two or three layers when the bladder is stretched. Therefore, as tension increases, the epithelial sheet is expanded, the number of observable cell layers will decrease and cell shape will change from cuboidal to squamous in appearance. As the impedance spectrum is a function of cellular organisation, it is reasonable to expect that it will vary with the volume of urine in the bladder. Figure 1.2 shows the relaxed and stretched urinary bladder tissue. The surface cells of the urinary bladder are the largest and their luminal surfaces are covered by a plasma membrane bearing plates of glycoprotein particles (plaques) embedded in its lipid bilayer. These arrays stiffen the membrane. When the epithelium is in a relaxed state and the surface area of the cells is reduced, the glycoprotein-lipid plates are partially taken into the cytoplasm within vacuoles, re-

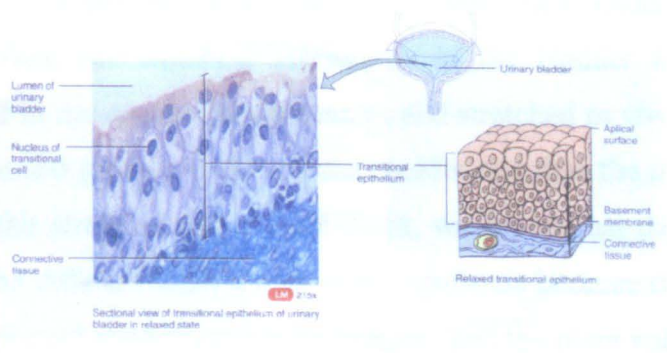
emerging onto the surface and to make a thin epithelial layer and thin squamous cells when its area increases once more through stretching. Previous modelling work by Walker on the effect of the cell nucleus on the impedance spectrum suggests that vacuoles would have little effect on the impedance spectrum (Walker 2001). In the stretched state, the effect of the plaques (in electrical terms) is to provide an additional thin membrane,  $0.5 \mu\text{m}$  in diameter and  $12 \text{ nm}$  in thickness (Lewis 2000), covering the surface, which would have a small effect on the spectrum.



a



b



c

**Figure 1.2 a) Transitional epithelium of the urinary bladder in relaxed and stretched states (a,b). Transitional epithelium in a relaxed state (c) (Tortora and Grabowski 2000). With permission from John Wiley & Sons**

Figure 1.3 shows plaques on the surface of relaxed bladder epithelium. Thus, the surface area of the relaxed cells is increased by the incorporation of plaques (disks) of membrane, which are stored in the cytoplasm and inserted into the apical plasma membrane when the mucosa is stretched by the accumulation of urine. This process is reversible and is accompanied by all cells changing shape and position within the epithelium.

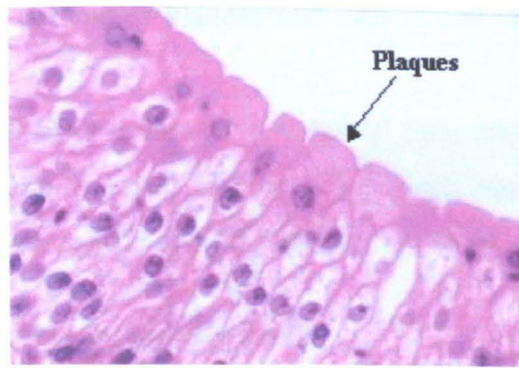


**Figure 1.3 Plaques present on surface of the relaxed bladder epithelium**

On the other hand, the transitional epithelium of the urinary bladder is impermeable to urine due to tight junctions; this may affect the electrical impedance of this organ because it is anticipated that the tight junctions will prevent ion movement through the extra-cellular space, thus resulting in high impedance especially at low frequencies. The tight junctions are very common among epithelial cells lining the urinary bladder. These junctions in the urinary bladder prevent fluid leakage through the bladder wall. The epithelial tissue of this organ consists of closely packed cells with little extra-cellular material between adjacent cells. When the electrical impedance of the bladder is measured, the bladder will be relaxed in the *ex vivo* measurements and stretched *in vivo* (surgeons usually use saline solutions and glycine to distend the bladder and thus the *in vivo* measurements will be made in this stretched state). As a result, we expect that the *in vivo* electrical impedance would be different from the *ex vivo* impedance because of the number of cell layers in the transitional epithelium; tight junctions; and the extra and intra cellular spaces in the two different states of the bladder. There is a brief description of tight junctions at the end of the histology section (section 1.2.3.3) because of their great importance in electrical impedance of the bladder tissue. The three regions in the urothelium are (Martin 1972; Lewis and Hanrahan 1990; Reuter 1992; Gray 1995):

- a) **Superficial cells:** these cells are large (cuboidal cells), and sometimes are elliptical depending on the distended or relaxed states of the bladder. They can be laid umbrella like over the smaller intermediate cells. When the bladder is distended they become flattened. The large superficial cells frequently bulge into the bladder lumen and are often binucleate (Figures 1.3 and 1.4).
- b) **Intermediate cells:** these cells are pyramidal in shape. The urothelium may be up to

5 cells thick in the contracted bladder and only 1 cell thick in the distended and flattened state.

- c) **Basal cells:** the basal layer is formed of cuboidal cells which are evident only in the contracted bladder and lie on a thin but continuous basement membrane. In the collapsed state, they are usually cuboidal almost columnar.

### 1.2.3.2 Lamina propria and Detrusor muscle

The lamina propria, a fibro-elastic connective tissue, is the inner layer of the urinary bladder and lies under the transitional epithelium and basement membrane (the basement membrane provides the physical support for the epithelium and provides a base for cell attachment). It forms a thick layer (varying in depth from 500  $\mu\text{m}$  in the fundus and interolateral walls to about 100  $\mu\text{m}$  in the trigone) (Eroschenko 2000). The lamina propria is shown in Figure 1.2 c or in Figure 1.4. The muscular coat or smooth muscle cells form three layers (inner, longitudinal; middle, circular and outer, longitudinal), include more than half part of the bladder wall thickness. See Figure 1.5 (Bailey 1984). Cellular-level modelling of cervical epithelium suggests that the injected current will penetrate into, and probably through, the lamina propria (Walker 2001). The measured impedance of cervical stroma is similar to the average impedance of muscle fibre (0.2-0.5  $\text{Sm}^{-1}$  varying with frequency in the frequency range of 10 Hz-1.5 MHz) see Figures 1.6 and 1.7, so electrically the lamina propria, the connective tissue and muscle would probably be considered to be a continuum. This will be used in cellular-level modelling of the bladder epithelium.



**Figure 1.4 Lamina propria (a connective tissue) is under the transitional epithelium and the basement membrane (Eroschenko 2000). With permission from Lippincott Williams & Wilkins.**

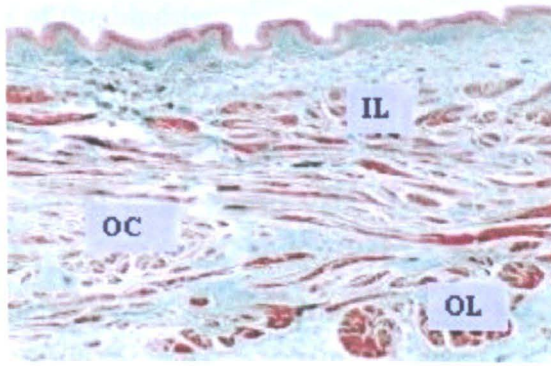


Figure 1.5 Urinary Bladder Muscles, IL: Inner Long Muscle OC: Outer Circular Muscle OL: Outer Long Muscle. Modified from (Young 2000)

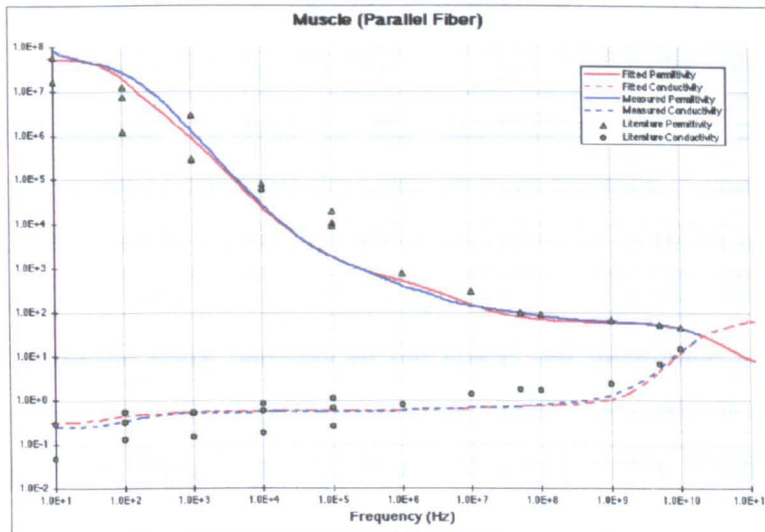


Figure 1.6 Conductivity in S/m and relative permittivity of the Muscle (Parallel Fiber) against frequency in Hz (Gabriel, Gabriel et al. 1996).

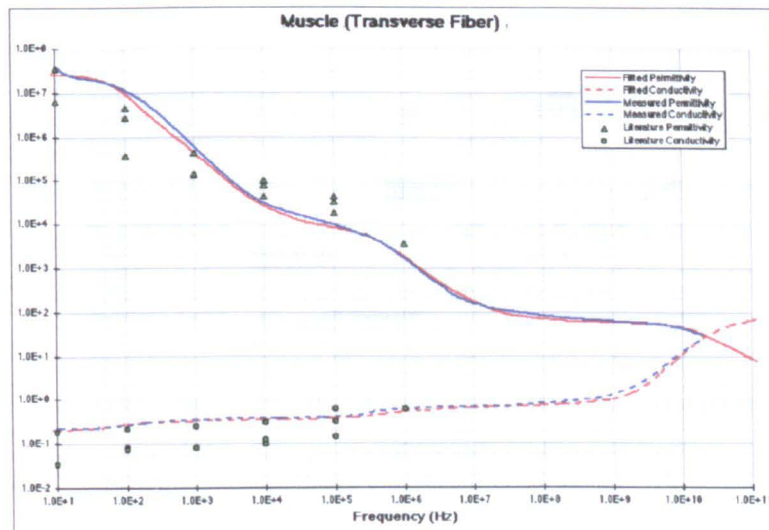
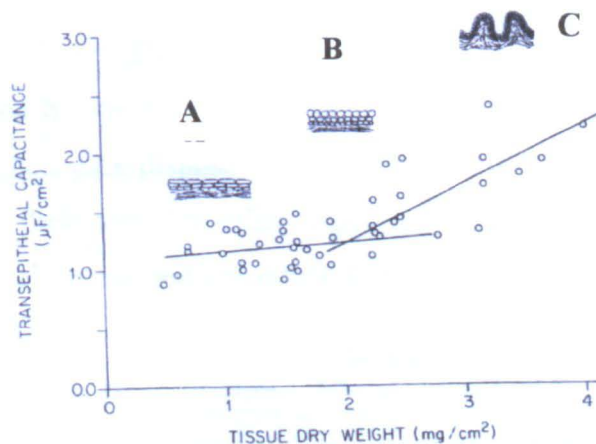


Figure 1.7 Conductivity in S/m and relative permittivity of the Muscle (Transverse Fiber) against frequency in Hz (Gabriel, Gabriel et al. 1996).

### 1.2.3.3 Tight junctions of the bladder

Epithelial tissue is used to form the inner lining of respiratory, digestive and urinary systems. In general, most of the epithelial and muscle cells are tightly joined. Tight junctions connect the cells of these tissues. This type of junction is common in the stomach, intestines and urinary bladder tissues. The unique barrier properties of the urothelial surface membrane permit urine storage (Lavelle, Meyers et al. 2000). In this junction, the outer surface of adjacent plasma membranes are fused together and because of that, prevent the passage of substances and ions through the extra cellular space, thus giving a high impedance at low frequencies. There is qualitative evidence from Clausen (1989) which suggests that these tight junctions may have some effects on the electrical impedances of the bladder in comparison with other organs. He summarised the methods involved in the quantitative analysis of transepithelial impedance for the study of transport processes in tight epithelia (Clausen 1989). There is also a good work done by Lewis et al about ion transport by rabbit urinary bladder, a tight epithelium. They used transepithelial and intra cellular electrical techniques to clarify the  $Na^+$ -specific entry pathway of the apical cell membrane and demonstrated that there is an inverse relationship between transepithelial capacitance and stretching of the bladder epithelium (Figure 1.8) (Lewis and Diamond 1976). Finally, finite element modelling at a cellular length scale indicates that tight junctions could affect the electrical impedance of cervical tissue. Tight junctions caused higher electrical impedance in normal cervical tissue than cancer type (Gonzales-Correa 2000; Walker 2001).



**Figure 1.8** Transepithelial capacitance of the rabbit urinary bladder in fully stretched (A), moderately stretched (B) and the relaxed states (C). Modified from (Lewis and Diamond 1976)

## **1.2.4 Pathology of the human urinary bladder**

One may expect that the structural changes caused in the bladder tissue would result in electrical impedance changes. Thus it is obviously important to discuss the pathology of the bladder. However for the purpose of this study, only the bladder abnormalities resulting from tissue structural changes will be introduced in this section. These abnormalities are divided into two categories: Non-Malignant and Malignant diseases.

### **1.2.4.1 Non-malignant diseases of the bladder**

There are several important diseases that are not malignant. They will be used in this work because the histopathological report of the biopsies (related to the electrical impedance measured area) includes some of these diseases such as: Inflammation, Oedema and Von Brunn's nests. (A detailed explanation of the biopsy procedure will be presented in the following chapters). The purpose of explaining these non-malignant diseases in this thesis is that they have some similarities with the morphology of malignant tissues. For example, bladder tissue with red patches cannot be visually identified as carcinoma *in situ* or only inflammation. Thus, it is the aim of this work to distinguish their respective electrical impedances. The effect of these diseases on the impedance spectrum will be compared using pathological reports of biopsies, in the following chapters.

#### **1.2.4.1.1 Inflammation and Oedema**

Inflammation is a local physiological response to tissue injury. It is not a disease in itself. By definition, if microbes, physical agents or chemical agents, damage cells, the response is called inflammation. This phenomenon is a defensive response and it is usually characterised by symptoms such as redness, pain, heat, swelling and loss of function. Inflammation aids disposal of microbes, toxins, or foreign materials at the injury site, prevents their spread to other organs and prepares the injured site for repair. Inflammation is usually classified according to its duration as: Acute inflammation (this is an initial, transient response to injury) and Chronic inflammation (this is a subsequent, a prolonged tissue reaction). Blood vessels in the injured site dilate and become more permeable, thus vasodilatation (an increase in diameter of blood vessels) occurs and permeability increases. The three stages for inflammation are: vasodilatation, phagocyte migration and tissue repair. Immediately after an injury, dilation of arterioles and increased permeability of capillaries produces heat, redness

(erythema) and oedema (Konishi, Morimoto et al. 1995) in the affected area. Oedema is excess fluid in the intercellular space and is recognized clinically by diffuse swelling of the affected sites (Underwood 2000). The increased permeability of capillaries allows leakage of clotting factors into tissue. Thus, clotting cascade occurs and fibrinogen is ultimately converted to an insoluble, thick network of fibrin threads that localise and trap invading microbes and block their spread. Electrical impedance increases at sites of bladder tissue inflammation because of the increasing number of cells in this area. As mentioned previously, oedema is another phenomenon occurring after injury. The resultant oedema permits fluid to move from the blood into tissue spaces. It is expected that increasing inflammation will cause an increase in impedance, but in contrast for oedema the impedance will decrease. The effect of inflammation and oedema on the measured electrical impedance of the urinary bladder will be discussed in this thesis.

#### **1.2.4.1.2 Interstitial Cystitis (IC)**

IC can be a debilitating urological disease. Urinary tract infection and IC have some similar characteristics. Many patients with IC have a past history of urinary tract infection (Lamm and Gittes 1977). In the case of interstitial cystitis, the term 'interstitial' is related to 'a space between' layers within the wall of the urinary bladder, and the term 'cystitis' refers to inflammation. IC is an inflammatory disease of the bladder not caused by known infectious agents. Its diagnosis should be considered when a painful bladder condition has not improved with antibiotics. Urinary cytology is the most helpful technique to diagnose this abnormality of the bladder, but repeated bladder biopsy with careful serial sectioning may be necessary to establish a diagnosis of malignancy. As this is an inflammatory response, we would expect it to result in an increase in impedance.

#### **1.2.4.1.3 Von Brunn's nests**

The most common urothelial variant is the Von Brunn's nests. They are proliferate, solid invaginations of urothelial cells into the lamina propria. Initially it was believed that this effect was caused by inflammation, but Von Brunn's nests are now considered to be a normal component of the urinary tract and they can be found in all urinary bladders. They are presumably caused by the repeated expansion and contraction of the urinary bladder and lower urinary tract structures. It is usual to observe biopsy specimens with

denuded mucosa or only a few malignant cells (Damjanov and Linder 1996).

#### **1.2.4.2 Malignant disease of the bladder (Bladder cancer)**

Bladder Cancer is an abnormal growth (tumour) in the lining of the urinary bladder. For the first time, a surgeon, Dr. Rehn reported three cases of bladder cancer in workers in the German dye industry in 1895. At present, bladder cancer is the fourth most common malignant neoplasm in men and the eighth in women. It is primarily a disease of men over 65 and is rarely diagnosed before the age of 40. Cigarette smoking is the most important risk factor, although work in the dye, rubber, or leather industries are also strongly associated with bladder cancer (the chemical agents may work as carcinogens in the bladder) (Silverman, Levin et al. 1989). Tumour cells have reduced cohesiveness, large nuclei, and are eccentric with irregular borders. The chromatin of these cells is granular and irregularly distributed. Bladder cancer refers to a change in morphology of one cell type into another that is considered aberrant for that location. For example, transitional epithelium frequently undergoes either squamous or glandular metaplasia (Reuter 1992). In the course of developing bladder cancer, a variety of urinary tract diseases such as chronic infections, bladder pain, irritation and frequent urination occur (Weiss and Stacey 1989).

Bladder cancer is usually divided into two types: superficial and invasive. According to reports, 75% of tumours are superficial, 20% are invasive and up to 5% have *de novo* metastasis. The disease can usually be controlled by local treatment. The accepted treatment strategy for patients with the superficial disease is transurethral resection. In terms of treating bladder cancer, surgery, radiotherapy and chemotherapy can be used alone or in combination. If the bladder tumour is more extensive, total or partial removal of the bladder may be necessary (cystectomy). Therefore, it is obviously important to detect this disease as soon as possible.

##### **1.2.4.2.1 Staging (grading) of bladder cancer**

Regardless of cell type, clinico-pathologic staging is the most important parameter for planning the treatment and diagnosis of bladder cancer. The most commonly used grading system is the Tumour-Node-Metastases (TNM) (Table 1.1). This classification recommended by the 'Union Internationale Contre le Cancer' (UICC). This system classifies the tumour depending on the level of invasion into the bladder wall as well as

the nodal and metastatic state of the patient (UICC 1997). This precise pathological classification has helped urologists in classifying different types of tumour (Table 1.2).

<b>TNM Grading System (1997)</b>	
<b>Primary tumour</b>	
<b>TX</b>	<b>Primary tumour can not be assessed</b>
<b>T0</b>	<b>No evidence of primary tumour</b>
<b>Ta</b>	<b>Non-invasive papillary carcinoma.</b>
<b>Tis</b>	<b>Carcinoma in situ: flat tumour</b>
<b>T1</b>	<b>Invades sub epithelial connective tissue</b>
<b>T2a</b>	<b>(inner half) muscle invasion</b>
<b>T2b</b>	<b>Deep (outer half Superficial) muscle invasion</b>
<b>T3</b>	<b>Invades perivesical fat</b>
<b>T3a</b>	<b>Microscopic</b>
<b>T3b</b>	<b>Macroscopic</b>
<b>T4a</b>	<b>Invades prostate, uterus, or vagina</b>
<b>T4b</b>	<b>Invades pelvic or abdominal wall</b>

**Table 1.1 TNM grading system of bladder cancer. Modified from (UICC 1997)**

<b>Stage or Grade grouping</b>	
<b>Stage 0</b>	<b>Tis</b>
	<b>Ta</b>
<b>Stage 1</b>	<b>T1</b>
<b>Stage 2</b>	<b>T2</b>
<b>Stage 3</b>	<b>T3a</b>
	<b>T3b</b>
<b>Stage 4</b>	<b>T4</b>

**Table 1.2 The staging of urinary bladder tumours. Modified from (UICC 1987).**

#### 1.2.4.2.2 Transitional Cell Carcinomas (TCC)

The majority of bladder cancers are Transitional Cell Carcinomas (TCC). It is one of the most common cancers, with approximately 13,000 new cases and 5400 deaths per year in the UK (Black, Bray et al. 1997). In addition, up to 40% of patients with high grade TCC will have synchronous or subsequent Carcinoma *in situ* (CIS). (Fleshner, Herr et al. 1996). 10-15% of patients with superficial TCC eventually progress to muscle-invasive and metastatic disease (Blair, Zahm et al. 1999).

**Incidence:** Transitional Cell Carcinomas range from: papillary to flat; non-invasive to invasive; and extremely well differentiated (grade 1) to highly anaplastic aggressive cancers (grade 3). Grade 1 are always papillary and rarely invasive, but may recur after removal. Grade 3 cancers can be papillary or flat, may cover larger areas of the mucosal surface and invade more deeply. TCC is divided into:

- Papillary
- Papillary and infiltrating
- Solid (sessile, nodular) and infiltrating
- Non-papillary, non-invasive, i.e., Carcinoma *in situ*

**Pathology:** Papillary TCC, grade 1 (non-invasive) is covered by thickened transitional cell epithelium (more than six cells thick). There is increased nuclear to cytoplasmic ratio (Silverberg 1988). Bladder cancer often presents as a spectrum of alterations to the urothelium ranging from minor changes in nuclear appearance to frank carcinoma, and from unifocal to multifocal mucosal involvement (Badalament, Ortolano et al. 1992). The non-papillary tumours are sessile, flat, nodular or ulcerated masses. When tumours first present, most of them are solitary while only 30% are multiple (Anderstrom, Johansson et al. 1980). In contrast to papillary tumours, which are usually pure transitional cells with some tubular structures, sessile and nodular tumours have foci of squamous and glandular structures or spindle cells and more frequently demonstrate muscle and lymphatic invasion.

#### 1.2.4.2.3 Carcinoma *in situ* (CIS)

Every invasive cancer arises by definition from Carcinoma *in situ* (CIS). It usually occurs as a multifocal disease of the bladder and may involve all regions of the urothelium. CIS is a high grade, highly malignant, flat and aggressive manifestation of

TCC that is likely to progress into muscle invasive cancer.

**Incidence:** Historically, Melicow first described CIS in 1952 as a superficial bladder cancer in areas of the bladder epithelium (Melicow 1952). Estimates of the incidence of CIS adjacent to papillary tumours are 10- 40% (Utz and Farrow 1984) and up to 75% are adjacent to invasive lesions (Prout, Koontz et al. 1983). It has a high propensity for invasion if left untreated. The typical cystoscopic appearance of CIS is an erythematous patch of the bladder mucosa that bleeds easily on contact. CIS (non-papillary tumours) are the major source of invasive and metastasising carcinomas in humans. An *in situ* stage of bladder carcinoma can often be recognised in patients with previous papillary or invasive tumours. The tissue of CIS can be shown as Figure 1.9.

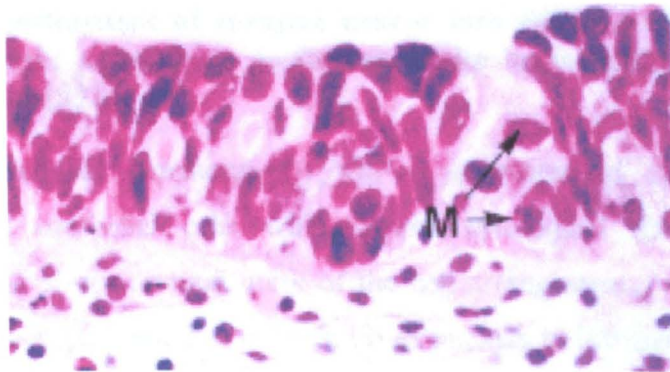


**Figure 1.9 Carcinoma *in situ* (CIS)**

**Stages:** Farrow (1984) has explained that invasive cancer is a dynamic evolution from the first occurrence of cytological alteration (epithelial atypia) to *in situ* cancer and then developing either into papillary or flat cancers. The most advanced disease can vary between high-grade (poorly differentiated) and low-grade (well differentiated) tumours (Farrow and Utz 1982). So, among the high grade TCCs, the flat pre-invasive lesion (CIS) is the most important route by which invasive cancer gradually develops into either a high-grade papillary stage or by direct progression to flat invasive cancer (Figure 1.10). Thus, this is a recognised step in the evolution of the most invasive bladder cancers:

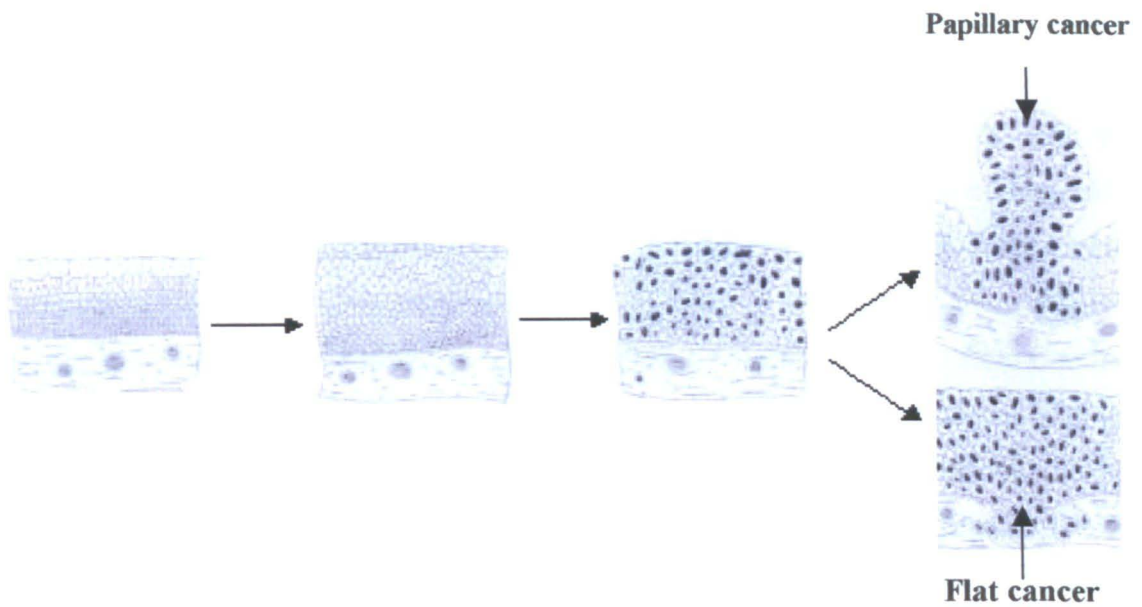


**Figure 1.10 Development of invasive cancer into either a high- grade papillary stage or by direct progression to flat or sessile invasive cancer. Modified from (Farrow and Utz 1982)**

**Pathology:** Urothelial carcinoma *in situ* is characterized by a flat, disordered proliferation of urothelial cells with marked cytological abnormalities including: increased nuclear size; non-uniformity of the cell arrangements; a variety of cell sizes, shapes and orientation; variation in the ratio of nucleus to intracellular liquid; reduction of cells cohesiveness; and loss of cellular polarity and mitoses (Ro, Staerkel et al. 1992). Thus these changes in structural parameters of the malignant bladder tissue, for example CIS, can cause significant bio impedance changes in the urinary bladder. It will probably be possible to characterise this important pre-cancerous malignant disease from the normal bladder tissue and from other abnormalities, in terms of their electrical impedances. CIS of the urothelium is often found as a multifocal change in areas between tumours, and in some bladders in which no obvious tumours are present. It is a precursor to invasive carcinoma (Underwood 2000). Finally, primary CIS of the bladder is recognised as a potentially lethal condition because of the high risk of it becoming invasive bladder carcinoma over time.

**Diagnosis:** A diagnosis of CIS at this time can be made when a population of malignant cells has replaced the entire thickness of the urothelium. It is most commonly seen in patients with high-grade papillary transitional cell carcinomas. The majority of patients develop invasive carcinoma within 3 years of diagnosis if left untreated (Damjanov and Linder 1996). From the viewpoint of the urologist, significant considerations for this

type of cancer are as follows: CIS of the bladder may be an early phase in the evolution of an invasive cancer, it tends to persist and may progress over time and is not precisely predictable using traditional diagnostic techniques. It looks like a red patch cystoscopically and is difficult to diagnose, thus an attempt was made to distinguish CIS from normal and other pathological states in the bladder epithelium using electrical impedance technique. However all of the malignant types of disease will be put into one major group named the 'Malignant group' including Partial Coverage of the Carcinoma *in situ* (CISp), Full Coverage of the Carcinoma *in situ* (CISf) and Carcinoma (Ca) in the measurement procedure. Then, using the respective biopsy reports, the electrical impedance of this group will be compared with the 'Non-Malignant group'. The Non-Malignant group includes Intact Epithelium (E), Ragged Epithelium (R), Denuded Epithelium (D) and Denuded Epithelium with Residual von Brunn's nests (DvB). More details will be in the materials and methods section.

### **1.3 A review of existing bladder cancer detection techniques**

There are different tests, but firstly because of simplicity, the patient will usually be asked for a urine sample, to test for blood and the possibility of urinary system infections. Various investigations are currently available to help with the diagnosis of bladder cancer as follows:

**Diagnostic Radiology:** Conventional *x-ray* has long been used as a method to evaluate urinary system disorders.

**Excretory Urography:** It is a type of *x-ray* examination specifically designed to study the kidneys, bladder, and ureters. After iodine-based contrast dye is injected intravenously, a series of radiographic images are taken at timed intervals. The kidneys are responsible for removing contrast from the blood and collecting it in urine. Abnormalities of the collecting systems can be identified. This technique has been regarded as the standard imaging technique for detection of urinary tract disorders. This technique reveals both the anatomic features of the urinary tract and the physiologic components of the kidneys. However this is not the best method for detecting bladder tumours, particularly if they are small in size.

**Urine Cytology:** Urine cytology is examining the urine samples of suspected patients under a microscope to look for cancerous or pre-cancerous cells. Urine cytology is often

used to detect tumours because it is a simple and non-invasive technique. Unfortunately, urine cytology does not detect low-grade lesions very well, since cellular changes are often very subtle in early malignancy. This technique is most helpful to detect bladder cancer but repeated biopsies with careful serial sectioning may be necessary to establish the diagnosis of malignancy.

**CT Scan and MRI:** Computed Tomography (CT Scan) and Magnetic Resonance Imaging (MRI) use a narrow *x-ray* beam and radio waves respectively to take detailed cross-sectional images of the organ. A computer then combines these images into a very detailed cross-sectional image. These images provide information about whether the cancer may have spread to tissue next to the bladder. These are used to assess large (Minsky and Chlapowski 1978) bulky tumours, lymphatic involvement, and the response of tumours to radiation or chemotherapy. Large (bigger than 5 cm) tumours or when the initial tumour is solid rather than papillary is appropriate to detect using this technique. Neither method can distinguish between surface bladder tumours and those that invade deep muscle tissue. In addition, CT Scans and MRI can not diagnose microscopic metastatic disease; for example, they only detect cancerous lymph nodes, that are 1 cm or larger in size.

**Ultrasound Scans:** These produce echoes of the urinary bladder tissues by using ultrasound waves and the pattern of echoes reflected by tissues can be useful in determining the size of a bladder tumour. The main disadvantage of this technique is the need to undertake the investigation under general anaesthesia and its poor definition of bladder wall invasion. Furthermore, this technique like CT Scan is unable to show accurately the depth of muscle invasion due to its inability to distinguish between individual layers of muscle wall (Syrigos and Skinner 1999).

**Cystoscopy:** Visual examination of the urinary tract is possible with a cystoscope (a thin, slender tube with a tiny camera attached and a light usually from a fibre optic cable) see Figure 1.11. In this procedure, a cystoscope is placed into the bladder through the urethra and permits the doctor to inspect the inside of the urinary bladder if suspicious areas of growth are seen, a biopsy (removing a small piece of tissue) will be taken for further histopathological examinations.

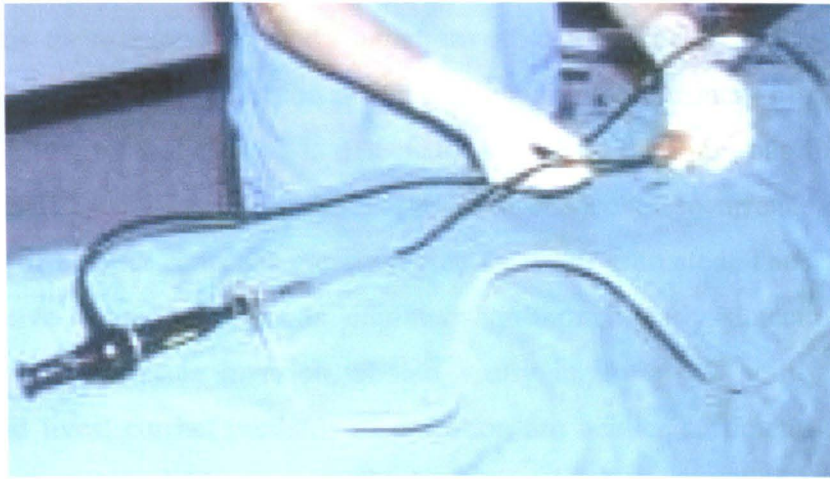


**Figure 1.11 A flexible scope: A useful diagnostic tool for the diagnosis of bladder tumours under local anaesthetic in the out patient department.**

When we use cystoscope to see inside of the bladder, CIS can be seen as a flat lesion (it can be difficult to diagnose) and can not be differentiated from other erythematous potentially benign areas, because it may be a red patch or velvety in appearance but not always visible. Thus a random biopsy and cytological analysis of the urine are required for definitive diagnosis. At present, definitive diagnosis can be made with a biopsy, usually under general anaesthesia, with resultant patient discomfort and morbidity, and relatively high cost. If the flexible type of cystoscope is used, it may not painful and there is no need for a general anaesthetic procedure, but under some circumstances such as taking tissue samples (biopsies), general anaesthesia may be recommended. Therefore, cystoscopy and biopsy remain the gold standard and common urological procedures for bladder abnormalities. In spite of the erythematous areas seen at cystoscopy, several different pathologies can be detected from simple inflammation to flat CIS in which significant pathology may be present in no obviously visible areas of abnormality.

There is another technique, which is optical biopsy in human urologic tissue using optical coherence tomography (Tearney, Brezinski et al. 1997). In this study, they introduced a non-invasive technology that may able to obtain optical biopsies or high-resolution cross-sectional images of the bladder tissue to improve the diagnosis of urinary tract disorders. In their method, they used 1300 nm light to pass through bladder tissue samples, which then reflected off the cell layers of the tissue. The reflection interfered with the original light to show morphological information about the bladder tissue. For *in vivo* work, a fibre optic endoscope was used to place inside the

bladder. This technique is currently under investigation. The weakness of the above methods is a lack of early detection of flat lesions within the urinary bladder. It is clear that the papillary type of tumour is detected more easily than non-papillary carcinoma because the first type can be seen by eye. The chance of recurrence, invasion and progression of bladder cancer is greatly increased if left untreated. Thus, the search for other effective detection methods continues. Although early detection of bladder tumours, prior to muscle invasion, should vastly improve our ability to save both bladders and lives, current methods of detection are neither sufficiently sensitive nor specific (Foresman and Messing 1997). Transitional cell carcinomas are divided into two major groups: Superficial and Muscle-invasive tumours, but most of them are of the superficial type, and approximately 15-20% are muscle-invasive carcinomas with pathologists playing a significant role in diagnosing bladder tumours (Lapham, Ro et al. 1997). The lack of an accepted standard for the histopathological diagnosis of transitional cell Carcinoma *in situ* poses a major problem for multi-institutional studies of this disease (Sharkey and Sarosdy 1997).

In the light of this background, it is possible that electrical impedance spectroscopy may be appropriate for the early detection of flat lesions and assessing bladder pathology. This technique will be detailed in the following chapter. Thus, this thesis considers the introduction of a novel minimally invasive diagnostic technique to detect bladder cancer and other abnormalities of the human urinary bladder. This is because of the potential of the technique to separate pathologic epithelium from normal epithelium as a result of changes in cell size, cell arrangement, and extra-cellular space.

## **1.4 Conclusions**

The epithelial tissues of the bladder are constructed from three different layers (superficial, intermediate and basal layer). These tissues are variable in appearance, depending on whether the bladder is relaxed or distended. The surface cells are the largest and the basal layer cells are the smallest. It is expected that structural parameters such as cell sizes in different layers of the bladder tissue, cell layers, extra and intra cellular spaces, and the relaxed or stretched state of this organ may change the electrical impedance of the urinary bladder tissue. Plaques (on the surface of the relaxed bladder epithelium) would not be expected to change the impedance, whereas tight junctions (between cells of the bladder tissue) will have a significant effect on the electrical

impedance of this organ. CIS is an aggressive form of bladder cancer with a high propensity for invasion if left untreated. These flat lesions cannot be differentiated from other benign areas thus they require biopsy for definitive diagnosis. Any changes in the structural parameters of the malignant bladder tissue, for example Carcinoma *in situ* (CIS) can cause significant electrical impedance changes in the bladder tissue. There are different diagnostic techniques to detect bladder abnormalities such as bladder cancer. However, it is possible that the minimally invasive technique of electrical impedance spectroscopy has a good ability for the early detection of flat lesions (CIS) and other abnormalities of the bladder tissue. Therefore, consideration of morphological changes in the abnormal urinary bladder may suggest alternative diagnostic strategies.

## Chapter 2

# Electrical Impedance Spectroscopy (EIS) and its applications to tissue characterisation: Technical background

## 2.1 Introduction

EIS involves driving electrical currents through electrodes into the body, measurement of the resulting potentials by other electrodes and then calculation of the transfer impedance. Different tissues may have distinguishing characteristics in the shape of the impedance spectrum. The aim of this project is to use the variation in the electrical impedance spectrum of normal and abnormal human bladder tissue (*in vivo* and *ex vivo*) to characterise the tissue. This measurement offers a promising minimally invasive method for the detection of pre-cancerous changes in the bladder. Can we introduce this novel, electrical impedance technique, as a new diagnostic method for the detection of bladder abnormalities? Are there any advantages or disadvantages with this method? Is it possible to apply this technique instead of other techniques in urology sections? The answers to these questions will depend on the evaluation of electrical characteristics of the bladder urothelium and the electrical impedance measurements of the bladder tissue in normal and abnormal states. An attempt will be made to answer these questions in this thesis. Initially the 4-electrode technique is discussed in this chapter.

## 2.2 4-electrode technique

The most common form of measuring tissue impedance is the tetra-polar or 4-electrode technique. This technique can measure transfer impedance (the ratio of measured voltage to applied current) of the urinary bladder. In the tetra-polar technique, a known current is driven between two electrodes and the resulting voltage is measured between the other two electrodes (Figure 2.1). This was used because it is designed to minimise the effect of electrode impedance. The principle is to use a constant current source with infinite output impedance and a voltage-measuring amplifier with infinite input impedance. Because no current flows across the receiving electrodes in the 4-electrode measurement technique, the electrode impedance does not contribute to the measurements and thus the measurement is a true reflection of the tissue transfer impedance. In contrast, in the bi-polar or 2-electrode technique the voltage across each

electrode is measured in addition to the voltage developed across the tissue. Thus this results in the incorrect analysis of the tissue electrical impedance and it is usually impossible to separate the tissue impedance from the electrode impedance, particularly with small electrodes, which have high impedance. Therefore, the 4-electrode technique allows more accurate analysis of the measured electrical impedance than the 2-electrode technique. Both the delivered current and recorded voltage will be supplied using a 4-electrode probe applied to the urothelium of the target bladder tissue. The technique requires that the probe be placed on the surface of the bladder tissue.

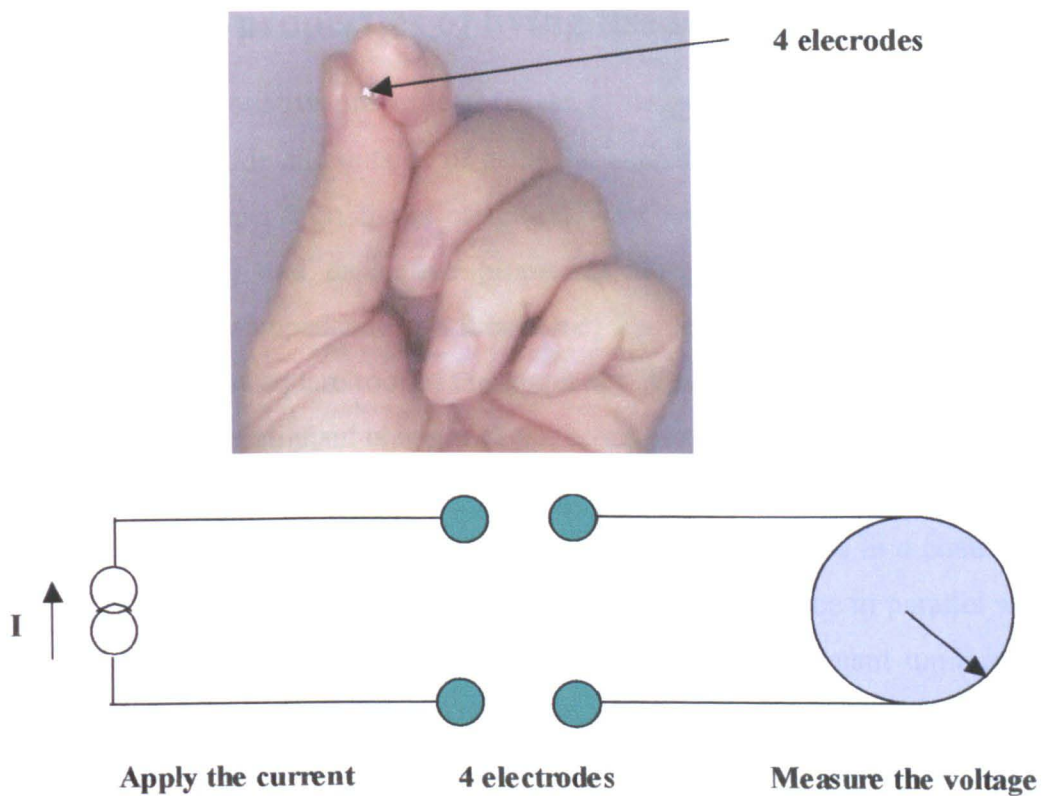


**Figure 2.1 4 Electrodes and their connections to both the current power supply and the voltage measurement system**

The electrical impedance spectroscopy systems that were used in this project are the ‘Mark 3.a Sheffield System’ and ‘Mark 3.5 Sheffield System’ (refer to chapter 3). The electrical impedance spectrum of the bladder tissue obtained by measuring impedance at different frequencies can be used for tissue characterisation. This reflects the physical properties of tissue. Biological tissues have a complex electrical impedance, which is a function of frequency, and their components have resistive and charge storage (capacitance) properties (equations 2.21 and 2.22). The real part of the impedance measurement is used in this work because the signal to noise ratio in this case is more than if the complex or imaginary part is used. Lu et al in 1996 showed that the

simulated imaginary part of the electrical impedance is affected to a greater extent than the real part (Lu, Hamzaoui et al. 1996). Stray capacitance is present between all connecting cables of the probe especially between pairs of drive and receive cables and its effect must be reduced to achieve accurate measurements. Such evidence provides the rationale for studying more about the electrical properties of biological tissue to understand the detection of bladder cancer. For this purpose it will be better to discuss the electrical properties and impedances of living tissue. The following section presents a discussion of the electrical properties of tissue.

## **2.3 Electrical properties of living tissue**

Living tissue has resistive properties because of its materials (nucleus, cell suspensions and cytoplasm) inside and outside of cells and capacitive properties because of the cell membrane (i.e. depend on tissue structure). The resistive properties arise from free charges (i.e. ions) and capacitive properties from bound charges. Philippon M. measured the tissue impedance as a function of frequency and he found that capacitance varied as the inverse square root of the frequency (Philippon 1921). Fricke H. et al first demonstrated that malignant changes of the breast tumour alter the impedance spectrum (Fricke and Morse 1926). They considered certain facts regarding the capacitance of tumour cells (malignant and benign) and placed biological tissue in a conductivity cell and believed that the cellular tissue represented a pure resistance in parallel with a pure capacitance. According to their reports, certain types of malignant tumours had high capacitance in comparison with benign tumours or inactive tissue. They measured tissue resistance and capacitance simultaneously at 20 KHz and reported: "... It will be seen that there is a very satisfactory separation between the tumours classified as malignant and those which are benign". So, according to their study, capacitance not only shows a separation of malignant and benign tumours, but also indicates a relationship between capacitance of the tumour type and the growing rate of the tumour. Schwan (Schwan 1957) published a comprehensive review of the electrical properties of tissues and cell suspensions from 10 Hz to 10 GHz. The biological tissues have complex electrical impedance, which are a function of frequency because of the components included in the tissues. These components have resistive and charge storage properties (Schwan and Kay 1957). Bio-impedance measurements give good information about electrochemical processes in the tissue and can hence be used for characterising the tissue or monitoring physiological changes. These measurements and their frequency dependence differ

greatly between different cell suspensions and tissues. If the physiological status of tissue changes, significant changes in the electrical properties are found, e.g. dry to moist or normal to pathological status. The benefits from impedance measurements in medicine and biology are potentially great and new applications are continuously under investigation and development.

Cole brothers, Kenneth S. Cole (1900-1984) and Robert H. Cole (1914-1990), considered analytical and mathematical treatments of tissue permittivity. Kenneth S. Cole worked with biological systems and cell suspensions but his brother worked with the dielectric properties of non-biological materials. Their common publications (1941) introduced the Cole-Cole dielectric equation that is commonly used in this field (Cole and Cole 1941). Then, Schwan from Pennsylvania University began some of the most important studies in the field of low frequency blood and blood serum conductivity, the conductivity of blood cells, body tissue properties in the ultra high frequency (UHF) frequency range, tissue relaxation and electrode polarisation. He interpreted the frequency dependence of muscle tissue capacitance as relaxation phenomenon. He was the first person to describe the  $\alpha$  dispersion in muscle tissue (1954) and determined the electrical properties of tissue, biological impedances and  $\alpha$ ,  $\beta$  and  $\gamma$  classification. It is usual that researchers characterise the electrical impedance of tissue as  $\alpha$ ,  $\beta$  and  $\gamma$ .

Schwan (1957) published a comprehensive review of the electrical properties of tissues and cell suspensions from 10 Hz to 10 GHz. He introduced the concept that biological tissues have complex electrical impedance, which is a function of frequency because of the components included in the tissues and these components have resistive and charge storage properties (Schwan and Kay 1957). Thus, the values of relative permittivity and conductivity of various tissues were tabulated at four frequencies (Pethig 1987). The publication of electrical properties of tissues and cell suspension by Schwan (1957), from 10 Hz to 10 GHz was a good background for this technique's application on characterisation of body tissues. Technological development, in the field of computer instrumentation, was important to obtaining rapid and exact measurements. Other workers such as Kenneth R. Foster and Herman P. Schwan (1989), Cole (1972), Pethig (1979) published their work in this field (Foster and Schwan 1989), (Cole 1972). The electrical properties of biological materials had begun about 110 years ago as the measurement of electrical resistance and capacitance became possible. The frequency dependence of electrical properties was very important to continue the role of this

technique in the wider area of different applications (Schwan and Kay 1957). The dielectric properties of biological materials provided important roles in characterising normal and cancerous tissues according to their permittivities. Their further studies showed the important effect of water content in tissue measurements and permittivity dependence was explained by the fact that cancer cells have a higher water content and sodium concentration than normal cells (Pethig 1984). The values of relative permittivity and conductivity for various tissues were tabulated at four frequencies (Pethig 1987). Finally, there is a widespread use of the parameters  $\sigma$  (conductivity) and  $\epsilon$  (permittivity) since they more directly relate to the electrical properties of tissue. In this section, different concepts of electrical properties of material will be reviewed:

### 2.3.1 Conductive and displacement currents

Electrical conduction in metallic (conductive) media is the result of the movement of electrons, but in biological tissues the movement of ions constitutes the current. The electrical properties of materials can be explored by passing a current through them, and can be used to characterise the material. When an electrical field is applied, there will be a potential difference of  $V$  between the opposite sides of the material. In tissue, there are resistive properties because of the materials (nucleus, cell suspensions and cytoplasm) inside and outside the cells. In this case, the movement of ions constitute a conduction current ( $I_c = \sigma V$ ).  $\sigma$  is the dielectric conductivity in  $S.m^{-1}$ .

Also, there is capacitive property because of movement of bound charges in the cell membrane (i.e. depending on the tissue structure) and in this case, this current is called the displacement current ( $I_d = \frac{dV}{dt} \epsilon \epsilon_0$ ).  $\epsilon_0 = 8.85 \times 10^{-12} Fm^{-1}$  is the permittivity of the free space and  $\epsilon$  is the relative permittivity (dimensionless). This means that the resistive properties and  $I_c$  arise from free charges (i.e. ions) and capacitive properties and  $I_d$  from bound charges. The first property determines the current density and the latter shows the charge density within the material. The dielectric conductivity and permittivity of the tissue are respectively the current and charge densities. Thus, the field applied to the tissue causes a current, which depends on two important dielectric parameters inside biological tissue. Thus living tissues exhibit simultaneously the properties of a conductor (includes a conductivity) and a dielectric (includes a

permittivity). Both conduction and displacement currents depend on the frequency of

the applied electrical field (Figure 2.2):

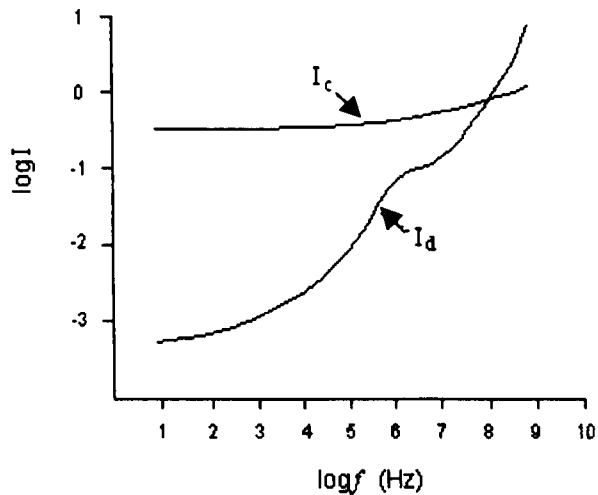


**Figure 2.2 Dependence of conduction and displacement currents on the frequency for a typical living tissue**

In Figure 2.2, it is important to note that the conduction current is very weakly dependent on frequency, but the displacement current exhibits strong frequency dependence. This graph is different for different materials and living tissues. However the living tissue is not pure resistance or capacitance and both conductivity and permittivity vary among different biological tissues.

### 2.3.2 Electrical parameters (Conductivity and Permittivity)

Electrical parameters such as dielectric conductivity ( $\sigma$ ) and permittivity ( $\epsilon$ ) have an important role in the electrical impedance spectrum calculation of the urinary bladder tissue. Also, it is necessary to have the electrical and geometrical parameters of the bladder tissue for the structural modelling procedure. For these purposes, the definitions mentioned in the last section are illustrated by an example with a parallel-plate capacitor (the space between the plates is a vacuum) with plate area  $A$  and separation of  $d$  (Figure 2.3):

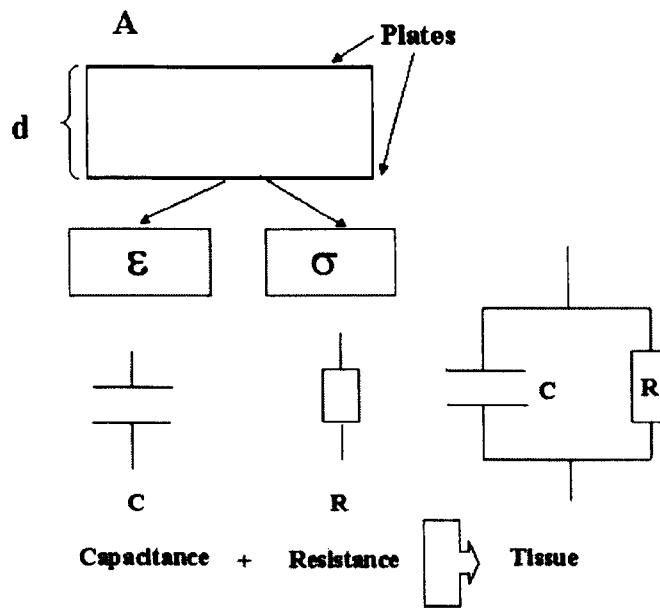


**Figure 2.3 The living tissue as capacitance and resistance equivalent**

A constant voltage difference of  $V$  is applied between the plates in Figure 2.3. The relation between the voltage difference ( $V$ ) and the electrical field ( $E$ ) across the plates is:

$$\vec{E} = \frac{V}{d} \cdot \hat{a}_E \quad (2.1)$$

i.e. where  $\hat{a}_E$  is the unit vector of the electrical field. The charge density  $D$  is:

$$\vec{D} = \epsilon_0 \vec{E} \quad (2.2)$$

Then,

$$D = \epsilon_0 \frac{V}{d} \quad (2.3)$$

The capacitance,  $C$  is:

$$C = \epsilon_0 \frac{A}{d} \quad (2.4)$$

When a material is placed between the two plates, because of material polarization between the plates, the dielectrically polarization charge density ( $\rho_s$ ) will occur inside

the material. The total charge density or displacement vector will be:

$$\vec{D} = \epsilon_0 \vec{E} + \vec{P} = \epsilon_0 \vec{E} + \kappa \epsilon_0 \vec{E} = \epsilon_0 (1 + \kappa) \vec{E} = \epsilon_0 \epsilon \vec{E} \quad (2.5)$$

By definition:  $1 + \kappa = \epsilon$ .  $\epsilon_0 E$  is the charge density of the vacuum,  $P$  is the charge density of the material,  $\kappa$  is the electrical susceptibility and  $\epsilon$  is the static relative permittivity of the material. The static capacitance in the case of a material being placed between two plates, will be:

$$C = \epsilon_0 \epsilon \frac{A}{d} \quad (2.6)$$

The circuit in Figure (2.3) includes a resistance in parallel with the capacitance, as tissue is a 'Leaky' dielectric. We know that the resistance  $R$  is:

$$R = \rho \frac{d}{A} \quad (2.7)$$

$\rho$  is the Resistivity of the material ( $\Omega.m$ ). As a definition, static conductance,  $G = \frac{1}{R}$

and  $\sigma = \frac{1}{\rho}$  is the static Conductivity of the material ( $S.m^{-1}$ ). Thus, the static conductance ( $G$ ) in parallel with the capacitance ( $C$ ) is extracted from the above equation:

$$G = \sigma \frac{A}{d} \quad (2.8)$$

Thus by considering these definitions, the equation (2.7) will be:

$$R = \frac{1}{\sigma} \cdot \frac{d}{A} = \frac{d}{\sigma \cdot A} \quad (2.9)$$

It is clear that when using static capacitance ( $C$ ) and conductance ( $G$ ) for the dielectric, the capacitance and conductance are at a frequency of zero.

If the static conductance ( $G$ ) is zero, the phase angle will be  $\frac{\pi}{2}$  (the current leads the

voltage by  $\frac{\pi}{2}$ ) and we have only a pure capacitance ( $C$ ) in Figure 2.3. Conversely, if the static capacitance ( $C$ ) is zero, the current and voltage will be in phase (phase angle will be zero) and thus we have only pure resistance ( $R$ ). However, in general the total complex admittance  $Y^*$  of a circuit made by a capacitance  $C$  parallel to a conductance  $G$  will be:

$$Y^* = G + j\omega C = \sigma \left(\frac{A}{d}\right) + j\omega \epsilon_0 \epsilon \left(\frac{A}{d}\right) = \left(\frac{A}{d}\right)(\sigma + j\omega \epsilon_0 \epsilon) \quad (2.10)$$

\* indicates a complex variable. For the complex conductivity, it can be assumed that:

$$\sigma^* = \sigma + j\omega \epsilon \epsilon_0$$

Thus,

$$Y^* = \frac{A}{d} \sigma^* \quad (2.11)$$

In the equation (2.10), the ideal capacitance ( $C$ ) has an admittance of  $j\omega C$ . This means that  $G = 0$ , thus we can define the complex capacitance ( $C^*$ ) as:

$$C^* = \frac{Y^*}{j\omega} = \frac{A}{d} \left( \frac{\sigma}{j\omega} + \frac{j\omega \epsilon_0 \epsilon}{j\omega} \right) \quad (2.12)$$

We know that  $j \cdot j = -1$  and if  $C = \epsilon_0 \frac{A}{d}$  is substituted in this equation it will change to:

$$C^* = \frac{Y^*}{j\omega} = \frac{A}{d} \left( -\frac{j\sigma}{\omega} + \epsilon_0 \epsilon \right) = \frac{A}{d} \epsilon_0 \epsilon^* = \epsilon^* C \quad (2.13)$$

This is because the complex capacitance  $G = 0$ . Therefore,  $C^*$  is equal to:  $C^* = \epsilon^* C$

If we choose:

$$\epsilon^* = \epsilon - \frac{j\sigma}{\omega \epsilon_0} \quad (2.14)$$

Then  $\varepsilon = \varepsilon^* + \frac{j\sigma}{\omega\varepsilon_0}$  and put the amount of  $\varepsilon$  in the equation  $\sigma^* = \sigma + j\omega\varepsilon\varepsilon_0$ , the complex conductivity will be:

$$\sigma^* = \sigma + j\omega\varepsilon\varepsilon_0 = \sigma + j\omega\varepsilon_0\left(\varepsilon^* + \frac{j\sigma}{\omega\varepsilon_0}\right) = \sigma + j\omega\varepsilon_0\varepsilon^* - \sigma = j\omega\varepsilon_0\varepsilon^* \quad (2.15)$$

Therefore, there is a relation between the conductivity and permittivity behaviour of the material. It is obviously shown by these equations that as the frequency ( $\omega = 2\pi f$ ) approaches zero, the equation  $\sigma^* = \sigma + j\omega\varepsilon\varepsilon_0$  changes to  $\sigma^* = \sigma$  and this means that the complex conductivity becomes purely real and in the high-frequency limit ( $\infty$ ), the equation  $\varepsilon^* = \varepsilon - \frac{j\sigma}{\omega\varepsilon_0}$  will change into:  $\varepsilon^* = \varepsilon$  and this shows that the complex permittivity becomes purely real. However, it is expected that the conductivity will be dominant at lower frequencies and the permittivity will be dominant at higher frequencies, Figure (2.4). Also, if we consider the effect of both resistance and capacitance in our real dielectric, the complex permittivity is:

$$\varepsilon^* = \varepsilon' - j\varepsilon'' \quad (2.16)$$

Where  $\varepsilon'$  and  $\varepsilon''$  are the real and imaginary parts of the complex permittivity ( $\varepsilon^*$ ) respectively. If we compare equation (2.14) with equation (2.16), the result will be as follows:

$$\varepsilon' = \varepsilon \text{ and } \varepsilon'' = \frac{\sigma}{\omega\varepsilon_0} \text{ or } \left( \varepsilon'' = \frac{\sigma}{2\pi f\varepsilon_0} \text{ because } \omega = 2\pi f \right)$$

The equation (2.16) can be rewritten as:

$$\varepsilon^* = \varepsilon' - j\varepsilon'' = \varepsilon' - j\frac{\sigma}{\omega\varepsilon_0} \quad (2.17)$$

Finally, Cole and Cole (1941) proposed an empirical function (Cole-Cole equation) similar to the equation (2.17). They used this function for all their work (Cole and Cole 1941; Cole and Cole 1942).

$$\varepsilon^* = \varepsilon_\infty - \frac{j\sigma_s}{2\pi f \varepsilon_0} + \frac{(\varepsilon_s - \varepsilon_\infty)}{1 + (j \frac{f}{f_c})^{1-\alpha}} \quad (2.18)$$

$\sigma_s$  is the conductivity at low frequencies,  $\varepsilon_s$  and  $\varepsilon_\infty$  are the limiting permittivity values at lower than  $f_c$  (centre or characteristic frequency) and higher than  $f_c$  respectively.  $\alpha$ , can be chosen to give a good fit to measured data ( $0 < \alpha < 1$ ). The above Cole-Cole equation describes the dielectric dispersion of tissues. For conductivity, we can use the following empirical equation which is similar to the above equation (Foster and Schwan 1989):

$$\sigma^* = \sigma_\infty + j2\pi f \varepsilon_0 \varepsilon_\infty + \frac{\sigma_s - \sigma_\infty}{1 + (-j \frac{f}{f_c})^{1-\alpha}} \quad (2.19)$$

$\sigma_\infty$  will be the tissue conductivity at very high frequencies. The electrical properties of a tissue are determined by a wide variety of behaviours that depends on frequency, polarisation, tissue type, water content, temperature and anisotropy. Much of the variability in tissue dielectric properties may be attributed to its water content. The conductivity of dielectrics is very low ( $< 10^{-10} \text{ Sm}^{-1}$ ) but where metals are the conductors the conductivity is very high ( $> 10^4 \text{ Sm}^{-1}$ ).

### 2.3.3 Dielectric dispersion in biological tissues

In general, the constituents of different biological tissues have similar properties. The variations in transfer impedance spectrum between different tissues are a result of the differing structures of the tissues-variations in intracellular and extracellular volumes, cell shape and size, cell organization. There are three dispersions over a wide range of frequency that must be considered to interpret electrical properties of tissues ( $\alpha$ ,  $\beta$  and  $\gamma$  dispersions). Schwan was the first person to describe the  $\alpha$  dispersion in muscle tissue and determined the electrical properties of tissue, biological impedances and  $\alpha$ ,  $\beta$  and  $\gamma$  classification (Schwan 1955; Foster and Schwan 1989). These dispersion regions can be summarised as follows:

1)  **$\alpha$  Region:**  $\alpha$  dispersion occurs at lower frequencies (a few Hz to a few KHz). This

region is associated with the ionic charges moving over the surface of the cellular membranes and the current can only pass through extra cellular fluids.

**2)  $\beta$  Region:** The  $\beta$  region (a few KHz to several MHz) covers middle frequencies. The current can pass through the tissue due to both an ionic current around the cells and capacitive charging of the membranes. Thus the current can pass through both intra and extra cellular fluids.

**3)  $\gamma$  Region:** This region occurs at higher frequencies (more than 10 MHz) due to the dipolar relaxation of the water molecules in soft tissues.

It is common for researchers to measure the electrical impedance of the tissue in the  $\beta$  range. The main idea behind using the  $\beta$  region by most researchers (including the author) is because changes in tissue structure affect the measured impedance in this region. Thus, most investigators concentrate on this region. The electrical impedance of the bladder tissue in  $\beta$  region is the main purpose of this thesis. Figure 2.4 shows these three dispersion regions.

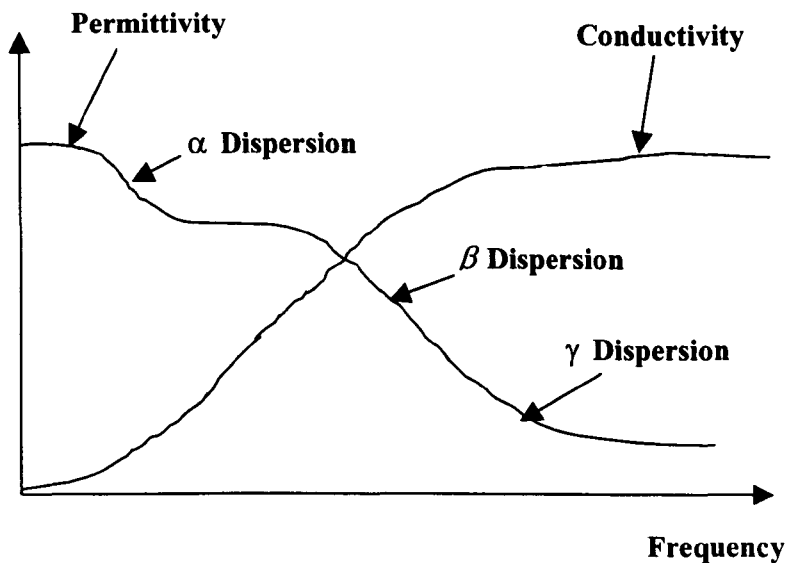


**Figure 2.4 Distribution of permittivity and conductivity of a typical tissue as a function of frequency. Modified from (Pethig and Kell 1987; Foster and Schwan 1989)**

For only one relaxation time constant (single dispersion), an equivalent electrical passive circuit for living tissue can be described by Figure 2.5:

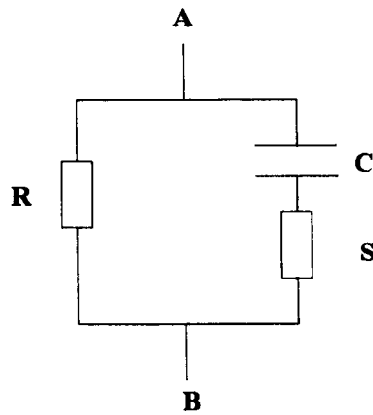


**Figure 2.5 Equivalent electrical circuits for biological tissue**

According to the Figure 2.5,  $S$  represents the intra-cellular resistance,  $C$  represents the membrane capacitance (related to the effect of the cell membrane) and  $R$  represents the extra-cellular resistance. The magnitude of these parameters varies according to tissue type. A better fit to biological data is obtained if  $C$  is a frequency dependent capacitance i.e. a time constant dispersion is introduced.

If a sinusoidal field (alternative voltage) is applied to the material, the resultant dielectric properties, permittivity ( $\epsilon$ ) and conductivity ( $\sigma$ ) will vary with frequency. Gabriel et al reviewed the dielectric properties of tissues in the literature and presented these in a graphical format (Gabriel, Gabriel et al. 1996). They then classified these parameters to be used by other researchers to get more electrical information from biological tissues and organs for further studies.

However, it will be interesting for researchers to gain good information about the electrical activity of normal and abnormal human organs. Also, there is a very important role for dielectric conductivity and permittivity parameters in terms of the structural modelling of every organ or tissue, because for this it is necessary to have the electrical properties and geometrical parameters of that organ or tissue. Thus, a number of dielectric parameters for the urinary bladder will be used in the structural modelling of this organ. Then the electrical impedance spectrum of normal and abnormal urinary bladder will be found by using the information in literature and geometrical parameters that will be found from histological sections manually. In this case, it will be possible to compare the measured impedance spectrum with the impedance spectrum resulting from the modelling procedure. Because this thesis is about bladder characterisation

using electrical impedance, the permittivity and conductivity for the bladder is shown in Figure 2.6. This plot was resulted from a study carried out by Gabriel in 1996. In this work, whole bladder tissue was obtained 24 to 48 hours after death and a conical probe used in conjunction with the impedance analyser. The permittivity and conductivity have been achieved through calculation from impedance measurements in the frequency of 10 Hz to 20 GHz (Gabriel, Gabriel et al. 1996).

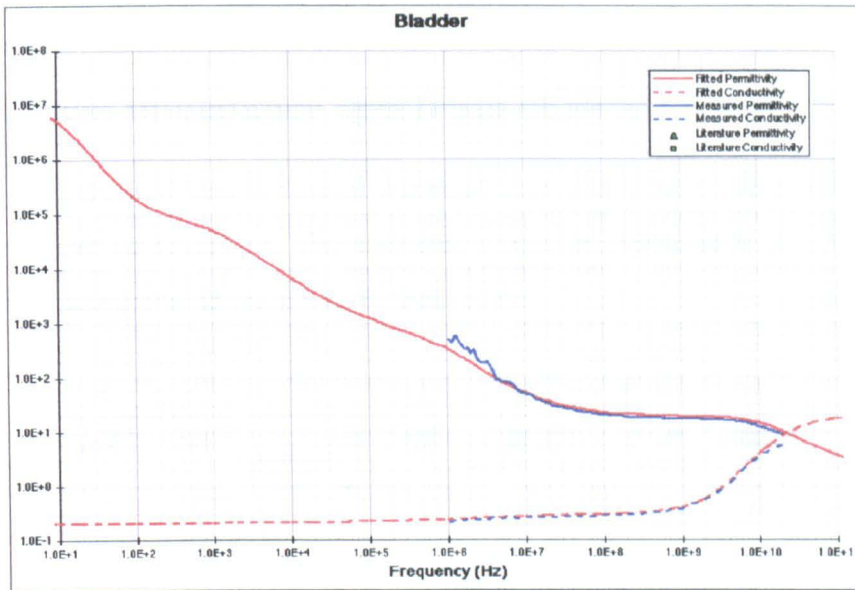


**Figure 2.6 Conductivity in S/m and relative permittivity of the urinary bladder against frequency in Hz (Gabriel, Gabriel et al. 1996).**

### 2.3.4 Effects of physical and physiological changes on tissue dielectric properties

There are different physical and physiological conditions that can have an impact on dielectric properties:

**Physical factors:** The extra-cellular water content of tissue and tissue composition are the physical parameters that have the most influence on tissue dielectric properties. It is expected that the variation of temperature may affect the dielectric properties. Between these factors, tissue water content is the dominant factor that determines tissue dielectric properties.

**Physiological factors:** There is wide range of physiological events or physiological conditions which can alter the dielectric properties of tissues (by altering the extra-

cellular water content). For example, pulmonary oedema greatly increases the dielectric constant and conductivity of lung tissue. In this thesis, different oedema states will be interpreted in terms of water dependent impedance. The other physiological factor is inflammation. Inflamed tissues have more cellular layers than normal tissue and they have the extra cellular space that differs from normal tissue. Thus their conductivity and the electrical impedance may be different from normal tissue. This factor is considered in this work as well as the effect of oedema.

## 2.4 Electrical impedance spectrum of living tissue

Initially it is important that electrical impedance is discussed mathematically and then other aspects can be reviewed. The complex electrical impedance of a leaky dielectric can be written using the equations (2.6) and (2.9):

$$Z^* = R + \frac{1}{j\omega C} = \frac{d}{\sigma A} + \frac{1}{j\omega \epsilon_0 \epsilon \frac{A}{d}} = \frac{d}{\sigma A} + \frac{d}{j\omega \epsilon_0 \epsilon A} = \frac{d}{A} \left( \frac{1}{\sigma} + \frac{1}{j\omega \epsilon_0 \epsilon} \right) \quad (2.20)$$

It is clear from this equation that the complex electrical impedance is frequency dependent.

The complex electrical impedance is usually written as follows:

$$Z^* = R + jX \quad (2.21)$$

$R$  is the real part and  $X$  is the imaginary part of the complex electrical impedance ( $Z^*$ ). It is common that Figure 2.5 describes the equivalent electrical circuit for a cellular medium. The complex electrical impedance of this circuit will be:

$$Z^* = \frac{R(S + \frac{1}{j\omega C})}{R + S + \frac{1}{j\omega C}} = \frac{R.S + \frac{R}{j\omega C}}{\frac{j\omega RC + j\omega SC + 1}{j\omega C}} = \frac{R.j\omega CS + R}{1 + j\omega RC + j\omega SC} = \frac{R + Rj\omega CS}{1 + j\omega C(S + R)}$$

If high frequency currents are applied to the circuit ( $f = \infty$ ), it can be written:

$$R_\infty = \frac{RS}{R + S} \text{ because capacitance } (C) \text{ will be short-circuited. It can also be assumed}$$

that the relaxation time constant of the tissue is  $\tau_c = C(R + S)$  and

$\omega_c = 2\pi f_c = \frac{1}{C(R+S)}$ . If we multiply the term  $Rj\omega CS$  by  $\frac{(R+S)}{(R+S)}$  and add  $R_\infty - R_\infty$  to

the numerator of this equation then the final form of this equation will be as follows:

$$Z^* = \frac{R + Rj\omega CS}{1 + j\omega C(S + R)} = \frac{R + Rj\omega CS \cdot \frac{S + R}{S + R}}{1 + j\omega C(S + R)} = \frac{R + j \frac{\omega}{\omega_c} R_\infty + R_\infty - R_\infty}{1 + j \frac{\omega}{\omega_c}} = \quad (2.22)$$

$$\frac{R_\infty (1 + j \frac{\omega}{\omega_c}) + R - R_\infty}{1 + j \frac{\omega}{\omega_c}} = R_\infty + \frac{R - R_\infty}{1 + j \frac{\omega}{\omega_c}} = R_\infty + \frac{R - R_\infty}{1 + j \frac{f}{f_c}}$$

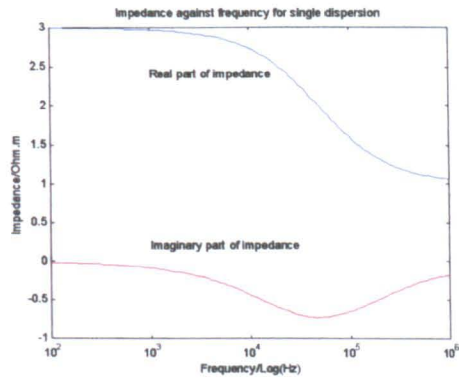
$f_c$  is the characteristic frequency. This is often referred to as the single dispersion Cole equation. For the multi-dispersion Cole equation one can refer to the work carried out by A. R. Waterworth (Waterworth 2000). For complex impedance, an empirical equation similar to but not the same as the equations (2.18) and (2.19), was introduced by (Foster and Schwan 1989):

$$Z^* = R_\infty + \frac{R_s - R_\infty}{1 + (j \frac{f}{f_c})^{1-\alpha}} \quad (2.23)$$

If equations (2.22) and (2.23) are compared to each other, the only difference is  $(1-\alpha)$  in empirical equation (2.23). This was introduced to give a good fit of the measured data with the equation (2.23) for living tissue. Thus  $\alpha$  can be chosen to give a good fit to measured data ( $0 < \alpha < 1$ ). Equation (2.23) generates a continuous dispersion of time constants. Different cells of the body have different time constants ( $\tau = S.C$ ) leading to the dispersion of time constants in tissue. It is important that equations (2.18), (2.19) and (2.22) or (2.23) show a relation among material properties (especially a frequency relation of the electrical impedance). Because this study is interested in measuring the electrical impedance of bladder tissue, the interpretation of the complex impedance equation (2.23), and its application to living tissue will be discussed in the following paragraphs. The real and imaginary part of this complex equation were extracted by several researchers, for example (McAdams and Jossinet 1995). The author simulated real and imaginary parts of  $Z$  against the frequency for the Cole equation and the

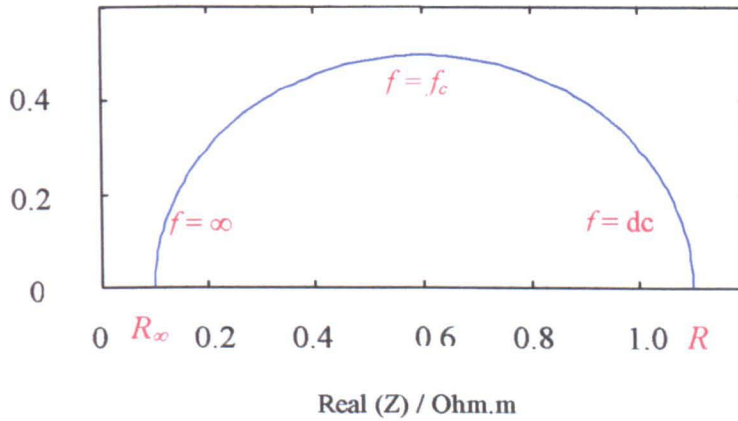
imaginary part against the real part of  $Z$  (Figure 2.7).

It is possible to use double and triple dispersion equations to find a figure similar to Figure 2.4, but in general, it is assumed that the shape of the impedance spectrum is the result of a continuous dispersion of time constants described by the parameter  $\alpha$  in equation 2.23. Figure 2.7 shows the real and imaginary parts of the impedance for  $\alpha = 0$  (i.e. a single time constant). In this case, the centre of the semi circle generated by the real part versus imaginary part plot lies on the real axis. In the more general case, for  $\alpha \neq 0$ , the locus of the semi circle lies below the real axis (the centre of semi circle depends on the value of  $\alpha$ ). The values of  $\alpha, R, S$ , and  $C$  can be found by curve fitting (Figure 2.7c). In Figure 2.7b, the low frequency impedance can be shown by  $R$  (the impedance of extra-cellular fluid), and for the high frequency impedance we can introduce  $R_{\infty}$  (the impedance of both extra-cellular and intra-cellular fluid in parallel). If we move from the lower frequency ( $f = \text{dc}$ ) to the higher frequency ( $f = \infty$ ), the measured real component of the data will decrease and the imaginary component will increase from zero to a maximum value and then it will decrease to zero. This maximum value will occur at a frequency that is called functional or characteristic frequency ( $f_c$ ). Details can be found in the following references: (Cole and Cole 1941; Schwan 1957; Foster and Schwan 1989).

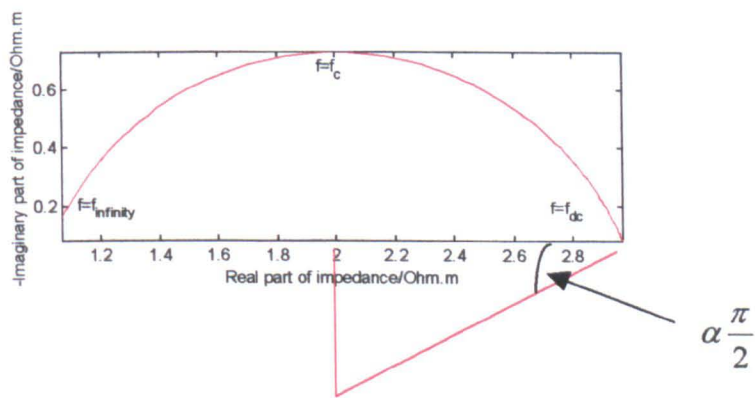


a

$-\text{Imag}(Z) / \text{Ohm.m}$



b



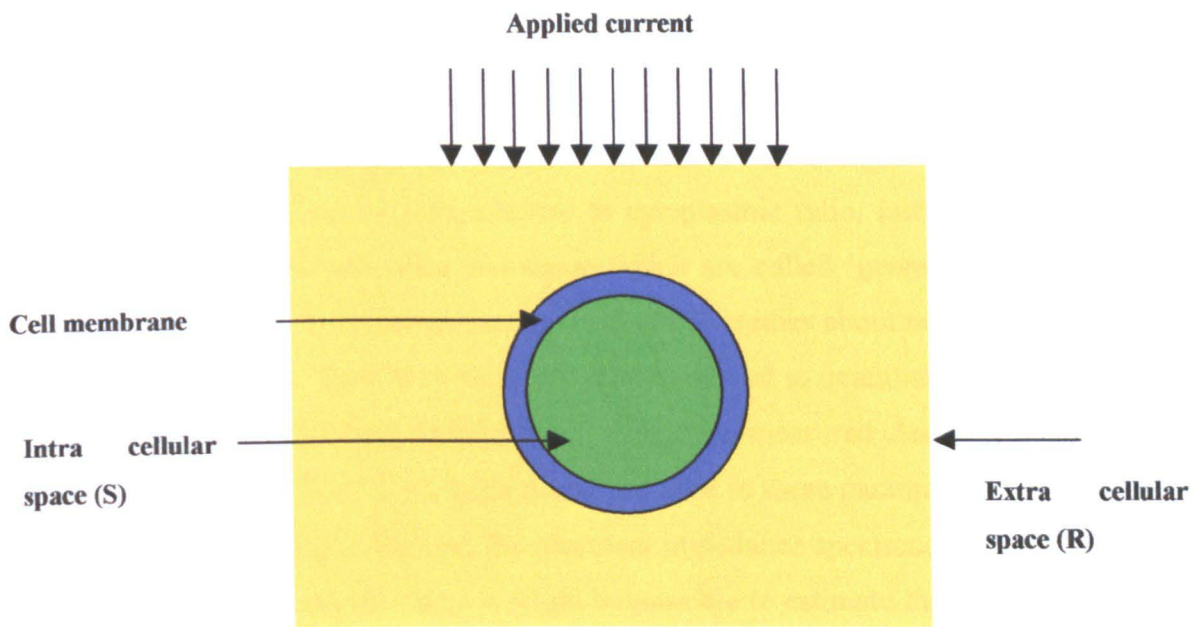
c

**Figure 2.7** Real and imaginary parts of impedance against the frequency for single dispersion (a). A parametric curve shows the imaginary part against the real part of impedance for  $\alpha = 0$  (b) and  $\alpha \neq 0$  (c). Modified from (Cole and Cole 1941).

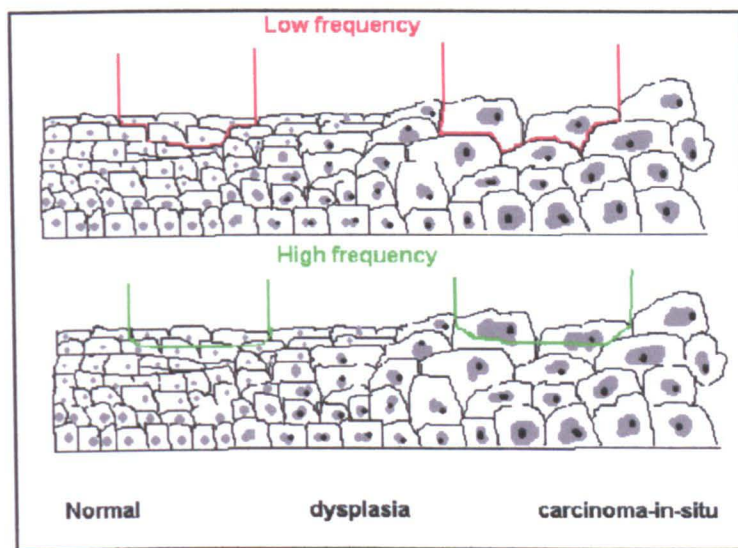
The circuit in Figure 2.5 is considered again to continue the electrical impedance discussions. At low frequencies (below 1 KHz), the current will only go through  $R$  (not through  $S$ ). But with increasing frequency the current passing through the S-C branch increases. If high frequency currents are applied, the currents can pass through the S-C branch because the capacitance of the cell membrane ( $C$ ) is short-circuited and the current can pass through both intra and extra cellular fluids. In this case, the concept of 'impedivity' instead of 'resistivity' is useful. The former is an AC equivalent of 'resistivity' (in DC). Therefore, the resistivity between points A and B varies as a function of applied current frequencies.

The characteristic frequency ( $f_c$ ) is different for every tissue and it is expected that it will be different in normal and abnormal tissues. However, if we consider real body tissue, it is expected that current will pass around the cell in the extra-cellular space (at low frequencies) (Figure 2.8, a and b). Furthermore, at high frequencies the current can pass through the cell membranes (the current can pass through both intra and extra cellular fluids). In fact, differences are at low frequencies because of (a) change in extra-cellular space and (b) loss of tight junctions. Also, at high frequencies (where structure can be ignored), malignant and non-malignant tissues have comparable impedance. The impedivity of a tissue depends on its biophysical parameters such as the amount, shape and orientation of cells, and ionic concentrations of extra and intra cellular space and cytoplasm.

The important matter that must be considered is that the electrical impedance drops with an increase in frequency (Foster and Schwan 1989; Brown, Smallwood et al. 1999). The living tissue cells are surrounded by and contain aqueous electrolytes that can conduct an applied current according to the current type, frequency, duration, and amplitude. This current conduction is a function of tissue liquids. When the tissue is changing from normal to abnormal (especially cancer), the distribution of tissue liquids (water) between intra and extra cellular space will change and so the measured conductivity and impedivity will also change at low frequencies. There is a significant change in the electrical properties when cells or tissues go from one physiological state to another, for example, normal to pathological. Therefore, knowing the absolute value or the range of typical values of impedance for different tissues in different states (normal or abnormal) will be very important. This important effect is the main concern of this work.



a



b

**Figure 2.8** The electrical current passes through the normal and abnormal living tissue (in low and high frequencies). Red and green lines represent the current path through the normal and abnormal living tissue.

## **2.5 Morphological parameters of normal and pathological tissue**

A literature review of the morphological parameters of normal and abnormal tissue will be presented in this section. The main reason behind this background is to discuss the size, shape and number of cells, nuclear to cytoplasmic ratio, intra and extra cellular spaces of the normal and abnormal tissue which are called 'geometrical parameters'. Although there have been many qualitative research studies about normal and abnormal cellular morphology, there have been few reports related to quantitative studies of these parameters. These structural parameters determine the measured electrical impedance of any living tissue. If there is any significant variation in these parameters in pathological conditions of the urinary bladder, the electrical impedance spectroscopy may be able to characterise these changes. Thus, it might be possible to estimate the structural changes in tissue according to the measured impedance spectrum. As stated earlier, these parameters will also be needed to model the structure of the urinary bladder tissue using finite element analysis in order to validate the measured electrical impedance. There are several historical studies (Schwan (1941); Geddes and Baker (1967) ) which provide useful information about the pathological status of the human body by measuring the bio impedance of different tissue types (Geddes and Baker 1967). Sugar, in 1968, carried out an electron microscopic study of the early invasive growth of human skin tumours and laryngeal carcinoma and reported an increase in the extra-cellular space of these tumours. This may be due to the loss of cellular cohesion (Sugar 1968). According to Sugar's report, the extra-cellular spaces in inflammation also increase but this increase is significantly less than in cancerous tissues.

In 1984, White et al investigated epithelial dysplasia by quantifying the volume of the intera-cellular space in normal and carcinogen treated hamster cheek-pouch epithelium. They found that there was a significant increase in extra-cellular space in cancerous tissue (White and Gohari 1984). They reported that extra-cellular space in dysplastic tissue (characterised by abnormality of development; alteration in size, shape and organization of cells) was approximately six times the volume of normal tissue. Extra-cellular space increased as dysplasia developed. Brown et al (2000) used the electrical impedance method to develop a screening technique for the detection of cervical precancers. If this were successfully applied in clinics, the doors would be opened for further practical studies related to other human organs. According to their results,

measurements made of normal squamous tissues were very different from those made of precancerous tissues. Brown et al believed that characteristics of the electrical impedance spectra of tissues could be explained by changes in cell arrangements (layering) and in the size of the nuclei. This relation suggests the possibility of deriving tissue structure from electrical impedance spectral measurements (Brown, Tidy et al. 2000). It is expected that one can develop their study for use with other organs. Finally in 2002, Walker et al applied a finite element modelling method to the structure of normal and precancerous cervical squamous epithelium. This work was developed from the previously mentioned study. In order to develop this, it was first necessary to find the mean values of a number of morphological tissue parameters such as: cell size and shape distribution, nuclear to cytoplasmic ratio and volume of extra-cellular space. They used image analysis of normal and pathological tissue sections to find these parameters (Walker, Brown et al. 2003). Walker et al modelled the electrical impedance of normal and pre-malignant cervical tissue using finite element analysis (Walker, Brown et al. 2000; Walker, Brown et al. 2002). They concluded that their finite element model could predict differences in electrical transfer impedance between normal and cancerous tissues as well as real measurements. Therefore, both modelling results and impedance measurements show that there was a significant change of impedance in malignant and normal tissues. Following this, the detection of impedance changes in the bladder tissue using finite element analysis would be possible. More discussion will be presented in Chapter 7 of this thesis.

### **2.5.1 Morphological parameters of normal bladder tissue**

Important morphological or geometrical parameters, such as the size, shape, changes of cell density with depth, nuclear to cytoplasmic ratio, intra and extra cellular spaces can be measured manually using pathological sections from normal and abnormal bladder tissue (see section 7.3). On the other hand, it is possible to find some of these parameters in literature, as reported in previous studies of the normal bladder: Walker in 1959, described three layers of transitional epithelium in the relaxed urinary bladder of mice (Walker 1959). However, cell sizes are independent of species, but number of cells in the tissue depends on size of animal. He described these layers as: a distal layer of very large surface cells, an intermediate layer of medium sized cells and a basal layer of small cells but without any quantitative values for the cell sizes. Another study, by Martin in 1972, also evaluated the bladder epithelium. In his study on the guinea-pig

bladder, he concluded that there are essentially three layers of cells in this relaxed epithelium: a layer of small basal cells; a middle or intermediate layer of pyriform cells, which vary in size and height with long cytoplasm; and a layer of surface cells which are large in size and often bi or multi-nucleate. Also, he found that during distension of the bladder, the stretched epithelium retains essentially three layers. The surface cells become flattened and thus increase their surface area, whilst the underlying cells become not only flattened but are displaced sideways and lie parallel to the basement membrane)(Martin 1972). Minsky and Chlapowski in 1978 reported that during bladder expansion, the surface cells change from a goblet shape to a flattened squamous shape (Minsky and Chlapowski 1978). There is a study from Ward et al (1986) that demonstrated that small cells of the basal layer of the human bladder epithelium are cuboidal and rounded with little cytoplasm. The intermediate cells (pyramidal cells) are larger, while big, single or multi-nucleated cells lie in the superficial layer of normal human urothelium (Ward, Stewart et al. 1986). All of the above mentioned references have no numerical measures. Lewis et al have improved the morphological study of normal bladder epithelium. According to their study, the rabbit urinary bladder in relaxed state has three layers, as has been reported before, but they also noted that the size of basal layer cells was approximately  $15 \mu\text{m}$ . The intermediate layer of cells had  $30 \mu\text{m}$  diameter and the superficial cells had a length of  $60\text{-}120 \mu\text{m}$  and a height of  $5\text{-}10 \mu\text{m}$ . Polygonal plaques of  $12 \text{ nm}$  thicknesses covered the apical membrane of the superficial cells occupying approximately 73% of the apical surface area, the remaining 27% being normal lipid bilayers (Lewis and Hanrahan 1990).

Finally, Lewis in 2000 introduced more evidence derived from a morphological study of normal mouse bladder epithelium. According to this study, the basal layer is germinal in nature with cells of a diameter of  $5\text{-}10 \mu\text{m}$ , and the intermediate cells of  $20 \mu\text{m}$ . The superficial umbrella-like cells are hexagonal, and depending on the degree of bladder stretch, range from  $50\text{-}120 \mu\text{m}$  in length (see Figure 2.9). The polygonal shaped plaques are approximately  $0.5 \mu\text{m}$  in diameter,  $12 \text{ nm}$  in thickness and occupy 70-90% of the apical surface area. Also, the superficial umbrella cells are joined together by tight junctions composed of four to six interconnecting strands and these junctions offer a physical barrier to the movement of substances between urine and blood (Lewis 2000).

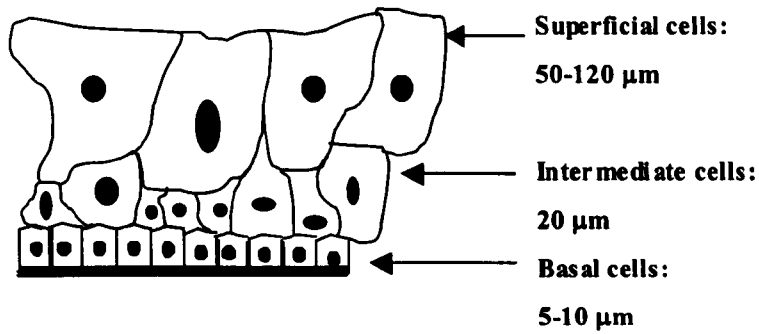


**Figure 2.9** The structure of the normal urinary bladder tissue. Modified from (Lewis and Hanrahan 1990)

### **2.5.2 Estimation of expected changes in morphological parameters of bladder tissue with pathology**

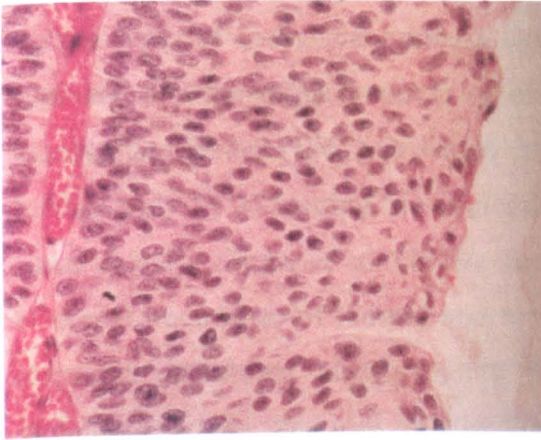
Evidence of pathology related changes in morphological parameters of the urinary bladder from the literature are discussed in this section. In carcinoma *in situ*, atypia (deviation from the normal case) and hyperplasia (abnormal increase in the number of cells in normal arrangement) in the bladder tissue is common. In these cases, a major change associated with precancerous and cancerous development in the tissue is an increase in the nuclear volume, which may be due to water absorption in pathologic conditions. There is usually no quantitative discussion of cell sizes in literature. However, cellular scale modelling by Walker et al has shown that changes in the nuclear volume has little effect on the impedance spectrum at nuclear volumes less than about 80% of the cell volume, as a result of the high conductivity of the nuclear membrane (Walker 2001). The cells shown in Figure 2.10b (TCC grade 2) are abnormally large and contain large and irregular nuclei with deeply stained, coarse chromatin. Lesions may vary considerably in overall cell size, nuclear size and configuration. Also, there may be an increase of mitotic activity (Utz and Farrow 1984). Moreover, this may alter the cell size distribution and therefore, the resulting impedance spectrum.

Carcinoma *in situ* is generally defined as a total replacement of the urothelial surface by cells which bear morphologic features of carcinoma, but which lack architectural alteration other than an increase in the number of cell layers, i.e., a flat lesion (Farrow

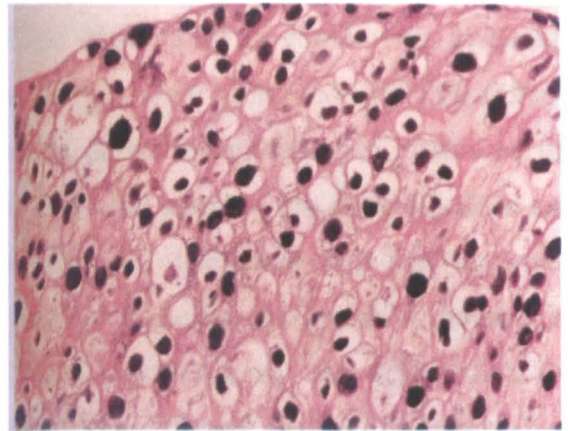
1992). Therefore, we would expect this to alter the impedance spectrum. In Transitional Cell Carcinoma (TCC), the most distinctive features are the spindle, pyramidal cell shapes and eccentric nuclei. Tumour cells are arranged in a tight cluster and show hyperchromatic nuclei and abnormal nucleocytoplasmic ratio (Ackerman 1981). Cytological appearance of TCC of the urinary bladder is shown as Figure 2.10. It is clear from Figure 2.10a that in grade 1 TCC, there are more than eight layers of urothelial cells with minimal nuclear abnormalities, well-preserved polarity of the cells and umbrella cells. Except for eccentric placement of the nucleus in some cells, these cells are indistinguishable from benign epithelium. Thus, it is not expected to be able to detect grade 1. But in Figure 2.10b, in grade 2 TCC, an increase of the number of cells and nuclear hyperchromasia, and a disturbance in polarity is seen. Also, significant nuclear crowding and overlapping are present. Finally, Figure 2.10c, grade 3 TCC, shows a considerable disturbed polarity, increased cell number and nuclear pleomorphism. Nuclear abnormalities include irregularity, coarse chromatin, enlarged nucleoli, hyperchromasia, mitoses and increased nuclear to cytoplasmic ratio (Farrow, Utz et al. 1976; Ro, Staerkel et al. 1992; Sonny and Samuel 1996). Therefore, we would expect these to change the impedance spectrum.

The limited quantitative data available in the literature for bladder cell sizes and other geometrical parameters such as extra-cellular space does not provide a scientific basis to construct accurate structural models of normal and malignant bladder tissue. However, this data can provide a reasonable estimation of expected morphological parameter changes of bladder tissue with pathology. The fact that there are clear morphological changes related to pathology suggests that the electrical impedance spectroscopy technique will be able to detect such changes in the urinary bladder tissue.

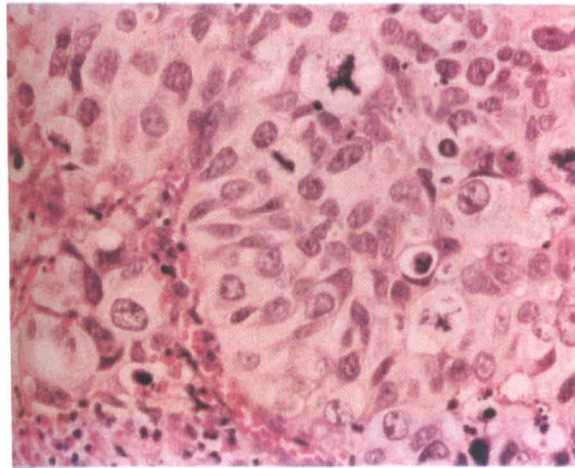
A detailed study of the bladder tissue specimens in the form of pathological sections will be required to obtain more accurate quantitative geometrical parameters for the bladder structural modelling procedure. These geometrical parameters resulting from both literature and measuring of the histological sections by the author are demonstrated in Tables 7.3 and 7.4 respectively. These data are related to normal and malignant bladder tissue for the latter study, however, only geometrical parameters for normal bladder tissue was obtained from the literature search.



**a: (magnification of 300)**



**b:(magnification of 400)**



**c:(magnification of 400)**

**Figure 2.10 Cytological appearance of TCC of the bladder. a) Transitional cell carcinoma, grade 1 b) Transitional cell carcinoma, grade 2 c) Transitional cell carcinoma, grade 3 (Sonny and Samuel 1996), Modified from Anderson's Pathology.**

## **2.6 Electrical impedance changes of malignant tissue and a new approach for detecting bladder cancer using EIS**

First of all, the historical developments of EIS to characterise different tissues will be reviewed. Fricke H. et al in 1926 first demonstrated that pathological tissue changes alter the impedance spectrum (Fricke and Morse 1926). They considered certain facts regarding the capacitance and resistivity of tumours (malignant and benign) at 20 KHz. Thus, they introduced the possibility of separating malignant tissue from benign, using measurements of the electrical properties of the tissue. According to their results,

certain types of malignant tumours have a high capacitance in comparison to benign tumours, and numerous tumours of different tissues were measured. Schwan (1941), Geddes and Baker (1967) provided information about the pathological status of the human body by measuring bio impedance of different parts of the body (Geddes and Baker 1967). Singh et al (1979) found significant differences between measured electrical impedance of normal and tumour tissues of the human breast. A number of electrical impedance measurements were taken using biopsy and resected tissue samples, and then they took *in vivo* measurements of different parts of human bodies. The most significant results were obtained from female breasts, some of which contained tumours (there are different plots showing different spectra of normal and abnormal breast tissue resistivities at 100 Hz-100 MHz). They suggested that useful clinical information about a breast tumour might be obtained using this technique and it was intended to continue this clinical evaluation (Singh, Smith et al. 1979). Ackmann and Seitz (1984) introduced complex electrical impedance measurements in biologic tissue and these measurements have been used to monitor a variety of physiological events (Ackmann and Seitz 1984).

Avis et al (1996) performed a pilot study to obtain basic information on the *in vitro* electrical impedance of the cervix at different frequencies and their aim was to produce a non-invasive cervical screening test (Avis, Lindow et al. 1996). Blad and Baldetorp (1996) used the 4-electrode technique at frequencies from 1.5 kHz to 700 kHz. They took several measurements to find the real and imaginary components of impedance, and the characteristic frequency of normal and tumour tissue of the human arm (*in vivo*) and mouse muscles (*ex vivo*). The characteristic frequency of tumour tissue (100 KHz) was higher than for normal tissue (20 KHz). Their results show that this method can be extended to a new application for the detection of tumour tissue using the electrical impedance technique (Blad and Baldetorp 1996). Jossinet and Lavandier in 1998 measured the impedance of the breast at 12 discrete frequencies from 488 Hz to 1 MHz. It is known that breast tissue is composed of both epithelial (lobules and ducts) and connective structures (adipocytes, fibroblasts, nervous and vascular structures). The measured spectra were sorted into three groups of normal, mammary gland, connective and adipose tissues, and three groups of pathological tissue-mastopathy, fibroadenoma and carcinoma. The low-frequency-limit resistivity and characteristic frequencies were calculated from the experimental data. No significant difference between groups of

normal tissue and benign pathology (mammary gland, mastopathy and fibro adenoma) was found. The carcinoma group differed from all the other groups at frequencies above 125 KHz. These results indicate that impedance spectroscopy is appropriate for the detection of breast cancer (Jossinet 1998). The measured electrical impedance by Jossinet and Lavandier (1998) shows a significant difference of impedance between breast carcinoma and the connective tissues of the breast freshly excised (Jossinet and Lavandier 1998). In their work, they plotted the imaginary part of the electrical impedance against the real part. They used the Kolmogorov-Smirnov statistical test (Press, Teukolsky et al. 1992) and correlation computations in the characterisation process.

Chauveau et al (1999) measured the bio impedance (real and imaginary components) in normal and cancerous female breast tissues with a 4-electrode technique (*ex vivo*). They used 10 KHz-10 MHz and reported that the electrical properties of normal tissue, surrounding tissue and carcinoma are significantly different and the shape of the impedance plots is different in the case of cancerous tissues. Thus, the electrical behaviour of mammary tissue could be used to develop a non-invasive technique for early breast cancer detection (Chauveau, Hamzaoui et al. 1999). This concurs with another study about breast tissue classification and breast cancer detection by electrical impedance spectroscopy. This study was done by Esterela da Silva et al (2000) as a minimally invasive technique (Da Silva, Desa et al. 2000). They used frequencies ranging from 488 Hz to 1 MHz and they showed that the plots of carcinoma tissues are significantly different to the plots of connective tissues (real components against imaginary components). The measured real component for carcinoma tissue was around 300-450  $\Omega$  and for connective tissue was more than 500  $\Omega$ .

Another study concerns the relation between tissue structures and imposed electrical flow in cervical neoplasia by Brown et al (2000). They took impedance measurements with a pencil probe with four gold electrodes at eight frequencies between 4.8 KHz and 614 KHz. They compared the normal and abnormal cervical tissues in terms of their extra-cellular resistance, intra-cellular resistance and cell membrane capacitance with each other. The final results show a significant separation between normal and abnormal cervical tissue. Therefore, their study showed the potential of this technique as a method for detecting pre-cancerous changes in the cervix (Brown, Tidy et al. 2000).

Another study investigated virtual biopsies in Barrett's Oesophagus using electrical impedance measurements with the multi frequency 4-electrode technique (Gonzales-Correa, Brown et al. 1999). The aim of their study was to show the possibility of differentiating two types of epithelia (squamous and columnar) in terms of their electrical impedances. Their measured data is as follows:

	9.6 KHz	19.2 KHz	138.4 KHz	76.8 KHz	153.6 KHz
<b>Squamous Median</b>	16.25	11.99	8.62	6.23	4.38
<b>Columnar Median</b>	4.12	3.99	3.74	3.39	3.14

**Table 2.1 *In vivo* electrical resistivity ( $\Omega.m$ ) measurements in the human oesophagus**

	9.6 KHz	19.2 KHz	138.4 KHz	76.8 KHz	153.6 KHz
<b>Squamous Median</b>	14.77	8.82	6.66	4.93	3.77
<b>Columnar Median</b>	5.35	4.91	4.63	4.41	3.63

**Table 2.2 *In vitro* electrical resistivity ( $\Omega.m$ ) measurements in the human oesophagus**

They applied this technique of electrical impedance spectroscopy in the Department of Medical Physics and Engineering at Sheffield University. In their work, 'Mk3.a Sheffield System', 7 different frequencies were used. According to their study, the electrical impedance method distinguishes significantly the squamous and columnar tissues of the oesophagus but there are some limitations to their work, such as the limitation of applied frequency and the effects of inflammation and oedema in their measured data. They have considered the inflammation effects on Barrett's oesophagus using low frequency (Gonzales-Correa, Brown et al. 2003). The final study that may be mentioned in this section is about the prostate tissue characterisation using this minimally invasive technique. Lee et al in 1999 used the electrical impedance measurements (frequencies ranging from 100 KHz to 4 MHz) to detect prostate cancer (Lee, Roberts et al. 1999). They used the 2-electrode technique, using probes constructed from two stainless steel needles. According to the published results, a cancerous prostate was found to have higher impedance than a normal prostate. The prostate cancer was found to have higher impedance ( $932 \pm 170 \Omega$ ) with the non-cancerous area of the same prostate having lower impedance ( $751 \pm 151 \Omega$ ) at 2 MHz

( $p < 0.0001$ ). They believed that bio impedance could potentially guide needle placement during prostate biopsy and thus improve sampling of tumours. Effects of inflammation and oedema of prostate tissues in their impedance measurements may limit their work. The 2-electrode technique also introduces additional limitations. It is known that the bipolar electrical impedance measurements of the tissue can be affected by electrode impedance (see section 3.2.1.2). The advantage of the mentioned studies is the presentation of a minimally invasive technique to characterise different tissues in the human body using electrical impedance measurements. However, they used a limited frequency range in their study, thus the characterisation of tissue would be poor.

## **2.7 Feasibility of the existing EIS equipment and methods to distinguish the normal and abnormal bladder tissue**

It has been proposed that electrical impedance spectroscopy can detect non-papillary carcinoma, carcinoma *in situ* (CIS) and other forms of urinary bladder malignancy. It is clear that the papillary types of tumours are easier to detect than non-papillary carcinoma, possibly because papillary tumours are often superficially invasive and visible (using the different methods in section 1.3). In this study, two impedance spectroscopy systems have been used to characterise the bladder urothelium. Keshtkar et al (2001) performed a study based on virtual bladder biopsy by bio-impedance measurements using the Mk3.a Sheffield System. A distinction between benign and malignant bladder tissues was found (Keshtkar, Smallwood et al. 2001). Other changes that might be useful in the detection of bladder abnormalities include tissue inflammation and oedema because of the number of cells in the tissue and water content respectively. If the number of cells in the tissue increases, the measured impedivity of the tissue increases. On the other hand, if the water content of the tissue increases, the related impedivity decreases (Smallwood, Keshtkar et al. 2002).

A second paper arising from this thesis is about electrical impedance spectroscopy and the diagnosis of bladder pathology (Wilkinson, Smallwood et al. 2002). A significant difference ( $p < 0.05$  at seven frequencies between 9.6 and 614 KHz) was found between normal and malignant urothelium. The equipment was found to have some disadvantages- limited frequency range (9.6 KHz – 614 KHz); the time required to choose and changing the gain selector of the system for every measurement; and the

calculation of impedivity using manual calibration factors for every measured data in impedance calculation procedure. A new system was therefore used to measure the electrical impedances over a wide range of frequencies (2 KHz-1.5 MHz), Mk3.5 Sheffield System. This system was further improved in order to measure the impedance at frequencies lower than 2 KHz (62.5 Hz-1.5 MHz) because it was believed that a better separation of malignant tissues from the benign type would be achieved using lower frequencies.

For the *in vivo* measurements in this thesis, a very small size probe (total diameter of 2 mm) was designed to go down through the endoscope into the urinary bladder. It was a technical challenge to find a suitable probe small enough to go through the endoscope and contact the human bladder urothelium.

An additional constraint is that there is little available time with which to take measurements since the surgeons do not want to have their surgery interrupted. In addition, the measurement procedure requires the taking of several impedance data measurements from one point of tissue, which is then averaged, and this is the impetus for improved impedance measurement equipment that can acquire more data in a second. It will be interesting to see if necessary improvements can produce a non-invasive, safe, rapid, and reproducible technique that has potential in clinical practice.

## **2.8 Conclusions**

The most common form of the application of the electrical impedance measurement technique, to characterise living tissue accurately, is the 4-electrode technique. This technique can minimise the effect of electrode impedance on the real measurement of tissue impedance, hence the transfer impedance of the urinary bladder can be measured in this work. Also, the real part of the complex impedance measurement is used in this work because the Signal to Noise Ratio (SNR) in this case is more than if the complex or imaginary part is used. It is important to study more about the electrical properties of biological tissue to understand the detection of bladder cancer using the electrical impedance spectroscopy technique. For this purpose, a discussion of electrical properties and impedances of living tissue was introduced. Conductive and displacement currents; electrical parameters (conductivity and permittivity) were

explained in detail when an electrical field is applied to the tissue. Living tissues including cells have small differences in electrical properties between each other thus three dispersions over a wide range of frequency were considered to interpret the electrical properties of tissues ( $\alpha$ ,  $\beta$  and  $\gamma$  dispersions). Also, it is common for researchers to measure the electrical impedance of the tissue in the  $\beta$  region. The main idea behind using this region is because of the tissue structure changes in this range. Thus measurement of the electrical impedance of the bladder tissue in this region is the main purpose of this thesis.

The electrical impedance spectrum of living tissue was explained mathematically to find its complex impedance, and then an empirical equation (Cole equation) was introduced similar to the calculated equation to fit the measured data in this equation. The electrical impedance drops with an increase in frequency which is important in the impedance spectroscopy field thus it was discussed in this chapter. Finally, if we consider real body tissue it is expected that current will pass around the cell in the extra cellular space at low frequencies and both extra and intra cellular space at high frequencies. This will affect electrical impedances related to different applied frequencies especially in normal and abnormal tissues (dependent on tissue morphology).

The morphological parameters of normal and abnormal tissue in general and for the urinary bladder were presented in this chapter. The main reason behind this background was to discuss the size, shape and number of cells, nuclear to cytoplasmic ratio, intra and extra cellular spaces of the normal and abnormal tissue (geometrical parameters). It is expected that these structural parameters are responsible for the amount of measured electrical impedance of any living tissue.

There are different investigations about the electrical impedance changes of malignant tissue in literature, such as cervix, breast, oesophagus and prostate using electrical impedance measurements. It has been proposed that electrical impedance spectroscopy as a minimally invasive technique can detect non-papillary carcinoma, carcinoma *in situ* and other forms of urinary bladder malignancy. It is clear that the papillary types of tumours are easier to detect than non-papillary carcinoma, possibly because papillary tumours are often superficially invasive and visible. Any significant variation in these parameters in pathological conditions of living tissue, the urinary bladder, can affect electrical impedance. Therefore, an estimation of the structural changes in cancerous

tissue causes alterations in the measured impedance, so it can be expected that the electrical impedance spectroscopy technique can be introduced to characterise the bladder urothelium. Therefore, the relationship between bladder tissue morphology and electrical impedance spectra in terms of a feasibility study is important. In addition, these parameters will be needed to model the structure of the urinary bladder tissue (in normal and abnormal cases) using finite element analysis to compare with the measured electrical impedance in this work. Therefore, in the light of these findings, it is possible that the bio impedance technique may represent a non-invasive, safe, rapid, and reproducible technique in clinical practice to characterise the urinary bladder tissue

# **Chapter 3**

## **Equipment**

### **3.1 Introduction**

This chapter will describe the equipment used for measuring the impedance spectrum.

### **3.2 Existing equipment and development of experimental protocol**

#### **3.2.1 Probe development**

##### **3.2.1.1 Introduction**

Existing probes are usually larger in diameter than that required for bladder EIS work and thus were not suitable for taking electrical impedance measurements of the urinary bladder (*in vivo*). Therefore, it was decided to design and construct a suitable probe for this work, thus different methods were used to construct, treat and perform safety tests on the probe. The applied current in the probe used in this study is high impedance and a very low sinusoidal ( $10\ \mu A$ ) alternating current. The main reason for the low current application is the safety regulation and to avoid saturating the receiver amplifier circuits; therefore the software for the measurement system determines this current. Using a low current and high frequency alternating current can minimise the risk of tissue stimulation. Tissue stimulation decreases with increasing frequency (Geddes and Baker 1989). In using the electrical impedance method (*in vivo*), the applied current must not stimulate or heat the tissues recognising the fact that the muscles such as nerve fibres, sensory receptors and body fluids all form part of the current circuit. Thus, the sinusoidal alternating current applied to the bladder tissue must be designed not to stimulate excitable tissues or cause any damage to the body. This section discusses probe construction, treatment and tests that have been effective and have the acceptable characteristics for this study. The calibration process of the probe to prepare for electrical impedance measurements will be introduced later. Initially, parameters such as 'Electrode impedance', 'Probe sensitivity' and 'Contact polarisation of probes' are discussed. These parameters must be considered at the time of probe design and construction to apply to the urinary bladder tissue in this work.

### 3.2.1.2 Electrode impedance

Before any electrical impedance can be measured, electrodes or a probe must be put in contact with the body tissue. These electrodes play the transducer role in terms of the conversion of ionic flow of currents (in the body) into an electronic current (in the wire). The electrical impedance probe is constructed from electrodes in a rectangular grid. If one uses a 2-electrode technique and puts these electrodes on the surface of living tissue, these will generate an electrical potential. For simplicity, a homogenous and semi-infinite medium is assumed to discuss the electrode impedance mathematically. It is clear that the resultant data will be a little different from the real media in the urinary bladder tissue (Figure 3.1):

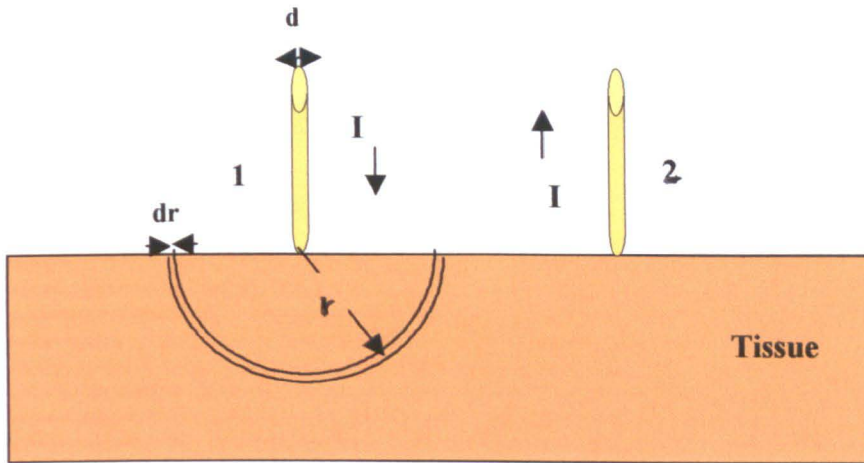


**Figure 3.1 2-electrodes in contact with tissue (tissue is assumed to be both homogenous and semi-infinite in extent,  $r \gg d$ ). Modified from (Brown, Smallwood et al. 1999)**

The relationship between the Electric field ( $\vec{E}$ ) and produced Electrical potential ( $\varphi$ ) can be written as follows:

$$\vec{E} = -\nabla\varphi \quad (3.1)$$

$\nabla$  is the gradient operator. We know from Ohm's law that:

$$\vec{J} = \sigma\vec{E} \quad (3.2)$$

$\vec{J}$  is the Current density and  $\sigma$  is the Conductivity of the homogenous region. Thus, if the equation (3.2) is substituted by equation (3.1), it can be written as follows:

$\frac{\vec{J}}{\sigma} = -\nabla\varphi \Rightarrow \vec{J} = -\sigma\nabla\varphi$ . The Current source density ( $\vec{I}_v$ ) is the divergence of  $\vec{J}$ , thus

$\nabla \vec{J} = \vec{I}_v = -\sigma \nabla^2 \phi$  and finally:

$$\nabla^2 \phi = -\frac{\vec{I}_v}{\sigma} \quad (3.3)$$

This equation is called Poisson's equation. For a single current source ( $i_v$ ), the potential will be:

$$\phi = \frac{1}{4\pi\sigma} \int \frac{i_v}{r} dV \quad (3.4)$$

The current in Figure 3.1 will spread out radially and the current density is  $\frac{I}{2\pi r^2}$ . Also the potential drop ( $dV$ ) across a thin hemispherical shell of thickness  $dr$  is:  $dV = \frac{i\rho}{2\pi r^2} .dr$ ,  $\rho$  is the resistivity of the tissue. Thus, if the potential at infinity is zero, the potential at radius  $r$  is equal to:

$$V(r) = i \int_r^\infty \frac{\rho}{2\pi r^2} dr = \frac{\rho i}{2\pi r} \quad (3.5)$$

It is known that a hemisphere and finite area ( $a$ ) of an electrode is:

$$a = 2\pi r^2 \Rightarrow r = \sqrt{\frac{a}{2\pi}}, r \text{ is the electrode radius. Therefore, } V = \frac{\rho i}{\sqrt{2\pi a}} \text{ or:}$$

$$\text{Electrode impedance} = \frac{\rho}{\sqrt{2\pi a}} \quad (3.6)$$

This is usually called the Spreading resistance (Brown, Smallwood et al. 1999). 4-electrodes are used in a similar way, with a uniform spacing 'a' along the x axis (Figure 3.2a). The potential difference between points 'a' and '2a', (V23) is being considered. For this purpose, an element of length  $\Delta x$  and cross-sectional area  $\Delta s$  with resistivity of  $\rho$  between the two electrodes is assumed. This element has a resistance of

$$\Delta R = \rho \frac{\Delta x}{\Delta s} \text{ and the potential difference across this element due to the current of}$$

$$\text{electrode 1 is: } \Delta V = \frac{I\Delta s}{2\pi x^2} \rho \frac{\Delta x}{\Delta s} \text{ because the current density along the line of the}$$

electrodes (X) for two current sources is given by: Current density =  $\frac{I}{2\pi x^2}$  and  $\frac{I}{2\pi(x-3a)^2}$

Therefore,

$$V_{2-3} | \text{Electrode1} = \frac{\rho I}{2\pi} \int_a^{2a} \frac{dx}{x^2} = \frac{\rho I}{4\pi a}$$

The potential difference between points 2 and 3, due to the current from electrode 4, will be the same as the above equation because the system is symmetrical and we assumed a semi-infinite uniform isotropic medium. Thus,

$$V_{2-3} | \text{Electrode4} = \frac{\rho I}{4\pi a}$$

Finally, the total is  $V_{2-3} = \frac{\rho I}{4\pi a} + \frac{\rho I}{4\pi a} = \frac{\rho I}{2\pi a}$  and thus the transfer impedance between

electrodes 2 and 3 is  $\frac{\rho}{2\pi a}$ . In these equations,  $\rho$  is the tissue resistivity and  $a$  is the area of the electrode in contact with tissue. In fact, in the 4-electrode technique, high output impedance current source is applied into the tissue and so this current is independent of load impedance and thus it seems to be a voltmeter with infinite input impedance between measurement electrodes because there is no voltage drop across electrodes as a perfect voltmeter draws no current (see Figure 3.2b). Therefore, in the 4-electrode technique, no current flows across the receive electrodes thus the electrode impedance does not contribute to the real measurements of the tissue (the applied current,  $I$  pass through the tissue transfer impedance,  $R_1, R_2, R_3$ ). Thus, the measured voltage across the receive electrodes is  $V = IR_2$ . Resistors,  $R$  in this figure represent the contact impedance of the electrodes and are higher than the real impedance of the tissue. Contact impedance of the electrodes using the Mk3.a (imaging system) is about  $\frac{2v}{2mA} = 1K\Omega$  and this will be  $\frac{5v}{10\mu A} = 500K\Omega$  using the Mk3.5 (spectroscopy system)

(personal communication with Dr. P. Milnes).

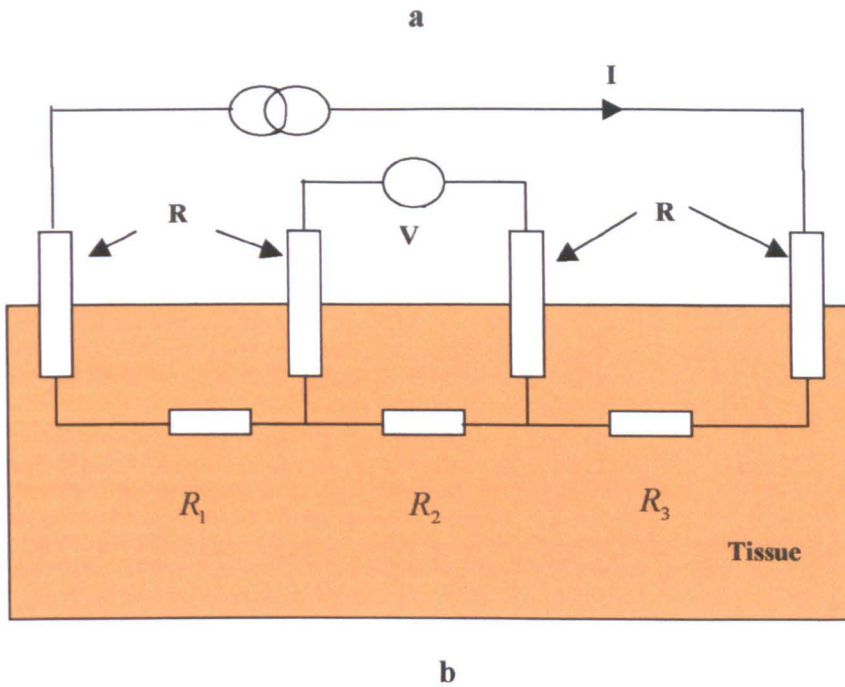
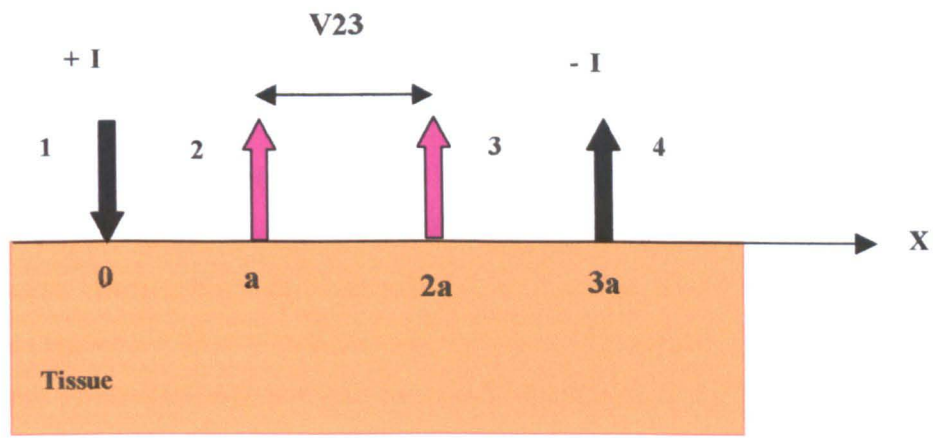


**Figure 3.2 a) 4-electrodes in contact with living tissue (tissue is assumed to be both homogenous and semi-infinite in extent). b) 4-electrodes are in contact with living tissue and are demonstrating  $R_1, R_2, R_3$  as tissue impedances,  $R$  as electrode contact impedance and  $V$  as a perfect voltmeter. Modified from (Brown, Smallwood et al. 1999).**

Therefore, most researchers are interested in using the 4-electrode technique in their electrical impedance measurements, thus the author has used this technique in this thesis. Furthermore, to minimize the effect of ‘electrode impedance’ on real electrical impedance measurements it is preferred that the area of electrodes in contact ( $a$ ) is chosen to be as large as possible due to the above mentioned electrode impedance equation (equation 3.6). Also, a rectangular arrangement of electrodes has been used in this thesis rather than planar (see Figure 3.2), because it was limited by the space available through the endoscope to go down into the urinary bladder (2 mm total

diameter). Therefore, the best electrodes arrangement in this case is rectangular and the total probe diameter (including 4 electrodes) was chosen to be only 2 mm (each electrode diameter is 0.5 mm and the edge to edge distance of electrodes is only 0.2 mm). Finally, according to above-mentioned paragraphs, this small diameter of the probe will cause increased contact impedance which has a detrimental affect on measurements. However, this is unavoidable because the probe must have a small enough diameter (2 mm) to enter the bladder via an endoscope.

### 3.2.1.3 Probe sensitivity distribution

Another probe parameter, which is important in designing the electrical impedance measurement probe, is the sensitivity distribution of the probe which determines the response of the system to local changes in tissue impedance. If we consider the circuit of Figure 3.2b, it will be easy to consider the sensitivity distribution. In this figure, if  $R_2$  increases,  $V$  increases and vice versa. Also, if  $R_1$  or  $R_3$  increases,  $V$  decreases and vice versa. Thus, the central region has positive and the sides have negative sensitivities (the volume represented by  $R_2$  has a positive sensitivity and this will be negative sensitivity for the volumes represented by  $R_1$  and  $R_3$ ). The probe sensitivity distribution is a description of a pattern of the current distribution in medium (the bladder tissue in this work). For example, this parameter for a planar array of electrodes is a function of the distances between electrodes and it decreases with penetration depth (in uniform medium) (Powell, Barber et al. 1987). The uniform or isotropic medium, as a definition, is a medium that different electrical parameters are constant everywhere. Therefore, increasing the separation of the current drive electrodes will give increased current penetration. The electrode separation is a trade-off amongst depth penetration, resolution and signal-to-noise ratio (SNR), and different arrangements of the electrodes will alter the trade-off (Bertemes-Filho 2002; Jones 2003). Increasing drive electrode separation will give deeper penetration but lower current density therefore lower SNR; increasing measurement electrode separation will give deeper detection and higher voltage (therefore high SNR) but decrease the resolution. Maximum averaged sensitivity occurs at a depth equal to 1/3 of the distance between two current injection electrodes in uniform medium (but in a non-uniform medium such as in living tissue, it is necessary to calculate the sensitivity distribution). In principle, we can optimise our probe sizes to gain a good sensitivity (Brown, Wilson et al. 2000) where it is required.

In the case of a probe to be passed through the cystoscope, the design is constrained by the orifice size and the need to maximize electrode area in order to reduce contact impedance. Brown et al used an isotropic medium to calculate the sensitivity but there are other studies that calculate the sensitivity in cellular media (non-uniform) using computational modelling because the sensitivity in this case depends on the medium morphology. In cellular medium the electrical spectra are extremely sensitive to the values of material properties thus sensitivity depends on morphology and can only be interpreted from computational modelling (Walker, Brown et al. 2002). One of the computational modelling results for the sensitivity of the urinary bladder is shown in the Figure 3.3 as follow (see Chapter 7 for modelling details):

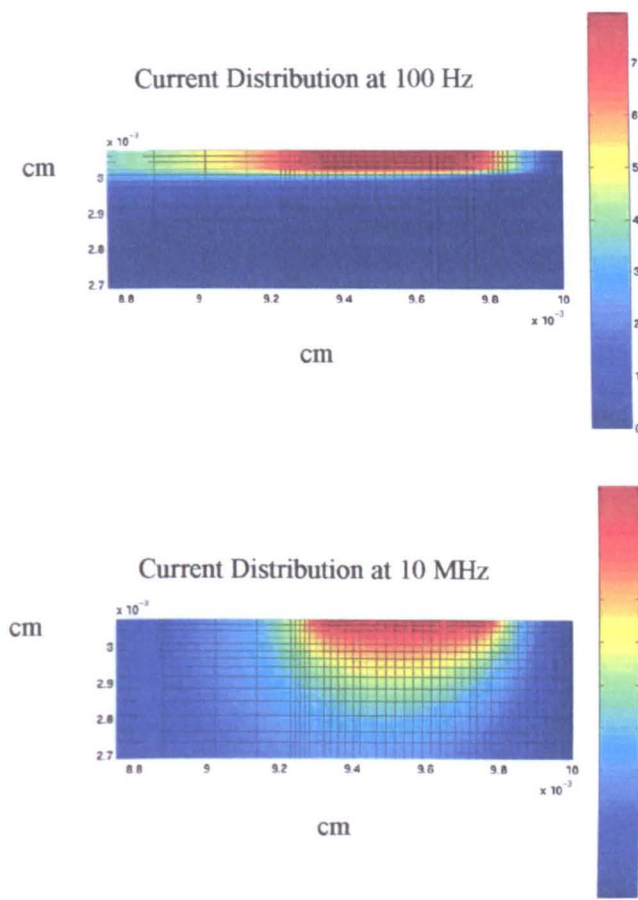


**Figure 3.3 Computational modelling (Finite element analysis) results for the current sensitivity distribution of the urinary bladder with  $30 \mu\text{m}$  thickness of mucosa (a combined study by the author and Dr. D. C. Walker)**

The calculated distribution of the sensitivity by Gonzales-Correa et al in 1999 showed

that about 90% of electrical impedance information in a uniform medium comes from a depth of 0.8 mm tissue using 4-electrode technique with 0.8 mm diameter electrodes and with an edge-to-edge distance of 1 mm between electrodes (Gonzales-Correa, Brown et al. 1999).

The electrode size (0.5 mm in diameter) and the edge-to-edge distance of 0.2 mm for the probe used in this study, would give a depth sensitivity of about 0.5 mm. Thus, the author used histopathologist's reports of biopsies of the bladder tissue (*in vivo* and *ex vivo*) over a depth range of 0.5 mm to compare these reports with the measured impedance data to distinguish the malignant and non-malignant bladder tissues. The probe measures average properties of a small number of cells. For example, the distance between two measuring electrodes plus the whole of the electrodes' size used in this work is about 1.5 mm (1500  $\mu\text{m}$ ). The biggest cell in the superficial layer of the bladder is about 100  $\mu\text{m}$  (depending on the degree of bladder stretch, range from 50-120  $\mu\text{m}$ ) (Lewis 2000). Thus, if this probe is placed on the surface of the urinary bladder tissue, the approximate number of occupied cells under these electrodes is 15 cells.

#### **3.2.1.4 Contact polarisation of probes**

If direct current (dc) is used, electrodes will be polarised and cause problems in bio-impedance measurements because of potential changes across the electrodes. It means that positive charges are produced at one drive electrode and negative charges in other drive electrode. These charges produce a potential difference across these electrodes because of the electrical field between two opposite charges in two electrodes. Charge carriers, ions within the living tissue and the electrons within the electrodes (such as metallic electrodes) have irreversible changes. For further explanation, according to Brown et al 1999, when metal electrodes are used, contact polarisation potentials will result from the fact that ions will diffuse into and out of the metal and these are actually noise sources in electrical impedance measurements because the measured data (potential differences) can be affected by these potentials.

Thus, it is usual that researchers use gold in electrodes as it greatly reduces chemical reactions between the probe and the electrolytes in the tissue. It eliminates oxidation of the metallic surface of probes and helps to establish good contact between tissue and probe. On the other hand, if a direct current (dc) passes through the electrodes, it will make small changes in electrode potentials (electrode polarisation). A very high input

impedance amplifier in measurement system (in data acquisition system) will minimise this effect because this effect is the result of direct current passing through the electrodes. Also, a good design of electrodes can reduce the effect of polarisation such as choosing chemically inert metals (Geddes 1972; Brown, Smallwood et al. 1999).

Finally according to the bad effect of contact polarisation of probe in measured impedance data, it must be minimised. In this project, gold electrodes were used because they are considered as chemically inert.

### **3.2.1.5 Probe construction, development and safety testing**

The probe used to measure the cervical tissue was 5.5 mm diameter (Brown, Tidy et al. 2000) and the probe used in the oesophagus was 3.2 mm diameter (Gonzales-Correa 2000). The design, construction, development and mechanical assembly of a smaller size probe (2 mm diameter) including 4 gold electrodes to use 4-electrode technique in the bladder tissue are the main purpose of this section. This process is very important because the injection of electrical current into the urinary bladder, *in vivo*, and taking impedance measurements, needs a very small size probe. The maximum permitted diameter of the probe is 2 mm in order to pass through the endoscope to measure the impedance inside the urinary bladder. In terms of tip designing process, the circular shape of the tip, instead of the planar shape, made the smallest configuration for the probe and thus this shape was chosen. Initially the sub-miniature coaxial cables were ordered from a UK based company (Axon Mini Coaxial Cable). The diameter of the cable core (inner conductor of the cable) is 0.15 mm and the total diameter of each cable is 0.72 mm and it is very flexible. The dimensions of cable parts, structure and its electrical characteristics are shown in Appendix (1). Subsequently, the factory was asked to fit 4 coaxial cables (PCX 36 K 08 O/D 0.5mm) inside a medical grade Polytetraflouroethylene (PTFE) tube with an outer diameter of 2 mm. This tube was used in this study because it can hold cables and electrodes closer, and has a good compatibility with biological media. The PTFE tube is flexible and has the ability to be wiped clean, and allows the probe to be passed through the biopsy channel of a cystoscope into the urinary bladder. The advantage of the cystoscope is its ability to see the measurement site inside the bladder. There are different steps in constructing this probe as follows: A small size plastic tip, 2 mm in diameter and 3.5 mm in depth was formed from black glass filled with nylon with 4 holes (about 0.5 mm diameters) to take

gold electrodes. See Appendix (2). A probe treatment process was used to fix the tip inside the PTFE tube and seal the junction area of tip and this tube to reduce mechanical shock and liquid leakage from the bladder into the probe. The ‘vacuum plasma’ method was used to remove fluorine atoms from the tube structure, which gives effective adhesion between the dental composite around the electrode connections and the cables at the end of the probe. This process is very important for protection against penetration or leakage of liquids from both sides of the tip. The whole tube is coiled to a diameter of about 10-15 cm during the plasma process. Cling film was wrapped around the PTFE tube to prevent fluorine atoms escaping from the other area of the tube (only about 2 cm of each tube end was exposed to the plasma process to remove fluorine atoms). The tube was placed inside a glass tube including argon gas at low pressure of  $2.5 \times 10^{-2}$  mbar (Figure 3.4), and treated in ‘argon plasma’ for 15 minutes at the power of 10 watts electrical field (plasma system power). High-speed electrons are produced by the electrical field and collide with argon atoms to produce ions. These ions collide with PTFE atoms then release fluorine, leaving free radicals. After the process, when the tube was exposed to the atmosphere outside of the system, oxygen atoms take the place of the fluorine immediately. Thus this treated area will be rough and there can be an effective adhesion between the dental composite, tube and tip. Figure 3.4 shows this process.

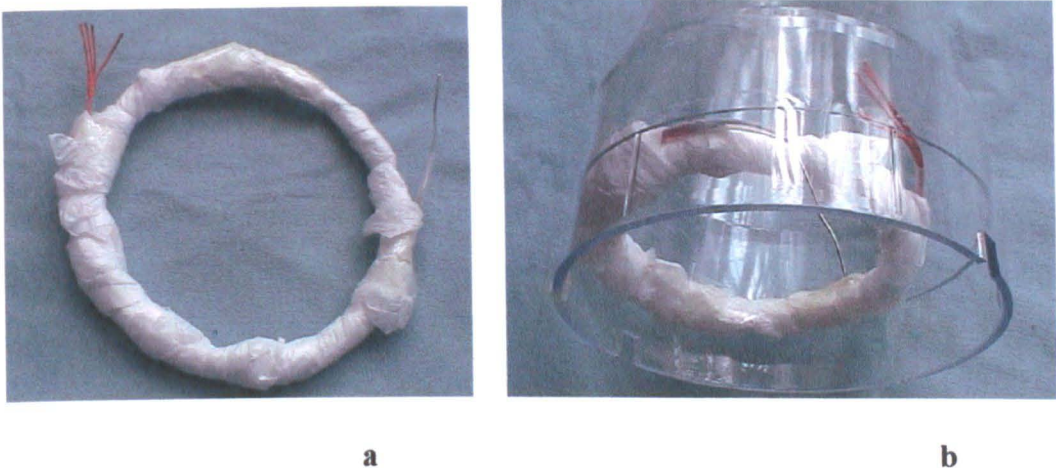


**Figure 3.4 a) PTFE tube was coiled to a diameter of about 10-15 cm (Cling film was wrapped around this tube except 2 cm of each tube end). b) PTFE tube was placed inside a vacuum plasma tube.**

After this treatment process, electrodes were cut in shape of rods (diameter 0.5 mm,

length 0.75 mm) from gold wire then fitted inside the tip holes. The outer jacket and screen of each sub-miniature coaxial cable stripped and removed 2 mm by a wire stripper (Abisollerer verstellbar, wire stripper adjustable, 0.25-0.80 mm). Then the core (0.15 mm in diameter) of the cable was inserted into the small hole of the tip (Figure 3.5) and it was soldered (a microscope aided the examination of the details of the work because the core of the cable and the electrode sizes are very small and thus need magnifying to look at the soldering process). Finally the tip and cables were carefully pulled back into the PTFE tube. The probe structure including 4 gold electrodes, tip, cables and PTFE is shown in Figure 3.5. The length of the assembly of probe is 60 *cm* for *ex vivo* work and 90 *cm* for *in vivo* studies. It is clear from the figure that one end of every electrode must contact the tissue and the other end must be soldered by cable for further connection to the measurement system. The connection of the probe to the multi-frequency single channel electrical impedance spectroscopy (Mk 3.a or Mk 3.5 Sheffield Systems) is a 9way connector as shown in Appendix (3).

Another probe treatment method was tried to get a fix and stabilise the probe to prevent any liquid leakage from the probe. Dental composite and ultraviolet radiation was used to fix the cables that are fitted into the PTFE tube. A drop of dental composite (Scotchbond multipurpose dental adhesive) added to the junction area of the tip (among gold electrodes, holes, cables and tube) to give a waterproof sealing in the tube using ultraviolet to gain sufficient sealing (Figure 3.6). The ultraviolet system was De Trey Dentsply, model EuroMax, (Canada). The ultraviolet exposure time to the composite site was about 1 minute on each side of the probe. This process maximised the strength of adhesive bond on the tube and composite joint area because of the removing of fluorine atoms (Caiazzo, Canonico et al. 1996). This adhesive effect can cause the best results by using vacuum plasma process thus the author used these two treatment methods together. The other face of the probe (made of 4 gold electrodes inside the tape and PTFE) must contact the bladder tissue lightly for electrical impedance measurements (Figure 3.7).

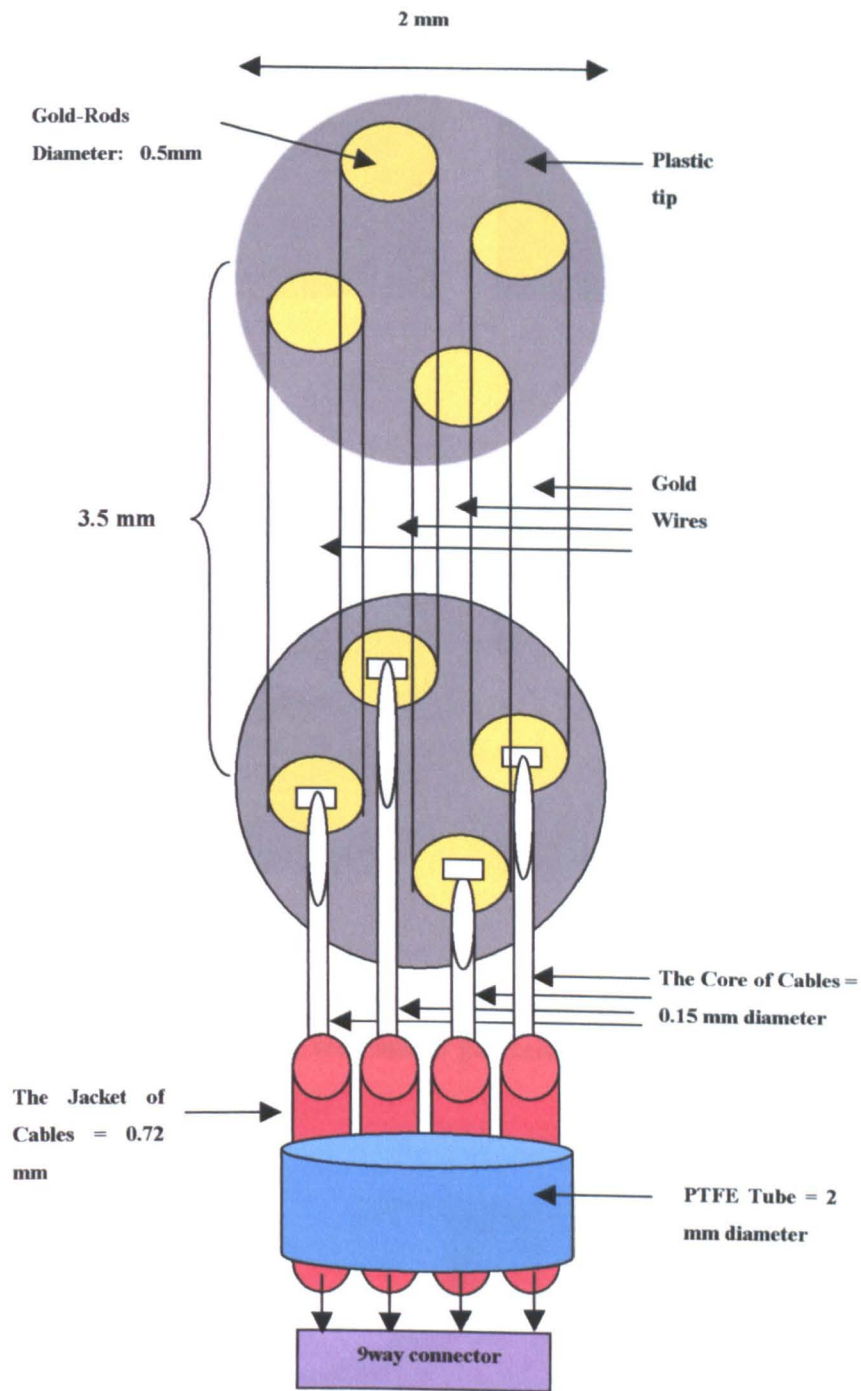


Figure 3.5 Probe structure



a



b



c

**Figure 3.6 Treatment of probe with ultraviolet: a) UV Source b) Equipment to treat the probe c) The probe treatment processing**

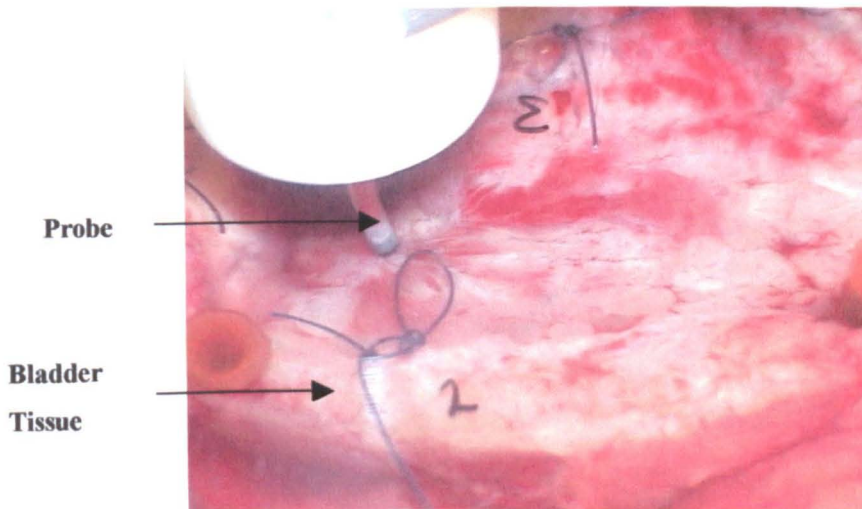


**Figure 3.7 Connection of the probe to the bladder tissue (*ex vivo*)**

Finally, a leak test was carried out to ensure that there is no leakage or penetration of liquids such as blood and other body fluids into the holes of the probe and this is important if fluid leakage is to be avoided. This treatment process was completed using air pressure. The author placed the constructed probe (the face or upper end of the probe including tip and electrodes) into a small tank of water then a positive pressure of air was applied to the other end of the probe (lower end of the probe). No bubbles in the water must be seen in this process (Figure 3.8). In the case of the existence of any hole along tip or tube, air bubbles can be expected to come out from the tube and these will be seen in the water. There was not any bubble in probes used in this study.

In the case of the second leakage test, the probe was placed into a specific fluorescent liquid (Martindale fluorescent; 1 gram in 5 ml, diluted in 5 ml water) about 30 seconds. Then the author applied a negative pressure on the other end (lower end) of the probe using a pump for about 1 minute (Figure 3.9). The surface of the probe was cleaned. After taking a fluorescent photograph, it was proved that whole surface of the film was black (no white area). Thus, it was interpreted that there had been no liquid penetration into the tip or tube from the fluorescent liquid. Therefore, it was proved that all of the probes used in this work were sealed and can be used safely in electrical impedance measurements of the body.

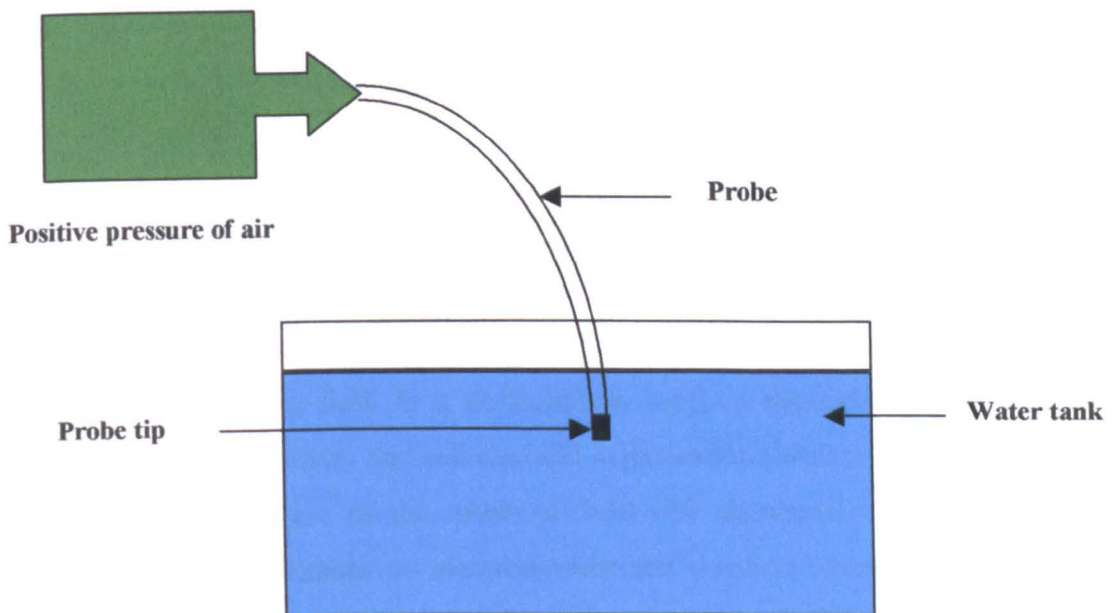


**Figure 3.8** Liquid leakage test of the probe using water and positive air pressure

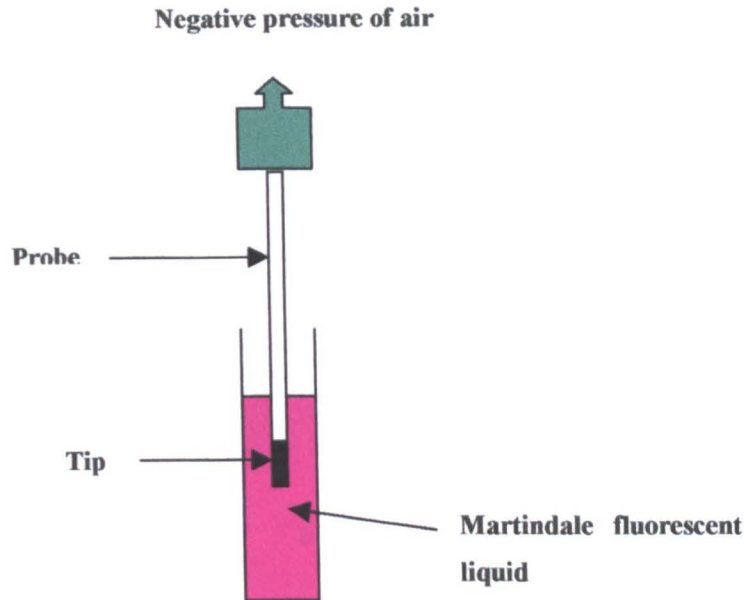
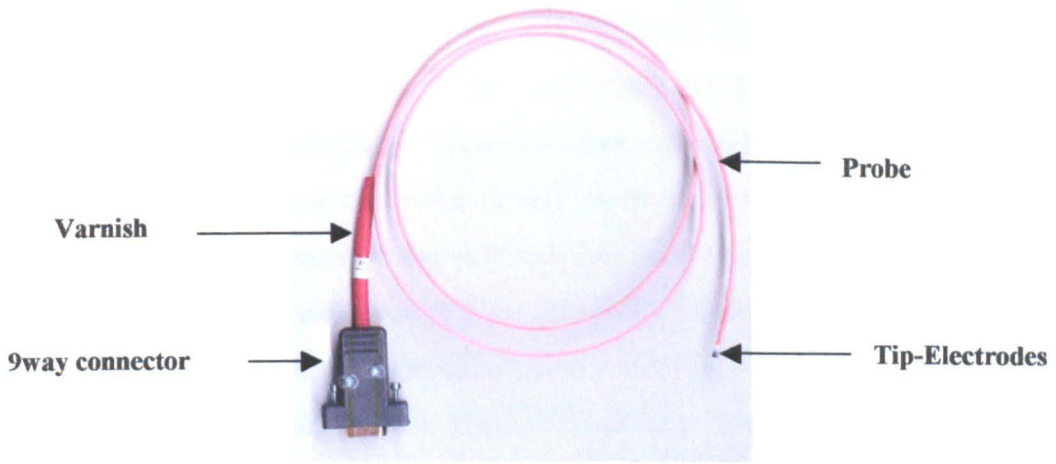


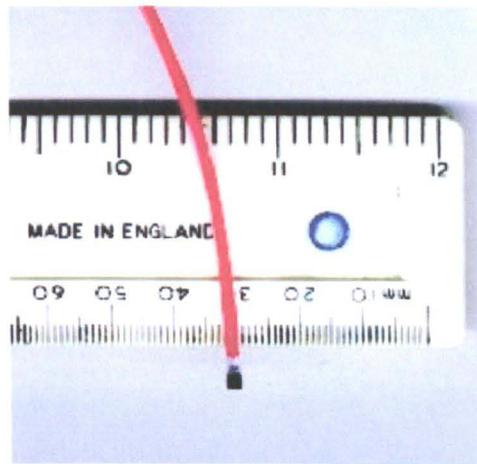
**Figure 3.9 Liquid leakage test of the probe using fluorescent liquid and negative air pressure.**

The electrical connection between ends of the cables was tested using an ohm meter to verify the electrical continuity. After these tests, the other end of the probe (lower end) was covered by a varnish to protect the cables from any mechanical shocks which may cause disconnections in cables (it was done under heating process). Approximately 3 mm of the jacket and screen of every cable was removed using a 0.25-0.80 mm wire stripper (Abisollerer verstellbar stripper). Following this, four cores and four screens of cables in this end were connected to a 9way connector such as Figure 3.10 using a soldering process (the location of cable-connector connections is shown in Appendix 3). Also one of 6 completed probes to use in this work is shown in this figure.

Finally, the probes are calibrated in a uniform isotropic medium (saline), so that the measured impedivity of a uniform medium is independent of the probe dimensions (the calibration procedure will be explained in Chapter 4). Cellular level modelling has shown that the current flow in a non-uniform medium depends on the relationship between electrode geometry and cell size and organisation (Walker, Brown et al. 2002). For electrodes which are of the order of 5-10 cell diameters, changes in measured impedivity due to tolerances on electrode size and position would be expected to be small compared to differences arising from the positioning of the probe relative to the cells.



a



b

**Figure 3.10 a) Completed probe b) A ruler shows the probe small size**

### 3.2.1.6 Results and discussions

To minimise the effect of the electrode impedance on measurements, the probe was made as large as possible. However, as there was limited available space for the probe to go down into the bladder, it was necessary to design a small probe of about 2 mm total diameter. The high electrode impedance resulting from the use of small diameter electrodes will reduce the measurement accuracy. To reduce this problem, some thought was given to designing a probe with the ability to expand within the bladder and increase the contact area. An argument is that the effective penetration depth in a uniform medium is a function of electrode separation, which therefore has to be small if

current is to be mainly confined to the thin epithelial layers. The most compromise amongst these requirements was 2 mm total diameter for the probe with 0.5 mm electrode diameter and electrodes separated from each other by about 0.2 mm. Gold electrodes were chosen for the probe in this study because it is chemically inert and causes no diffusion of ions from the electrode into the body and vice versa. In the probe construction process, the existence of a sub-miniature coaxial cable has a very important role in this work because of its small size. It would have been impossible to do this study without the small size cables. The PTFE tube and two-treatment process (vacuum plasma and ultraviolet exposure to seal the tip, tube and cables) are very important in the construction of the probe. Finally, the electrical safety and other safety tests using positive and negative air pressure in water tank and fluorescent liquid respectively were necessary to ensure optimal working condition of the probe.

### **3.2.1.7 Conclusions**

The existing probes used for measurements in cervix and oesophagus were too large in diameter and thus not suitable for electrical impedance measurement from the urinary bladder (*in vivo*). A suitable probe was designed and constructed for this work. This new and developed probe was constructed realising different limitations because of the allowed diameter for the probe to pass through the endoscope. Different methods were employed to construct, treat and perform safety tests for the probe for qualifying working condition. Six probes were constructed and all of them are working properly at present. This is the reason that all of the afore-mentioned instructions to design, construct and treat the process were followed in the best possible manner. Therefore, it is expected that the constructed probe in this section can measure accurately the electrical impedances of the urinary bladder tissue after the probe calibration. The calibration process of the probe is very important and it is necessary to take accurate impedance measurements of the tissue and thus it will be explained in the following chapter.

The existing electrical impedance spectroscopy equipment, Mk 3.a and Mk3.5 Sheffield Systems in Medical Physics and Engineering Department of Sheffield University will be described in the following section.

## **3.2.2 Electrical impedance spectroscopy systems**

### **3.2.2.1 Introduction**

Electrical impedance spectroscopy (EIS) systems can be designed to obtain high accuracy measurements. Basic components used in spectroscopy and imaging systems is current source, voltage measurement, demodulator and computer interface. The purpose of this section is to provide a description of these components in both general and spectroscopic types of Mk 3.a and Mk3.5 Sheffield Systems.

Initially, the first component, current source will be explained. The current source with high output impedance applies a constant current into tissue. Then, other important and basic parts of the equipment, the differential amplifier for measuring the resulting potential differences, the computer interface, data acquisition unit and the electrical safety will be described. Finally, both Mk 3.a and Mk3.5 Sheffield Systems will be discussed in detail. The general principle is straight forward:

1. Generate a suitable frequency sine wave.
2. Convert the voltage signal from the sine wave generator to a bipolar current signal.
3. Drive the current signal into one pair of electrodes.
4. Detect the resulting voltage signal at a second pair of electrodes.
5. Demodulate the signal to extract the in-phase component at the drive frequency.

The two systems use different drive and demodulation techniques. Mk3.a is conventional, with a single drive frequency at a time and synchronous demodulation, with 8 frequencies from 9.6 KHz to 1.2 MHz. Mk3.5 use 30 frequencies over a range from 2 KHz to 1.6 MHz, with 3 drive frames each containing the sum of 10 frequencies. Each drive frame is of different length, chosen so that frequency in the frame has an integral number of cycles. Demodulation is by FFT and having an integral number of cycles within the frame removes the need for windowing prior to the FFT, as there is no spectral leakage.

### 3.2.2.2 Current source and generator

The amplitude of the constant current drive in electrical impedance systems is of the order of milliampere or less. The main reason is safety regulation. However, a lower current than the maximum permitted current may be necessary to prevent the receiving amplifier circuits from saturating. In order to get a constant current source, high output impedance is necessary to minimise the effect of contact impedance.

Denyer et al designed, constructed and tested high output impedance current source circuits (supply-current sensing current source) for application in electrical impedance tomography systems (Denyer, Lidgley et al. 1994). Their experimental tests confirmed the theoretical predictions and produced a graph showing the output impedance of their circuit for different frequencies (100 KHz-1 MHz). The output impedance was more than 1 MΩ for currents at 100 KHz and 50 KΩ for currents at 1 MHz frequency. Therefore, it is possible to obtain acceptable output impedances for current sources but the design of a circuit to produce a current source with higher output impedance at higher frequencies is very difficult. It is usual that a 'voltage- controlled current source' is designed to convert a sine wave ( $V_{in}$ ) voltage into a current. For this purpose, there are different forms of circuits that have been considered by extensive research in this field of study as follows:

#### 3.2.2.2.1 Supply-Sensing Current Source

The 'Supply-Sensing Current Source' was introduced by Wilson (Wilson 1981) and then it was used by a number of researchers using an operational amplifier (op-amp) in electrical impedance equipment as in Figure 3.11. In this circuit,  $i_{m1}$  and  $i_{m2}$  are current

mirrors and  $i_2 = I_{Load} + i_{m2}$  also,  $\frac{V_{in}}{R_1} + i_1 = i_{m1}$ . If  $i_{m1}$  and  $i_{m2}$  are ideal,  $i_1 = i_2$  and

$i_{m1} = i_{m2}$ .  $i_1 = i_2 \Rightarrow \frac{V_{in}}{R_1} + I_{Load} + i_{m2} = i_{m1}$  since  $i_{m1} = i_{m2} \Rightarrow \frac{V_{in}}{R_1} = -I_{Load}$ . Therefore,

$I_{Load} = -\frac{V_{in}}{R_1}$ . In this case, the load current will be independent of the load impedance

( $R_L$ ).

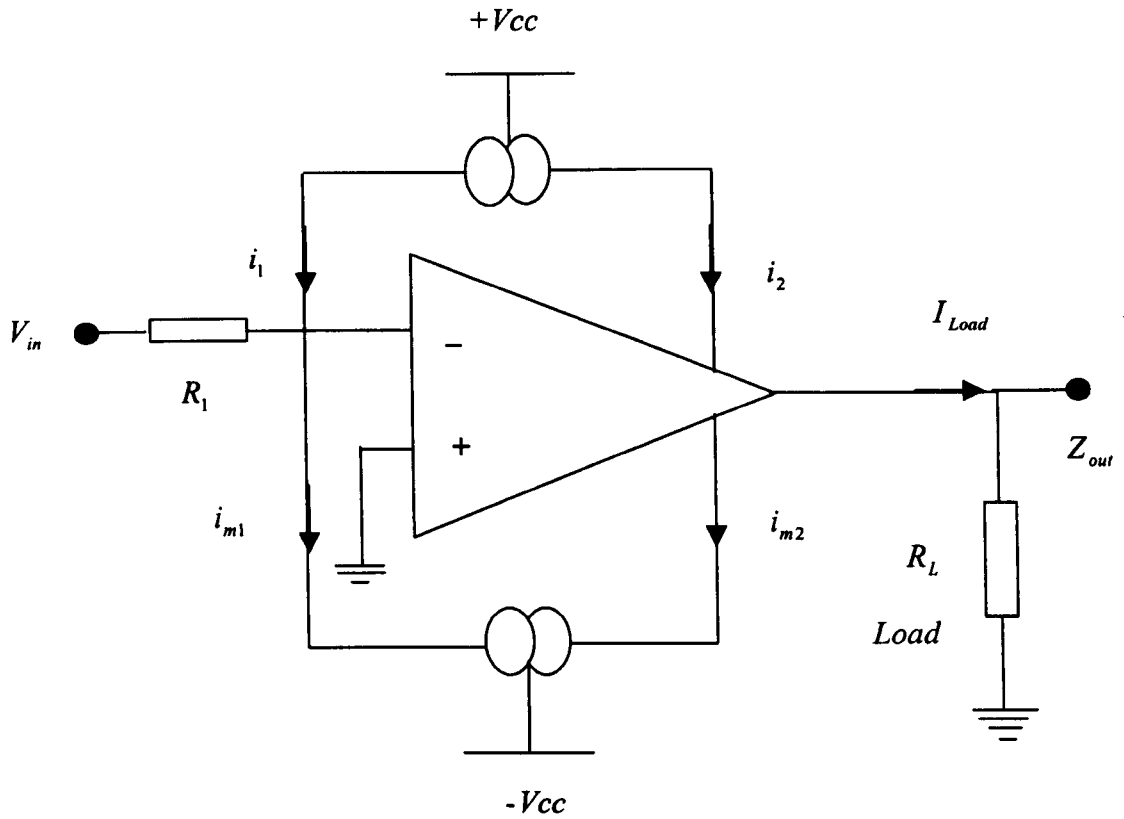


**Figure 3.11 Supply-Sensing Current Source**

The output impedance of this circuit will be as equation (3.7) (Denyer, Lidgley et al. 1994).

$$Z_{out} = A\lambda R_1 \quad (3.7)$$

$A$  = Open loop voltage gain of the op-amp.

$\lambda$  = The ratio of output current to controlling current for the current mirrors.

Table (3.1) shows the number of researchers that used Supply-Sensing Current Source and reported the value of  $Z_{out}$  at different frequencies:

Author	$Z_{out}$	Frequency
Leung et al (1990)	$2M\Omega$	10 KHz
	$300K\Omega$	100 KHz
Record et al (1990)	$2M\Omega$	100 KHz
Denyer et al (1994)	$600K\Omega - 8M\Omega$	100 KHz
	$200K\Omega$	500 KHz

**Table 3.1 The number of researchers that used Supply-Sensing Current Source, Modified from (Boone and Holder 1996).**

Bertemes-Filho designed an improved version of this current source and achieved an output impedance of  $70\text{ K}\Omega$  at  $1\text{ MHz}$  (Bertemes-Filho, Brown et al. 2000). This design is used in the Mk3.5 system.

### 3.2.2.2.2 The Howland circuit generator

The Howland circuit has been used in the majority of ‘voltage-controlled current source’ type of the current generators in both electrical impedance tomography and spectroscopy equipment. The basic form of this circuit is shown in Figure 3.12. This figure demonstrates a single op-amp with both positive and negative feedback. In this circuit, the total current,  $I$  will pass through  $R_1$  and  $R_2$ . At the negative input of the amplifier:

$$\begin{cases} I = \frac{V_{in} - V}{R_1} \\ I = \frac{V - V_{out}}{R_2} \end{cases} \Rightarrow \frac{V_{in}}{R_1} + \frac{V_{out}}{R_2} = V \left( \frac{1}{R_1} + \frac{1}{R_2} \right) \quad (3.8)$$

At the positive input of the amplifier:

$$V = \frac{R_3 \parallel R_L}{(R_3 \parallel R_L) + R_4} V_{out} = \frac{\frac{R_3 R_L}{R_3 + R_L}}{\frac{R_3 R_L}{R_3 + R_L} + R_4} V_{out} = \frac{R_3 R_L}{R_3 R_L + R_3 R_4 + R_L R_4} V_{out} \quad (3.9)$$

The load current,  $I_L$  is given by:

$$I_L = \frac{V}{R_L} \quad (3.10)$$

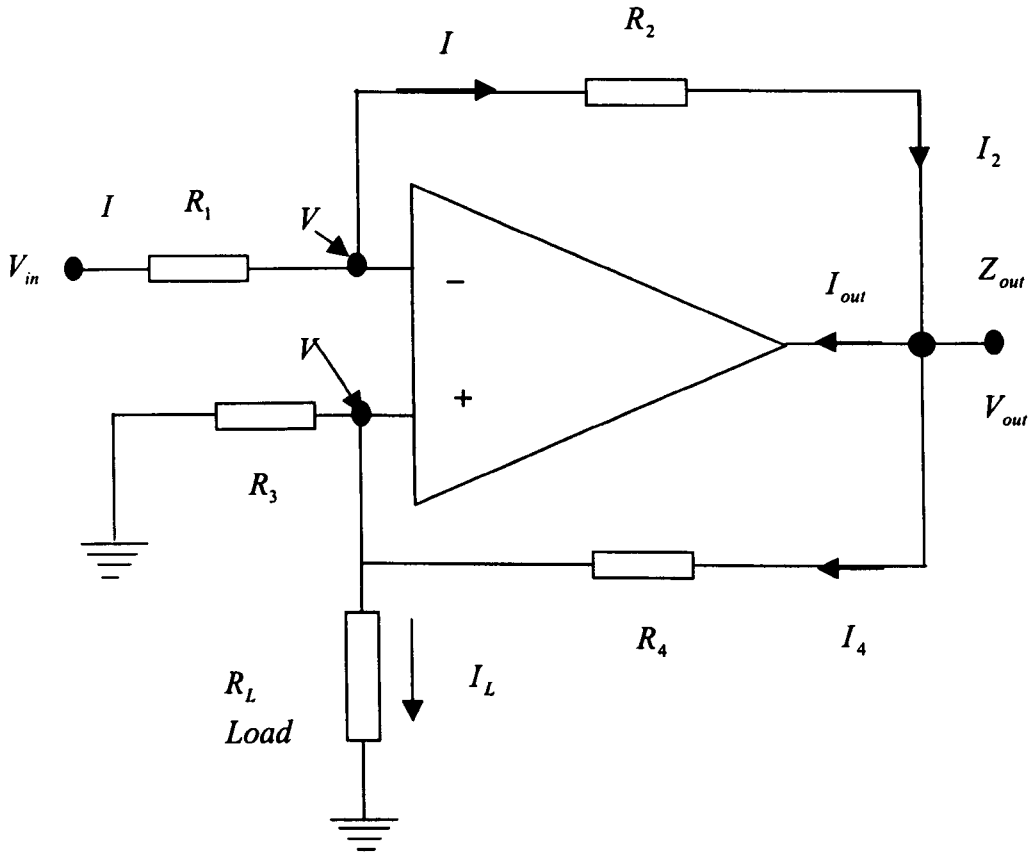


**Figure 3.12 Howland basic circuit**

Equation (3.9) can be re-written as  $V_{out} = V \frac{R_3 R_L + R_3 R_4 + R_L R_4}{R_3 R_L}$  and if we put this

value of output voltage into the second part of equation (3.8), we get:

$$\frac{V_{in}}{R_1} + \frac{R_3 R_L + R_3 R_4 + R_L R_4}{R_2 R_3 R_L} V = V \left( \frac{1}{R_1} + \frac{1}{R_2} \right)$$

$$\Rightarrow V \left( \frac{R_3 R_L + R_3 R_4 + R_L R_4}{R_2 R_3 R_L} - \frac{1}{R_1} - \frac{1}{R_2} \right) = -\frac{V_{in}}{R_1}$$

$$\Rightarrow V = \frac{V_{in}}{R_1 \left( \frac{1}{R_1} + \frac{1}{R_2} - \frac{R_3 R_L + R_3 R_4 + R_L R_4}{R_2 R_3 R_L} \right)}$$

Therefore using this equation, equation (3.10) becomes:

$$I_L = \frac{V}{R_L} = \frac{V_{in}}{R_L R_1 \frac{R_2 R_3 R_L + R_1 R_3 R_L - R_1 R_3 R_L - R_3 R_1 R_4 - R_1 R_L R_4}{R_1 R_2 R_3 R_L}}$$

$$\Rightarrow I_L = \frac{V}{R_L} = \frac{V_{in}}{R_L \left( \frac{R_3 R_1 R_4}{R_2 R_3} - \frac{R_1 R_L R_4}{R_2 R_3} \right)}$$

$$\Rightarrow I_L = \frac{V_{in}}{R_L \left( 1 - \frac{R_1 R_4}{R_2 R_3} \right) - \frac{R_1 R_4}{R_2}} \quad (3.11)$$

If  $R_1 = R_2 = R_3 = R_4$ ,  $I_L = -\frac{V_{in}}{R_1}$  can be found from the equation (3.11). Therefore  $I_L$

is independent of  $R_L$ . However  $I_4 = \frac{V_{out} - V}{R_4}$  and  $I_2 = \frac{V_{out} - V}{R_2}$ . Since  $R_2 = R_4$

thus,  $I_2 = I_4$ , therefore, no current is drawn from the output of the op-amp ( $I_{out} = 0$ ).

Therefore, the output impedance is infinite. In practice, mismatching among these resistors, stray capacitance, and finite amplifier gain limit the output impedance, although it will remain high.

Bootstrapping cables and using driven screens can reduce stray capacitance and thus increase the output impedance of the current generator. Table 3.2 shows researchers' reports used Howland circuit generators to find the output impedance.

Author	$Z_{out}$	Frequency
Rigaud et al (1990)	5M $\Omega$	50 KHz
Jossinet et al (1994)	1M $\Omega$	2 MHz

**Table 3.2 Researchers that used the Howland circuit for Current Source, modified from (Boone and Holder 1996).**

To maintain a high output impedance of the circuit over the whole frequency range (in multi-frequency systems), without any oscillation of the circuit, requires suitable adjustment of the feedback circuit. Bertmes-Filho compared the modified Howland circuits by both measurement and simulation with current mirror type circuits for current generators (Bertemes-Filho, Brown et al. 2000). The maximum variation of output current with frequency for the modified Howland circuit was 2 % and for mirror type circuits was 1.6 %. In addition, the output impedance for frequencies up to 100 KHz, for both circuits was greater than 100 K $\Omega$  and neither circuit had this output impedance at 1 MHz. They suggested that the results of the two type circuits are approximately the same.

### **3.2.2.3 Voltage measurement, differential amplifier and demodulator**

The receive circuit-voltage measurement part has to approximate to a perfect voltmeter, so it is necessary to reduce the effect of common-mode voltage and to increase the input impedance. A preamplifier (buffer) is usually used to increase the input impedance of the measurement circuits. Measurement errors can occur if there is a buffer mismatch. The differential amplifiers increase the amplitude of the desired signal (measured data potential differences) from the order of millivolts to the order of volts and reject any common mode voltage in the signal. The differential voltage at input terminals will be between 100  $\mu V$  -10  $mV$ . Hence, the signal resulting from the amplifier will be proportional to the electrical impedance of the tissue under measurement. The instrumentation amplifiers are used in electrical impedance systems as signal measurement circuits. These amplifiers are a combination of two pre-amplifiers and one op-amp differential amplifier (Figure 3.13).

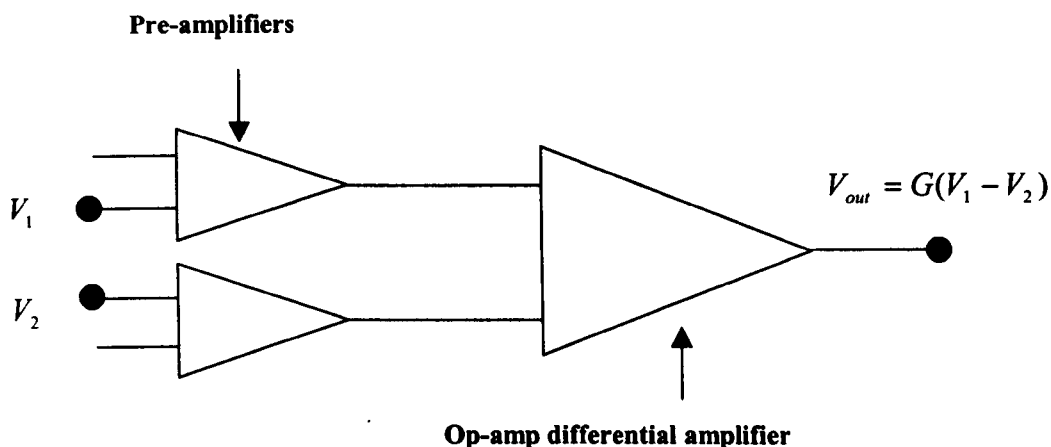


**Figure 3.13 Instrumentation amplifier**

$V_1$  and  $V_2$ , the input resultant differential voltages are connected to the measurement electrodes (these two electrodes are connected to the target tissue).  $V_{out}$  is the resultant amplified signal using the differential gain ( $G$ ). One of the aims in improving the measurement circuits is to reduce the effect of common-mode voltage and increasing of the input impedance. Finally, as was mentioned before, most researchers are interested in choosing the real part of measured complex impedance. Thus, to separate the real part, a demodulator circuit must be used in this part of the equipment. Therefore, the real component, quadrature signal component, will be separated from the in-phase component by using a demodulator. Also, bootstrapping cables can reduce the effect of stray capacitance and thus increase both the output impedance of the current source and the input impedance of the amplifier in the measurement part.

#### **3.2.2.4 Computer interface and data acquisition unit**

After the voltage measurement procedure, the resulting signal is analogue. Thus, it must be digitised to pass into the computer. In electrical impedance equipment, a data acquisition card is usually interfaced to a computer for this purpose (analogue-to-digital converter). Also, a rapid transmission process (high speed) is needed to transfer the signal into the computer for storage. Zhu Q. S. et al introduced a high-speed data acquisition system in 1994. In their system design, they achieved a high data acquisition speed while maintaining sufficient system accuracy. They achieved a speed of 25 frames per second for the data acquisition part and used video-speed A/D converter (Zhu, McLeod et al. 1994).

### **3.2.2.5 Electrical safety in EIS**

An isolated negative-feedback current source is a suitable way to apply in voltage controlled current sources for safety regulations. Hence, the patient will be isolated from the current source circuit by a transformer. According to safety regulations, the amplitude of the constant current applied in these systems (EIT and EIS) must be the order of milliamper ( $mA$ ) or less. According to IEC601 (International Electrotechnical Commission based in Geneva, Switzerland), the 'patient auxiliary currents', and in this study the electrical currents between electrodes are limited by different system frequencies (less than  $100\ \mu A$  from 0.1 Hz to 1 KHz and less than  $0.1\ mA$  per KHz up to  $10\ mA$  for above 100 KHz). For more information about electrical safety in EIT, see a study carried out by Lionheart et al (Lionheart, Kaipio et al. 2001).

### **3.2.2.6 Mk3.a Sheffield System**

#### **3.2.2.6.1 General description**

The first electrical impedance spectroscopic multi-frequency system was designed and built in the Medical Physics and Engineering Department of Sheffield University. A good description is given by Brown et al. (Campbell, Harris et al. 1994). Figure 3.14 shows the Mk3.a Sheffield System. This system is similar to the electrical imaging system and includes two isolated boxes, one small and one big. The small box includes the Gain Selector, V/I Converter and Preamplifiers and is located near the patient (*in vivo*) or sample (*ex vivo*) as close as possible during impedance measurements. This is because the probe can be passed through the endoscope easily (without extension or applying more force). A suitable gain must be selected since the reading data must not be saturated. The big box includes the Power Supply and Current Generation. The author will discuss the related electronics and circuit analysis in detail in this chapter.

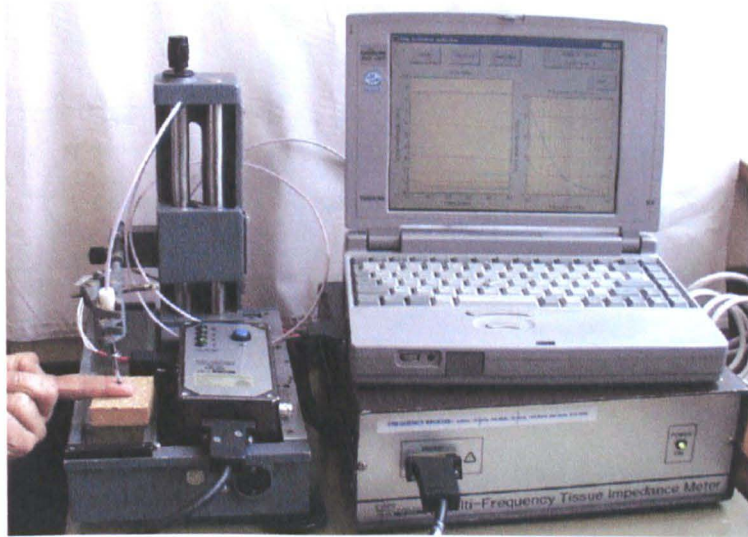


**Figure 3.14 Mk3.a Sheffield System**

The Mk3.a Sheffield System is a multi-frequency (7 frequencies) electrical impedance system that was used at the beginning of this study to characterise the bladder tissues *in vivo* and *ex vivo*. The applied frequencies are shown in Table 3.3. The related circuits are shown in Appendix 4 and Appendix 5. They measure the transfer impedance by passing a current between two electrodes of a 4 electrodes probe. Two other electrodes measure the resulting potential. There are 7 frequencies in a 1:2:4:8:16:32:64 sequences.

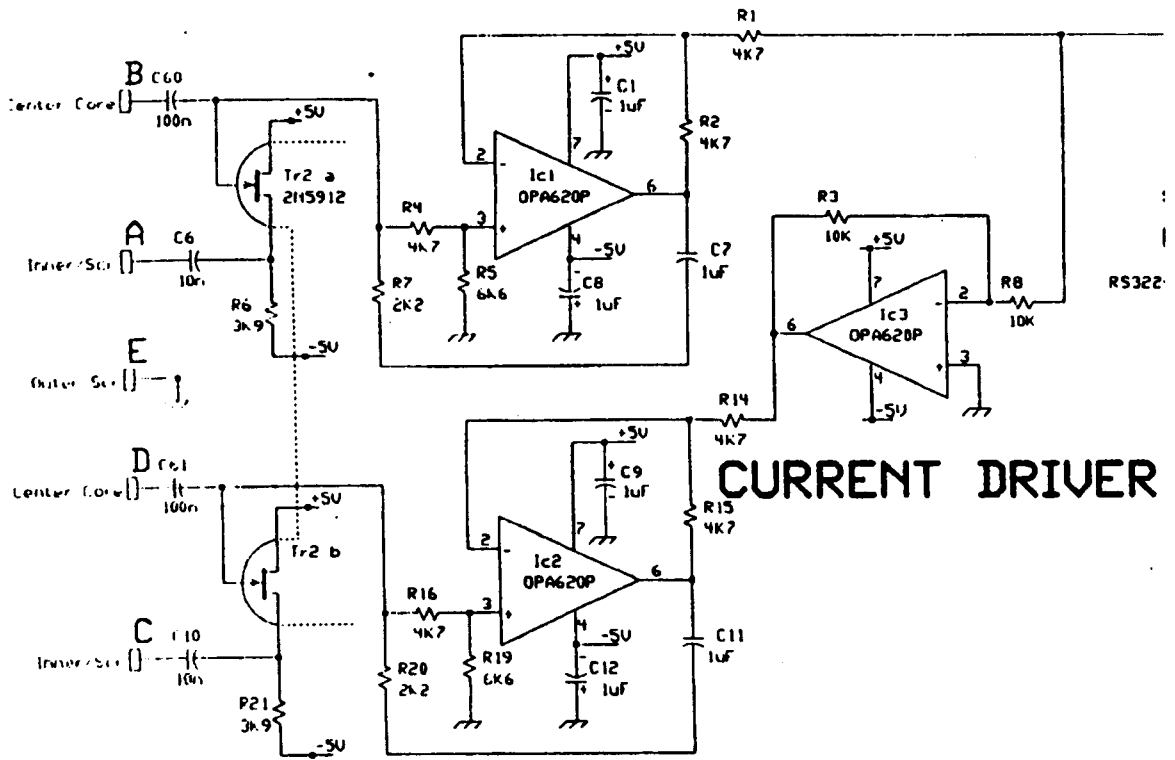
9600	19200	38400	76800	153600	307200	614400
------	-------	-------	-------	--------	--------	--------

**Table 3.3 Frequencies used in Mk3.a Sheffield System in Hz**

The sine wave is generated by a walking-ring counter with a variable clock speed to generate different frequencies.

### **3.2.2.6.2 Current Generation**

A voltage controlled current source is used to apply the current ( $2\text{mA } p - p$ ) between two drive electrodes (Appendix 4, IC1 and IC2 in current driver). The V to I converter (IC1 and IC2) are shown on the current driver part of Appendix 4 (or Figure 3.15). In this circuit, IC3 generates an inverted signal which is applied to one of the electrodes, '-' Drive, and a non-inverted signal results from IC2 with IC3 and is applied to another electrode, '+' Drive. The resistors R7 and R20 in the current driver region determine the output currents. See Figure 3.15:



### CURRENT DRIVER

**Figure 3.15 Current driver of Mk3.a Sheffield System**

Initially, (see Appendix 5), the current is generated in a digitally controlled Clock (IC11), which operates at selected frequencies on pin 1 (9.8 KHz) and pin 2 (19.6 KHz). The output of IC11 (pin 2) is divided by 16 using IC13, and the final result is a sinusoidal waveform on pin 6 of the IC15 (Figure 3.16).

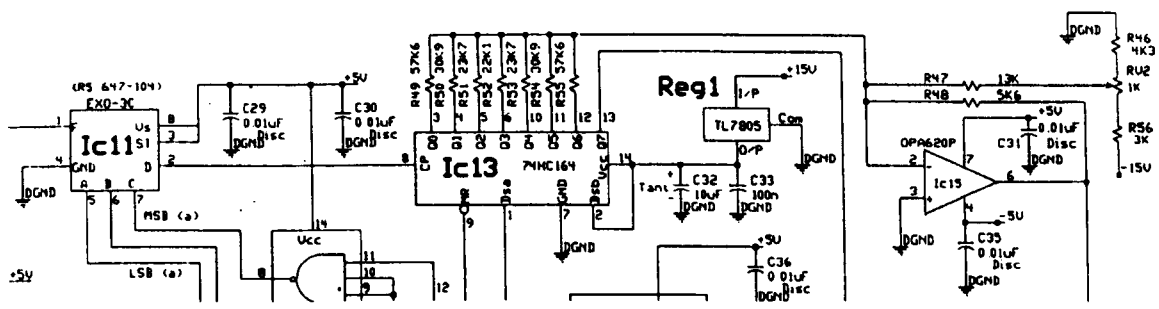


**Figure 3.16 Current generation of Mk3.a Sheffield System**

Furthermore, there are two integrated circuits, IC9 and IC10, as dividers controlling the frequency of this sinusoid every 3.3ms. Therefore, they produce epochs of 9.6, 19.2, 38.4, 76.8, 307.2 and 614.4 KHz. The 2V p-p sinusoidal waveform drives IC17 (used

as demodulator) (Figure 3.17).

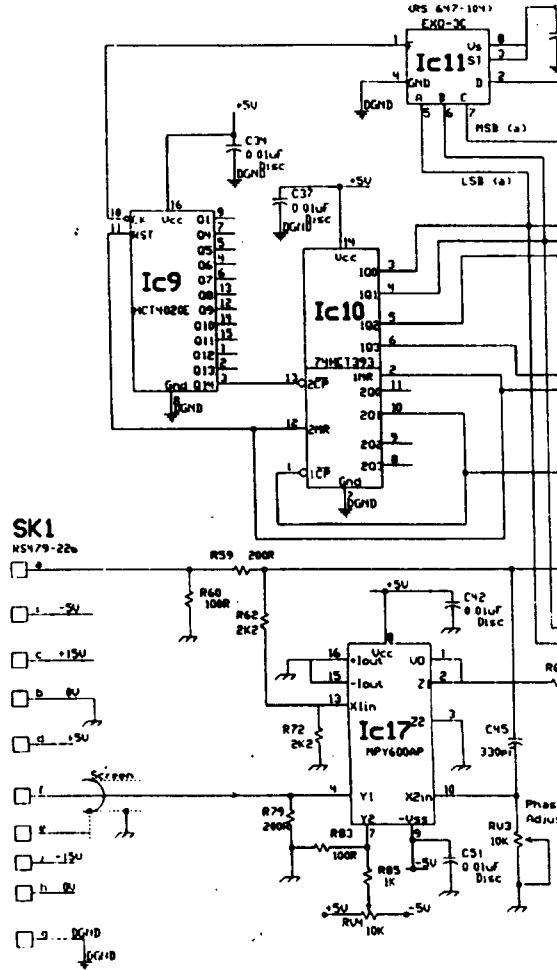


**Figure 3.17 Frequency controller and demodulator of Mk3.a Sheffield System**

### 3.2.2.6.3 Voltage measurement

The parallel voltage receivers measure the voltage of electrodes. Actually, the input potentials across C15 and C22 are applied to IC5, IC6 and IC7 (differential amplifier) and then on to IC8 of Appendix 4. (Figure 3.18):

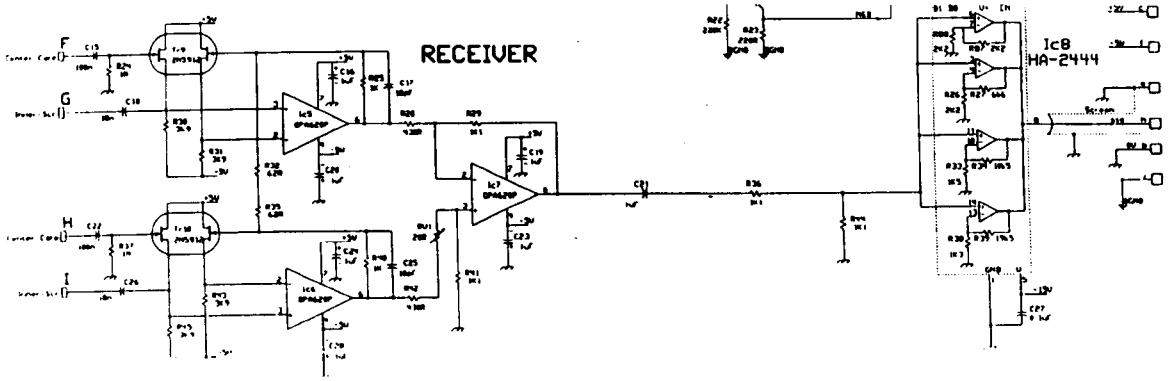


**Figure 3.18 Voltage measurement of Mk3.a Sheffield System**

The IC8 gain is controlled by the gain select logic circuitry (IC4, Tr6, Tr7 and etc.). It is a programmable gain amplifier. Four gains present (1,2,4,8) on the small box of the system result from this part of the circuit (Figure 3.19).

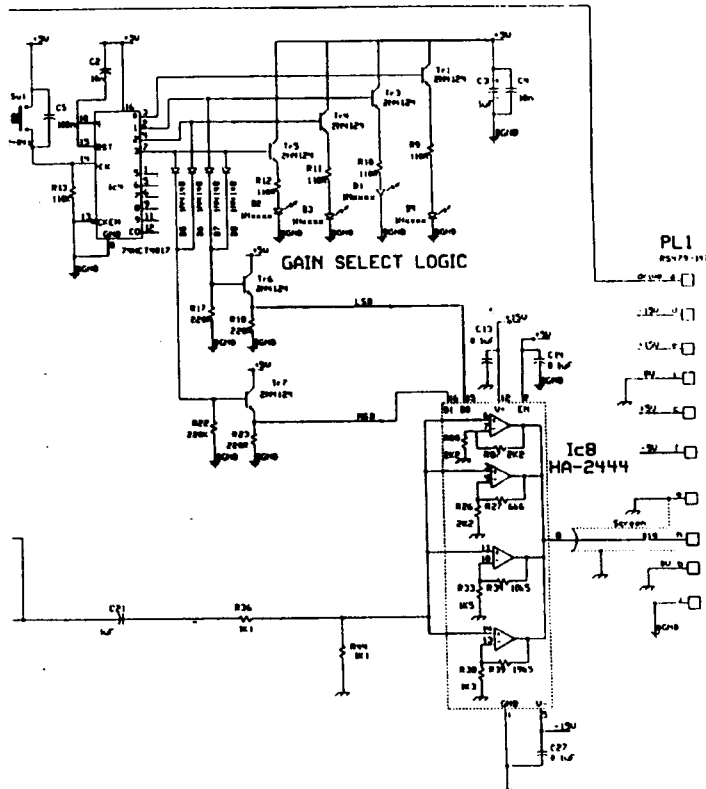


**Figure 3.19 Gain controller circuit of Mk3.a Sheffield System**

The output of IC8 (pin 8), feeds the Y input of the analogue multiplier IC17 and the X input of the analogue multiplier results from the current in R62 (Appendix 5). The large signals are amplified moderately but small signals are amplified more and more, thus signal to noise ratio (SNR) improves. The IC17 output (pin 1 and 2) is the in-phase component of the recorded potential and IC18 is a low pass filter to remove the carrier

frequency and also forms a full wave rectifier. IC19 is a demultiplexer. Finally, the current flows to eight isolation amplifiers and the output is passed to the DAS-8 data acquisition card (Figure 3.20).

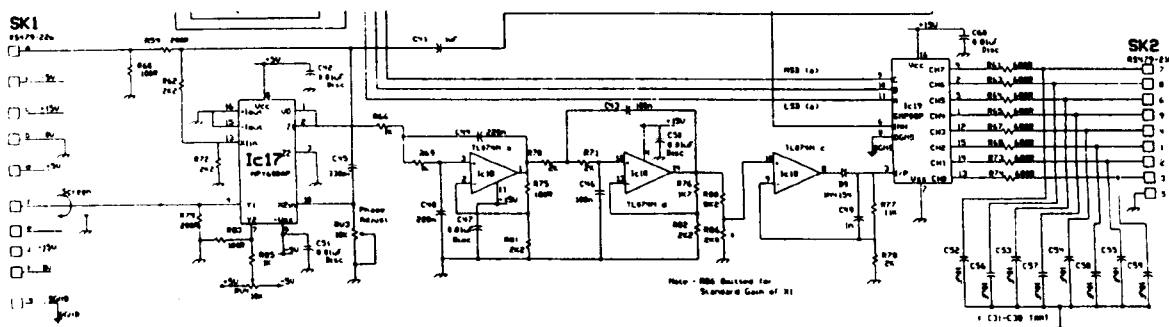


**Figure 3.20 Low pass filter and demultiplexer of Mk3.a Sheffield System**

### 3.2.2.6.4 Computer interface

The computer interface in this system provides the control of the required frequency sequence and drive configuration. The signal is passed to the analogue to digital converter (ADC). This system uses a 12bit ADC with 10 V input voltage. The data acquisition system is Daqbook 120, IOtech Inc. Also, the measured signal will be saved in a computer for more analytical studies of the measured data (Metherall 1998).

### 3.2.2.6.5 Electrical safety

The PC and data acquisition system are isolated from the analogue part (via Opto-isolators).

### 3.2.2.7 Mk3.5 Sheffield System

#### 3.2.2.7.1 General description

Mk3.5 Sheffield system, which has been used to characterise the bladder urothelium in this study, works in 30 frequencies at 25 frames per second and is completely different from the older system. There are three inter-level sets of frequencies with a 1:2:4:8:16:32:64:128:256:512 relationship and base frequencies of 2000, 2400, 3000 Hz:

2000	2400	3000
4000	4800	6000
8000	9600	12000
16000	19200	24000
32000	38400	48000
64000	76800	96000
128000	153600	192000
256000	307200	384000
512000	614400	768000
1024000	1228800	1536000

**Table 3.4 Frequencies (in Hz) used in MK3.5 Sheffield System**

It includes two boxes (Power Supply and Data Acquisition Unit) and a laptop shown as in Figure 3.21. This system combines a laptop computer with measurement hardware. The laptop is used to collect and analyse data obtained from the measurement hardware.

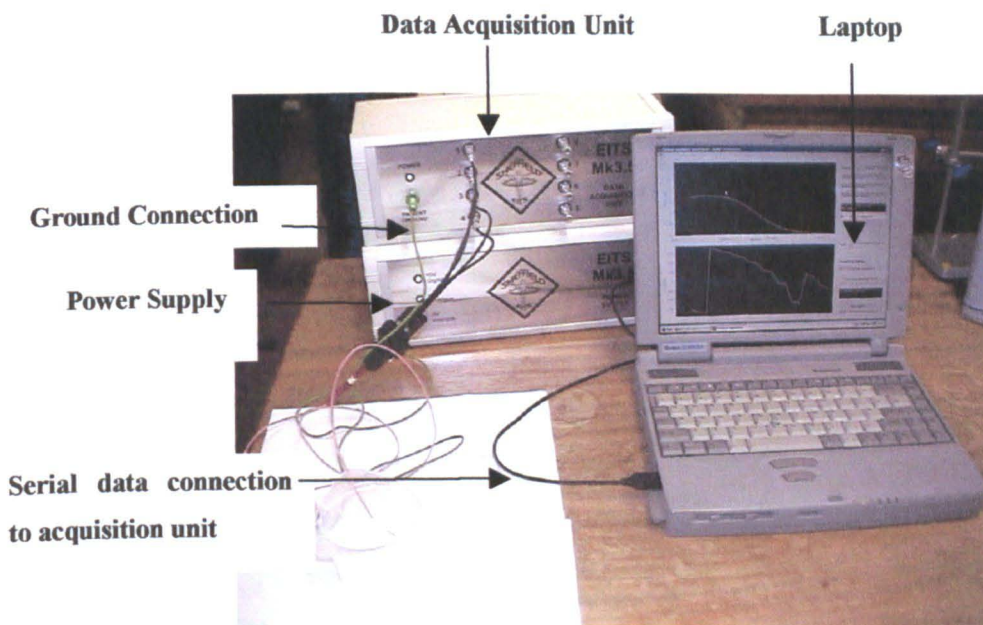


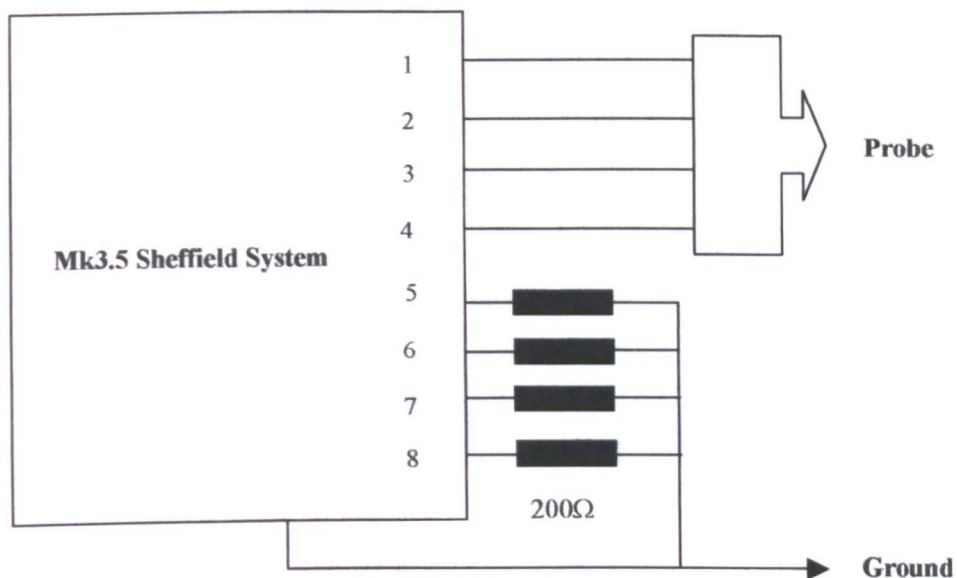
**Figure 3.21 Mk3.5 Sheffield System (data acquisition system)**

The Mk3.5 Sheffield System uses 8 electrodes to both inject current and measure voltage using different combinations of drive and receive electrodes and it is designed for imaging purposes. The applied current in this EIT system, for imaging of e.g. the thorax, is  $1\text{ mA}$ . However, it can easily be converted to electrical impedance

spectroscopy measurements for characterising the electrical properties of the tissues (the current in the spectroscopic version of this system is only  $10\ \mu A$ ). For spectroscopy, only four of the electrodes (2, current drive and 2, voltage receive) were used. Four resistors (each  $200\ \Omega$ ) were used as dummy loads on the other four electrodes' connection to the measurement system (see Figure 3.22). The software produces plots of the probe readings (in  $\Omega.m$ ) in real time to allow the user to check if there is a good reading before storing the data in a connected laptop for further calculation and data analysis. This portable computer reads 50 values for each measurement point and stores them as a Matlab file. Thus, readings can be averaged to reduce the measured noise. Data acquisition involves two distinct processes:

- 1) The hardware must be initialised and the DSPs booted. This permits information go from the PC to measurement hardware.
- 2) Data collection (Information transfer from the hardware to PC).

The respective circuit diagrams are attached in Appendixes 6 and 7. The system contains eight Data Acquisitions (DAQs) circuits connected to a motherboard. Each electrode is connected to a data acquisition board and each DAQ board includes a Texas Instruments 549 DSP. There is an analogue-to-digital converter for data measurement purpose and a digital-to-analogue converter for current drive and these eight DAQs boards are connected to a motherboard by high-speed synchronous serial links. The motherboard has a micro-controller to control both data transfer to and from the DSPs. A simple diagram is shown in Figure 3.23. Both Mk3.a and Mk3.5 Sheffield Systems use triaxial cables for connection of the electrodes and the system electronics with the outer screen earthed to reduce the capacitance coupling between electrodes and the inner screen bootstrapped to the voltage on the central conductor to minimise the capacitance to earth (Wilson, Milnes et al. 2001). Finally, in the first system, analogue demodulation was used, but in the latter system, digital signal processing is used for both the current generation and demodulation of the measured data.



**4 Electrodes connection**

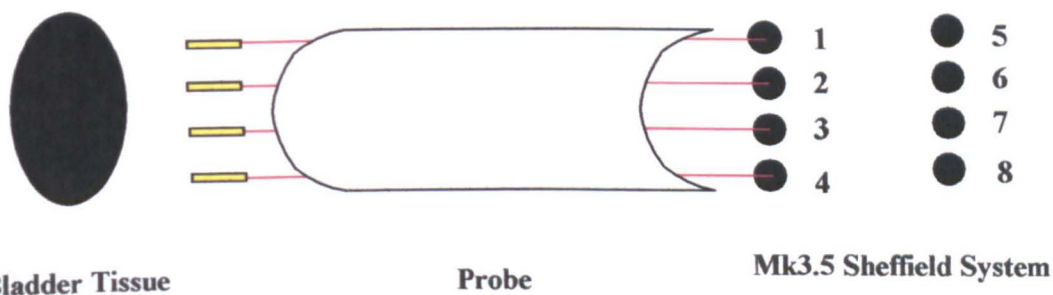
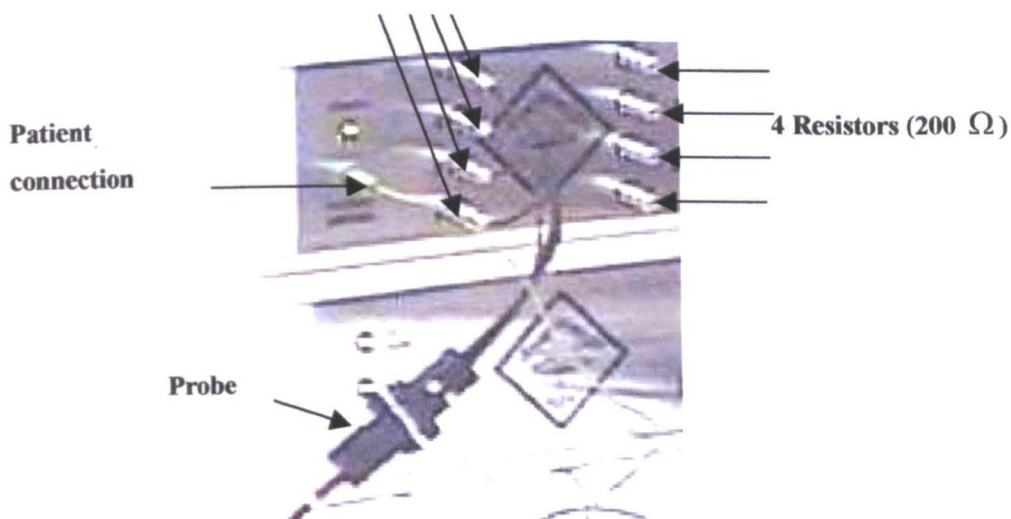


**Figure 3.22** Four Connectors were used to connect the probe to the measurement system of the Mk3.5 Sheffield System (Electrodes 1 and 2 are Current Drive, Electrodes 3 and 4 are Voltage Drive) and 4 Resistors ( $200\ \Omega$ ) were used to block another 4 Electrode Connections (Connections 5, 6, 7 and 8).

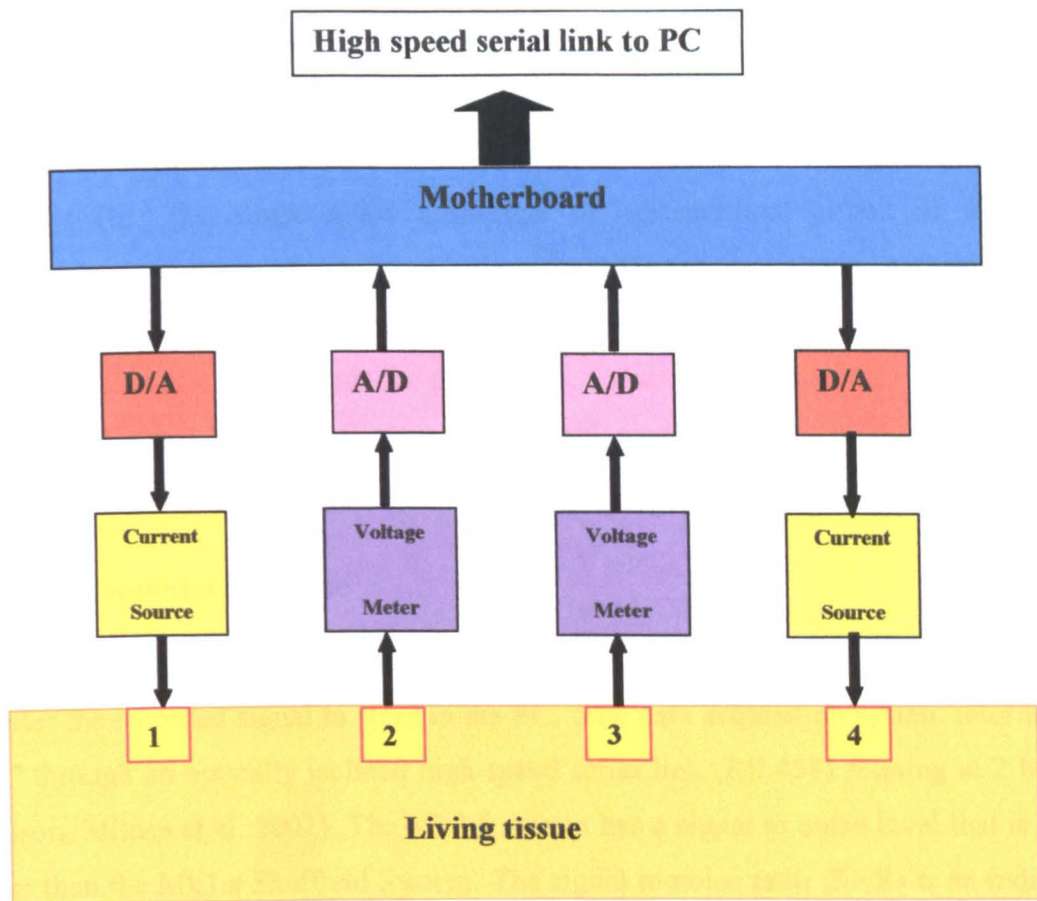


**Figure 3.23** Diagram of 4 electrodes connections to the data acquisition system in Mk3.5 Sheffield System (D/A is digital-to-analogue converter and A/D is analogue -to-digital converter and the numbers 1, 2, 3 and 4 are the contact point of electrodes with tissue).

### 3.2.2.7.2 Current Generation

The Mk3.5 Sheffield System contains eight identical data acquisition boards, which contain DSPs to generate the drive frequencies. It uses a precision balanced voltage controlled current source using modified Howland circuits by Dr. P. Bertemes-Filho in section 3.2.2.2.2 (Bertemes-Filho, Brown et al. 2000). The applied current to the bladder tissue in this study is  $10\mu\text{A}$  p-p.

### **3.2.2.7.3 Voltage measurement**

There are 8 Data Acquisition Modules (DAQs), which record and analyse data from respective channels. The measurement hardware is microprocessor-controlled and uses digital electronics technology. It measures both real and imaginary components of impedance at 30 separated frequencies on a logarithmic scale between 2 KHz and 1.6 MHz. The voltage measurement circuit of Mk3.5 Sheffield System can be shown in Appendix (6). The single-ended amplifiers of measurement circuit in the Mk3.5 Sheffield System are configured to measure the differentiate voltage. A third electrode is used for the reference potential (it is connected to the tissue under study). The difference between inputs and the third input (ground) is called the Common-mode voltage and must be rejected by a differential amplifier with high common mode rejection ratio (CMRR).

### **3.2.2.7.4 Computer interface**

The receive module samples the differential voltage then communicates with the PC to transfer the recorded signal to store in the PC. The data acquisition system interfaces to a PC through an optically isolated high speed serial link (RS 458) running at 2 Mbits/s (Wilson, Milnes et al. 2001). The Mk3.5 system has a signal to noise level that is 10 dB better than the Mk3.a Sheffield System. The signal to noise ratio (SNR) is an indication of how effectively the system works. If this is very high, the noise errors in our measured data will decrease. The improved SNR is a result of technical improvements over the older analogue demodulation method, particularly the use of digital signal processing for both the current generation and demodulation of the measured data.

### **3.2.2.7.5 Electrical safety**

This system is optically isolated from the PC to keep the leakage current low, because of electrical safety.

### **3.2.2.8 Conclusions**

It is very important to have a constant current source in electrical impedance systems with high output impedance to minimise the effect of contact impedance between probe and tissue. A number of high output impedance current source circuits have been designed, constructed and tested by several researchers for application in electrical impedance tomography systems. These are usually a 'voltage- controlled current

source' which are designed to convert a sine wave voltage into a current (Supply-Sensing Current Source or Howland circuit generator). In the Mk3.a Sheffield System, a voltage controlled current source was used to apply the current between two drive electrodes of the probe and in the Mk3.5 Sheffield System, the current drive of the system was designed using Howland circuits. In the circuit designed for EIS, a preamplifier (buffer) is used to increase the input impedance of the measurement circuits. In the Mk3.a system, the gain is controlled by the gain select logic circuitry and a programmable gain amplifier. In addition, analogue circuits are used in this system. In the Mk3.5 system, the measurement hardware is microprocessor-controlled and uses digital electronics technology. It measures both real and imaginary components of impedance at 30 separated frequencies on a logarithmic scale between 2 KHz and 1.6 MHz. After voltage measurement procedure, the analogue signal is digitised to pass into the computer.

In electrical impedance equipment, a data acquisition card is usually interfaced to a computer for this purpose (analogue-to-digital converter). In the Mk3.a system, the signal is passed to the analogue to digital converter (ADC). This system uses a 12bit ADC with 10 V input voltage. The data acquisition system is Daqbook 120, IOtech Inc. In the Mk3.5 system, the data acquisition system interfaces to a PC through an optically isolated high speed serial link (RS 458) running at 2 Mbits/s. The signal to noise of the Mk3.5 system is 10 dB better than the MK3.a system and uses digital signal processing for both the current generation and demodulation of the measured data. Finally, the systems are optically isolated from the PC to keep the leakage current low because of electrical safety.

### **3.3 Conclusions**

There are some important aspects related to the impedance measurement procedure such as existing equipment (probe and EIS systems). The existing probe in our department was bigger in diameter and thus it was not suitable to take electrical impedance measurement from the urinary bladder (*in vivo*). Therefore, it was decided to design and construct a suitable probe for this work. As a result, this new and developed probe was constructed realising different limitations because of the allowed diameter for the probe to pass through the endoscope. Finally different treatment procedures were applied to

the constructed probes to prevent the liquid leakage and to consider electrical safety. In the probe used in this study, 4-electrode technique, the effect of electrode impedance in actual measurements must be minimised. This could be achieved using large probes but because of permitted limited available space for the probe to go down into the bladder, the author designed and constructed a small probe (2 mm total diameter) inside a PTFE tube. The electrodes used in this study must be chemically inert to prevent ion diffusion from the electrode into the body and vice versa. Gold electrodes were chosen for this purpose. Finally, several treatment and test procedures were applied for safety purposes.

The electrical impedance systems have different characteristics, such as a current source and generator with high output impedance, a suitable voltage measurement part to measure small signals received from the measuring electrodes, a computer interface and a data acquisition unit. Both Mk3.a and Mk3.5 Sheffield Systems were used in this work to measure the electrical impedance of the bladder urothelium. A voltage controlled current source was used to apply the current in the first system and the improved Howland circuits were used in the latter system. In addition, a programmable gain amplifier was used in the first system. Analogue circuits are used in the Mk3.a but digital technology is used in the Mk3.5 Sheffield System. Therefore, the SNR of the latter system is better than the first one.

In the Mk3.a system, the calculation of impedivity using manually calibration factors for every measured data in impedance calculation procedure causes a disadvantage for this system. Therefore, it was improved to measure the electrical impedances in wide range of frequencies, Mk3.5 Sheffield System. This system then was improved to get wider frequencies, especially lower frequencies (62.5 Hz-1.5 MHz) because it was believed that a significant separation of malignant tissues from the benign type could be presented using lower frequencies. Thus, this developed impedance spectroscopy system is suitable to characterise the bladder tissue.

# Chapter 4

## Impedance measurement methods, data acquisition, storage and analysis

### 4.1 Introduction

The physical dimensions of the different probes used in this study will have an effect on the measurements, and thus these probes must be unified using a calibration process. The calibration of the probes using known conductivity saline solutions in both impedance spectroscopy systems that were used in this study will be discussed. Then the electrical impedance measurements of the urinary bladder, data acquisition, storage and analysis in this work (which are divided into two different groups namely *ex vivo* and *in vivo*) are described. In the data measurement procedure, we started with *ex vivo* studies because this removed the need for the small probe to go down an endoscope. Otherwise, if we choose to use only *in vivo* measurements, the number of our samples is severely limited by the availability of suitable patients who have agreed to electrical impedance measurements from their bladder. It is expected that the results coming from these two types of measurements will not be identical. This is because the experimental conditions for these two studies will be different for the following reasons:

- 1) Patient body temperature in *in vivo* study will be different from the resected bladder tissue temperature in the laboratory (*ex vivo* study).
- 2) There is no blood circulation in a resected bladder, and the resulting cell death will progressively change its electrical impedance. To minimise this problem, the bladder must be transferred to the histopathology department for examination within one hour.
- 3) Handling of the resected bladder may cause changes in the measured electrical impedance due to additional inflammation of the tissue.
- 4) Existence of glycine inside the urinary bladder (*in vivo* study). It is expected that the resistivity of the glycine inside the bladder will cause an increase in the real impedance results for malignant and non-malignant tissues.
- 5) Bladder cells are usually relaxed in *ex vivo* and extended in *in vivo*. In the former, the number of cells in bladder tissue epithelium is greater than in the latter.

The above-mentioned factors will cause differences in the measured impedances of the urinary bladder for *ex vivo* and *in vivo* studies. Initially, the author will discuss the probe calibration method and then the *ex vivo* and *in vivo* impedance measurement methods, data acquisition, storage and analysis will be explained.

## **4.2 Probe calibration**

When the impedance of the bladder tissue is measured using one probe (*ex vivo* or *in vivo*), this probe will be dirty between procedures and it must then be cleaned using sterilisation process (at least one hour). Therefore, the author needed another probe to continue the measurement process and thus in total used four probes in this work. These probes must be calibrated before any measurement procedure in order to unify the results. This means that if we measure one place on the tissue with each of the probes, the resulting impedances should be the same. Therefore, to ensure comparability between these probes, and before any electrical impedance measurement, the probe must be calibrated using different known (uniform) conductivity saline solutions. Thus, the author calibrated every probe separately using different systems: Mk3.a and Mk3.5 Sheffield Systems. For this purpose, the probe calibration procedure in these systems is explained separately as follows:

### **4.2.1 Probe calibration using Mk3.a Sheffield System**

The principle of the calibration procedure is to relate the measured transfer impedance to a known uniform conductivity by means of a calibration factor for each measurement frequency. Initially, the Mk3.a Sheffield System and saline solutions with different conductivities were prepared to begin the probes calibration. Therefore, it was necessary to obtain volts-to-impedance factors for all of the gains and frequencies. For explaining the calibration procedure, firstly ten different saline solutions were prepared using a conductivity meter (Model 470 Portable Conductivity/TDS Meter, HI 8633- constructed by Hanna instruments) to determine the exact amount of conductivity of every saline solution (Figure 4.1). According to the specifications of this conductivity meter, it is possible to obtain accurate readings across the range of 0.1-200 mS/cm with the accuracy of 1% full scale. This is using a 9 volt battery with 100 hours of continuous use within 0-50 °C environment (the author used this meter in the room temperature) and indicates that the instrument will be sufficiently accurate for the purposes of this calibration.

Conductivity (mS/cm) ⇒	0.30	0.37	0.82	1.42	2.20	2.83	5.04	5.75	6.66	7.40
------------------------	------	------	------	------	------	------	------	------	------	------

The reason that the author used these conductivities was because they cover the full range of the bladder tissue conductivity which may exist. After collecting the above-mentioned saline solutions, the respective readings of every solution were taken using the electrical impedance measurement system and then stored in a portable computer (Laptop) for further analysis. These readings were taken at all of the gains (1, 2, 4, and 8) and at seven distinct frequencies in KHz (9.6, 19.2, 38.4, 76.8, 153.6, 307.2, 614.4).



**Figure 4.1 Conductivity Meter**

The calibration process for one of the probes with different saline solutions is shown in Table 4.1. There is a combination of readings using 10 different saline solutions and 4 different system gains. The second row of this table represents the conductivity of ten different saline solutions in mS/cm that were measured using a conductivity meter and the third row determines the resistivity of respective saline solutions in  $\Omega.m$ .

Saline Solution No.	1	2	3	4	5	6	7	8	9	10
Conductivity (mS/cm) ⇒	0.30	0.37	0.82	1.42	2.20	2.83	5.04	5.75	6.66	7.40
Resistivity (Ohm.m) ⇒	33.33	27.03	12.19	7.04	4.54	3.53	1.98	1.74	1.50	1.35
Gain 1 ↓	Y1	Y2	Y4							
2		Y3	Y5	Y7						
4				Y8	Y10	Y12	Y14	Y16	Y18	Y20
8					Y11	Y13	Y15	Y17	Y19	Y21

**Table 4.1 Calibration Process for Mk3.a Sheffield System (Conductivity and Resistivity) Y1-Y21 are the impedance measurement system readings at Laptop screen (their values are shown in Table 4.2).**

All the readings (from 1 to 21) in the measurement system presented in Table 4.1 are represented in Table 4.2 at 7 frequencies as follows:

Frequencies (KHz) ⇒	9.60	19.20	38.40	76.80	153.60	307.20	614.40
Readings (Volts) ↓							
Y 1	3.78	4.17	4.27	4.27	3.94	1.94	0.04
Y 2	3.27	3.66	3.77	3.85	3.67	2.24	0.04
Y 3	6.65	7.39	7.59	7.81	7.42	4.51	0.04
Y 4	1.71	1.89	1.95	2.00	2.1	2.2	1.25
Y 5	3.52	3.86	3.98	4.12	4.37	4.32	2.70
Y 6	7.15	7.81	8.02	8.35	8.80	8.60	3.83
Y 7	2.48	2.64	2.66	2.69	2.88	3.01	3.37
Y 8	5.11	5.40	5.44	5.53	5.85	6.05	7.44
Y 9 *	10.00	10.00	10.00	10.00	10.00	10.00	0.04
Y 10	3.25	3.40	3.42	3.46	3.63	3.80	4.82
Y 11	6.61	6.92	6.95	7.04	7.39	7.68	10.00
Y 12	2.79	2.94	2.93	2.95	3.05	3.16	3.91
Y 13	5.72	5.98	5.98	6.04	6.24	6.42	8.68
Y 14	1.55	1.60	1.58	1.57	1.64	1.68	1.93
Y 15	3.21	3.31	3.28	3.30	3.39	3.48	4.16
Y 16	1.38	1.41	1.40	1.38	1.44	1.47	1.65
Y 17	2.89	2.95	2.91	2.92	2.99	3.05	3.55
Y 18	1.19	1.22	1.20	1.17	1.23	1.25	1.39
Y 19	2.48	2.53	2.49	2.49	2.55	2.59	2.97
Y 20	1.10	1.12	1.10	1.07	1.13	1.14	1.26
Y 21	2.31	2.35	2.31	2.30	2.36	238	2.70

\* Y9 was not considered because it was 10 volts and high (because of the measurement system saturation).

**Table 4.2 Calibration Process, readings in volts at seven frequencies for Mk3.a Sheffield System**

Readings >10V are rejected as saturation, and <0.5V because of large errors at low voltages arising from the demodulation.

The Conversion Factor for Gain 4 (from Reading Y8) using saline solution with the resistivity of 7.04  $\Omega m$  will be as follows:

Frequency (KHz)	9.60	19.20	38.40	76.80	153.60	307.20	614.40
Conversion Factor ( $\frac{\Omega m}{Volt}$ )	1.38	1.30	1.29	1.27	1.20	1.16	0.95

**Table 4.3 Conversion Factor for Gain 4 and reading Y8 at 7 frequencies**

The conversion factors for other data (Y10, Y12, Y14, Y16, Y18, Y20) in different saline solutions at Gain 4 were calculated from Tables 4.1 and 4.2. Finally the conversion factor at Gain 4 for 7 readings at 7 frequencies is as follows:

Calibration Factor (Ohm.m/Volt)	9.6	19.2	38.4	76.8	153.6	307.2	614.4
Gain 4 from Y8	1.38	1.30	1.29	1.27	1.20	1.16	0.95
Gain 4 from Y10	1.40	1.33	1.33	1.31	1.25	1.20	0.94
Gain 4 from Y12	1.26	1.20	1.20	1.20	1.15	1.11	0.90
Gain 4 from Y14	1.28	1.24	1.25	1.26	1.21	1.18	1.03
Gain 4 from Y16	1.26	1.23	1.25	1.26	1.21	1.18	1.05
Gain 4 from Y18	1.26	1.23	1.25	1.28	1.22	1.20	1.08
Gain 4 from Y20	1.23	1.20	1.22	1.26	1.19	1.18	1.07

**Table 4.4 Conversion Factors for Gain 4 and for 7 readings at 7 frequencies ( $\frac{\Omega.m}{Volt}$ )**

The conversion factors are calculated for every gain and frequency, and thus the author averaged the Conversion Factors for each frequency using different saline solutions to obtain more accurate factors. The average of the rows 2-8 from Table 4.4 at 7 frequencies is the Conversion Factor at Gain 4:

Calibration Factor (Ohm.m/Volt)	9.6	19.2	38.4	76.8	153.6	307.2	614.4
Gain 4	1.29	1.26	1.26	1.26	1.20	1.17	1.00
Standard error of mean	0.02	0.02	0.02	0.02	0.01	0.01	0.01

**Table 4.5 Conversion Factor for Gain 4 at 7 frequencies ( $\frac{\Omega.m}{Volt}$ )**

The Conversion Factor for Gain 8 was calculated in the same way as for Gain 4. In this case, the readings Y11, Y13, Y15, Y17, Y19, and Y21 were used:

Calibration Factor (Ohm.m/Volt)	9.6	19.2	38.4	76.8	153.6	307.2	614.4
Gain 8	0.60	0.59	0.59	0.59	0.58	0.57	0.48
Standard error of mean	0.01	0.01	0.01	0.01	0.01	0.01	0.01

**Table 4.6 Conversion Factor for Gain 8 at 7 frequencies ( $\frac{\Omega.m}{Volt}$ )**

Finally, having these factors, thus related to every gain of the system separately, it was necessary to use them for the respective measurements in the same gain (Gains 4 and 8 were usually used in this work). This factor is the amount that every *Computer Reading*

must be multiplied by to find the equivalent impedivity (*ex vivo* or *in vivo*) in  $\Omega.m$ . This was performed when the author calculated the impedivity of the measured point using Matlab programme (a simple programme written by the author to apply for all of the probes' calibrations).

#### 4.2.2 Probe calibration using Mk3.5 Sheffield System

The calibration process for Mk3.5 is similar to the above-mentioned method but there is no gain selection or manual calculation of calibration factors. In fact the measured data using different saline solutions (similar to the Mk3.a system) by the Mk3.5 Sheffield System is saved directly in the calibration files in Matlab programme. Figure 4.2 shows the set-up of this system and saline solution during calibration process (probe placed inside a known saline solution).

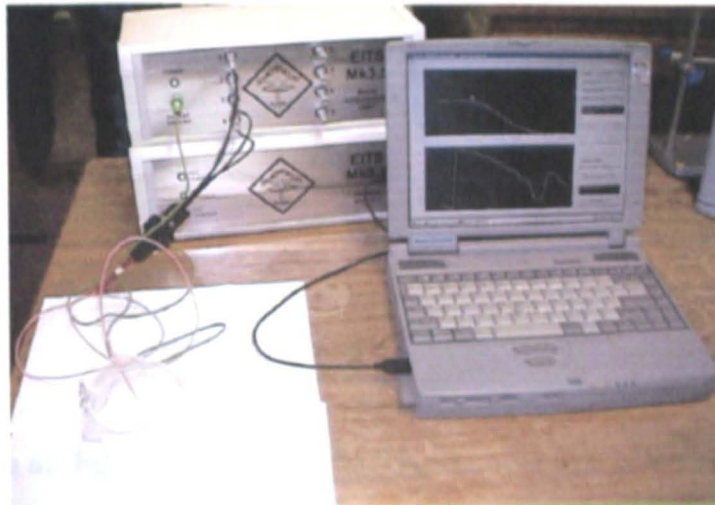


**Figure 4.2 Probe calibration (Mk3.5)**

During calibration of probes procedure using this system, a series of saline solutions with different resistivities, were used (Table 4.7):

Saline Solution No.	1	2	3	4	5	6	7	8	9	10
Conductivity (mS/cm) $\Rightarrow$	0.30	0.37	0.82	1.42	2.20	2.83	5.04	5.75	6.66	7.40
Resistivity (Ohm.m) $\Rightarrow$	33.33	27.03	12.19	7.04	4.54	3.53	1.98	1.74	1.50	1.35

**Table 4.7 Calibration Process for Mk3.5 Sheffield System (Conductivity and Resistivity)**

To first order, there is a linear relationship between the resistivity of saline solutions and the measured readings at all frequencies except at higher frequencies. One of the calibration curves at 2 KHz is demonstrated in Figure 4.3 (the \* symbols indicate the measured data points and the solid curve indicates the best line fitting to this data at lower impedances). Therefore, it is not possible to calibrate the probe at higher frequencies thus at these frequencies, a number of spikes in the impedance spectra are appeared. At lower impedances, it is clear from the fitted line to the readings that the relationship between the saline impedance and these readings can be linear. However, at higher impedances, other factors become apparent and the measured readings fall below its true value and thus, the relationship between saline impedance and the measured readings will be non-linear. The data plateaus at higher impedances. These curves are stored in laptop for further calculations of measured impedance of tissue. In fact, these apply to the computer readings to obtain the actual electrical impedance measured data in the real impedance measurements in  $\Omega m$  (calibration in memory).

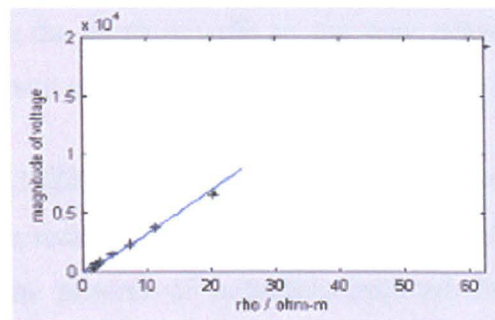


**Figure 4.3 One of the calibration curves (the vertical axis is in arbitrary units)**

When we are using the measured system to characterise actual tissues in terms of electrical impedances, first of all we must load a respective calibration file. After that, the calibration factors will be applied automatically in real time to find the final results. Finally, in the probe calibration procedure for both impedance spectroscopic systems used in this work, the calibration factor may not change over time because it depends on the probe structure, size and cable length. However, there was a small (insignificant) change of the conversion factors for each probe. Both bipolar and tetrapolar impedance measurements are made during the calibration process. The measured bipolar impedance at different load impedances is used to provide an estimate of the output impedance of the current generator, which can then be used to correct the tetrapolar impedance measurement for the effect of the non-ideal current source.

### 4.3 Electrical impedance of resected bladder (*ex vivo* study)

For *ex vivo* study, a whole or partial part of the patient's urinary bladder was used in this study to measure the electrical impedance immediately (within one hour) after excision. 35 patients (27 male and 8 female) were investigated. Specimens from cystectomies with malignant and non-malignant bladders were used. The range of patient ages at the time of cystectomy was between 37 and 79. A brief description of their details is shown in the Table 4.8. The malignant bladders were resected for Transitional Cell G3pT2 disease (19), G3pT2 disease with squamous or sarcomatoid differentiation (3), G3pT2 with CIS (8), G3pT3 disease (1) and refractory G3pT1/CIS disease (3). These patients had operations at the Royal Hallamshire Hospital in Sheffield between March 1999 and September 2001. All of the electrical impedance measurements were carried out within 1 hour of resection to ensure that the physiological condition of the bladder tissue was as near as possible to the *in vivo* state (Foster and Schwan 1989). The reason for this can be discussed as follows: Galeotti (1902) was probably the first to note changes in resistivity accompanying the death of cells as the time passed after tissue resection. In excised tissues, he observed an initial increase followed by a decrease in resistivity.

In addition, Crile et al (1922) found the resistivity of tissue was substantially constant during the first hour after removal from the body (Crile, Hosmer et al. 1922). Also, there is an investigation of the process of ischaemia-induced disturbances in the rat liver, employing the electrical bio-impedance technique. The electrical bio-impedance was measured continuously over 6 hours by the 4-electrode method. The findings of this study suggested the possibility of bio impedance data changes in liver tissue or the tissue structure changes because of ischaemic changes (Konishi, Morimoto et al. 1995) and implies that *ex vivo* results may not completely replicate *in vivo* results after a few hours of tissue resection. However, these *ex vivo* results may replicate *in vivo* results if the electrical impedance measurement applies within one hour after the bladder resection. Therefore, the sample transferring, sample preparation and *ex vivo* measurements were carried out within 1 hour after the bladder resection. Also, the bladder sample was transferred from the theatre to the histopathology department with minimum disturbance and with care. The specimens of malignant bladder contained bladder and prostate tissue (in male), and bladder and uterus tissue (in female). These were collected from the operating theatre and taken immediately to the pathology department. Initially, the bladder is similar to a balloon thus the bladder was cut and

opened by one of the urological pathologists. After opening the bladder, it was pinned to a corkboard in order to keep it fixed without extensive folding of the bladder wall or applying any tension to the bladder specimen (Figure 4.4). The connection of the probe to the bladder sample and the prepared human cystectomy sample are shown in this figure. Because of the probe fixing and to minimise the applied pressure from the probe to the measured area of the tissue, the probe was passed through a PVC tube:

**The bladder sample connection**

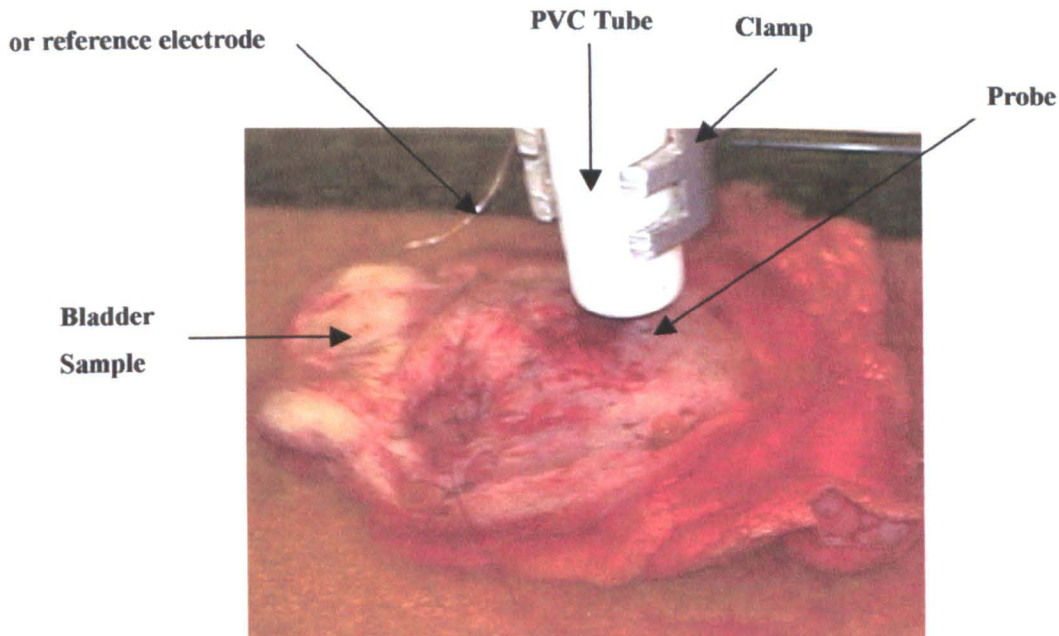


**Figure 4.4 Resected bladder sample under the probe (the bladder specimen was pinned to a corkboard). The diameter of PVC tube is about 3 cm.**

Thus, in this figure, it is shown that the probe was passed through a PVC tube with a bore just wide enough to pass the probe through its centre because the probe must be applied to the tissue with known pressure.

Number	Age	Sex	Reason For Cystectomy
1	63	M	G3pT2
2	69	F	G3pT2
3	70	M	G3pT2 Sarcomatoid tumour and CIS
4	62	M	G3pT2
5	57	M	G3pT2
6	67	F	Interstitial cystitis
7	76	M	G3pT2
8	57	M	Chronic Pyocystis
9	58	M	G3pT2
10	52	M	G3pT1 and Carcinoma in situ
11	71	M	G3pT1 and Carcinoma in situ
12	77	M	G3pT2 and Carcinoma in situ
13	72	M	G3pT2
14	64	M	G3pT2
15	61	F	G3pT2
16	62	M	G3pT2 and Carcinoma in situ
17	60	M	G3pT1 refractory post treatment
18	61	M	G3pT2
19	71	M	G3pT2
20	44	M	G3pT2 with squamous differentiation
21	70	M	G3pT1 and Carcinoma in situ
22	37	F	Painful bladder syndrome
23	71	F	G3pT2
24	72	M	G3pT2
25	68	M	G3pT2
26	46	F	Painful bladder syndrome, post cystoplasty
27	73	M	G3pT3
28	68	M	G3pT2 with squamous differentiation
29	51	F	Benign painful bladder
30	49	M	G3pT2 and Carcinoma in situ
31	57	M	G3pT2
32	63	M	G3pT2
33	65	M	G3pT2 and Carcinoma in situ
34	78	M	G3pT2
35	68	F	Vesico-vaginal fistula following extensive pelvic surgery

**Table 4.8 Age (mostly in their 60's and 70's), sex and reason for cystectomy in 35 *ex vivo* patients**

The effect of applied pressure on the measured impedance will be studied. Thus, it will be shown in this thesis that if the applied pressure increases, the electrical impedance will be increased. This effect appears because the probe compresses the bladder tissue and thus may squeeze out extra-cellular liquids from the probe tissue interface, thus increasing the electrical impedance at low frequencies. Furthermore, the probe must be applied perpendicular to the surface of the bladder tissue to increase the contact surface area between probe and the tissue. The PVC tube was mounted in a clamp to prevent any movement of the probe and allow the measurements to be reproduced. The measurement

procedure using Mk3.a and Mk3.5 Sheffield Systems is different. In the Mk3.a system, the measurement procedure is simple thus 15 impedance spectra are collected immediately after pressing the 'acquire' button (these readings averaged to reduce the noise) but in the second system, there are different settings for the data acquisition unit such as choosing 'Real part', 'impedivity' and 'the number of sampled data'. The number of the sampled for the *ex vivo* study is set to 15 (as for the Mk3.a Sheffield System). The required time for taking 15 impedance spectra is about 22.5 second. After the preparation of the bladder sample, the measurement equipment, Mk3.a or Mk3.5 Sheffield System was used to perform the impedance measurement (Figure 4.5). Before any measurement, all the system connections must be checked, and then the probe must be placed over the sample. Also, the reference lead, in Figure 4.5b must be connected to the tissue.

Figure 4.5 shows the probe attached to the equipment and a laptop connected to the Mark 3.5 Sheffield System to record the measured data from this electrical impedance system. These data were analysed to gain the final results or plots. A probe adaptor connects 4 cables of the probe to the system. Finally, three readings were taken from each point by removing the probe completely from the mucosa and then re-applying it. This was done in order to assess the reproducibility of the measurements. The time required measuring one point under the mentioned condition is a few seconds. Then, punch biopsies were taken exactly from the measured area and were put separately in numbered containers in formalin solution. The punch biopsy size was 3mm (1mm wider than the probe size) for two reasons:

- 1) The orientation of the specimen (mucosal surface) is important. If the sample size is smaller than 3 mm, it will be difficult for the pathologist to orientate and thus, cause difficulties interpreting the histology reports.

- 2) The smaller samples are difficult to handle without any tissue disruption.

The process of pathological assessing these specimens by the pathologist is discussed later. The bladder tissue will be in relaxed state (this will be extended if we measure the impedance of the bladder tissue *in vivo*). It is clear that cell layers, cell sizes and cell shapes are different in relaxed and extended bladder. Therefore, it is expected that resulting impedance of the relaxed and extended bladder will be different. Following this, the state of the bladder will be considered in the bladder structural modelling using

finite element analysis to compare the modelled impedance results with the measured data. The area of specimen that displayed erythema or seemed macroscopically different from the other areas (according to the pathologist's suggestion) were chosen to carry out the measurements and sampled immediately from there. The data from malignant bladder tissue usually also resulted from these areas. Other areas of the bladder tissue were used to give the normal or non-malignant measurements. Readings were performed at room temperature.

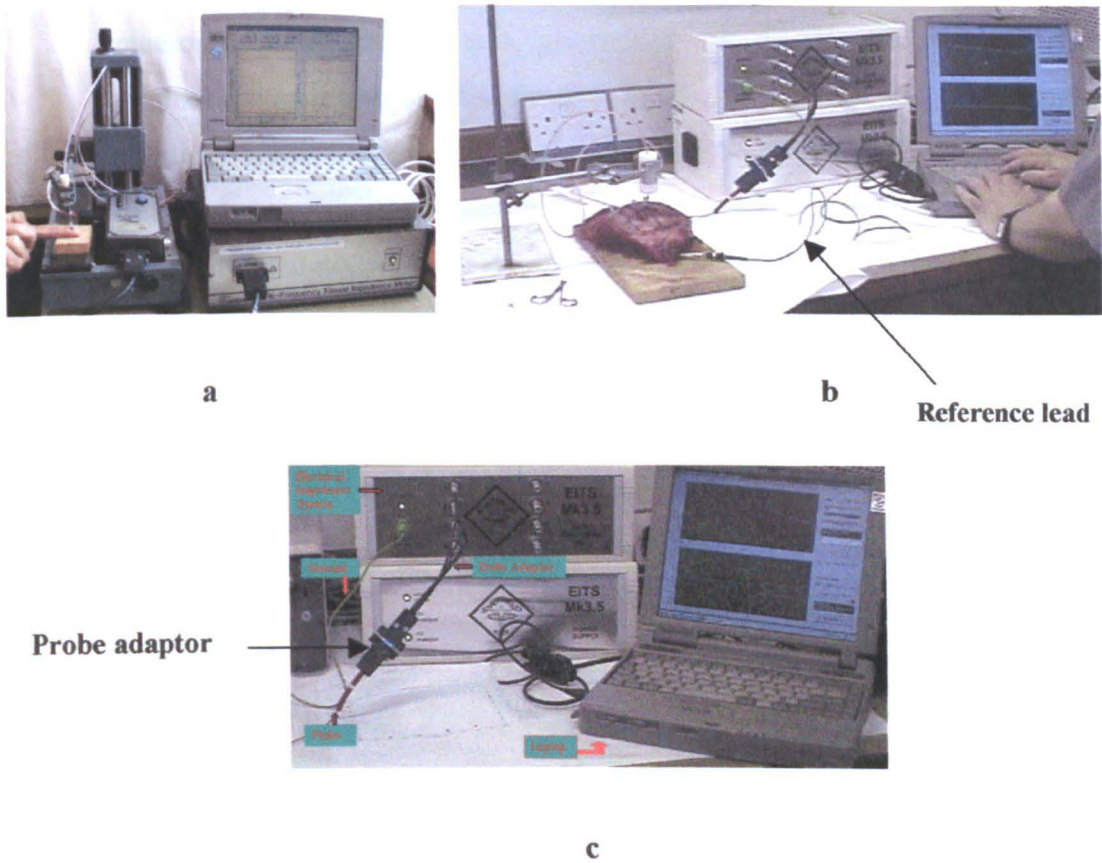


**Figure 4.5 a) Mk3.a Sheffield System b and c) Mk3.5 Sheffield System**

#### **4.4 Biopsy and tissue sampling procedure**

The tissue sampling process is performed in the Histopathology department as follows. Tissue samples were taken from the measurement sites to compare the measured data with the pathological results immediately after impedance measurements. It is very important to discuss the tissue sampling process and the histopathological processing of

tissues because it is the intention to relate any changes in tissue structure to changes in the measured electrical impedance spectrum. After removal of the tissue samples from the body (*in vivo*) or from the excised samples (*ex vivo*), they were put separately in numbered containers with a solution of fixative (to fix the cells of the bladder tissue), formalin solution after which they were sent to the urological pathologist.

Finally, the samples of tissue were processed and then prepared for microscopic examination as follows:

- 1) **Fixation:** After the tissue sample arrived in the histopathology laboratory, a macroscopic description was given and the tissue was selected for light microscope examination. The fixation was made in buffered (10% formal saline) solution. In this process, the tissue structure was fixed by the formation of cross-links between proteins. Thus, it will be in a stable state to assess accurately the normality or abnormality of the tissue.
- 2) **Dehydration:** The specimens were processed through graded alcohols which replaces the water in the samples by pure solutions of alcohol.
- 3) **Clearing:** The alcohol in the samples was removed and cleared in chloroform.
- 4) **Embedding:** The tissue samples were embedded in paraffin wax to make solid tissue blocks.

After the embedding process, the tissue samples can be cut into sections. They were cut at 4  $\mu\text{m}$  thickness using a microtome. Then, the sections were floated on water and transferred to slides. Three sections were placed on each slide. Haemotoxylin and eosin staining was performed on all formalin-fixed, paraffin embedded sections to see the epithelium and tissue morphology. See Figure 4.6

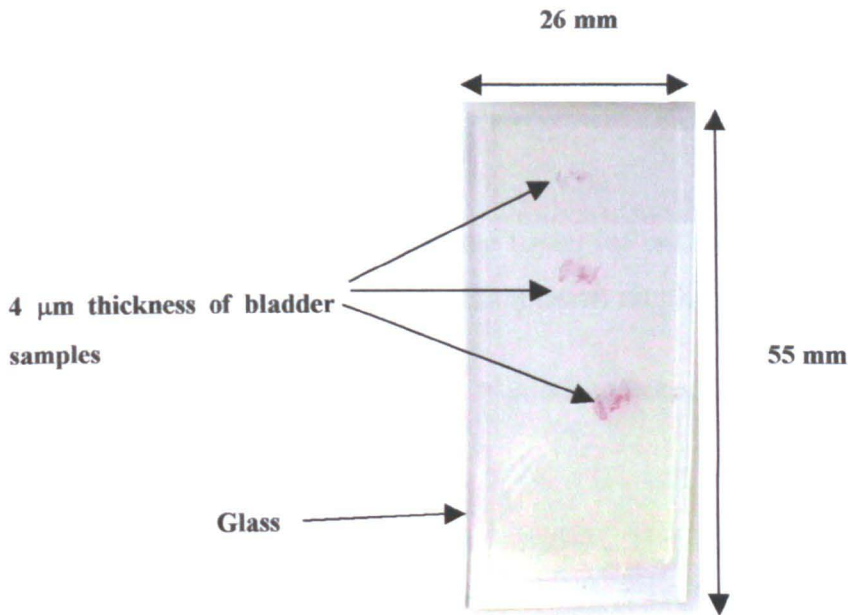


**Figure 4.6 A typical slide of histopathological sections**

#### **4.4.1 Histological classification**

The tissue sample (after initial measurements) was processed and viewed by a urology histopathologist under a light microscope using histopathology slides to determine the organisation and shapes of the cells. According to the reports, changes of the urothelium were classified histologically into seven subgroups. The degree of oedema and inflammation was noted because the effect of these on the measured data of the normal and abnormal bladder will be shown in this research. The histopathological assessment characterised the first 500  $\mu\text{m}$  of the mucosal surface, consistent with the depth of the electrical impedance spectroscopy measurement. There is a sensitivity of about 95% for electrical impedance measurements at this depth in isotropic medium (Gonzales-Correa, Brown et al. 1999). Finally, the specimens were classified according to one of the following schemes:

##### **A. Non -Malignant:**

- 1) Intact Epithelium (E)**
- 2) Ragged Epithelium (R)**
- 3) Denuded Epithelium (D)**
- 4) Denuded Epithelium with Residual von Brunn's nests (DvB)**

## **B. Malignant:**

- 1) Partial Coverage Carcinoma in situ (CISp)**
- 2) Full Coverage Carcinoma in situ (CISf)**
- 3) Carcinoma (Ca)**

A more detailed classification of the tissue for each sample includes separate scores for the degrees of both oedema and inflammation ranging from 0 to 3.

For oedema: (0 = no oedema, 1 = mild oedema, 2 = moderate oedema, 3 = severe oedema).

For inflammation: (0 = no inflammation, 1 = mild inflammation, 2 = moderate inflammation, 3 = severe inflammation).

Patients with aggressive CIS may have denuded epithelium because of epithelium lifting off the underlying lamina propria and this may cause a classification problem for the pathologist (Lee, personal communication).

By using this classification system, scoring the degree of oedema and inflammation and also considering the effects of all the possible parameters on the measurements, we classified disease by the measured bio-impedance of the bladder as explained in the following chapters. The photographs of the epithelium classifications including different degrees of oedema and inflammation (ranging from 0 to 3) are shown in the Figures 4.7 to 4.18 (all of the figures are magnification 100):

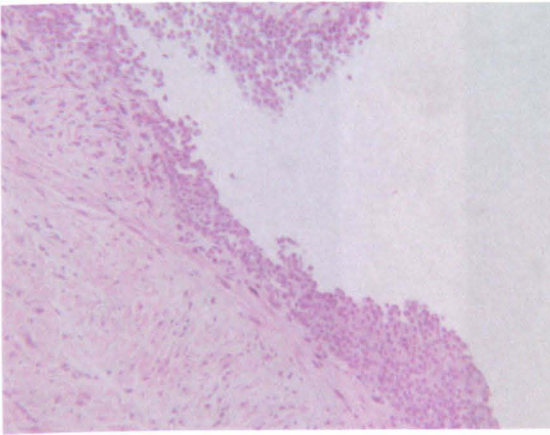


**Figure 4.7 The Normal Epithelium**

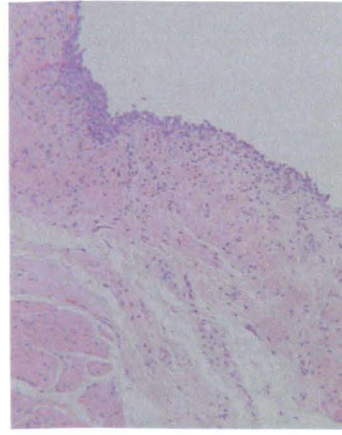


**Figure 4.8 Ragged Epithelium (R)**

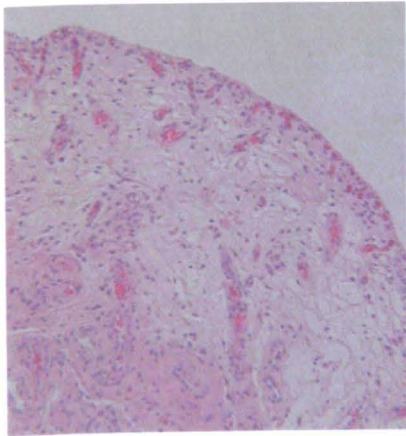


**Figure 4.9 Denuded Epithelium (D)**

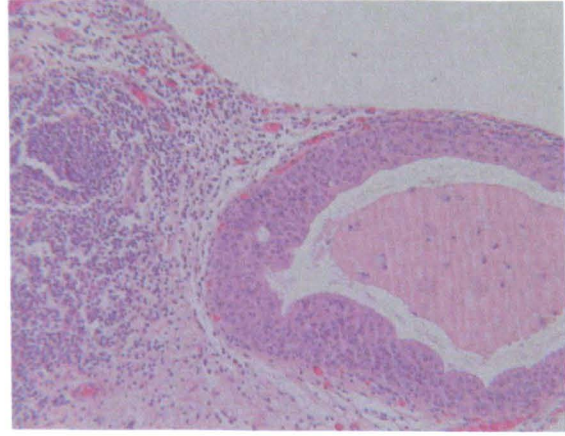


**Figure 4.10 Denuded Epithelium with Residual von Brunns nests (DvB)**

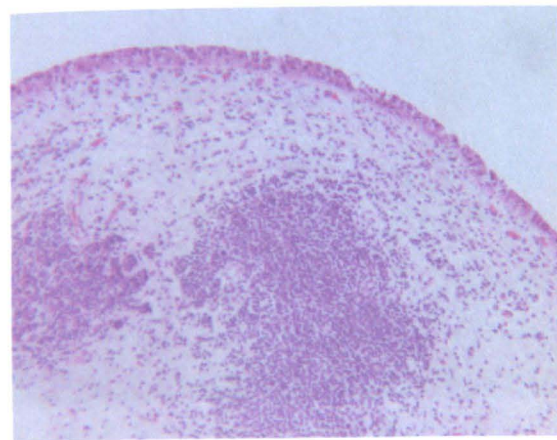


**Figure 4.11 Full Coverage *Carcinoma in situ* (CISf)**

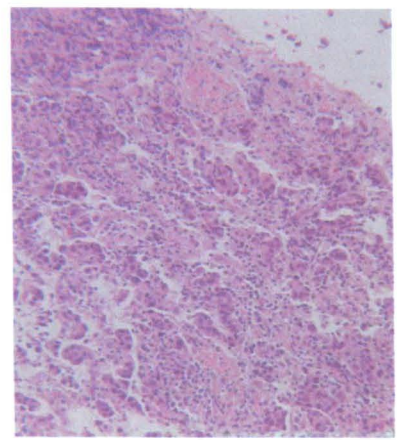


**Figure 4.12 Carcinoma (Ca)**

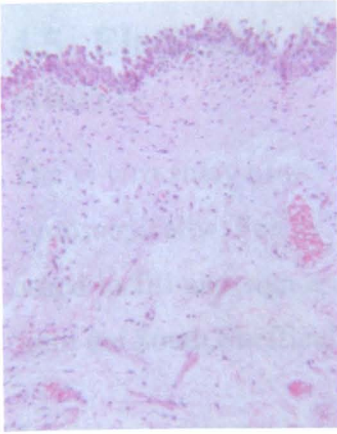


**Figure 4.13 Oedema 1(Mild)**

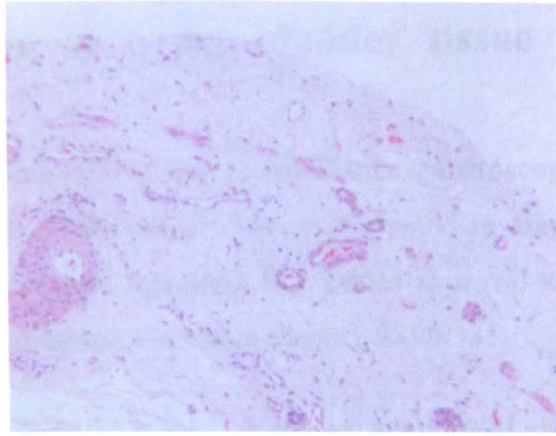


**Figure 4.14 Oedema 2 (Moderate)**

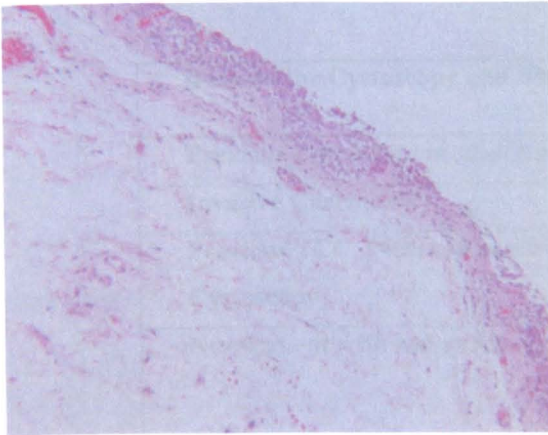


**Figure 4.15 The Oedema 3 (Severe)**

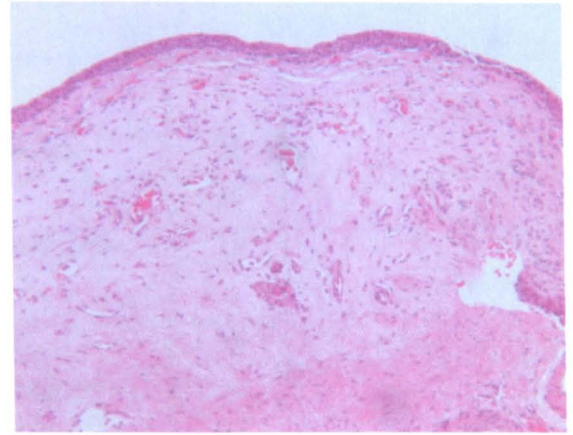


**Figure 4.16 Inflammation 1 (Mild)**

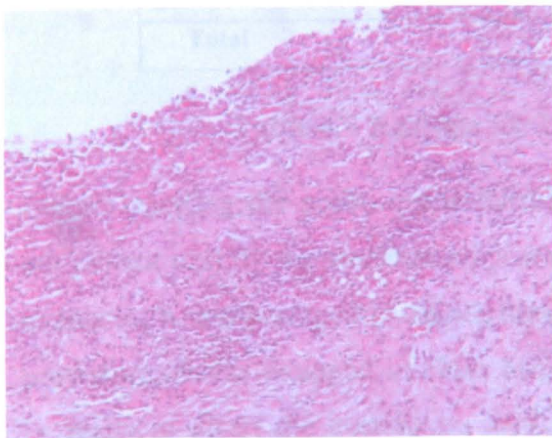


**Figure 4.17 Inflammation 2 (Moderate)**

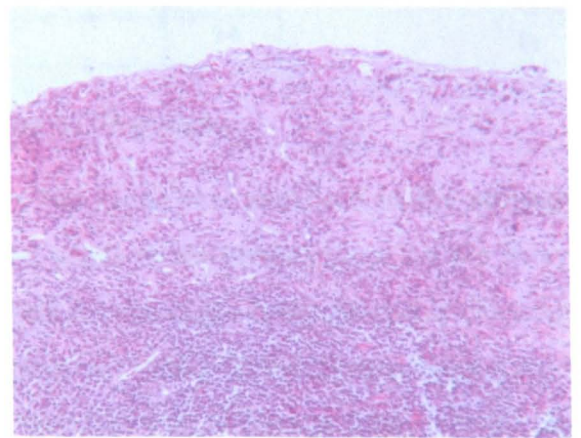


**Figure 4.18 Inflammation 3 (Severe)**

## 4.5 Electrical impedance of living bladder tissue (*in vivo* study)

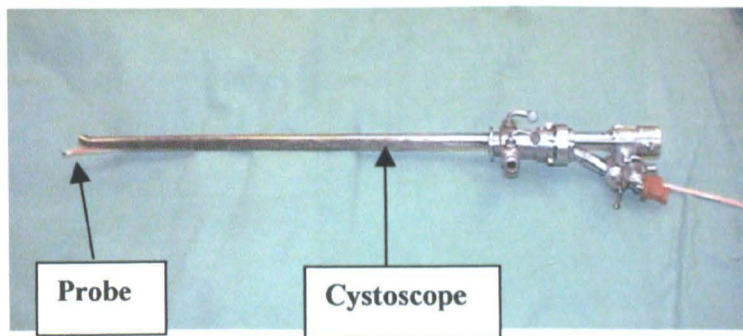
The *in vivo* study of the bladder tissue with electrical impedance spectroscopy was done cystoscopically. For *in vivo* study, every patient who participated in this study was asked to fill and sign a questionnaire. See Appendix (8). Ethics approval was obtained from the South Sheffield Ethics Committee, reference number SS99/335.

*In vivo* measurements were taken from 74 patients between April 2000 and December 2003, at the Royal Hallamshire Hospital in Sheffield. The patients were recruited for various reasons as shown in the following table:

Reasons for Cystoscopy and Biopsies		
Previous <i>Carcinoma in situ</i> /Grade 3 disease		21
Invasive Carcinoma		10
Previous TCC. New red patch seen at flexible Cystoscopy		13
New Patient with red patch	With concurrent TCC	16
	Without TCC	7
Previous TCC, 3 months check post resection		5
Other (1 Irritative symptoms small bladder, 1 Interstitial Cystitis)		2
Total		74

**Table 4.9 Reasons for biopsies in 74 patients**

Before inserting the probe inside the bladder, the probe was sterilised in the urology out-patient unit. In the sterilisation process, the whole of the probe except for the 9way connector was submerged in the sterilising liquid for about one hour. After this cleaning procedure, it was wrapped in clean tissue papers to transfer to the theatre. This would be ready to insert the cystoscope inside the bladder. The following figure shows the cystoscope including sterilised probe and whole of the measured system (Mk3.5), which is set up for *in vivo* work:



a

Connection to the patient  
body (reference electrode)



b

**Figure 4.19 a) Cystoscope including probe b) Cystoscope and whole measurement system**

For following the *in vivo* impedance measurement method, the surgeon usually inspected the whole of the urinary bladder using a flexible cystoscope. In this procedure, the cystoscope was inserted inside the bladder to find abnormal points within the bladder to perform our measurements. When an abnormal area was identified, this area was marked using 'Indigo Carmine' via a 1 mm diameter sclerosing endoscopy needle (Diagmed, UNO-JECT, ref. AS0081018). The 'indigo carmine' is a blue coloured liquid. This 'needle' and 'Indigo Carmine' are shown in the Figure 4.20:

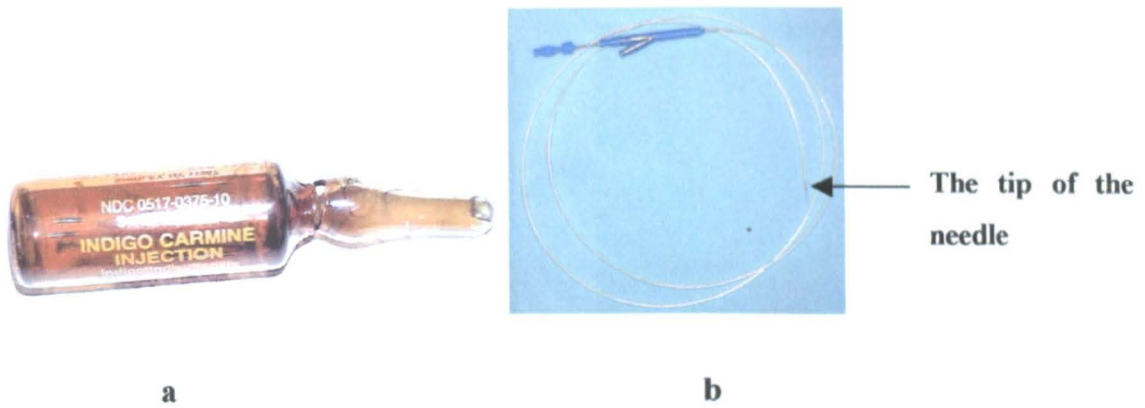


**Figure 4.20 Indigo carmine (a) and Sclerosing endoscopy needle (b) used to mark inside of the bladder to choose the impedance measurement point and then taken the biopsies from this point.**

Diathermy equipment (using electrical heat and spark to mark the tissue) is usually used to mark inside of the bladder to select one point of the urinary bladder tissue in operating procedure. It was not used because it could affect the electrical impedance measurements by burning the tissue in measurement area. Therefore, the dye method was used to mark the measured point of the bladder for *in vivo* study. It was expected that the indigo carmine injection into the bladder tissue would cause minimal tissue disruption to subsequent electrical impedance measurements.

In addition, the measurement point is about 5 mm away from the colour marked point, thus the author tried to cancel any possible side effects of the injected colour liquid on the measured real impedance of the bladder tissue. After coloured marking the bladder, the cystoscope (including the probe) was inserted inside the bladder immediately and then it was used to find the marked points to perform impedance measurements. Finally, the impedance readings were taken from near the marked point (about 5 mm away) using the probe inside the cystoscope. The Figure 4.21 shows this process.

It was usual that two or three points were chosen for measurement purpose in this work. A biopsy was then taken immediately from the same point in order to correlate readings with biopsies as in the *ex vivo* cases. These biopsies were placed in formalin in separate pots and then sent for histopathological analysis (as in *ex vivo* study) to identify its pathological status and different degrees of oedema and inflammation.

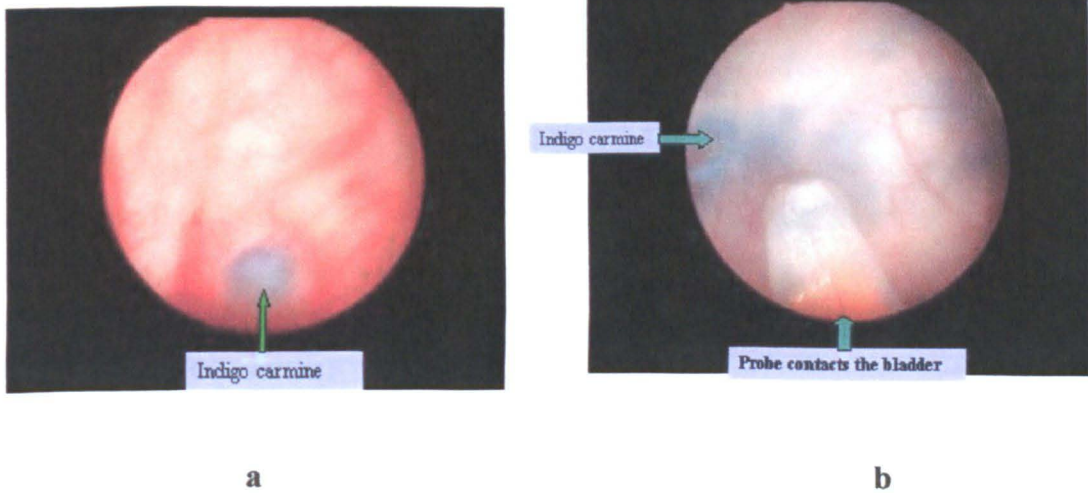


**Figure 4.21** One of the cystoscopy photos of the inside of the bladder a) A blue mark has been made with the indigo carmine b) Probe contacts the bladder tissues near the blue area

## 4.6 Data acquisition, storage and analysis

### 4.6.1 Introduction

Bladder cancer, especially carcinoma *in situ* is one of the most important cancers to diagnose for humans. As mentioned in Chapter 1, carcinoma *in situ* is an aggressive form of bladder cancer and highly invasive if left untreated. This flat lesion cannot be differentiated cystoscopically because it appears as a red patch and there is no significant difference between this lesion and a simple inflammation or other erythematous, benign areas of the urinary bladder. Therefore, the only way to diagnose this important lesion is to analyse the randomly taken biopsies from the red areas (definitive diagnosis); other diagnostic techniques to detect carcinoma *in situ* remain experimental. Some researchers have shown that the electrical impedance measurements can differentiate cervical interstitial neoplasia from normal cervical tissue, and squamous from columnar tissue in the oesophagus. Following this, the effectiveness of this minimally invasive technique was assessed to characterise various pathological changes, especially to differentiate carcinoma *in situ* from the normal urothelium in the human urinary bladder (*ex vivo* and *in vivo*). Therefore, the main aim of this study was to develop a non-invasive and novel screening technique to distinguish malignant and non-malignant areas in the urinary bladder. This chapter will explain the impedance data acquisition; storage and analysis procedure of the impedance readings taken from

freshly excised human bladders (*ex vivo*) and the bladders of patients in theatre (*in vivo*) from March 2000 to September 2001. Two different electrical impedance spectroscopy systems (Mk3.a and Mk3.5 Sheffield Systems) were used in this study. In addition, an improved Mk3.5 Sheffield System that is able to measure the impedances at lower frequencies than the two above-mentioned systems was used for the *in vivo* study from March 2003 to December 2003.

#### 4.6.2 Data acquisition

Before any data acquisition procedure, a patient information and impedance measurement form was used to provide useful information on each patient (*in vivo*) and each resected bladder (*ex vivo*). This was slightly different for the spectroscopic systems (Appendix 9). In addition, the laptop screen that connected to the impedance measurement system to take the impedance data from the bladder tissue was slightly different for these systems. Figure 4.22 demonstrates the screen of a laptop connected to the Mk3.a Sheffield System.

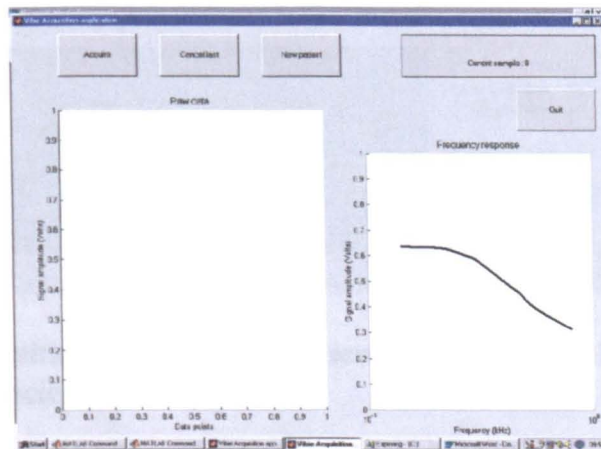


**Figure 4.22 Data acquisition on laptop screen: Mk3.a Sheffield System**

The laptop screen for the Mk3.5 Sheffield System (2 KHz-1.5 MHz) and its improved version to measure the impedance at lower frequencies (62.5 Hz-1.5 MHz) is shown in Figures 4.23 and 4.24. These figures clearly demonstrate the measurement conditions that must be set before each measurement and then applied at the time of impedance readings using the data acquisition button. Then, after a few seconds, about 5 seconds for the Mk3.a and the Mk3.5 Sheffield Systems (to take 10 readings and find the average) and about 10 seconds (to take 5 readings and find the average) for the improved version of the Mk3.5 Sheffield System, we can take other measurements.

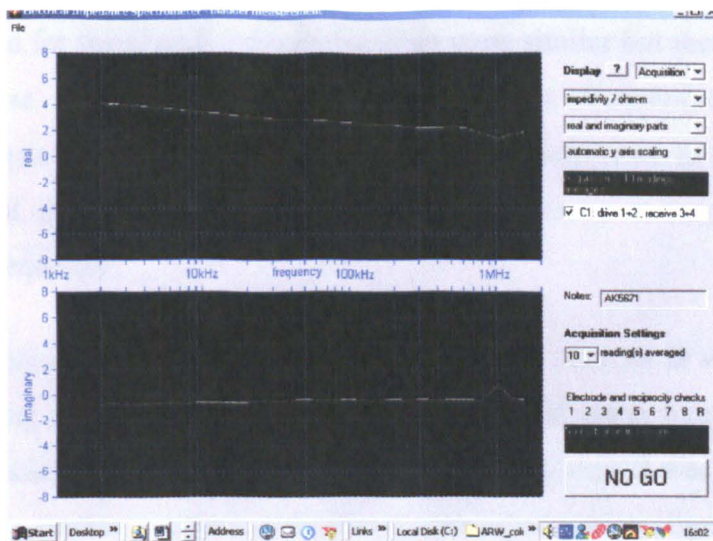


**Figure 4.23 Data acquisition on the laptop screen: Mk3.5 Sheffield System**

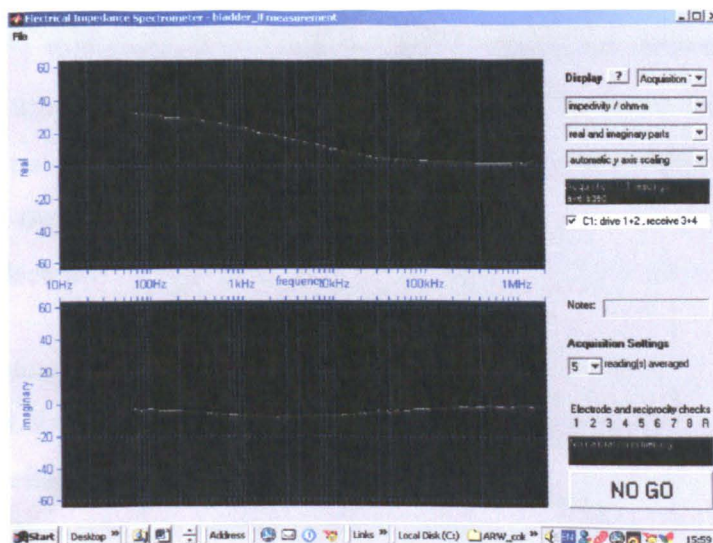


**Figure 4.24 Data acquisition on the laptop screen: Improved Mk3.5 Sheffield System for lower frequencies**

The laptop screen of the measurement system shows the electrical impedance measurement settings of one typical impedance measurement of bladder tissue including a typical measured data (real part of impedance against frequency). The upper parts of the screen in Figures 4.23 and 4.24 show that for the Mk3.5 system, the real part of impedance was taken under the following conditions shown on the right hand side of the screen:

- impedivity / ohm.m, -real and imaginary parts, -automatic y-axis scaling, -drive 1+2 and receive 3+4
- acquisition settings for 10 readings averaged (Mk3.5) and 5 readings averaged (improved Mk3.5).

These conditions for the Mk3.5 improved system were similar but there were 5 averaged readings because this system was working at lower frequencies and hence the measurement time had to be increased. The measurement time is determined by the requirement that the time frame has to contain the exactly one cycle of the lowest measurement frequency

It must be mentioned that the improved system was used only for *in vivo* studies and the main aim of using this system was to evaluate the effect of lower frequencies (from 62.5 Hz) on the transfer impedance of the human urinary bladder. It was expected that this lower frequency system would provide better separation of malignant bladder tissue from the benign tissue. Furthermore, the author added the results of this system to the measurements resulting from the Mk3.5 system (*in vivo*) to increase the measured points, especially malignant points, to assess the difference between malignant and benign human urothelium as accurately as possible. We were interested in taking readings from patients usually under anaesthesia (*in vivo*), with the minimum of interference in the surgical procedures; thus the number of readings (acquisition settings) was selected at 5 to give a measurement time of about 10 seconds.

Finally, by pressing the data acquisition button, impedance readings were saved on the laptop hard disk for each point separately for further data analysis. These data will be analysed in this chapter.

### **4.6.3 Data storage**

The storage of data on computer after taking impedance readings and saving temporarily on laptop hard disk was carried out using Matlab *structures*. *Structures* are Matlab arrays with named 'data containers' called *fields* which can contain any kind of data. It was thus possible to save patient data, histological results and numerical data in a structured and searchable form. The instructions to produce the necessary files are demonstrated in Appendix 10. The 7 frequency data for the Mk3.a, 30 frequency data for the Mk3.5 and 60 frequency data for the improved Mk3.5 plus the respective histopathology reports (normal, epithelium denuded, ragged epithelium, carcinoma, carcinoma *in situ*, the degree of inflammation and oedema) were transferred to these files. Therefore, in this step both the two numerical data and the related histopathology reports were transferred into a 'data base file' for further analysis. The added numerical and histological reports process can be summarised as following: A Matlab m.file,

AppendRecord applied to each measured point (new\_data) to find the new 'data base file' (OutputFile). 'InputFile' was the file before the current impedance measurement. Thus, the instruction in Matlab was:

```
function[]=AppendRecord(InputFileName,OutputFileName,new_data)
```

An 'AppendRecord' m.file is added as Appendix 11. Finally, all numerical (impedance data) and histopathological reports of patients used in this work were transferred to the following databases subject to *ex vivo* or *in vivo* studies for further analysis in the next section:

For Mk3.a Sheffield System: Bladder\_Data\_Mk3a\_Ex\_23, Bladder\_Data\_Mk3a\_In\_36

For Mk3.5 Sheffield System: Bladder\_Data\_Mk35\_Ex\_16, Bladder\_Data\_Mk35\_In\_20

#### **4.6.4 Data analysis**

The data analysis presented in this chapter is an analysis of electrical impedance readings taken on freshly excised human bladders (*ex vivo*) and from patients with undiagnosed erythematous areas of their bladders (*in vivo*). In addition, the process of data fitting programmes will be presented in this section to obtain scatter plots that can reasonably distinguish the malignant and non-malignant areas of bladder tissue.

##### **4.6.4.1 Data extraction and classification**

The aim of this section is to extract and classify the mean spectra of measured impedance data (real part) and the histopathological reports of each measured point and then sort them into separate arrays by applying an m.file on the data stored in data base files. This m.file was called 'GetClassifiedSpectra' as follows:

```
function[..]=GetClassifiedSpectra...(InputFileName)
```

It is shown for clarity as in the following example for the data extraction from the *Ex vivo* state of the Mk3.a system:

```
[E_1_3Spectrum,E_1_2Spectrum,Ca_3_0Spectrum,Ca_1_1Spectrum,...]=  
GetClassifiedSpectraExVivoMK3a(InputFileName)
```

In part (1), all of the measured impedance data related to each histopathology report and the reports are written, e.g., Ca\_3\_0Spectrum (the impedance of carcinoma point of the bladder including the degrees of 3 for inflammation and 0 for oedema respectively). In part (2), 'InputFileName' is the data base file called 'Bladder\_Data\_Mk3a\_Ex\_23' and including all of the impedance data and histopathological reports related to all measured points of the resected bladders of 23 patients (*ex vivo*). The final results of this data extraction and classification procedure is an array of data such as 'Non\_malignant Spectrum' and 'Malignant Spectrum' that demonstrates several arrays of impedance readings related to benign and malignant areas of 23 resected bladders respectively using the Mk3.a Sheffield System. This procedure was applied for oedema and inflammation data and also for *in vivo* and the data of the other measurement system. The malignant and benign classifications are shown in 4.4.1. Finally, the author used the histopathological reports to analyse the impedance data to plot different forms of graphs to evaluate the difference between benign and malignant areas of the urinary bladder especially to characterize the carcinoma *in situ* from the erythematus or inflamed areas of the bladder. These graphs will be discussed in Chapter 5.

#### 4.6.4.2 Fitting a model to the measured data

The fitting process, such as the Cole equation fitting programme, yields an equation that is a description of the measured data. There are different forms of fitting process and important parameters of Figure (2.5) such as  $R$ ,  $S$  and central frequency ( $f_c$ ) of the tissue that are used to characterise tissue in terms of electrical impedance. Therefore, this involves fitting a theoretical expression to the measured data at many points and if more and more parameters are used (if possible), the accuracy of the fitting will be increased and thus a good fitting of models to the measured data may be obtained. The fitting method used a 'least squares minimization algorithm'. This programme minimises the difference between the measured data ( $Z_a(f_i)$ ) and values predicted by model ( $Z_b(f_i)$ ) at different frequencies and uses the following equation:

$$y = \text{least squares minimization} = \sum_{i=1}^N [Z_a(f_i) - Z_b(f_i)]^2 \quad (4.1)$$

Where,

$N$  = The number of frequencies ( $N=7$  for Mk3.a Sheffield System)

$f_i = 9.6 \text{ KHz}-614.4 \text{ KHz}$ ,  $Z_a(f_i)$  = The impedance of measured data at  $i$  th frequency

$Z_b(f_i)$  = The impedance of modelled data at  $i$  th frequency.

In accordance with this equation, the reduction in the value of  $y$  indicates that the modelled data are approaching that of the measured data. Lower noise levels will give lower values for  $y$ . However, noise is always present in the measurements, and, thus, the best-fit curve will be always non-zero. The parameters used in the fitting process can be used to distinguish differences between the malignant bladder tissue and benign area. Lu et al used the Cole equation fitting programme to fit to the measured data (Lu, Brown et al. 1995). They used  $R$ ,  $S$  and central frequency ( $f_c$ ) as fitting parameters because these parameters play an important role in impedance measurements of the tissue. There is further discussion about this method in their published paper. Also, three parameter modelling was introduced by Lu et al (Lu, Hamzaoui et al. 1996). They discuss three methods of fitting the Cole equation to measured data (using only real part, using both real and imaginary parts by fitting these parts separately and using these two parts by fitting simultaneously). Comparing these methods, it is clear that the first method (using only the real part) was normally less noisy than the others. They used the measured data of animal tissues (*in vitro*) to demonstrate a close fit to the Cole equation using only the real part of the electrical impedance. In accordance with the above discussion, only real part of measured impedance was used in this work to fit the Cole equation to measured data of the bladder tissue. The fitting software (Matlab-m.file) that the author used in this study to fit the data was written by A. R. Waterworth (Waterworth 2000). These models allow comparison between different tissue types. The Cole equation gives an impedance profile similar to those obtained from the tissue electrical impedance measurements (real and imaginary components) thus, the Cole equation can describe the measured data. Therefore, the Cole equation fitting process can be applied to the measured data to quantify changes in tissue states from normal to abnormal. For example, Brown used this method to differentiate between normal and abnormal cervical tissue (Brown, Tidy et al. 2000). A suitable statistical test to evaluate the differences between these groups is the other aim of this section.

#### 4.6.4.3 Statistical method

In this study, it is usual that two groups of measured impedance data are compared with each other; thus, to study the difference between these groups it must be determined whether they are related or independent groups. Therefore, one must consider use of suitable statistical tests to evaluate the significance of differences between these two groups. As the measured impedance data related to these groups demonstrated, it was impossible to consider all of the corresponding sets of data as normally distributed (i.e. the data had evidence of non-compliance with the Gaussian or Normal distributional assumptions). Thus, this excluded the application of statistical tests based on Gaussian distribution. Therefore, a non-parametric test was needed in this work. However, there are several statistical tests in non-parametric statistics: Chi-Square, Wilcoxon-Mann-Whitney test and Kolmogorov-Smirnov-Two-Sample test.

The Chi-Square test for two independent groups may be used to show the significance of differences between two independent groups. The data used in this test must consist of frequencies in discrete categories, thus it cannot be used in this study. On the other hand, the Wilcoxon-Mann-Whitney test can be used if at least ordinal measurement has been achieved for the variables and thus there is an assumption that limits the application of this test for the measured impedance data in this work. Finally, the Kolmogorov-Smirnov-Two-Sample test, that is a non-parametric statistical test, can be used to determine whether two independent samples have been drawn from populations with the same distribution. No assumptions are made about the data distribution of two measured groups using this test. To apply this test, one determines the cumulative frequency distribution for each group. In this test, two groups in a cumulative frequency distribution are arranged, then by subtraction, the difference between the two groups' cumulative distributions at each point is determined. Then the largest difference is chosen to determine that. The Kolmogorov-Smirnov-Two-Sample test is more powerful in all cases than Chi-Square test. It also seems to be slightly more efficient than the Wilcoxon-Mann-Whitney test for small samples, but for large samples the converse is the case (Siegel 1988). The author used both SPSS software and a Matlab programme to apply the Kolmogorov-Smirnov-Two-Sample test for the measured impedance data.

## 4.7 Conclusions

The calibration of the probes using known conductivity of the saline solutions was carried out in this chapter in both impedance spectroscopy systems used in this work. Also, the impedance measurement methods (*ex vivo* and *in vivo*) were discussed to take impedance readings from the urinary bladder. Then, the tissue sampling process was described because it is common that a small sample of tissue is taken from the site of the electrical impedance readings to compare the measured data with the pathological results immediately after impedance measurements. After that, the processing of tissue samples by a urology histopathologist and a classification of tissue specimens according to their reports was explained. Finally, data acquisition, storage and analysis were discussed in detail to arrive at a reasonable evaluation of the electrical impedance of the bladder tissue in benign and malignant states. The result of impedance readings for these two types of bladder tissue and the differentiation between these readings will be presented in the next chapter.

## **Chapter 5**

# **Electrical impedance measurements in urinary bladders**

## **5.1 Introduction**

The results presented in this chapter are related to the analysis of measured data taken on freshly excised human bladders (*ex vivo*) and the patients under anaesthesia (*in vivo*). In addition, data analysis related to each impedance measurement point is compared with the analysis of biopsies from the same point of the bladder as an existing gold standard bladder cancer technique.

## **5.2 Electrical impedance measurement results and discussion**

Two spectroscopic systems, Mk3.a and Mk3.5 Sheffield Systems were used in this study. The results of the data analysis of the bladder tissue transfer impedances will be compared with the analysis of biopsies taken from the same points and then the final results will be discussed to characterise the human bladder urothelium.

### **5.2.1 *Ex vivo* study**

In *ex vivo* work, 305 points (from 35 freshly excised bladders from patients) were studied in terms of their biopsy reports (histopathological analysis) matching them to the electrical impedance measurements. 32 points have been discarded (19 points because of difficulties in identifying the mucosal surface histologically; and, 13 points due to difficulties with poor impedance recordings or data interpretation).

#### **5.2.1.1 Mk3.a Sheffield System results and discussion**

The author began this work using the first system (Mk3.a Sheffield System) at 7 frequencies and measured the resected bladders of 23 patients in March 2000. The number of points measured was 158, but the number of records that have not been classified due to difficulties with data interpretation was 20. Thus, the number of electrical impedance readings from these resected bladders was 138 (116 points non-malignant and 22 points malignant as indicated by histology). However, after several months, the new system (Mk3.5 Sheffield System) that includes a wider range of frequencies than the Mk3.a Sheffield System became available; thus it was decided to

use this system. The new system can work at lower and higher frequencies than the old system and so were of interest in this study.

### 5.2.1.1.1 Reproducibility of the impedance readings

After taking 3 independent readings per point from the human bladders (to show the reproducibility of these readings), the measured data were analysed using both the probe calibration process and computer based Matlab software. These readings were usually not more than 8% difference. The following figure demonstrates one of the plots to evaluate the reproducibility of the impedance readings of the bladder tissue:

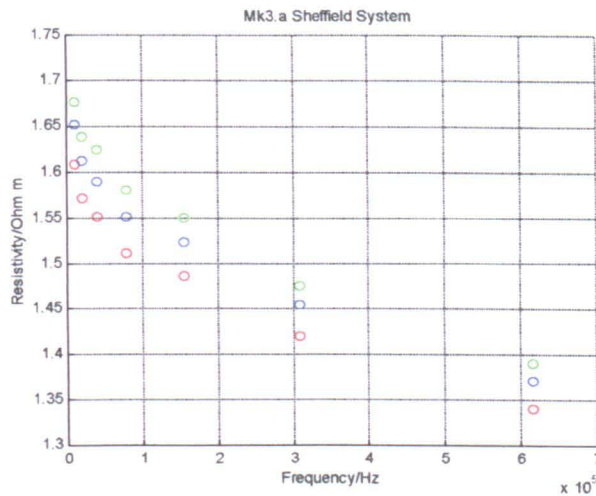
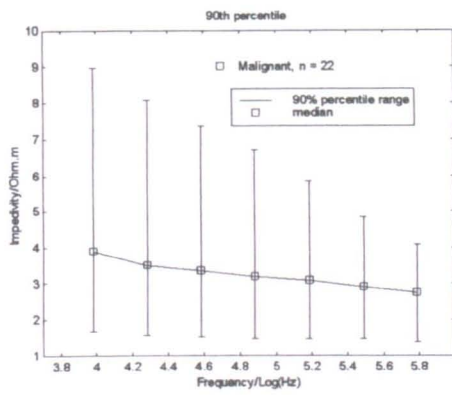


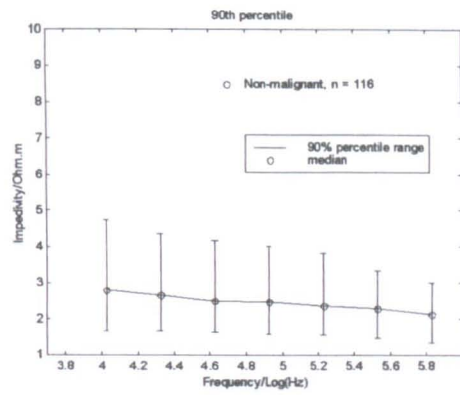
**Figure 5.1 Evaluation of reproducibility of the measured data using 3 independent readings per point**

### 5.2.1.1.2 Separation of malignant impedance from the benign

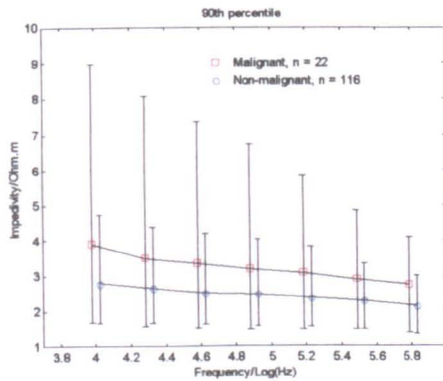
After calculation and mathematical analysis of measurements using both the probe calibration process for the chosen probe in every reading and computer based Matlab software, the effect of malignancy on benign bladder tissue readings was identified. Figure 5.2 demonstrates the difference of impedance between benign and malignant areas of the bladder tissue. Figure 5.2a and b show the median and 90% percentile ranges for malignant and non-malignant areas respectively and c shows the comparison for the range of impedance for the two groups (the 90% percentile range is defined as the range of values which contains 90% of the data). The error bars in Figure 5.2d demonstrate standard error of mean.



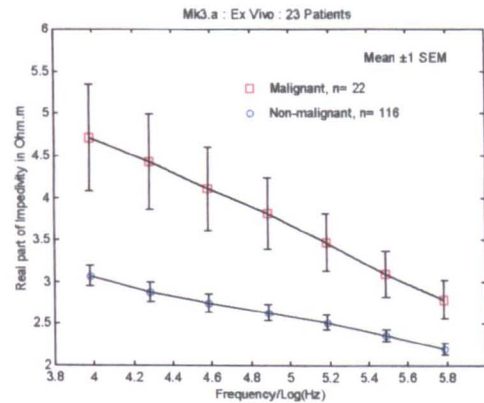
a



b



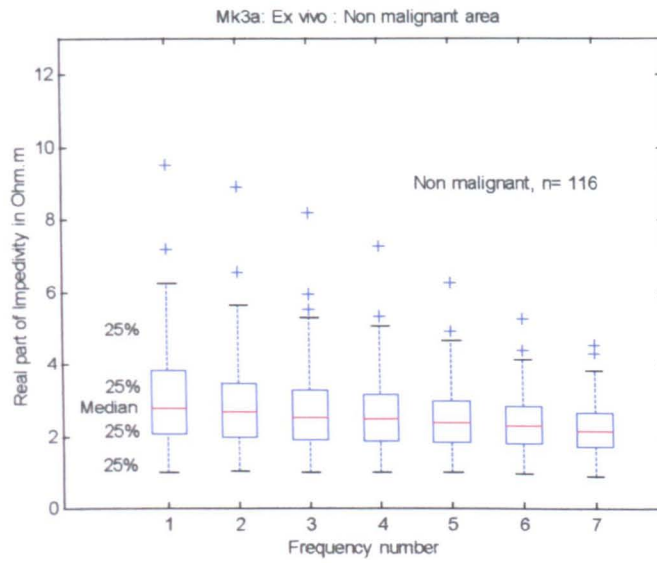
c



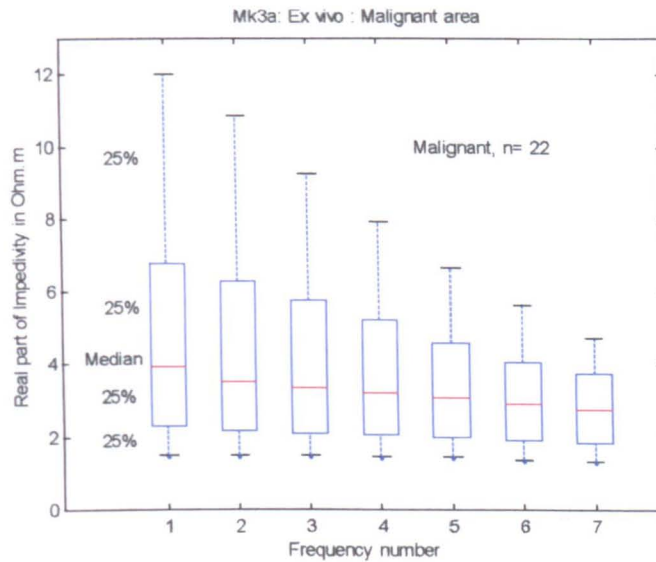
d

**Figure 5.2 Median and 90% percentile ranges for malignant (a) and non-malignant (b) points of the bladder tissue separately and together (c). d) Real part of impedivity versus log of frequency for normal and malignant bladder tissue in the Mk3.a Sheffield System**

In addition, the statistical analysis in Matlab, boxplot m.file (the MathWorks) was used to determine how the malignant and benign impedance spectrum was distributed accurately to choose a reliable statistical test to compare the impedance in both pathological and normal groups (Figure 5.3). This means that the type of data distribution has an important role in the selection of statistical method.



**a**



**b**

**Figure 5.3 The distribution of measured impedance data in non-malignant (a) and malignant (b) areas of the urinary bladder using Mk3.a Sheffield System**

According to these plots, the measured data in two groups are not normally distributed in 4 different vertical areas (the areas that include 25% of readings). Therefore, this measured impedance for benign and malignant points had evidence of non-compliance with the Gaussian or normal distributional assumptions (to use a parametric test) for both malignant and non malignant areas. Following this, the author used a non-parametric test, Kolmogorov-Smirnov-Two-Sample test to evaluate the difference

between these two benign and malignant groups. According to calculations of data resulting from measurements using the Mk3.a Sheffield system for assessing the malignant and non-malignant tissue, the impedance of the malignant group was higher than that of the non-malignant group at all of the frequencies according to the Kolmogorov-Smirnov 2 Sample Test ( $p < 0.01$ ). See Figure 5.2d. The box plot can be expressed as the following figure:

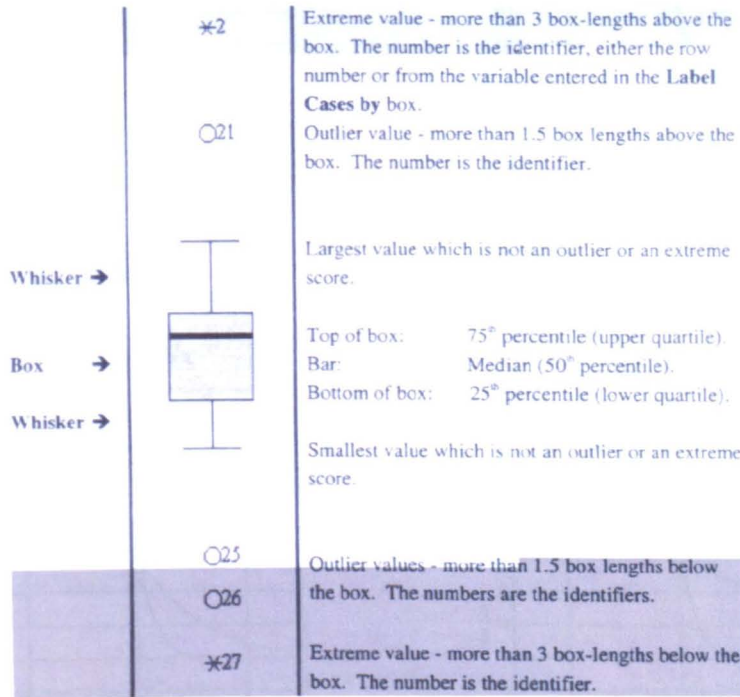


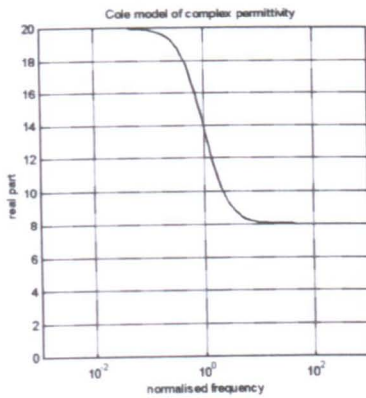
**Figure 5.3c Structure of a box plot display**

However, it is clear from these results that classification of individual samples as malignant or non-malignant is not possible in this data set because of the large degree of overlap of the two groups.

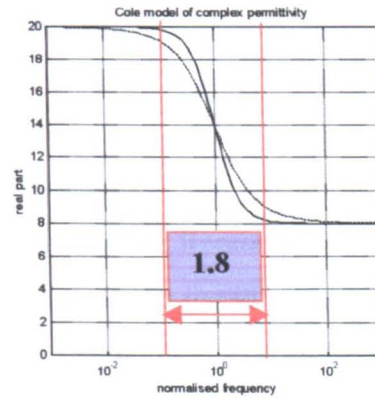
### 5.2.1.1.3 Evaluation of impedance spectrum linearity

If we plot the real part of permittivity spectrum against frequency for different values of  $\alpha$ , ( $0 < \alpha < 1$ ) in equation 2.18, the resulting plots are shown in Figure 5.4. In this figure, for  $\alpha = 0.2$ , the curve is expected to be the spectrum of permittivity or impedivity for the bladder tissue because the value of  $\alpha$  for the many tissue samples is about 0.2 (Brown, Leathard et al. 1995). The logarithm of the lowest frequency (9600 Hz) using Mk3.a System is 4 and the logarithm of the highest frequency (614400 Hz) is 5.8. Thus, the difference between these values will be  $5.8 - 4 = 1.8$  decade and hence, the

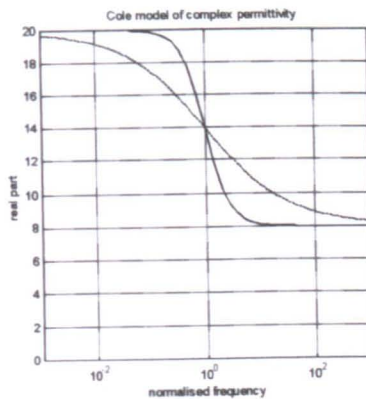
impedance spectrum occurs in this area (red area) of Figure 5.4b. If the centre frequency for the tissue lies at the mid-point of the measurement range, the tails of the sigmoid curve will not be seen. And the distribution will appear to quasi-linear. Therefore, the value of  $\alpha$  and the used lower and higher frequencies have an important role in controlling the shape of the curve (impedivity against frequency) from a sigmoid ( $\alpha = 0$ ) to a straight line ( $\alpha = 0.8$  or higher).



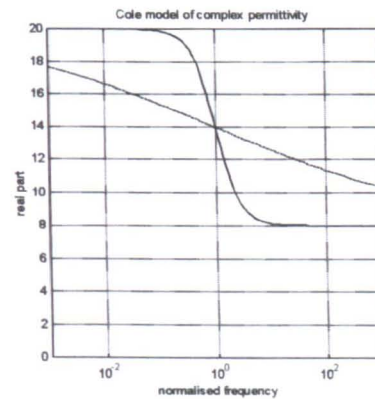
a)  $\alpha = 0$



b)  $\alpha = 0.2$



c)  $\alpha = 0.5$



d)  $\alpha = 0.8$

**Figure 5.4** The real part of permittivity against frequency using assumptions such as:  $\epsilon_{\infty}=8$ ,  $\epsilon_0=20$ , shows that for the different values of  $\alpha$ , the shape of this spectrum is changing from a sigmoid ( $\alpha = 0$ ) to a straight line ( $\alpha = 0.8$  or higher). Dashed lines demonstrated the shape changes using different values of  $\alpha$

The Cole equation predicts a sigmoid curve for the impedance spectrum. However, both the malignant and benign impedance spectra in this study appeared essentially linear (this is shown in Figure 5.2d).

#### 5.2.1.1.4 The Cole equation fitting

The Cole equation was fitted to the measured data in this work. As mentioned before, the fitting software (Matlab-M.file) that the author used in this study to fit the data was written by A. R. Waterworth. He introduced CNLSFIT software (Complex Non-linear Least Squares Fitting of the Cole equation to measured or simulated data) (Waterworth 2000). The parameters  $R$ ,  $S$ ,  $C$  and  $\alpha$  were used as fitting parameters. The real part of impedivity was used to separate malignant points from the benign area of the urinary bladder. The fitted parameter  $\frac{R}{S}$  from the Cole model was used to create scatter plots.

These plots show individual values of impedance differences of the bladder impedance measurements. The natural logarithm of resistivity at the lowest frequency ( $R$ ) over the resistivity at the highest frequency ( $S$ ) was plotted against the resistivity at the lowest frequency for benign and malignant bladder tissue using the Cole equation fitting (Figure 5.5). Almost all the measured data were acceptable because there were only 4 data cancellations due to poor measurement procedures between non-malignant data. This figure shows the resistivity of malignant points is approaching the right hand side. It is clear from Figure 5.5 that the electrical impedance of malignant bladder tissue is generally higher than the non-malignant tissue, but that classification of individuals is not possible in this data set.

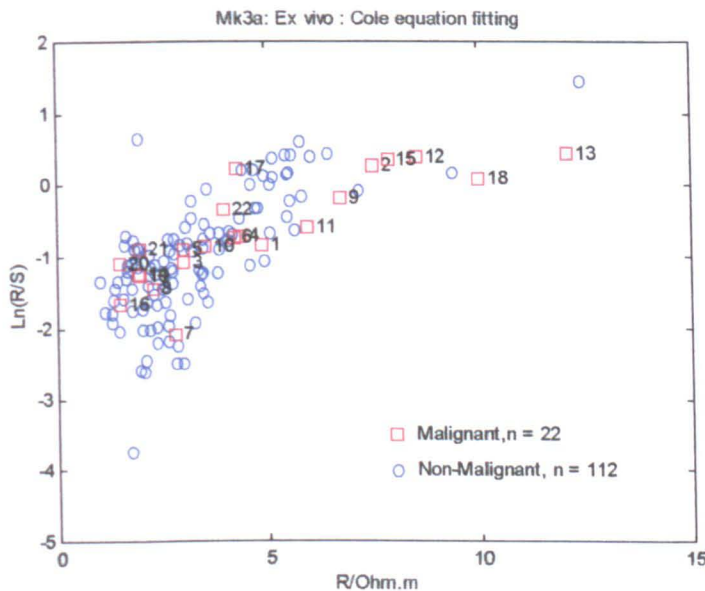


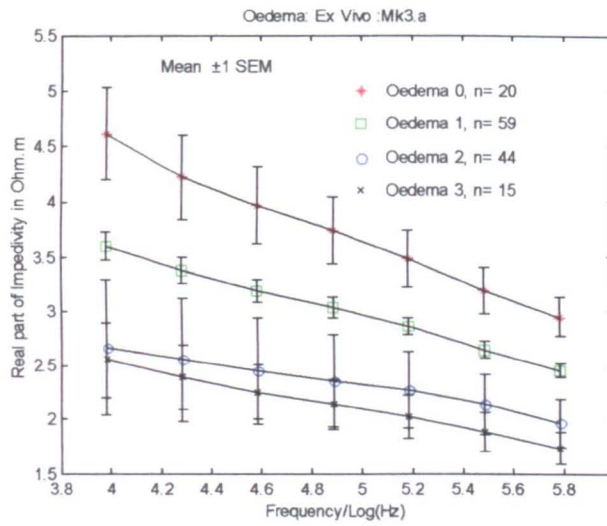
**Figure 5.5** The Cole equation fitting for benign and malignant bladder tissue in the Mk3.a Sheffield System (the numbers show the position of 22 malignant points exactly)

### 5.2.1.1.5 The effect of inflammation and oedema on measured impedance

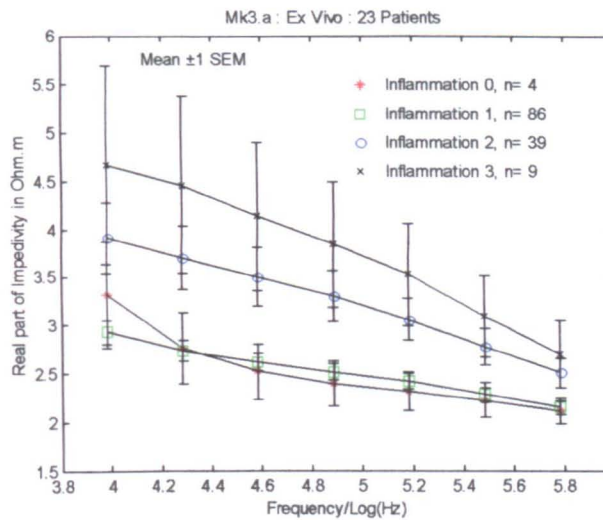
Although the grouped data are significantly different, Figure 5.5 shows that it is not possible to classify individual measurements directly. Cervical measurements demonstrated that malignant and non-malignant epithelial tissue could be separated on an  $\frac{R}{S}$  against  $R$  scatter plot (Brown, Tidy et al. 2000). Re-examination of the histological specimens showed varying degrees of inflammation and oedema. These pathological factors were considered as two sub-pathological groups and their effect on electrical impedance was explored.

According to the different grades of these two effects, two plots including the related impedance changes are shown here. Figure 5.6a demonstrates a decrease in the tissue impedance with increasing oedema. Figure 5.6b shows the opposite effect of inflammation on the measured impedance (a gradual increase in the tissue impedance with increasing inflammation). This figure includes both malignant and benign measured points and thus only the effect of oedema and inflammation are considered. Firstly, we can note that there are significant differences between oedema grades 0 and 1 ( $p < 0.001$  at lower and  $p < 0.01$  at higher frequencies), and between grades 1 and 2 ( $p < 0.001$ ) at all 7 frequencies. However, there is no significant difference between oedema grades 2 and 3.

Secondly, when the effect of inflammation on the measured impedance of the bladder (*ex vivo*) was assessed, this abnormality of tissue showed an opposite effect on the measured impedance of the bladder tissue. Figure 5.6b shows these effects on the impedance changes. According to this plot, if the degree of inflammation increases, the resulting impedance will increase. The impedivity differences between grades 1 and 2 was significant at  $p < 0.02$ . Also, the Kolmogorov-Smirnov 2 Sample Test shows that the inflammation grade 1 and grade 3 demonstrates a significant difference at 7 frequencies ( $p < 0.002$ ) but no significant differences occurred for grades 2 and 3 or 0 and 1. However, it is clear that the impedance of the bladder tissue increases if it is inflamed tissue and the impedance decreases if it includes more oedema.



a



b

**Figure 5.6 a) Effect of different degrees of oedema (0= no oedema and 3= severe oedema) and b) inflammation (0= no inflammation and 3= severe inflammation) on the impedance measurements of the bladder tissue in the Mk3.a Sheffield System**

### 5.2.1.1.6 Evaluation of individual points of the malignant data in the benign area

The incidence of inflammation and oedema on the malignant points which fall in the non-malignant area and on non-malignant points which fall in the malignant area may evaluate these individual points. For example, for the first case, malignant points which fall in the non-malignant area are shown in Table 5.1. No clear picture emerges from this analysis now.

Point No	7	8	14	16	20	21
Oedema classification	1	2	2	1	1	1
Inflammation classification	1	1	2	3	1	2

**Table 5.1 The malignant points which are categorised in non-malignant area with the respective pathological reports**

#### **5.2.1.1.7 Separation of Carcinoma *in situ* (CIS) from the inflammation area**

Finally, as mentioned before, the appearance of carcinoma *in situ* (CIS), the early stage of bladder cancer, is similar to an inflamed area of the bladder, a red patch area. Thus, it will be very important and one of the main aims of this thesis is to distinguish this early stage of bladder cancer from the inflamed benign area. Therefore, the impedance of CIS was compared with the impedance of different degrees of inflammation (0, 1, 2 and 3). However, after using the Kolmogorov-Smirnov 2 Sample Test, there was no significant difference between the impedance of CIS and the different inflammation degrees of the bladder using Mk3.a Sheffield System.

#### **5.2.1.2 Mk3.5 Sheffield System results and discussion**

In the Mk3.5 Sheffield System, *ex vivo*, the number of electrical impedance readings from the patients was 152 but the number of records that were not classified due to difficulties with data interpretation was 7. Thus, a total number of 145 (118 points non-malignant and 27 points malignant) points were measured.

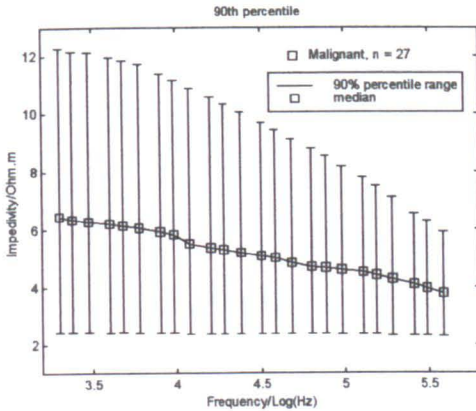
##### **5.2.1.2.1 Reproducibility of the impedance readings**

At every measured point of the bladder, 3 individual readings were taken to ensure the reproducibility of the work. These readings were usually not more than 8% difference.

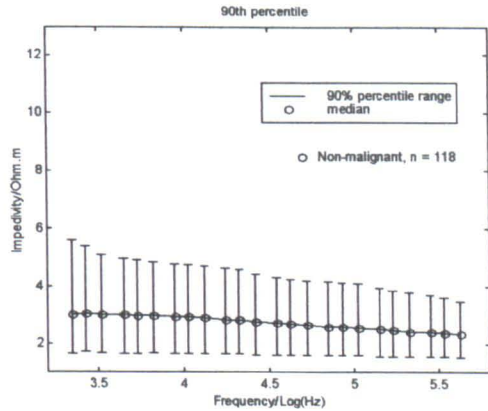
##### **5.2.1.2.2 Separation of malignant impedance from the benign**

After mathematical analysis of the readings similar to that described in the last section for Mk3.a, the malignant and non-malignant bladder tissue data were evaluated. From the calculation of the respective data for the measurements made using the Mk3.5 Sheffield system, the impedivity of malignant points was again higher than that of non-malignant points (Figures 5.7). This figure demonstrates the difference of impedance

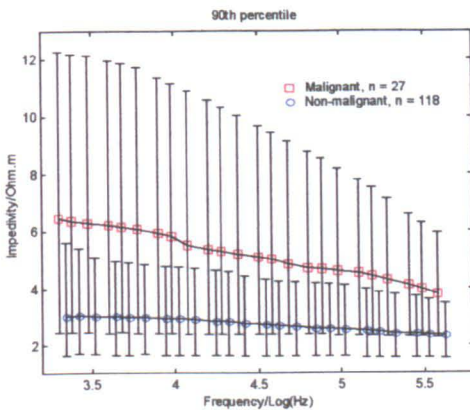
between benign and malignant areas of the bladder tissue. The working frequency range for the impedance system was limited to 1 MHz or less by system errors caused by the high load impedance due to the small electrode area. Figure 5.7a and b show the median and 90% percentile ranges for malignant and benign areas respectively and c shows the comparison for the range of impedance for the two groups. The error bars in Figure 5.7d demonstrate standard error of mean.



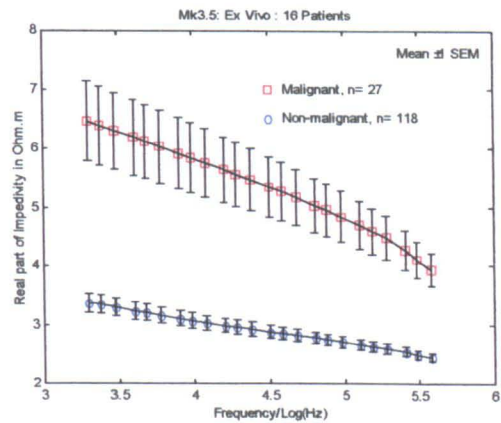
a



b



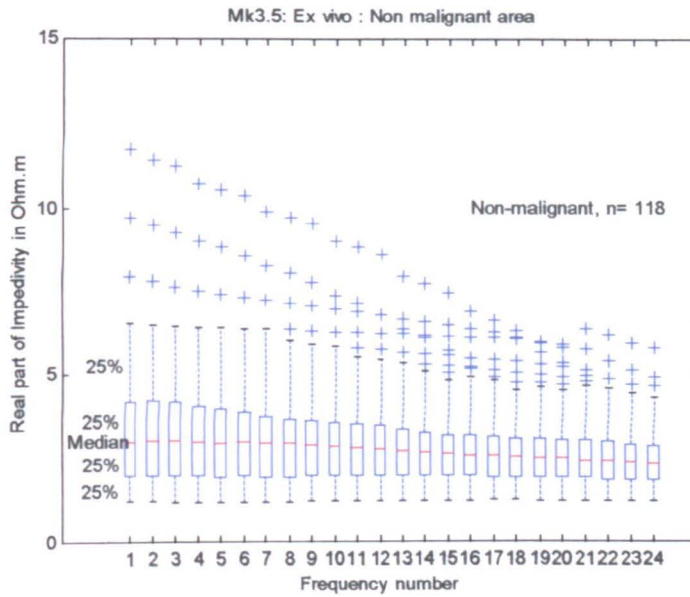
c



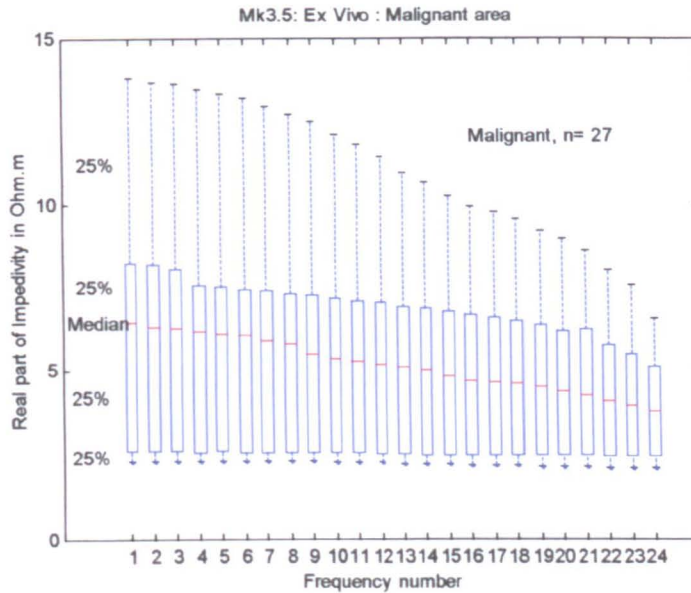
d

**Figure 5.7 Median and 90% percentile ranges for malignant and non-malignant points of the bladder tissue separately (a and b) and together (c). d) Real part of impedivity versus log of frequency for normal and malignant bladder tissue in the Mk3.5 Sheffield System**

In addition, there is a plot that was produced using boxplot instruction to find the distribution of the measured impedance spectrum for two malignant and benign groups (Figure 5.8a and b).



a



b

**Figure 5.8 The distribution of measured impedance data in non-malignant (a) and malignant (b) areas of the urinary bladder using Mk3.5 Sheffield System**

These plots demonstrated that the impedance readings for both malignant and benign areas of the bladder using Mk3.5 Sheffield System were not normally distributed (in 4 different vertical areas including four different 25% of readings). Thus, there was no evidence of Gaussian or normal distributional assumptions. Therefore, a non-parametric test, Kolmogorov-Smirnov-Two-Sample test was applied to data to evaluate the difference between the two groups statistically. According to the calculation of

respective data for the measurements using the Mk3.5 Sheffield System, the resistivity of the malignant group was higher than that of the non-malignant group at all of the frequencies ( $p < 0.0001$ ), but it is clear that the overlap of the groups will preclude the classification of individual measurements as normal or malignant.

### 5.2.1.2.3 The Cole equation fitting

The resultant scatter graph for the Mk3.5 Sheffield System from the Cole equation fitting is shown in Figure 5.9. This figure shows the impedance of malignant points is usually approaching the right hand side and the impedance of benign points is usually placed on the left hand side (similar to Figure 5.5). The scatter plot includes 25 out of 27 malignant points and 98 out of 118 non-malignant points. A satisfactory fit could not be made to the remaining data within the bounds on the parameter values because there were uppers and lowers bounds on  $R, C, S, \alpha$  and cause a maximum error on the fitting procedure.

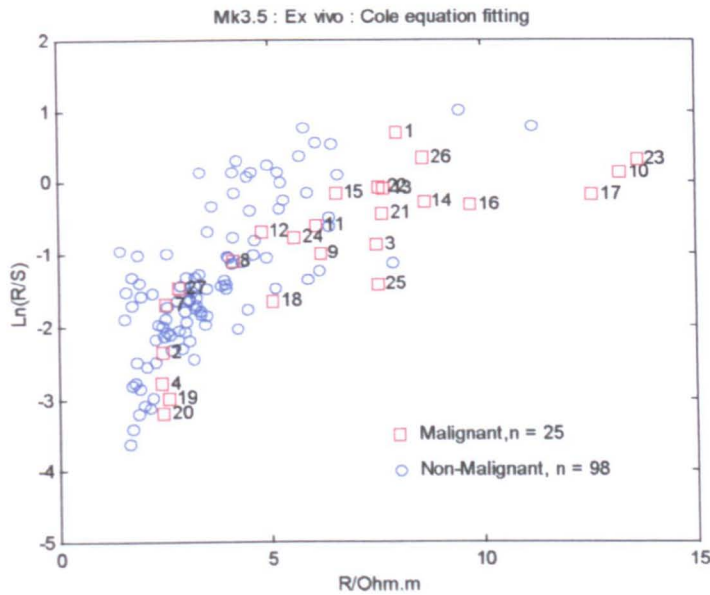
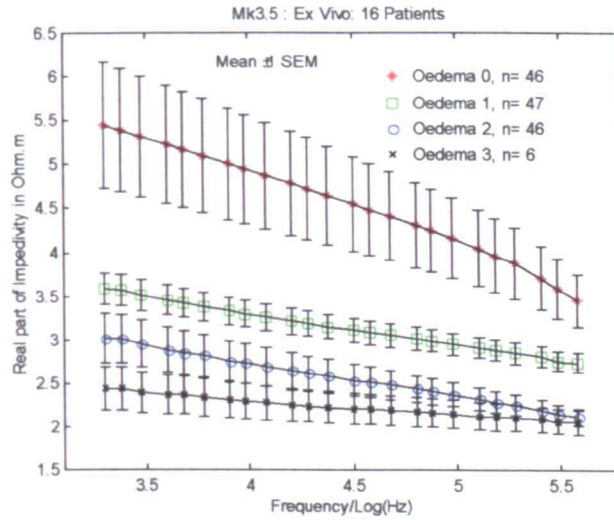


**Figure 5.9 The Cole equation fitting for normal and malignant bladder tissue in the Mk3.5 Sheffield System (the numbers show the position of 25 malignant points exactly)**

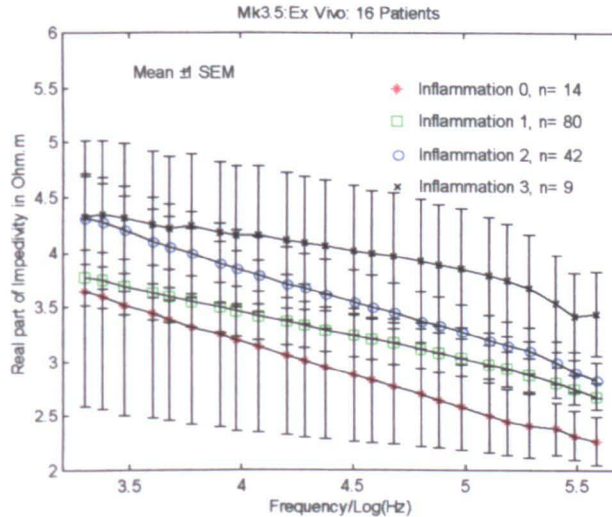
### 5.2.1.2.4 The effect of inflammation and oedema on measured impedance

The effect of oedema and inflammation on measured data is shown in Figure 5.10. There is a mixture of malignancies and benign measured points in these figures and thus only the effect of oedema and inflammation were considered. There is no significant difference between the grades of oedema and inflammation except between

oedema 0 and oedema 1 which have significant differences with ( $p < 0.007$ ) and oedema 1 and oedema 2 ( $p < 0.003$  at lower and  $p < 0.001$  at higher frequencies). However, according to this figure, it is clear that the impedance of the bladder tissue usually increases if it is inflamed tissue and the impedance usually decreases if it includes more oedema.



a



b

**Figure 5.10 a) Effect of different degrees of oedema (0= no oedema and 3= severe oedema) and b) inflammation (0= no inflammation and 3= severe inflammation) on the impedance measurements of the bladder tissue in the Mk3.5 Sheffield System**

**5.2.1.2.5 Evaluation of individual points of the malignant data in benign area**

As previously discussed for Mk3.a, there are some malignant points that have small impedances and hence they are placed on left hand side of Figure 5.9 (also, some benign points are placed on the right hand side). The incidence of inflammation and oedema on the malignant points which fall in the non-malignant area and on non-malignant points which fall in the malignant area may evaluate these individual points. For example, for the first case, malignant points which fall in the non-malignant area are shown in Table 5.2. No clear picture emerges from this analysis.

<b>Point No</b>	<b>2</b>	<b>4</b>	<b>7</b>	<b>19</b>	<b>20</b>	<b>27</b>
<b>Oedema classification</b>	<b>1</b>	<b>1</b>	<b>1</b>	<b>2</b>	<b>2</b>	<b>2</b>
<b>Inflammation classification</b>	<b>1</b>	<b>0</b>	<b>0</b>	<b>0</b>	<b>0</b>	<b>0</b>

**Table 5.2 The malignant points which are categorised in non-malignant area with the respective pathological reports**

**5.2.1.3 Results and discussion of the Combined Mk3.a and Mk3.5 Sheffield Systems**

The two measurement systems, Mk3a and Mk3.5 use different current sources, different measurement amplifiers, and different demodulation systems, so it is of interest to compare the measurements made with the two systems over the same frequency range. If two plots in Figures 5.2d-5.7d are compared, the non-malignant area of the bladders has an impedance of about 2.2 Ohm.m (at lower frequencies=9.6 KHz) and 3 Ohm.m (at higher frequencies=614 KHz). In addition, the plots obtained using percentile and boxplot for non-malignant data demonstrate a similar data distribution using these two impedance measurement systems (Figure 5.11a, b, c and d). Finally, Figure 5.11e shows these two sets of measured data against the logarithm of frequency. This shows a little difference between the mean of measured data (about 5%) but the error bars overlapped. The following equation shows the relationship between the mean values of two data at 7 frequencies:

$$\text{mean(Non\_malignantSpectrum\_MK3a)/mean (Non\_malignantSpectrum\_MK35)=} \tag{5.1}$$

0.9974 0.9713 0.9614 0.9576 0.9573 0.9470 0.9559

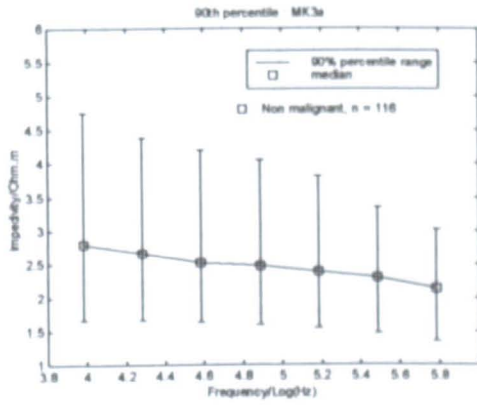
According to Figure 5.11a and b, the 90 percentiles for both systems are the same and in addition their boxplots (c and d) show a similar distribution (not normal) for the measured data. Therefore, the author used the Kolmogorov-Smirnov 2 Sample Test to evaluate any difference in the measured data between the two systems. There is no significant difference ( $p < 0.993$  at 9.6 KHz and  $p < 0.163$  at 614 KHz) between the impedance of non-malignant areas measured using Mk3a and Mk3.5 Sheffield Systems and thus, these data can be pooled.

Therefore, if we combine the malignant points together (and the benign points together) that have been measured by Mk3.a and Mk3.5, at 7 interface frequencies, we will increase the number of patients to 36 and the total measured data will be 305. But 32 readings have not been classified due to difficulties with data interpretation; thus 273 readings will be considered in this section.

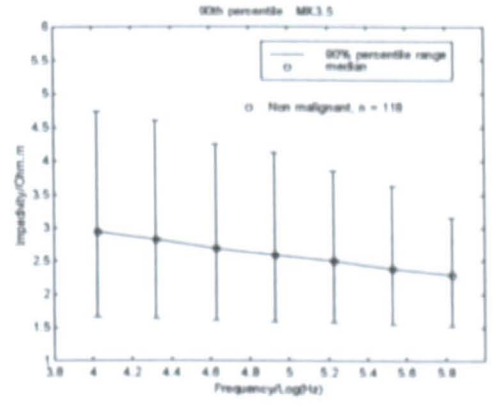
#### **5.2.1.3.1 Separation of malignant impedance from the benign**

There are 90% percentile graphs (Figure 5.12a, b and c) and the average of malignant and benign data against frequency (Figure 5.12d, including error bars, mean  $\pm$  1 standard error of mean). The mentioned graphs can characterise malignant and non-malignant points.

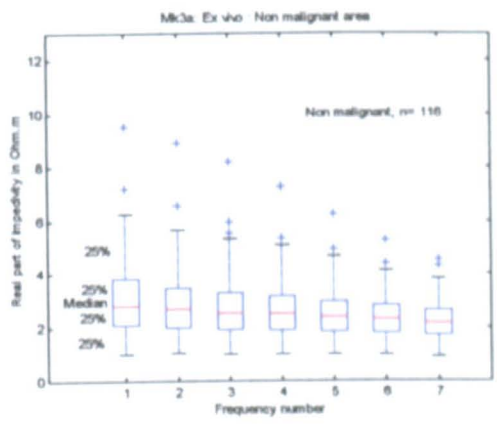
This figure can be compared with Figure 5.2 (Mk3.a) and Figure 5.7 (Mk3.5) to find the effect of the number of measured points on the electrical impedance (there is a reasonable relation between the error bars and the mean values in these figures and the number of points). It is clear that when the number of measured points increases in combined plots, the mean values approach the real values and the error bar ranges decrease relative to the graphs of these systems separately. Therefore, the result of using the combined procedure is to obtain more and more accurate impedance readings and hence the accurate bladder tissue characterisation using electrical impedance spectroscopy.



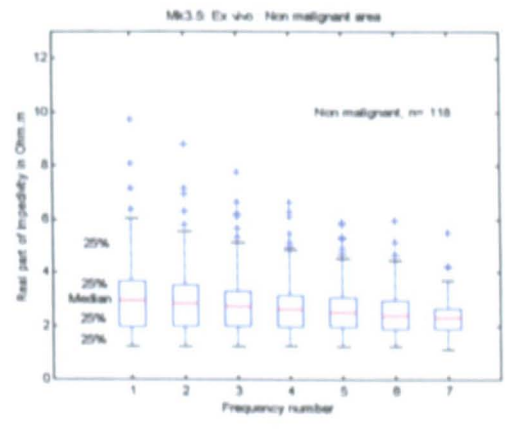
a) Mk3a



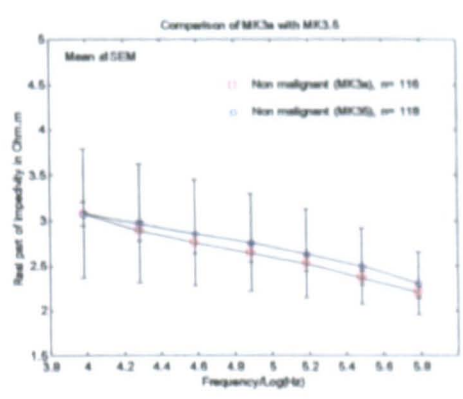
b) Mk3.5



c) Mk3a

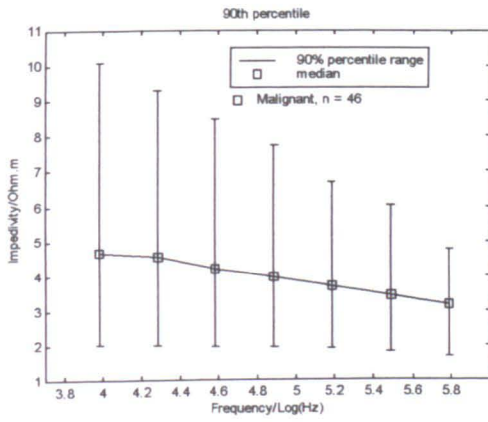


d) Mk3.5

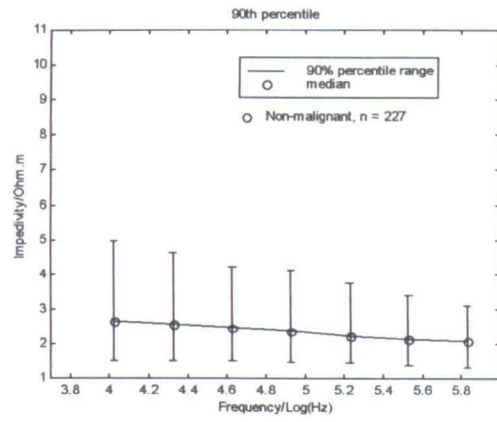


e) Mk3.a and Mk3.5

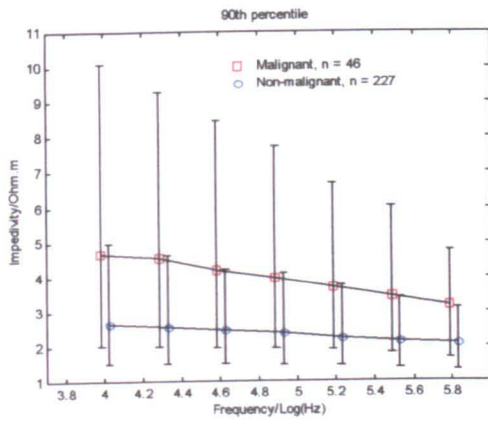
Figure 5.11 Comparison of the measured non-malignant impedance data using Mk3a and Mk3.5 Sheffield Systems with each other.



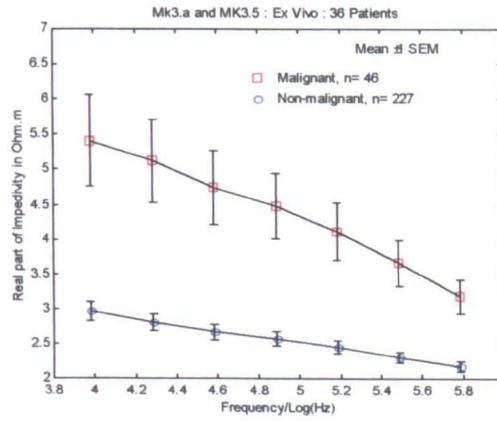
a



b



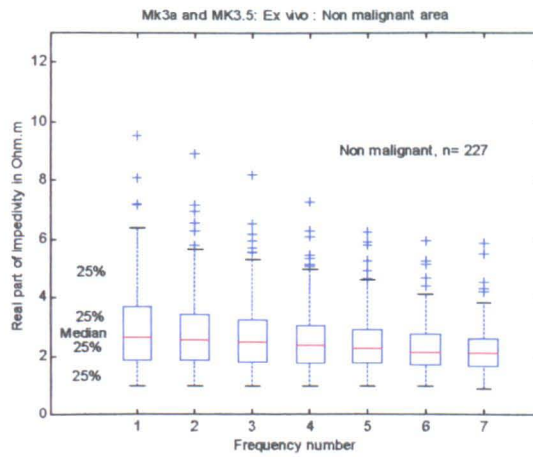
c



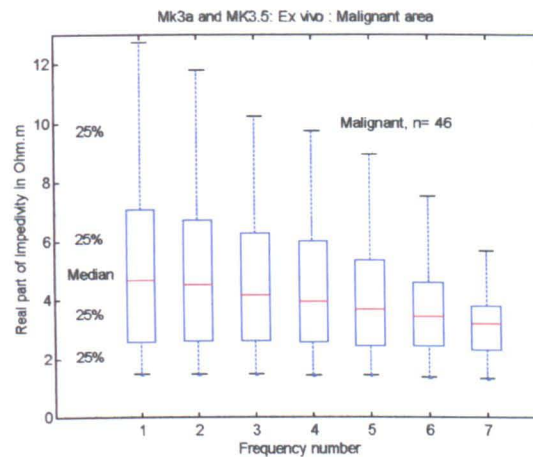
d

**Figure 5.12 Median and 90% percentile ranges for malignant and non-malignant points of the bladder tissue separately (a and b) and together (c). d) Real part of impedivity versus log of frequency for normal and malignant bladder tissue in the combined form of Mk3.a and Mk3.5 Sheffield Systems**

In addition the boxplots in this case show the data distribution. As was mentioned before, the data distribution is not normal and thus a non-parametric statistical technique must be used to evaluate the significant difference between the malignant and benign areas (Figure 5.13).



**a**



**b**

**Figure 5.13 The distribution of measured impedance data in non-malignant (a) and malignant (b) area of the urinary bladder using combined Mk3.a and Mk3.5 Sheffield Systems**

According to the non-parametric statistical test, Kolmogorov-Smirnov 2 Sample Test, the impedivity of malignant points was higher than non-malignant points at all of the frequencies ( $p < 0.000001$ ).

### 5.2.1.3.2 The Cole equation fitting

The scatter plot using Cole equation fitting for this case of study is:

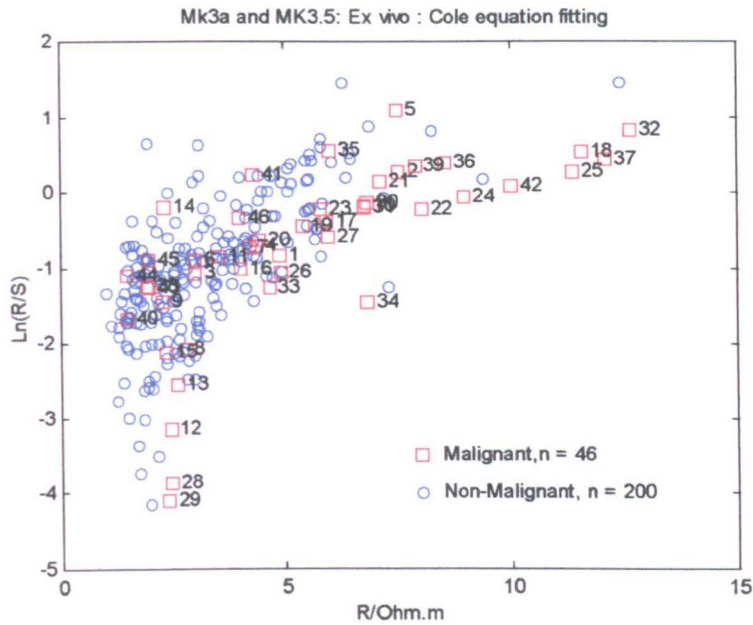
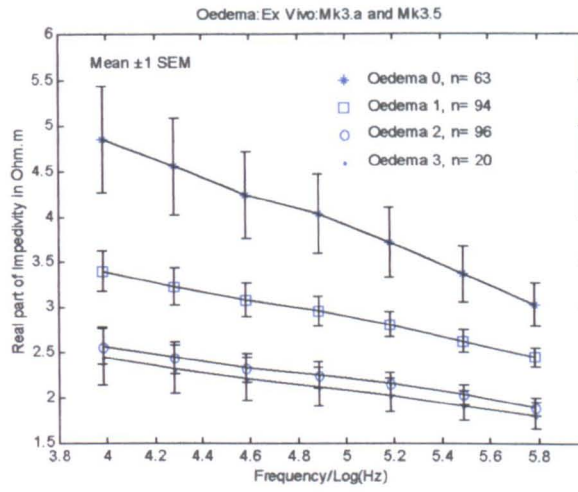


**Figure 5.14 The Cole equation fitting for normal and malignant bladder tissue in the combined form of Mk3.a and Mk3.5 Sheffield Systems (the numbers show the position of 46 malignant points exactly)**

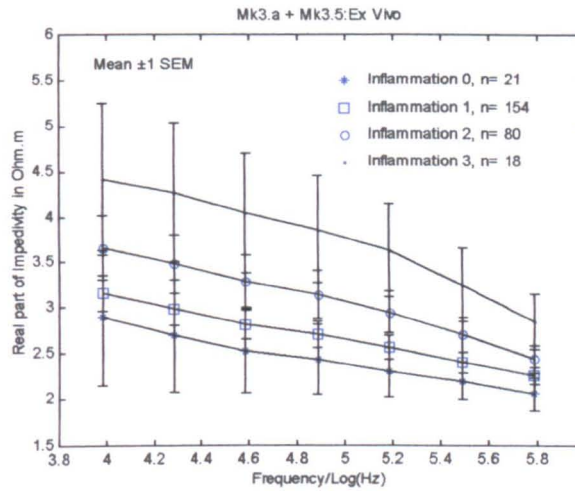
This scatter plot includes the total malignant and benign points of Figures 5.5 and 5.9; there is a good separation of these two groups in left and right hand side areas. However, the impedance of malignant area of the bladder tissue placed in the right hand side, and the readings related to benign area are in the left hand side of the graph.

### 5.2.1.3.3 The effect of inflammation and oedema on measured impedance

Following this, the combined graphs for the variation of oedema and inflammation degrees with electrical impedance of bladder tissue (*ex vivo*) using Mk3.a and Mk3.5 Sheffield Systems at 7 frequencies are shown in Figure 5.15. These plots are improved (the error bars are smaller than the error bars in Figures 5.6 and 5.10) because the number of measured data is more than using Mk3.a or Mk3.5 separately.



a



b

**Figure 5.15 Effect of different degrees of oedema (a) and inflammation (b) on the electrical impedance measurements of the bladder tissue in the combined form of Mk3.a and Mk3.5 Sheffield Systems**

The calculated results using the Kolmogorov-Smirnov 2 Sample Test show that there is a significant difference between oedema grade 0 and grade1 ( $p < 0.0001$ ); oedema grade1 and grade 2 ( $p < 0.0001$ ) but no significant difference between oedema grade 2 and grade 3. In addition, the impedivity of inflammation grades 2 and 3 were significantly different at all of the frequencies ( $p < 0.02$ ). Also, there is a significant difference between inflammation grade 1 and grade3 ( $p < 0.0001$ ) but no significant difference between inflammation grade 0 and grade 1.

**5.2.1.3.4 Separation of Carcinoma *in situ* (CIS) from the inflammation area**

Presented below are some plots that demonstrate the difference of the measured data in CIS and inflammation. The first two plots (Figure 5.16) enable differentiation of the CIS measured data from all of the inflammation data (grades 0 and 1) of the non-malignant group significant ( $p < 0.01$ ):

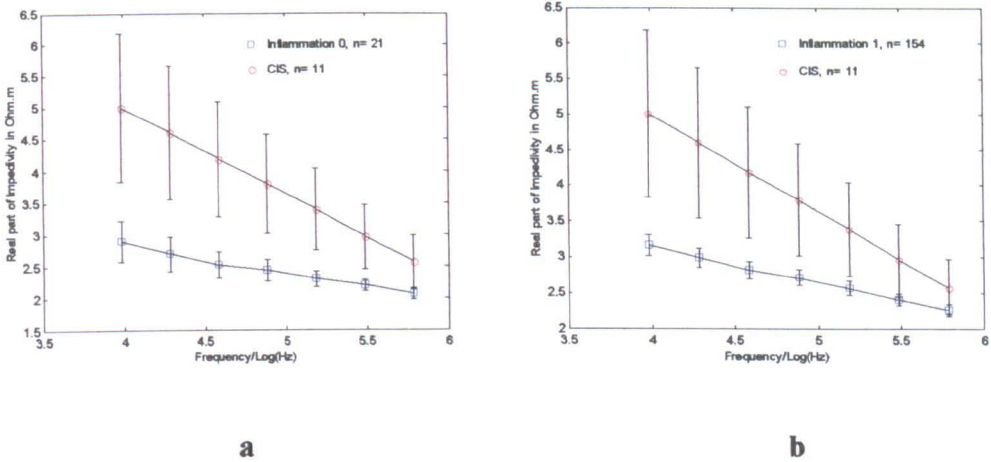


**Figure 5.16 Differentiating CIS from Inflammation grades 0 (a) and 1 (b) of the bladder tissue using the combined form of Mk3.a and Mk3.5 Sheffield Systems (error bars are mean  $\pm$ 1 standard error of mean)**

However, Figure 5.17a and b show there is no significant difference between CIS measured data and all of the inflammation data (grade 2 ( $p < 0.3$ ) and grade 3 ( $p < 0.4$ )) of the non-malignant group:

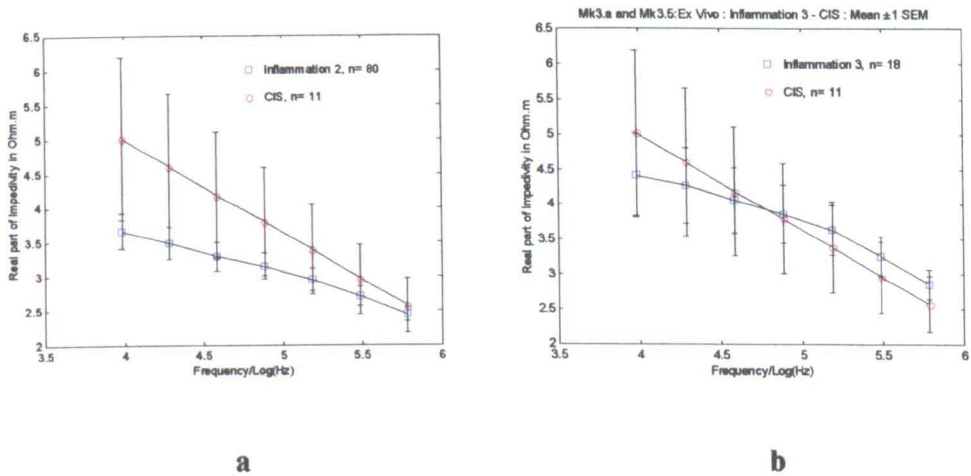


**Figure 5.17 Differentiating CIS from Inflammation grades 2 (a) and 3 (b) of the bladder tissue using the combined form of Mk3.a and Mk3.5 Sheffield Systems (error bars are mean  $\pm$ 1 standard error of mean)**

There is a significant difference between CIS Inflammation grade 2 and only Inflammation grade 2 of all the non-malignant measured data ( $p < 0.001$ ) as shown in the following figure:

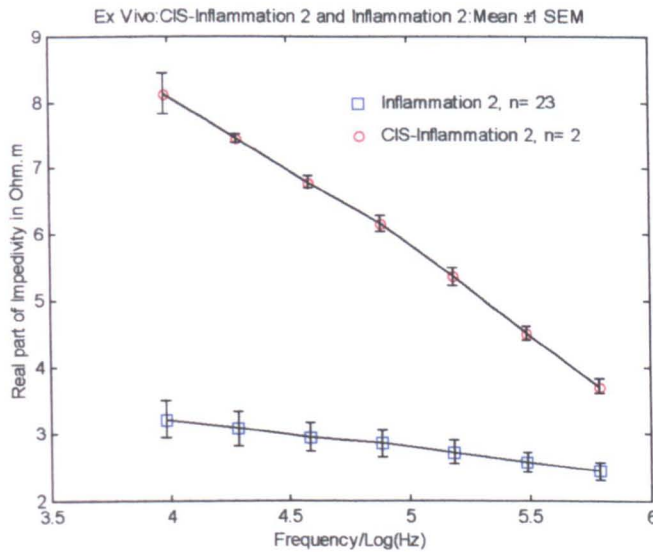


**Figure 5.18 Differentiating CIS- Inflammation grade 2 from Inflammation grade 2 of all non-malignant measured data of the bladder tissue in using the combined Mk3.a and Mk3.5 Sheffield Systems**

#### 5.2.1.4 Conclusion

As explained in this chapter, the aim of this thesis is to assess the effectiveness of the electrical impedance method at differentiating between benign and malignant urinary bladder tissues. For this purpose, the impedance measurements of the urothelium were carried out in two *ex vivo* and *in vivo* states. The first case was discussed in this section and the latter are presented in the next section. Thus, a total number of 305 biopsies from 35 freshly excised bladders (immediately after operation) from patients were studied using two electrical impedance spectroscopic systems.

It was demonstrated that the impedance of the malignant group of points in the bladder is significantly higher than the benign group of points, but this minimally invasive technique cannot be used to classify individual measurements. It has been shown that different degrees of oedema and inflammation might explain the scatter in the impedance of individual points. Oedema causes a decrease in measured impedance (oedema increases the fluid in the extra-cellular space) and inflammation causes an increase in the impedance by infiltrating more and more cells in the lamina propria of the tissue. Finally, an important message of this section can be the separation ability to

distinguish carcinoma *in situ* (CIS) from the different degrees of the bladder tissue inflammation, because the common sign of these pathological changes in the bladder tissue surface is the existence of red colour using a cystoscope. There were significant differences between CIS and Inflammation with degrees of 0 and 1, but in more severe cases of inflammation (degrees 2 and 3) the change in the impedance of the tissue is of the same value as when CIS presents. Therefore, this impedance technique at present can not distinguish CIS from the severe inflammation accurately.

## **5.2.2 *In vivo* study**

### **5.2.2.1 Measured transfer impedance of the bladder**

In this part of work, a total of 223 points from 74 patients were studied to take electrical impedance measurements. As mentioned in methods section, all patients were under anaesthesia.

### **5.2.2.2 Mk3.a Sheffield System results and discussion**

The number of points measured was 109, but the number of records that have not been classified due to difficulties with data interpretation was 7. In fact the number of non-malignant points was 97 and the number of malignant points was 5 points.

#### **5.2.2.2.1 Separation of malignant impedance from the benign**

After mathematical analyses of readings, using the computer based Matlab software, the 90% percentile graphs demonstrated the data distribution in both malignant and benign groups (Figure 5.19a, b and c). Then, the separation of mean value of the impedance related to malignant points from the benign area of the bladder was considered (Figure 5.19d).

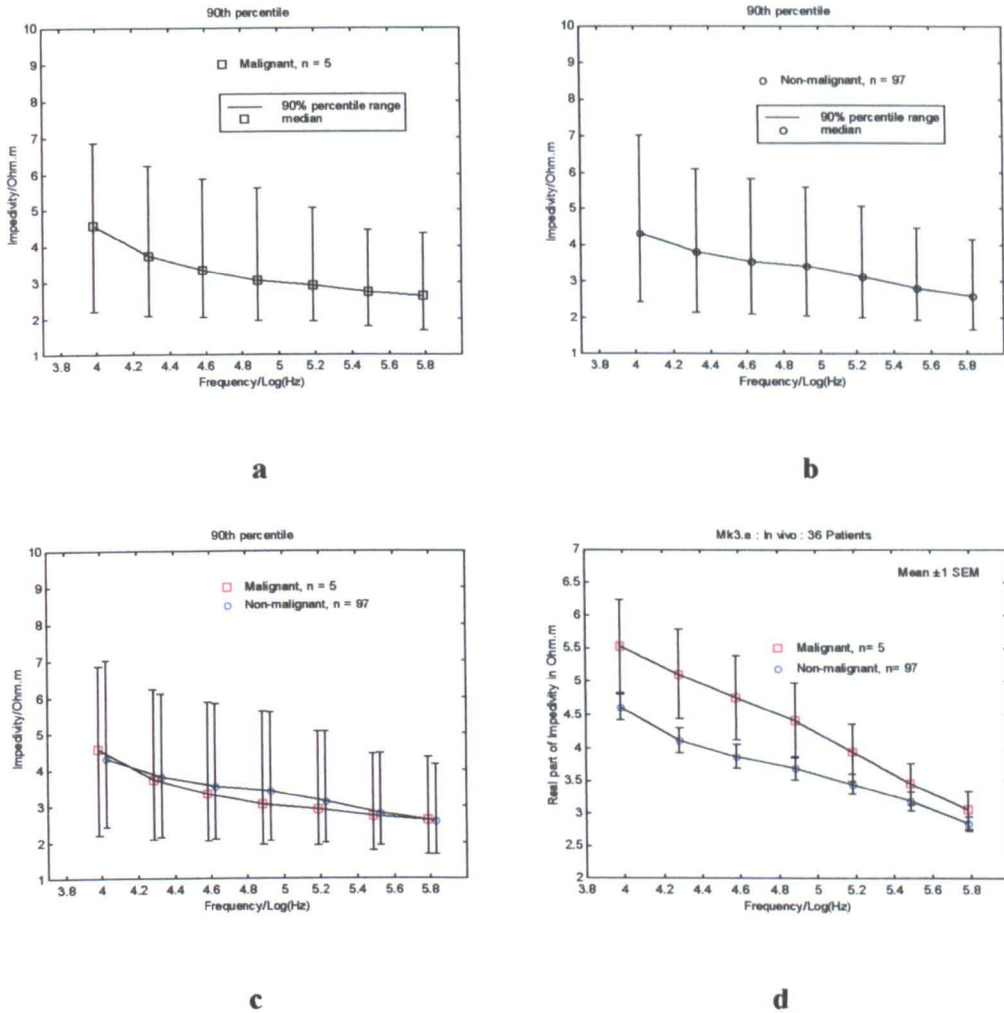
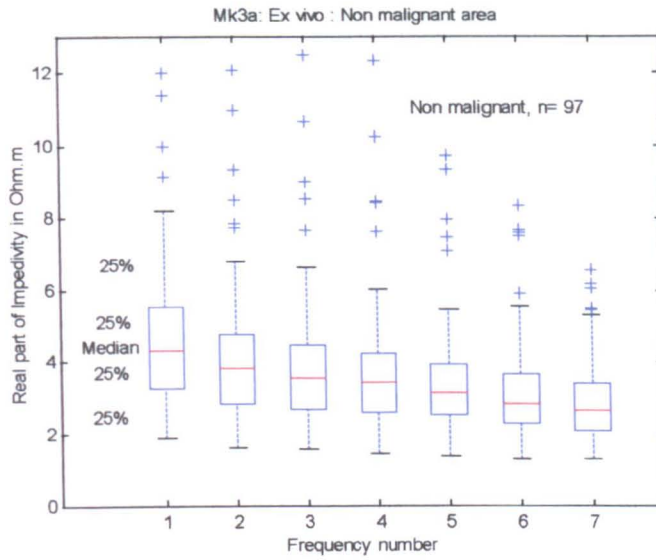
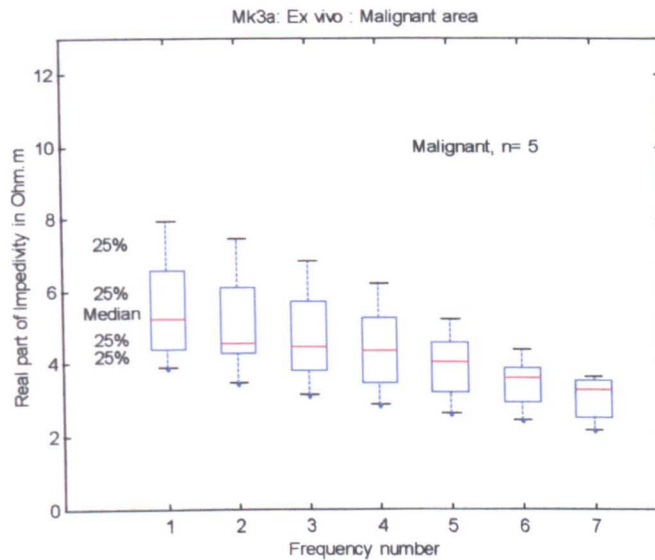


**Figure 5.19 Median and 90% percentile ranges for malignant (a) and non-malignant (b) points of the bladder tissue separately and together (c). d) Real part of impedivity versus log of frequency for normal and malignant bladder tissue in the Mk3.a Sheffield System**

Following this the graphs resulted from boxplot in Figure 5.20 shows a non-normal distribution for the measured data and this means that we can use a non-parametric statistical method (the Kolmogorov-Smirnov 2 Sample Test) to separate the malignant area from the normal area of the bladder. According to Figure 5.19d, the result of the Mk3.a Sheffield System shows no significant difference between malignant and non-malignant groups at the two highest frequencies as shown in the following plot. There is a significant difference between Malignant and Non-malignant groups ( $p < 0.01$ ) for lower frequencies.



**a**



**b**

**Figure 5.20** The distribution of measured impedance data in non-malignant (a) and malignant (b) areas of the urinary bladder using Mk3.a Sheffield System

#### 5.2.2.2.2 The Cole equation fitting

There is a plot that resulted from the Cole equation fitting in to measured *in vivo* data (Figure 5.21) but the impedance of malignant points are similar to the impedance of benign area and hence they are overlapped. Therefore, there is not more discussion about their differences here and need to have more measurements to evaluate their differences.

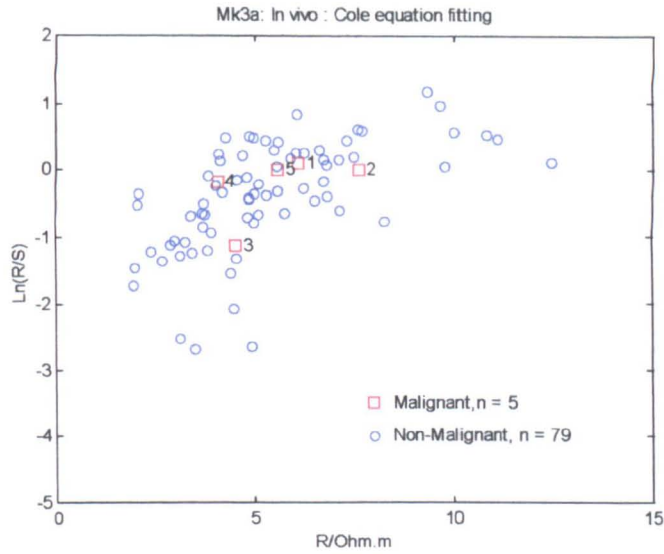


**Figure 5.21 The Cole equation fitting for benign and malignant bladder tissue in the Mk3.a Sheffield System**

### 5.2.2.3 Mk3.5 Sheffield System results and discussion

The number of points measured was 114 from 38 patients, but the number of records that have not been classified due to difficulties with data interpretation was 8. In fact the number of non-malignant points was 80 and the number of malignant points was 26 points.

#### 5.2.2.3.1 Separation of malignant impedance from the benign

The impedance readings of Mk3.5 were analysed using Matlab software and finally the malignant and non-malignant bladder tissue data were evaluated. The 90% percentile graphs demonstrated the data distribution in both malignant and benign groups (Figure 5.22a, b and c). Then, the impedivity of the malignant group was again higher than that of the non- malignant group (Figures 5.22d).

As we know, boxplot can demonstrate the impedance data distribution resulting from malignant and non-malignant areas. Thus, according to these plots which are shown in Figures 5.23a and b, the both data distributions are not normal. Therefore, a non-parametric statistical technique, the Kolmogorov-Smirnov 2 Sample Test used to evaluate the significant difference between the malignant and benign areas. These results show a significant difference between malignant and non-malignant groups

especially at lower frequencies (for 2-76.8 KHz,  $p < 0.0001$  and for 96-192 KHz,  $p < 0.001$  and for higher frequencies,  $p < 0.01$ ).

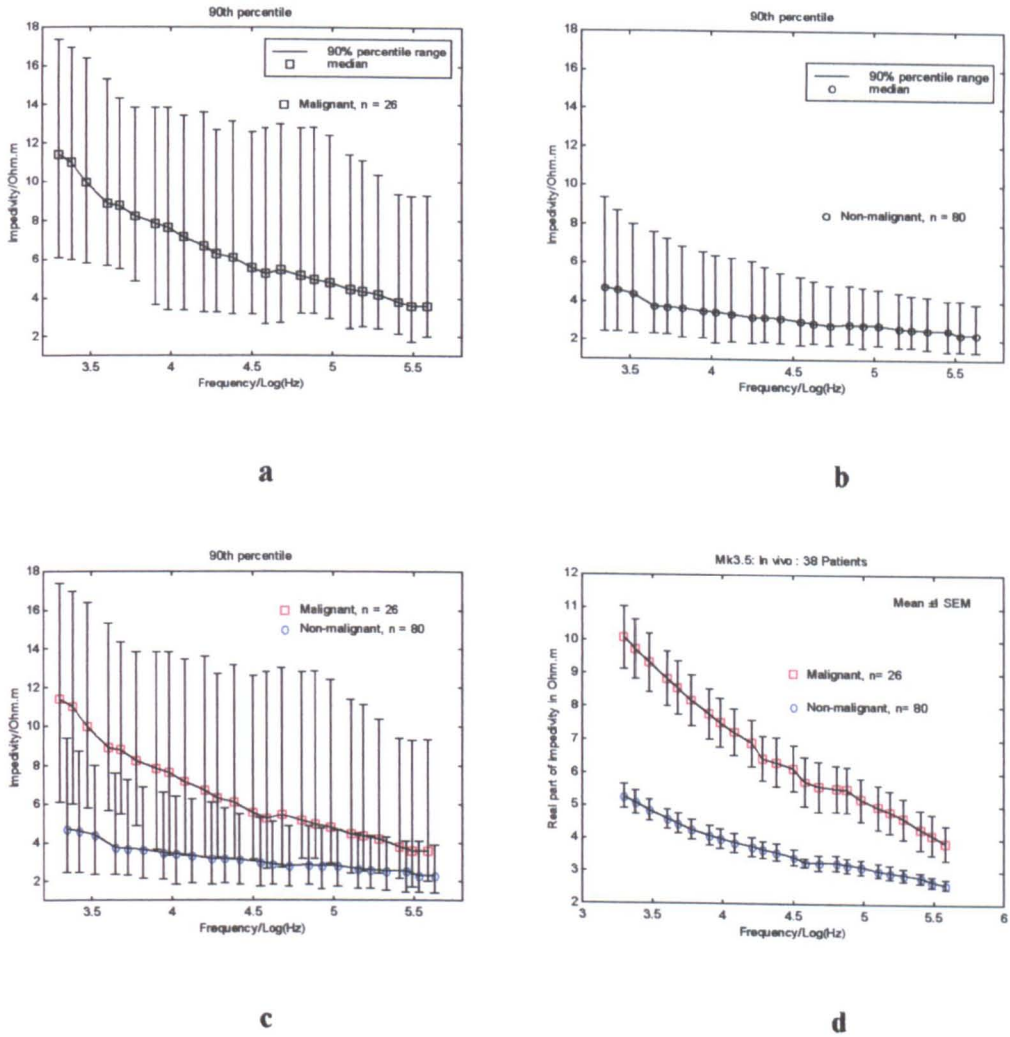
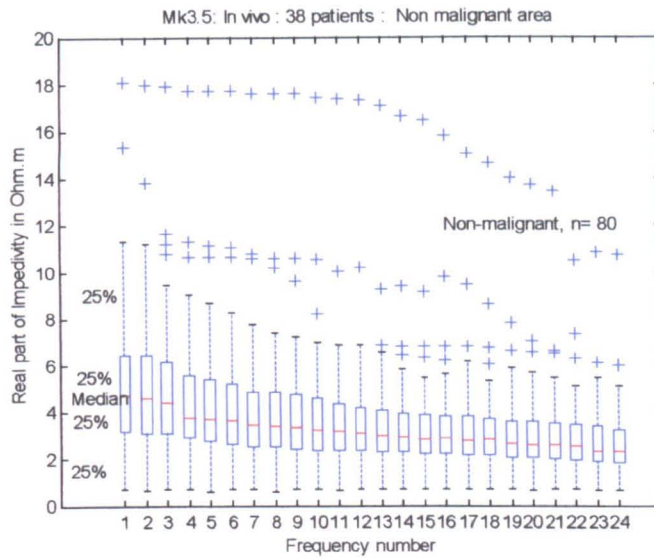
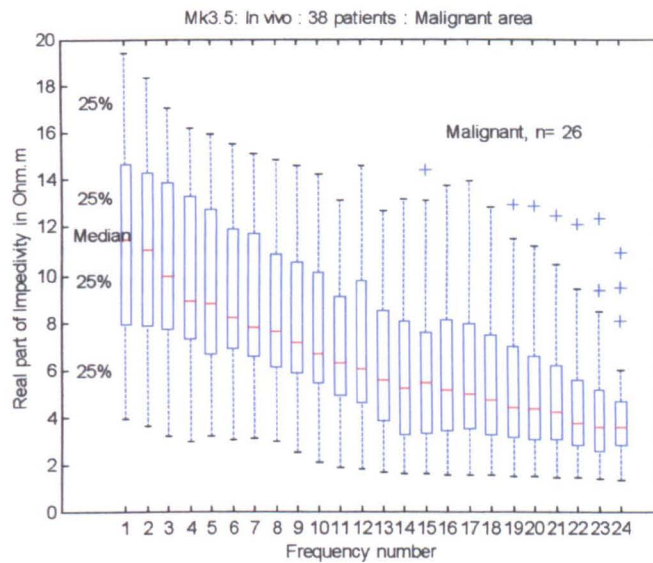


**Figure 5.22 Median and 90% percentile ranges for malignant (a) and non-malignant (b) points of the bladder tissue separately and together (c). d) Real part of impedivity versus log of frequency for normal and malignant bladder tissue in the Mk3.5 Sheffield System**



**a**



**b**

**Figure 5.23 The distribution of measured impedance data in non-malignant (a) and malignant (b) areas of the urinary bladder using Mk3.5 Sheffield System**

**5.2.2.3.2 The Cole equation fitting**

The following scatter plot using the Cole equation fitting demonstrates the separation of malignant and non-malignant areas in this case. This figure shows higher values

of  $R/S$  and  $R$  for malignant tissue. The scatter plot includes 73 out of 80 non-malignant points and 24 out of 26 malignant points. A satisfactory fit could not be made to the remaining data within the bounds on the parameters values.

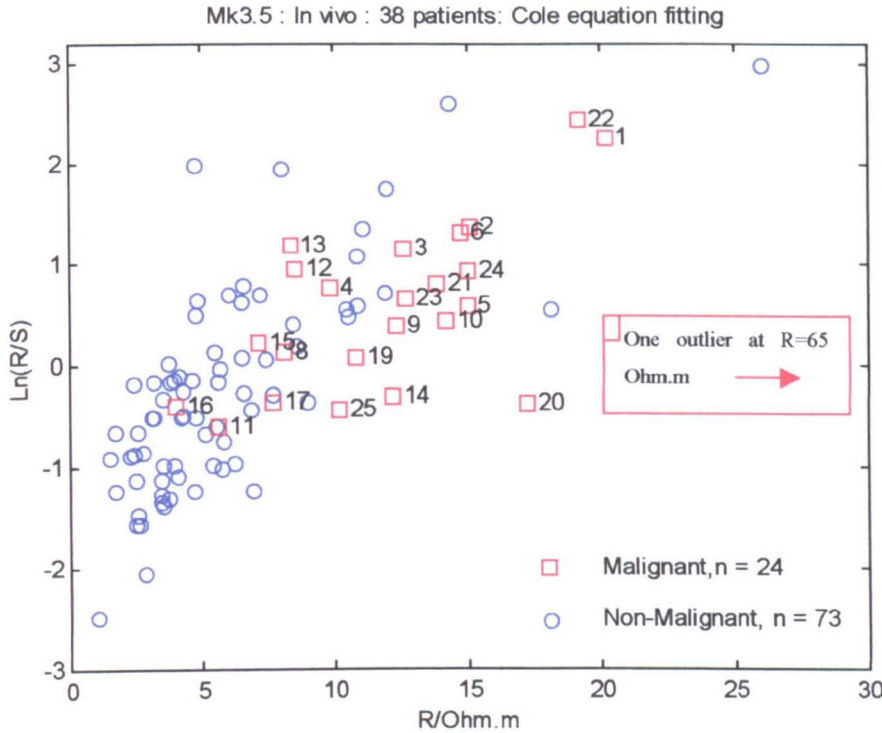


**Figure 5.24** The Cole equation fitting for normal and malignant bladder tissue in the Mk3.5 Sheffield System (one malignant point is located at  $R=65 \Omega m$  and  $\ln R/S=0.2$ )

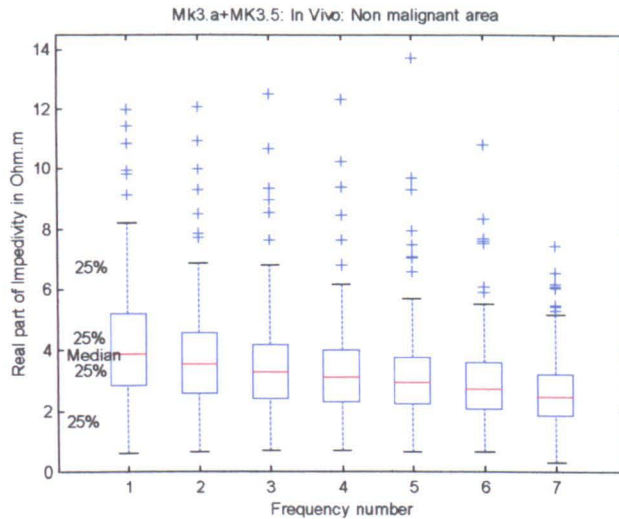
**5.2.2.4 Results and discussion of the Combined Mk3.a and Mk3.5 Sheffield Systems**

A total number of 31 malignant and 177 non-malignant points from 106 patients (*in vivo*) were used in this study.

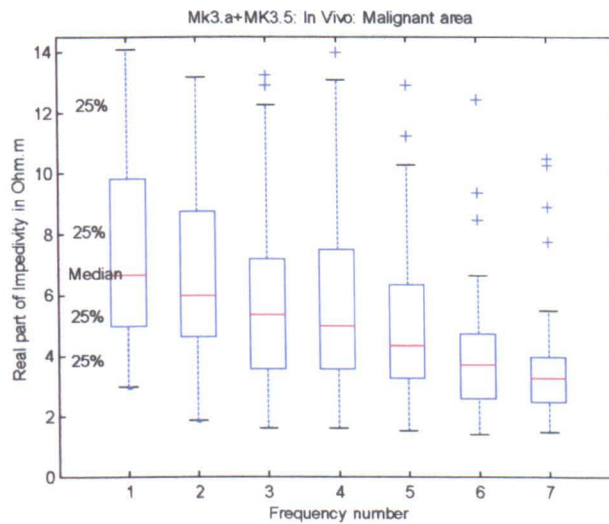
**5.2.2.4.1 Separation of malignant impedance from the benign**

The combined measured data from Mk3.a and Mk3.5 Sheffield Systems in 7 frequencies, similar to the frequencies of Mk3.a System was analysed in this section. However, the impedance data measured from the malignant and benign area of the bladder was not normally distributed (Figure 5.25) thus the non-parametric statistical test was used to evaluate the difference of these two groups of data. Therefore, there is a significant difference between malignant and non-malignant area of the bladder using

the Kolmogorov-Smirnov 2 Sample Test ( $p < 0.0001$  at lower and  $p < 0.01$  at higher frequencies). In addition, median and 90% percentile ranges of the impedance readings, and the separation plot for malignant and non-malignant points of the bladder tissue are shown in Figure 5.26.

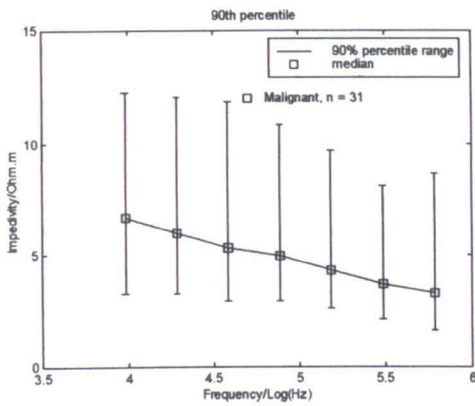


**a**

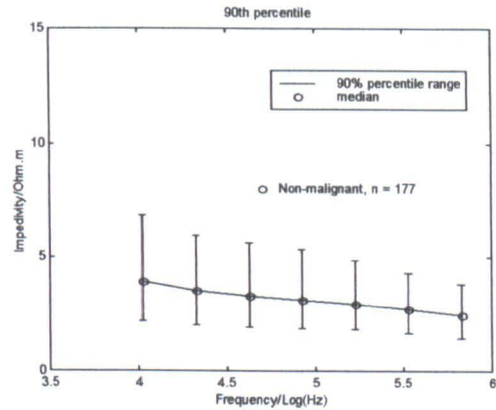


**b**

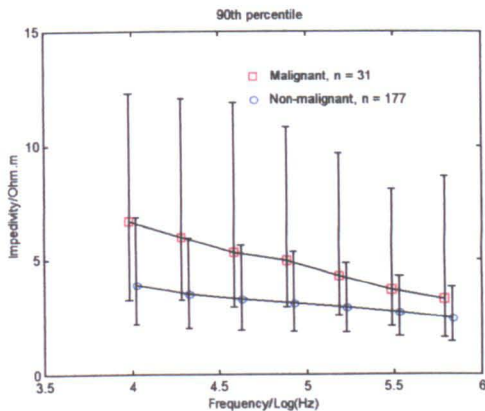
**Figure 5.25** The distribution of measured impedance data in non-malignant (a) and malignant (b) area of the urinary bladder using combined Mk3.a and Mk3.5 Sheffield Systems



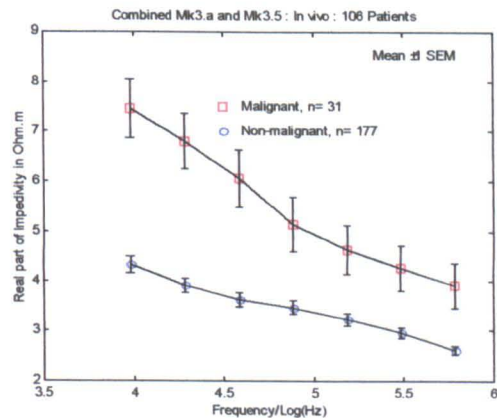
a



b



c



d

**Figure 5.26 Median and 90% percentile ranges for malignant and non-malignant points of the bladder tissue separately (a and b) and together (c). d) Real part of impedivity versus log of frequency for normal and malignant bladder tissue in the combined Mk3.a and Mk3.5 Sheffield Systems**

#### 5.2.2.4.1 The Cole equation fitting

The Cole equation fitting in to the measured data of the combined Mk3.a and Mk3.5 Sheffield Systems is shown in Figure 5.27. When the Mk3.a and Mk3.5 systems are used separately to measure the impedance of the tissue, the numbers of measured points that are fitted successfully using the Cole equation fitting procedure are different than if we combine all of the data, then extract data at a selection of frequencies. However, the

distributions of applied current in tissue are different using these two systems at selected frequencies. Therefore, if combined data of these measurements (at only 7 frequencies) are used for the fitting procedure, the received data loses some information because of the reduced signal to noise ratio (SNR).

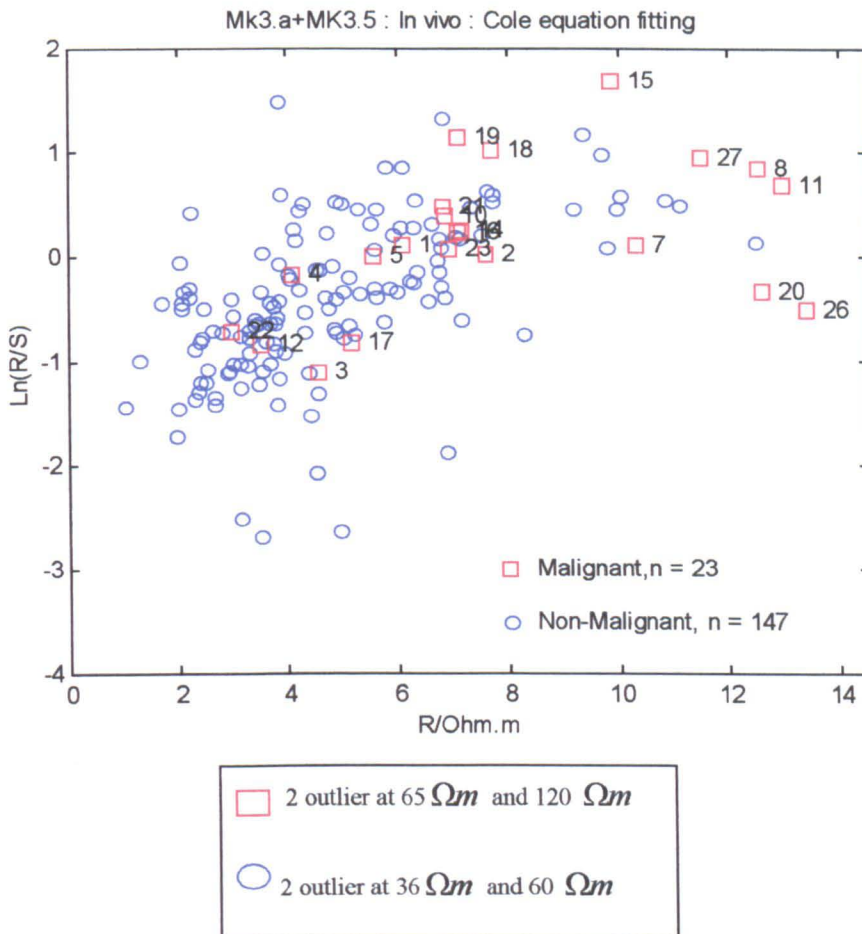


**Figure 5.27** The Cole equation fitting for benign and malignant bladder tissue in the combined Mk3.a and Mk3.5 Sheffield Systems (Malignant: 2 outlier at 65  $\Omega m$  and 120  $\Omega m$  and Non-malignant: 2 outlier at 36  $\Omega m$  and 60  $\Omega m$ )

Finally, the effect of different degrees of oedema and inflammation in the combined Mk3.a and Mk3.5 Sheffield Systems was assessed, and according to Kolmogorov-Smirnov 2 Sample Test, there is a significant difference between oedema grades 1 and 2 ( $p < 0.001$ ), oedema grades 1 and 3 ( $p < 0.01$ ) at all of the frequencies (Figure 5.28). Finally, the effect of inflammation degrees on measured electrical impedances assessed and the calculated results shows a significant difference between inflammation grades 2 and 3 ( $p < 0.02$ ); grades 1 and 3 ( $p < 0.05$ ); and no significant differences among others (Figure 5.29).

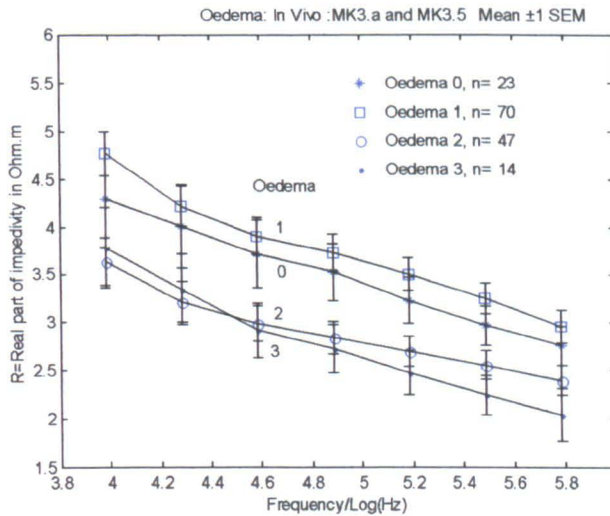


**Figure 5.28 Effect of different degrees of oedema (0= no oedema and 3= severe oedema) on the electrical impedance measurements of the bladder tissue in the combined Mk3.a and Mk3.5 Sheffield Systems**

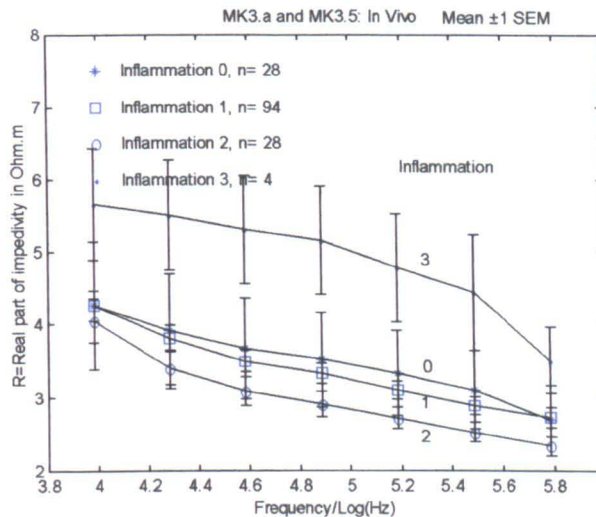


**Figure 5.29 Effect of different degrees of inflammation (0= no inflammation and 3= severe inflammation) on the electrical impedance measurements of the bladder tissue in the combined Mk3.a and Mk3.5 Sheffield Systems**

### 5.2.2.5 Conclusion

The aim of this section, similar to the last section is also to assess the effectiveness of the electrical impedance method at differentiating between benign and malignant urothelium. For this purpose, the impedance measurements of the urothelium were carried out *in vivo* states. A total number of 209 biopsies from 68 freshly excised

bladders were studied using two electrical impedance spectroscopic systems. It was shown that the impedance of the malignant group is similar to the *ex vivo* state, significantly higher than the benign group. Also, the plot resulting from the Cole equation fitting demonstrated that the impedance of malignant area of the bladder approaches to the right hand side and the reading of benign area are placed in the left hand side of the plot. Finally, the separation of different degrees of inflammation and oedema in the *in vivo* study is not as well as the *ex vivo* case. This mean that the strong correlation between the degrees of inflammation and oedema of the *ex vivo* study has not been seen in *in vivo* work. The reason may be a result of the tissue handling procedure in the *ex vivo* study. The separation between CIS and inflammation was not carried out in this section because the number of CIS measured impedances was only 3 and it is not valid to assess this procedure.

### **5.2.3 Lower frequency study of the urothelium (*In vivo*)**

The tight junctions of the epithelium affect the low frequency impedances (Jones 2003). To investigate the effect of barriers of the urothelium, such as tight junctions on the electrical impedance at very low frequencies, the Mk3.5 Sheffield System was modified to reduce the minimum measurement frequency to 62.5 Hz. It was expected that the measured impedance for normal tissue at lower frequencies would be greater than the impedance of the malignant area. A trial series in this frequency range was performed over the period January 2003 until December 2003. A total of 18 patients including 51 measured points were used in this experiment in theatre 1 and 2 in the Royal Hallamshire Hospital.

The modified Mk3.5 Sheffield System works at 60 frequencies in the range of 62.5 Hz-1.5 MHz. At lower frequencies, the data acquisition is performed with each of the 30 frequencies of Table 3.4 being reduced by a factor of 32 (the first frequency is:  $\frac{2000}{32} = 62.5$ , the second frequency is:  $\frac{2400}{32} = 75$  and...). Thus, the whole range of frequency is shown in Table 5.3.

62.5	75	93.75	125	150	187.5	250	300	375
500	600	750	1000	1200	1500	2000	2000	2400
2400	3000	3000	4000	4000	4800	4800	6000	6000
8000	8000	9600	9600	12000	12000	16000	16000	19200
19200	24000	24000	32000	32000	38400	38400	48000	48000
64000	76800	96000	128000	153600	192000	256000	307200	384000
512000	614400	768000	1024000	1228800	1536000			

**Table 5.3 Frequencies (in Hz) used in the modified Mk3.5 Sheffield System**

In the measuring procedure, the acquisition time is increased because of the requirement that the time frame contain a minimum of 1 cycle of the lowest frequency.

### 5.2.3.1 Separation of malignant impedance from the benign

The malignant and non-malignant areas of the bladder were evaluated using lower frequency measurement system. Initially, the boxplots (Figure 5.31) show that the distribution of impedance data in both cases are not distributed normally, thus the non-parametric test, Kolmogorov-Smirnov 2 Sample Test, was applied to these data. There were different values for  $p$  and usually significant difference between malignant and non malignant areas at low frequencies but no significant difference at high frequencies. The  $p$  values at different frequencies are shown in Table 5.4.

Frequency	$P$ value
62.5 Hz- 6 KHz	$p < 0.0001$
8 KHz- 24 KHz	$p < 0.0001$
32 KHz- 76.8 KHz	$p < 0.001$
96 KHz- 192 KHz	$p < 0.07$
256 KHz-1.5 MHz	Not significant

**Table 5.4 The  $p$  values of statistical analysis of malignant and non-malignant bladder tissue using modified Mk3.5 System**

Figure 5.30 shows the separation of the mean value of malignant and non-malignant impedance data using the low frequency system (error bars demonstrated the standard error of mean in this figure). It is clear that the separation between the groups increases at lower frequencies.

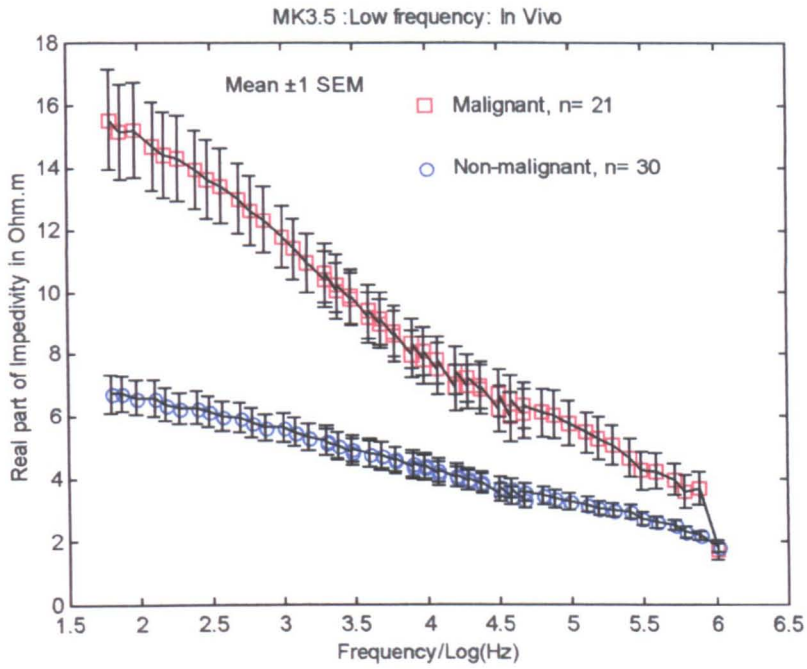
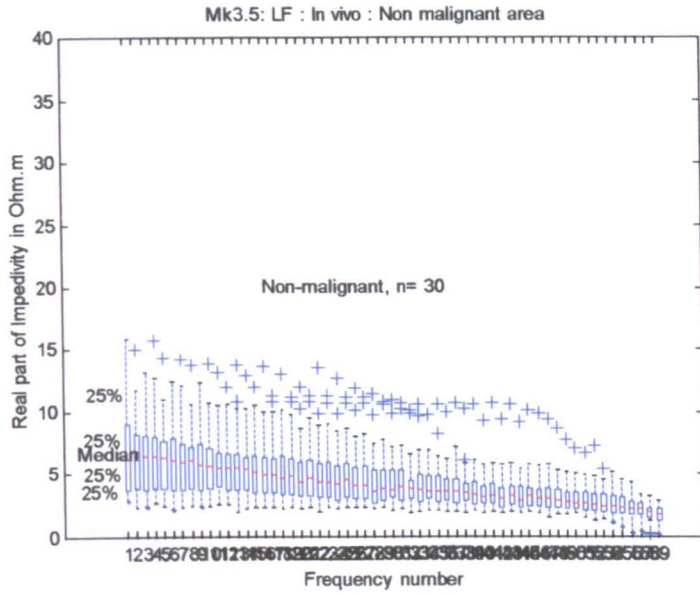
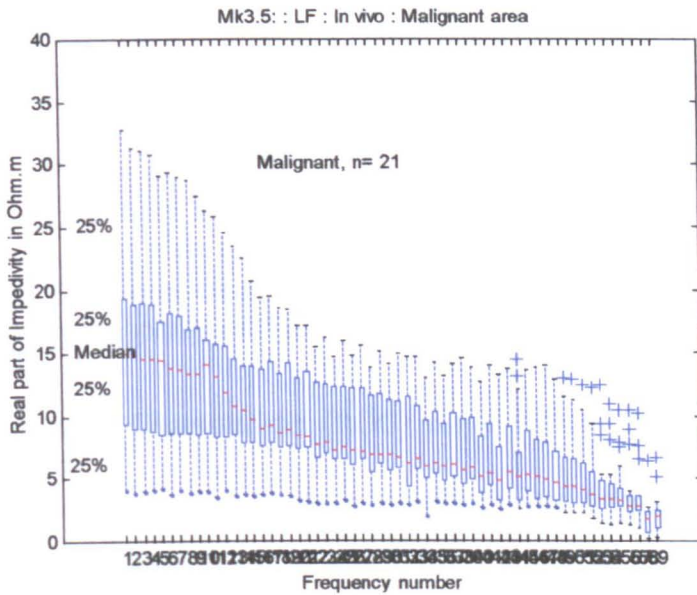


**Figure 5.30 Real part of impedivity versus log of frequency for benign and malignant bladder tissue in the modified Mk3.5 Sheffield System**



a



b

**Figure 5.31** The distribution of measured impedance data in non-malignant (a) and malignant (b) areas of the urinary bladder using modified Mk3.5 Sheffield System

### 5.2.3.2 The Cole equation fitting

There is a plot that resulted from the Cole equation fitting in to the measured *in vivo* data using the modified Mk3.5 Sheffield System. There were 20 malignant and 29 non-malignant points which were fitted successfully (a satisfactory fit could not be made to one non-malignant and one malignant points within the bounds on the parameter values). The resulted scatter plot demonstrated a good separation of these groups from each other (Figure 5.32).

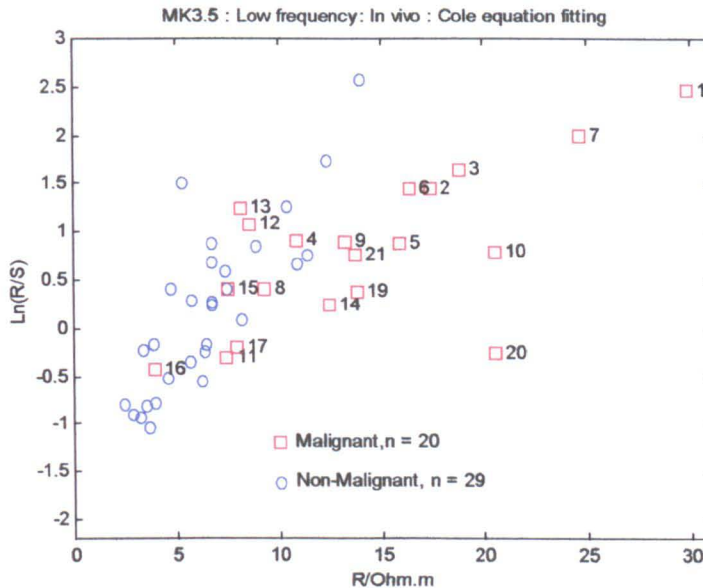


**Figure 5.32** The Cole equation fitting for benign and malignant areas of the bladder tissue using the modified Mk3.5 Sheffield System

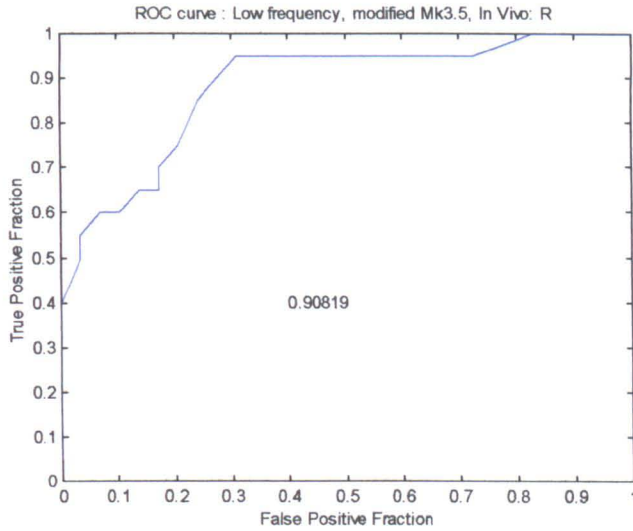
The Receiver Operating Characteristic (ROC) curve for the parameters  $R$  and  $\frac{R}{S}$  is shown in Figure 5.33. The area under the curve (for  $R$ ) is 0.91 and the standard error on the area under the curve (Hanley and McNeil 1982) is given by:

$$SE = \sqrt{\frac{\theta(1-\theta) + (n_A - 1)(Q_1 - \theta^2) + (n_N - 1)(Q_2 - \theta^2)}{n_A n_N}} \quad 5.1$$

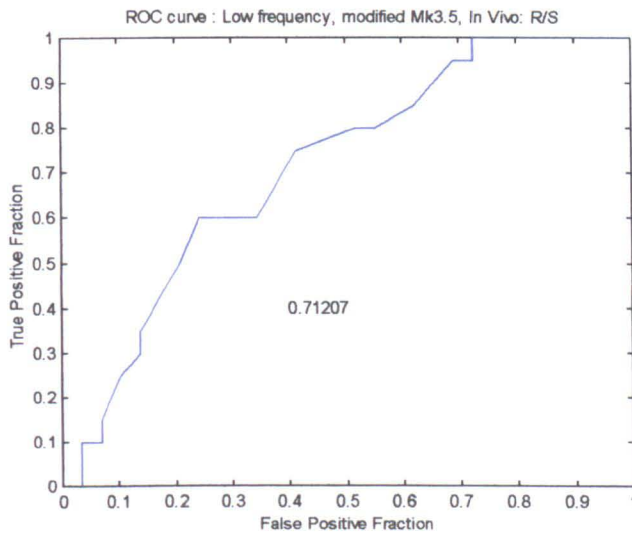
Where  $\theta$  is the area under the curve,  $n_A$  and  $n_N$  are the number of abnormal and normals respectively, and  $Q_1$  and  $Q_2$  are estimated by:  $Q_1 = \frac{\theta}{(2-\theta)}$  and

$Q_2 = \frac{2\theta^2}{(1+\theta)}$ . For the above curve, the area is  $(0.91 \pm 0.07)$ . If  $R = 7.2\Omega m$  is taken as

the boundary between normal and malignant points, there is 1 false negative out of 20 and 9 false positive out of 29, i.e. a PPV (Positive Predictive Value = true positives / all positive tests) of 95% and NPV (Negative Predictive Value = true negatives / all negative tests) of 69%. If the prediction boundary is moved to include all of the malignant points, the PPV is clearly 100%, and the NPV falls to 17%.



**a**



**b**

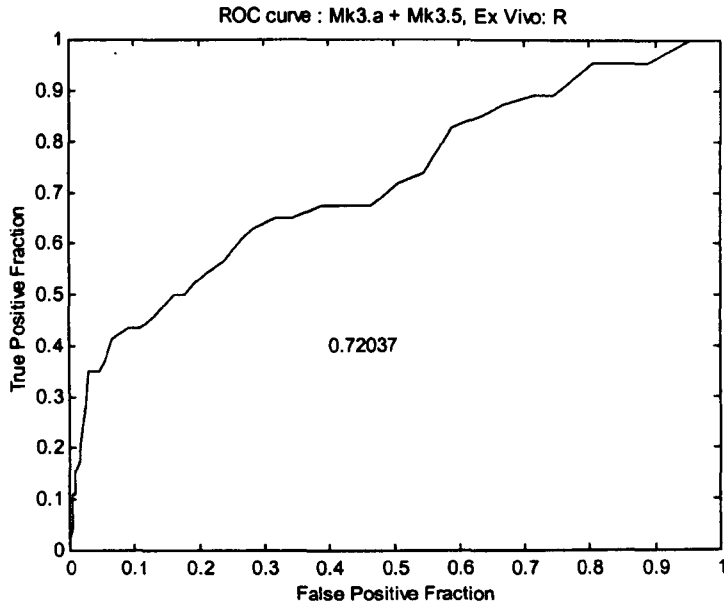
**Figure 5.33** The ROC curve for the parameter  $R$  (a) and parameter  $\frac{R}{S}$  (b) using the modified Mk3.5 Sheffield System (*in vivo* study)

### 5.2.3.3 Conclusion

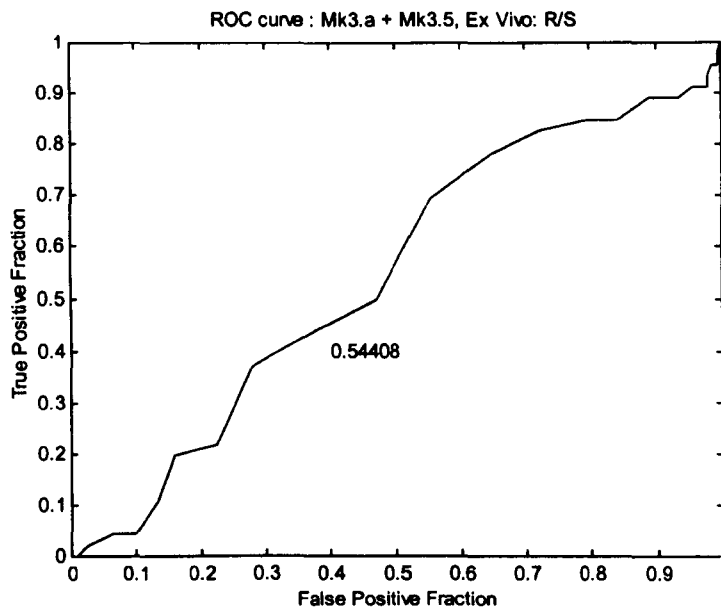
It was predicted that the measured impedance from benign bladder tissue at lower frequencies would be higher than the impedance of the malignant area. The electrical impedance of 18 patients (a total of 14 malignant and 21 benign points) were measured using the modified Mk3.5 Sheffield System. The resulting data demonstrated a confirmation of the last impedance data: the impedance of malignant area was significantly higher than the impedance of non-malignant area. In addition, there was a better separation of impedance at lower frequencies (lower than 2 KHz, Figure 5.30). The plot resulting from the Cole equation fitting demonstrated that the impedance of the malignant area of the bladder approaches to the right hand side and the reading of the benign area are placed in the left hand side of the figure. The ROC demonstrates that  $R$  alone, given the small number of points in the sample, provides reasonable separation between benign and malignant points. If the aim of the screening procedure is to exclude normal patients, who would otherwise be subjected to an invasive procedure which is not without risk, then an NPV of 17-69% may be acceptable.

### 5.2.4 Receiver Operating Characteristic curve (ROC) application on the combined *ex vivo* and *in vivo* results

The scatter plot suggests that classification of malignant areas may be possible, but the false-negative and false positive rate may be high. This has been explored using Receiver Operating Characteristic (ROC) curves for the parameters  $R$  and  $\frac{R}{S}$  separately. The ROC curve for the parameters  $R$  and  $\frac{R}{S}$  was used for the results of the Cole equation fitting scatter plots from Figures 5.14 (combined Mk3.a and Mk3.5, *ex vivo* study) and 5.27 (combined Mk3.a and Mk3.5, *in vivo* study). The results are shown in Figures 5.34 and 5.35 (the areas under the ROC curves are demonstrated in figures). These ROC curves show that individual classification is possible.

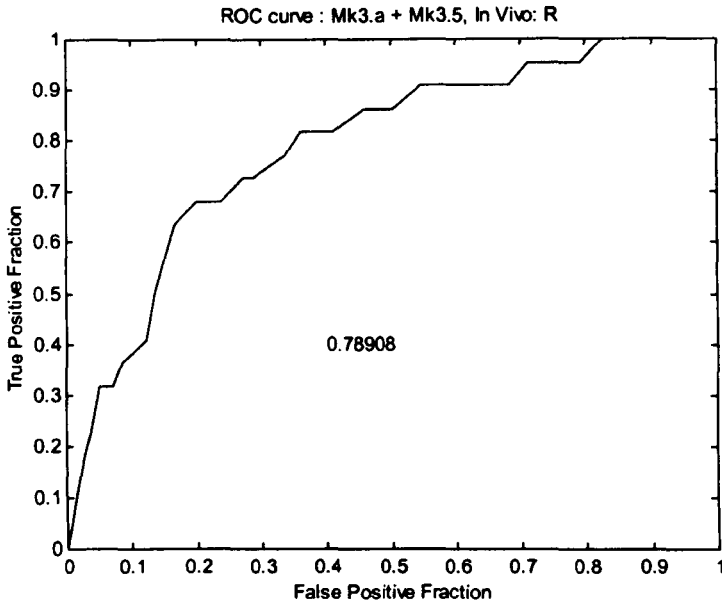


a

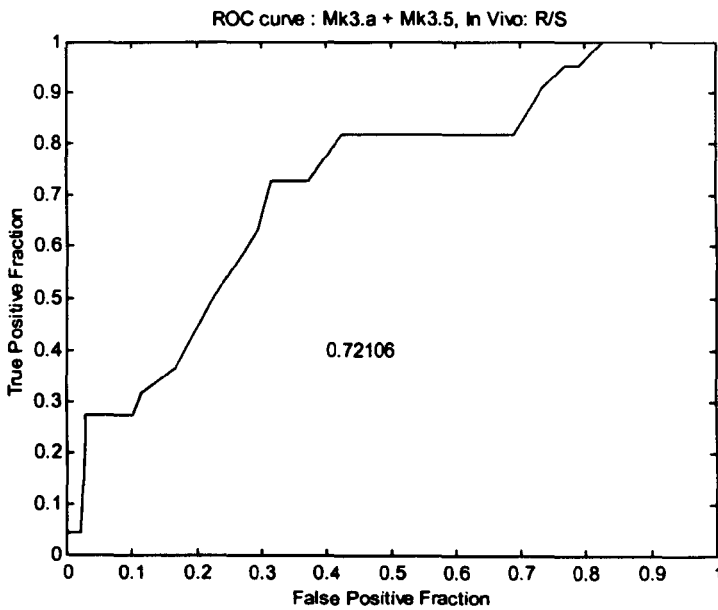


b

**Figure 5.34** The ROC curve for the parameters  $R$  and  $\frac{R}{S}$  using the combined Mk3.a and Mk3.5 Sheffield Systems (Ex vivo study): a)  $R$  b)  $\frac{R}{S}$



a



b

**Figure 5.35** The ROC curve for the parameters  $R$  and  $\frac{R}{S}$  using the combined Mk3.a and Mk3.5 Sheffield Systems (In vivo study): a)  $R$  b)  $\frac{R}{S}$

## 5.3 Conclusions

The electrical impedance data of the human urothelium were measured using Mk3.a and Mk3.5 Sheffield Systems both *ex vivo* and *in vivo* and compared with histopathological reports of the biopsies which had been taken from the measurement area. These impedance data distributions were evaluated in both groups and in both *ex vivo* and *in vivo* cases using boxplots. Thus, the data distributions were not normal in all of the cases and therefore, a non-parametrical statistic test, the Kolmogorov-Smirnov 2 Sample Test, was used to assess their separation. The separation of these readings related to the malignant and non-malignant groups were evaluated in each case and revealed a significant difference between these two groups, especially at lower frequencies (see section 5.2.3). The impedance of malignant and benign areas for the *in vivo* study is respectively a slightly higher than the impedance of these areas in the *ex vivo* study. Possible reasons are: 1) Existence of glycine inside the urinary bladder for the *in vivo* study, which increases the measured impedance (see section 6.4). 2) The time between the bladder resection and taking impedance data for the *ex vivo* study. This can decrease the impedance of the bladder tissue in the *ex vivo* case relative to the time duration (Galeotti 1902).

The Cole equation fitting procedure was used to generate a scatter plot of the malignant and non-malignant points: in general, malignant points had higher values of  $R$  and  $\frac{R}{S}$  than the non-malignant points. To evaluate the individual points which were not placed in their group, their related histopathological reports including the effects of inflammation and oedema on the measured impedance of the urothelium were considered (for example, a few malignant points were placed in the non-malignant area and vice versa). It was confirmed in this study that the inflammation caused increasing impedance and the oedema caused a significant reduction in the measured impedance of the bladder tissue (sections 5.2.1.1.5, 5.2.1.2.4 and 5.2.1.3.3 in the *ex vivo* study). Finally, an important message of this chapter can be the separation ability to distinguish carcinoma *in situ* (CIS) from the different degrees of the bladder tissue inflammation, because the common sign of these pathological changes in the bladder tissue surface is the existence of red colour using a cystoscope (see section 5.2.1.3.4). There were significant differences between CIS and inflammation with degrees of 0 and 1, but in more severe cases of inflammation (degrees 2 and 3) the change in the impedance of the

tissue is of the same value as when CIS is present. Therefore, this impedance technique at present cannot accurately distinguish CIS from the severe inflammation.

Extension of the measurements to lower frequencies showed an increasing separation of the impedance spectra at low frequencies. A priori, the impedance of malignant tissue would be expected to be lower than normal tissue (lower tight junctions; increased extra-cellular space), and this is found in cervical tissue. The anomalous results in bladders tissue remain to be explained. The ROC curve for the extended frequency measurements includes an area of 0.91 with an SE of 0.07, indicating that the technique could provide diagnostic information. An important provision is that the data relates to individual biopsies, and not to individual patients, and the aim is to identify patients with malignancy who require further investigation. Therefore, ROC curves showed that individual classification is possible. An appropriate strategy would be to repeat the analysis using, for each patient, the individual measurement which had the greatest value of  $R$  (i.e. the measurement with the highest likelihood of malignancy). However, there are too few patients in this series for this procedure to yield reliable results.

# Chapter 6

## The effects of experimental conditions on bio-impedance measurements

### 6.1 Introduction

There are different experimental conditions or parameters which are expected to affect the resulting electrical impedance of the urinary bladder such as the reproducibility of the measurements, the probe size, the value of applied pressure over the probe, the effect of the bladder volume changes and of different liquids of the bladder on impedance reading. Some of these important parameters will be discussed in this chapter. The effect of applied pressure and the bladder volume changes on measured results will be described. These effects usually exist in the experimental area, and may cause significant effects on the measured data and thus will be considered in this chapter. In addition, it is expected that the bladder volume changes may have an effect on the measured results as well as the applied pressure. These parameters are also described in this chapter. Furthermore, the effect of Glycine and Saline solution inside the bladder is important because they are expected to change the transfer impedance of the bladder. Glycine is usually used in bladder surgery in the theatre to make an insulation medium for electro-surgery and the extension of the mucosa and saline solution is usually used to wash the inside of the bladder after bladder surgery and to extend the mucosa. Thus, the impedance measurements were usually performed under these conditions.

### 6.2 The effect of applied pressure on measured results (*ex vivo*)

#### 6.2.1 Introduction

This section will discuss an important experimental condition, the applied pressure on the probe, which was expected to affect the reproducibility of the measured electrical impedance of the bladder. It is important to consider this effect *in vivo* or *ex vivo*. Therefore, this section is mainly concerned with the standardization or optimisation of the applied pressure (force). However the reading of electrical impedance is known to differ if different pressures are applied to the tissue. These changes depend on the size of the probe according to the following pressure calculation. When the probe is applied to

the bladder tissue, the applied pressure has an effect on the measured electrical impedance data because it compresses the tissue and may squeeze out extra-cellular water. A study carried out by Gonzalez-Correa (2000), he showed that excessive pressure on the squamous and columnar tissue can increase the measured impedance and it reached a maximum change of about 50% at the highest pressure. The electrical impedance of the bladder was measured in the *ex vivo* case. However, the bladder tissue was in the relaxed state and all of the measurements were taken from points that had benign histology reports. If the probe radius ( $r$ ) is small, the increased pressure ( $P$ ) effect due to the equation (6.1) will be very high.

$$P = \frac{F}{A} = \frac{W}{\pi.r^2} \quad (6.1)$$

$W$ , in this equation, is the applied weight or the applied force over the probe. The probes used in this study have a radius of 1 mm, therefore:

$$P = \frac{W}{3.14 \times 10^{-6}} \quad Pa. \quad (6.2)$$

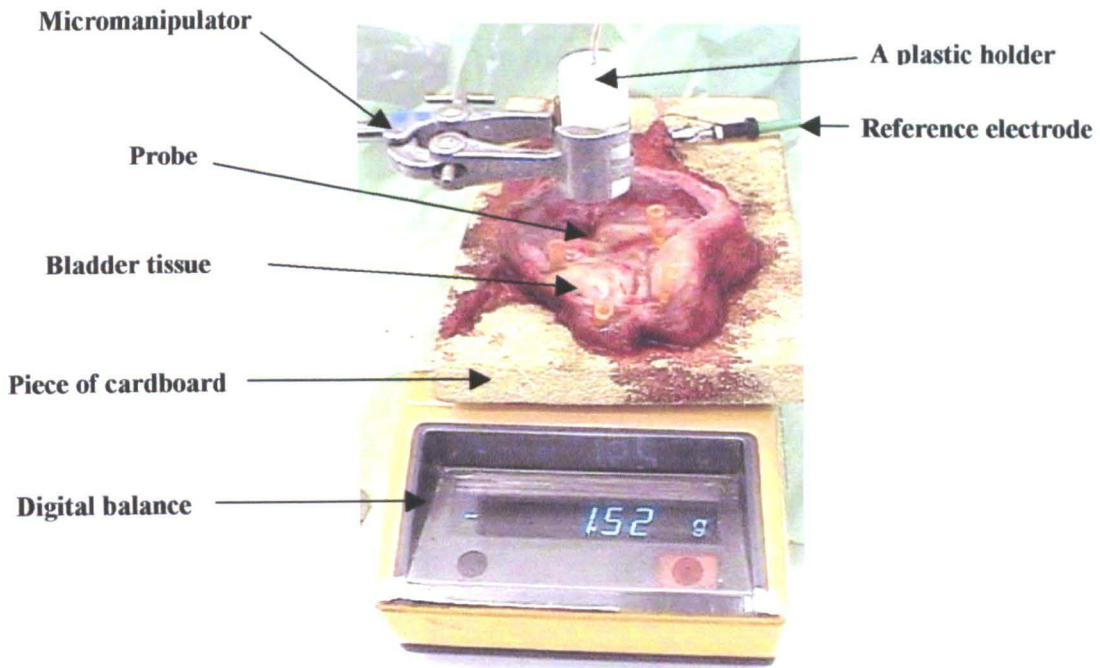
If we use a larger probe area (a larger contact area between probe and the bladder tissue), the applied pressure will be decreased according to the equation (6.1). Therefore, the author used a larger contact area of one probe (5 mm radius), using a plastic disc to cover the probe. The measured impedance results can then be compared with the results of the same probe (without the disc). It is expected that this pressure would be decreased because of the larger probe (5 mm radius) area compared to the probe without the disc (1mm radius). Also, in this process, a digital balance was used to determine the exact weight or applied pressure in the two cases. The reason for this study was to assess the effect of applied pressure on the impedance measurements using two different contact area sizes and if this could be optimised.

### 6.2.2 Measurement method

In this section, first of all, the reproducibility of the measurements for every point was considered. Therefore, an experiment was carried out on 6 resected bladders assessing a total of 60 points (10 points per patient). Every point included 3 independent impedance measurements. The main aim of this experiment was the evaluation of the reproducibility of the impedance measurements to demonstrate the reliability of

repeated measurements. Because of the effect of applied different pressures on the repeated measurements, this matter was studied in detailed. When the applied pressure on the probe is changed, the bladder wall thickness will change and which may alter the electrical impedance of the bladder wall. Different forces were used to assess the effect of pressure on the measured impedance of the bladder tissue. The following experiment was carried out using bladder tissues taken from three patients *ex vivo*. Immediately after resection, the bladder was opened in the histopathology department by a histopathologist. It was extended on a small piece of cardboard (15 x 7 cm) and fixed with pins. The Mk3.5 Sheffield System and a digital balance were set up to measure the electrical impedance of the sample under a defined pressure (see Figure 6.1). This figure shows an opened bladder sample on a digital balance, the fixed probe inside a white plastic holder using a micromanipulator (Figure 6.1a) and the Mk3.5 Sheffield System (Figure 6.1b).

The role of the balance in this study was to determine the force applied over the sample. In this method, as this figure shows, the probe was fixed in a micromanipulator and then pushed downwards to increase the pressure over the bladder tissue. This was pushed until a visible indentation appeared to ensure that the probe and tissue connection was completed. The digital balance shows a typical weight that was applied over the surface of the resected bladder tissue (the tissue is in the relaxed state). After each reading and before taking the next one, the bladder tissue was allowed to redistribute. This was done by removing the probe from the surface of the bladder and reapplying it after about 10 seconds.



a



b

**Figure 6.1 Set-up of bladder sample, probe, digital balance and Mk3.5 Sheffield System to assess the effect of applied pressure on the measured electrical impedances**

The author chose three newly resected bladders including different measured points (Table 6.1a) and then applied an m.file (written by the author) in Matlab programme to assess the applied force on the bladder in 7 different groups (Table 6.1b).

Patient 1			Patient 2				Patient 3			
Point 1 gf	Point 2 gf	Point 3 gf	Point 1 gf	Point 2 gf	Point 3 gf	Point 4 gf	Point 1 gf	Point 2 gf	Point 3 gf	Point 4 gf
3.3	1.5	2.7	5.0	5.8	1.7	1.5	7.7	6.7	6.8	6.9
5.9	3.6	4.5	15.5	14.8	5.4	9.3	14.5	14.8	13.6	14.0
8.3	6.4	11.3	25.0	24.0	13.1	15.5	20.0	25.4	23.5	23.4
9.6	11.0	14.2	35.8	35.1	22.0	25.1	24.2	45.5	40.7	43.1
17.7	14.0	18.1	47.6	45.1	33.2	35.6	40.6	68.9	55.9	55.9
23.7	19.8	22.4	59.5	53.6	48.6	44.7	54.1	88.1	64.1	77.3
28.2	24.0	23.0	71.3	67.8	59.2	53.5	86.6	108.5	73.0	96.5
							99.9	140.9	85.4	111.5
							150.6	159.9	93.9	145.9
							167.7	163.1	126.5	185.4

**Table 6.1a The forces applied to the three resected bladder tissues to study the effect of different pressures on the bladder tissue impedivity (the reading of the balance in grams was proportional to the applied force, gf).**

Groups	Number of measurements	Force value (gf)
Group 1	8	0-5
Group 2	11	5.1-10
Group 3	16	10.1-20
Group 4	17	20.1-40
Group 5	16	40.1-70
Group 6	11	70.1-120
Group 7	8	120.1-200

**Table 6.1b 7 force groups were used to assess the effect of force on the measured impedance in three resected bladders (gf=gram force)**

At every point, different forces were applied to assess the resultant impedance. Three readings were taken per point and per applied force to assess the reproducibility of the measurements. The digital balance was adjusted to show zero including the bladder sample and thus the balance reading was the grams force of the applied force on this bladder tissue. A finite pressure over the probe was applied by hand and then the

reading at every applied pressure was stored in a connected laptop computer (Figure 6.1b) for further calculation using a Matlab computer- based programme.

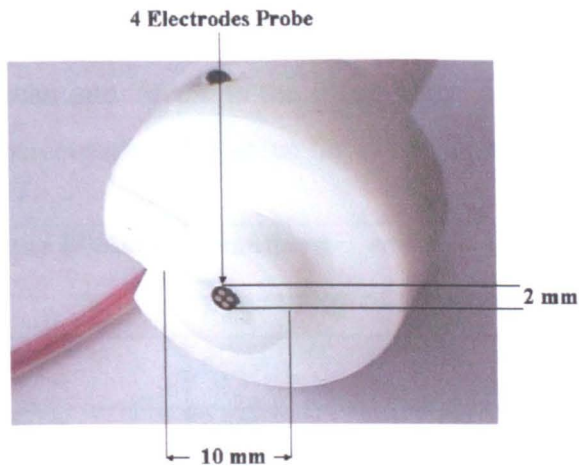
The probe could go down and up easily inside the clamp and the pressure was applied only to the probe and not to the clamp. As was mentioned above, to assess the reproducibility of every measurement, 3 independent readings were taken after every measurement and the probe was removed from the bladder tissue surface and then replaced as accurately as possible in the same position. The 3 measurements were averaged (these readings were usually not more than 8% difference). The minimum force required to produce the first record-able reading on the bladder tissue or a visible indentation was variable in the different points of three bladders, 1.5 gf (4.7 KPa)- 7.7 gf (24 KPa) but its mean value was 4.5 gf (14 KPa). To achieve lower pressures, the probe was modified by increasing the radius of the contact area (from 1 mm to 5 mm). See Figures 6.2b and c. Two further resected bladders were used for low pressure measurements. Large and small probes were used separately in 5 different force groups to assess the effect of probe contact area on the results (Table 6.2).

Groups	Number of measurements		Force value (gf)
	Small probe	Large probe	
<b>Group 1</b>	28	5	0-5
<b>Group 2</b>	24	40	5.1-20
<b>Group 3</b>	34	30	20.1-50
<b>Group 4</b>	45	38	50.1-100
<b>Group 5</b>	86	112	100.1-400

**Table 6.2 5 force groups were used to assess the effect of probe contact area on the measured impedance using two resected bladders (gf=gram force)**



a



b



c

**Figure 6.2 Probe size affects electrical impedance measurements. a) Small size (1 mm radius) probe b) Large size (5 mm radius) probe c) Large size probe with cable (the probe was placed in the centre of the white plastic disc and then secured in its place using a screw)**

### 6.2.3 Measured results and discussions

Initially, the reproducibility of the measurements using small size probe for every point is very important in this study. Thus, the results of 6 resected bladders assessing a total of 60 points (10 points per patient) were plotted as Figure (6.3) (every point included 3 independent impedance measurements). This figure shows the mean value of the measured data against frequency with related error bars. The main aim of this experiment was the evaluation of the reproducibility of the impedance measurements to demonstrate the reliability of repeated measurements. In this figure, every coefficient of variation, ( $Var = \frac{SD}{Mean}$ ), can demonstrate an indication of its reproducibility. *SD* is the standard deviation of mean and *Mean* is the mean value of the 3×10 measured data. The standard error as a percentage of the mean for every bladder is shown in Table 6.3.

<b>Resected Bladder</b>	<b>Standard error as a percentage of the mean</b>
<b>Bladder 1</b>	40%-10%
<b>Bladder 2</b>	14%
<b>Bladder 3</b>	10%
<b>Bladder 4</b>	25%
<b>Bladder 5</b>	100%-23%
<b>Bladder 6</b>	32%-7%

**Table 6.3 The standard error as a percentage of the mean for the measured impedance of 6 resected bladders (using small sized probe)**

It is clearly seen that the impedance measurements using small sized probe are not perfectly reproducible and therefore the effect of different applied forces can be a major problem. Thus, this effect will be assessed in this section. Following this, the author carried out another experiment to assess the effect of larger contact area of the probe. Thus, 10 resected bladders were used with small probes and 10 resected bladders with large probes using different applied forces to compare their reproducibility (3×8 measured data per bladder) (Figure 6.4a and b). The applied forces are shown in plots.

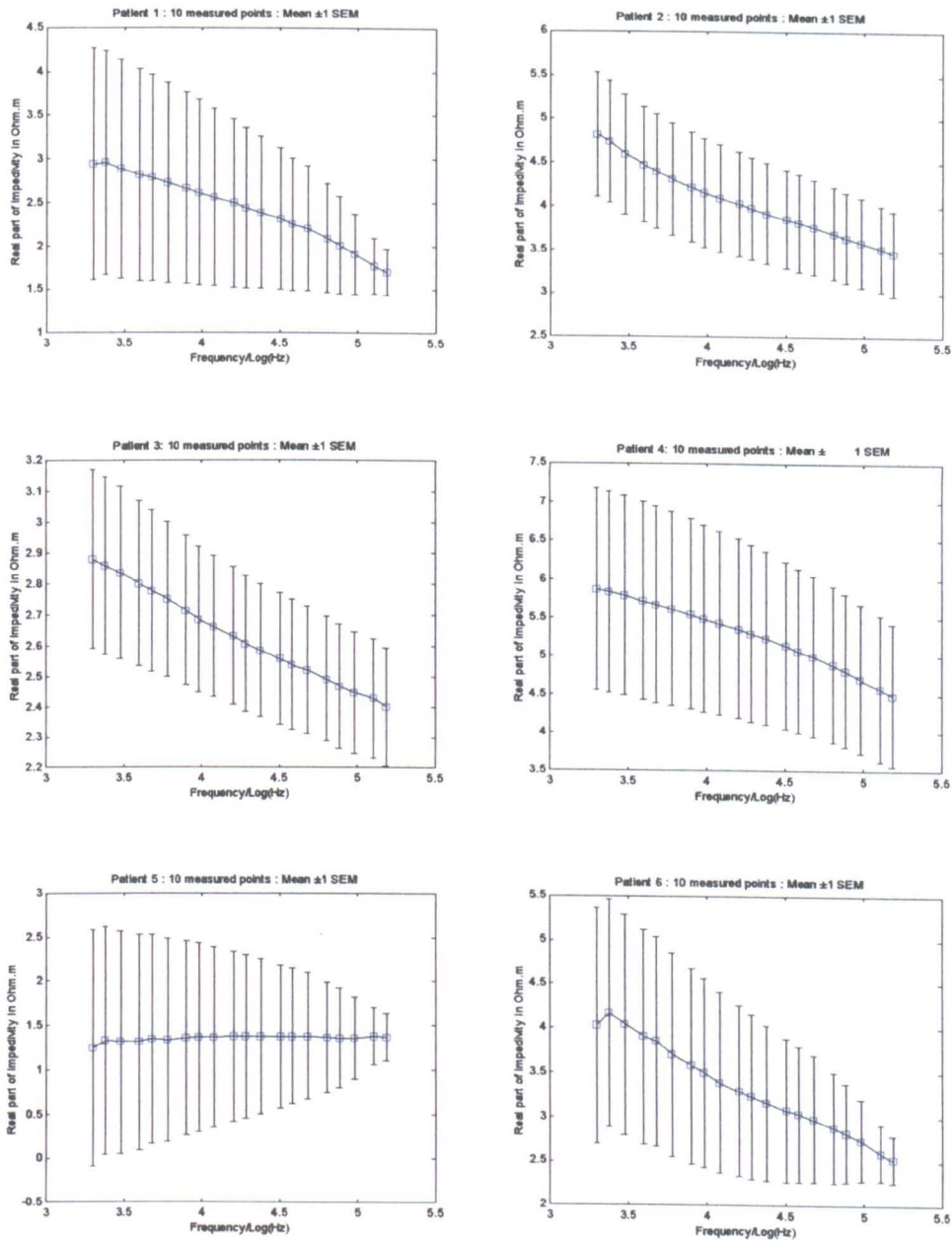


**Figure 6.3** The reproducibility of the measurements resultant from the 6 resected bladders without pressure using small probe (each point is the average of 3 different measurements from that point). The calculated coefficient of variation ( $Var = \frac{SD}{Mean}$ ) for these plots are: Var 1 = 1.20, Var 2 = 0.46, Var 3 = 0.28, Var 4 = 0.69, Var 5 = 1.20, Var 6 = 0.27.

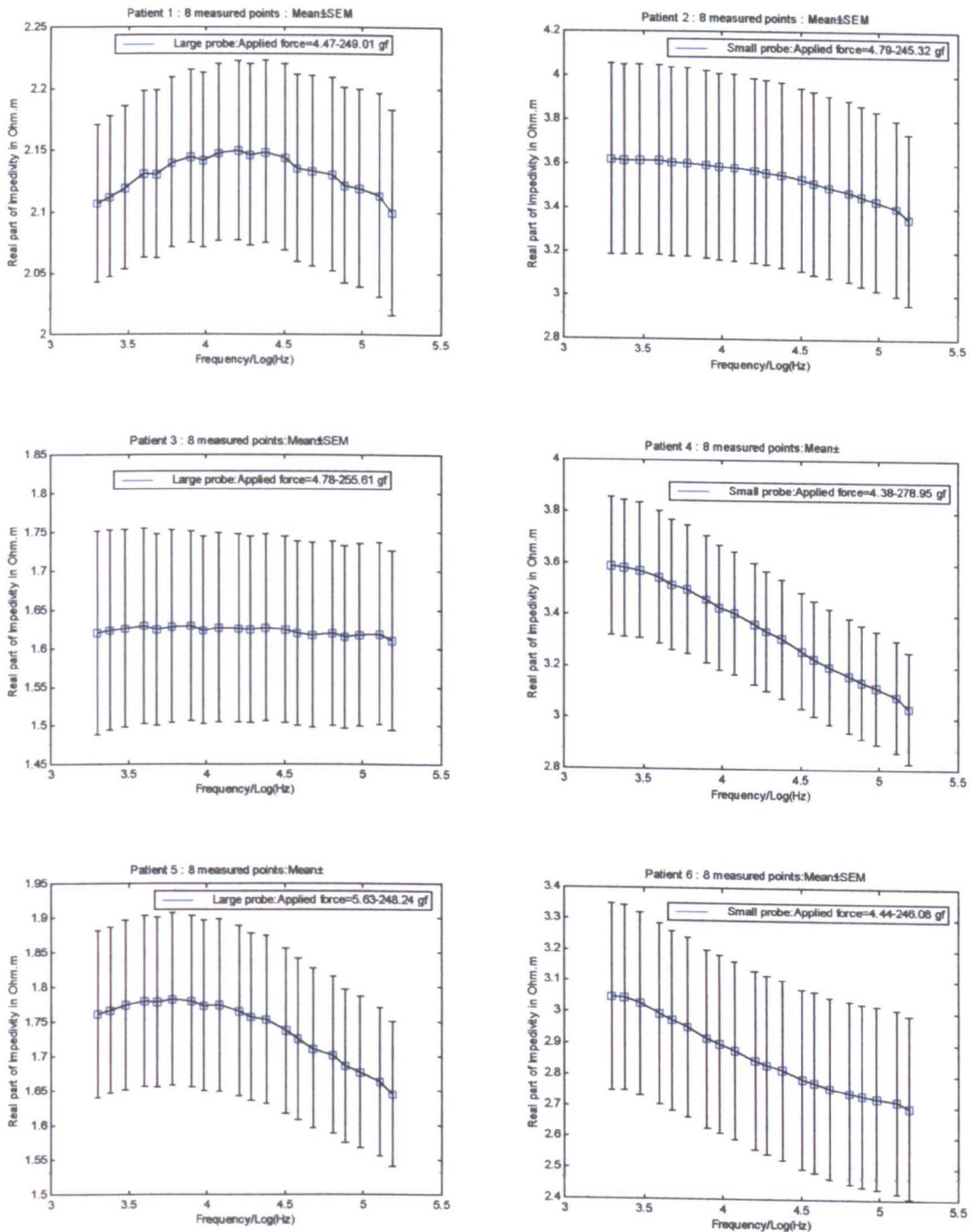
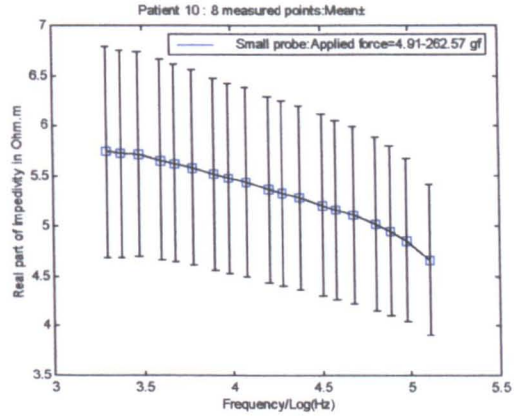
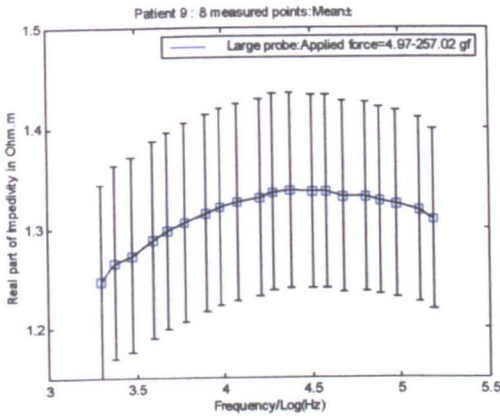
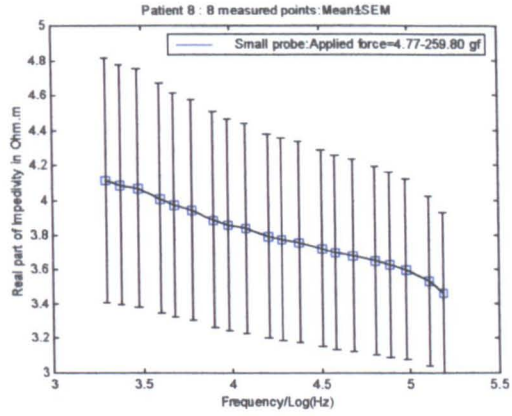
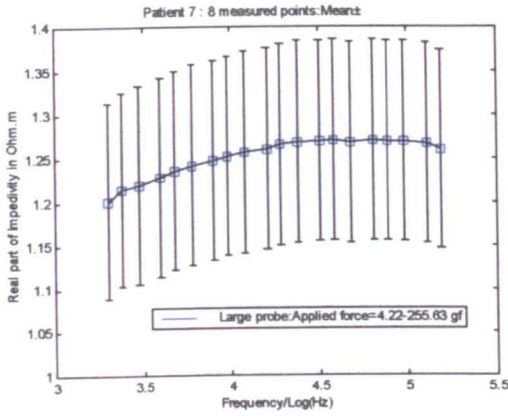


**Figure 6.4a** The reproducibility of the measurements resultant from the 6 resected bladders with pressure (each point is the average of 3 different measurements from that point). The calculated coefficient of variation ( $Var = \frac{SD}{Mean}$ ) for these plots are: **Var 1 = 0.11, Var 2 = 0.33, Var 3 = 0.21, Var 4 = 0.20, Var 5 = 0.19, Var 6 = 0.29.**

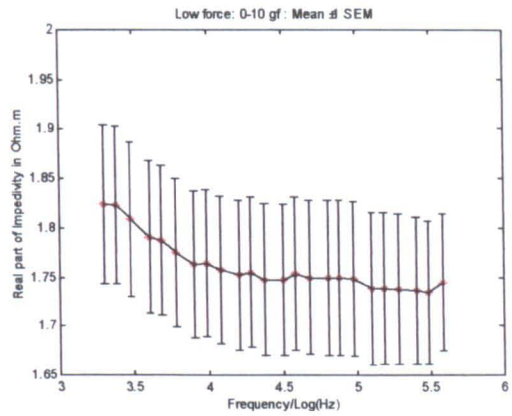
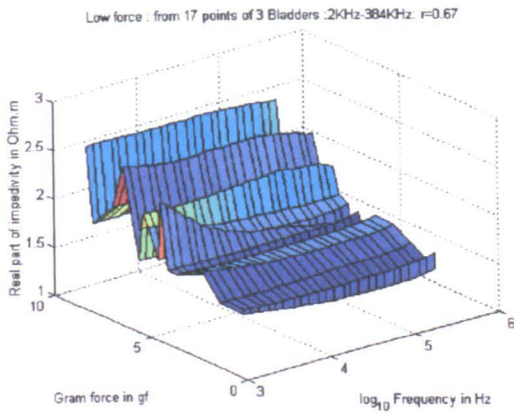
**(Left hand side: using large probe, Right hand side: using small probe)**



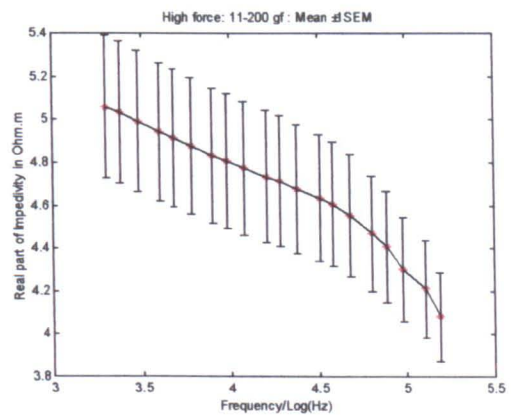
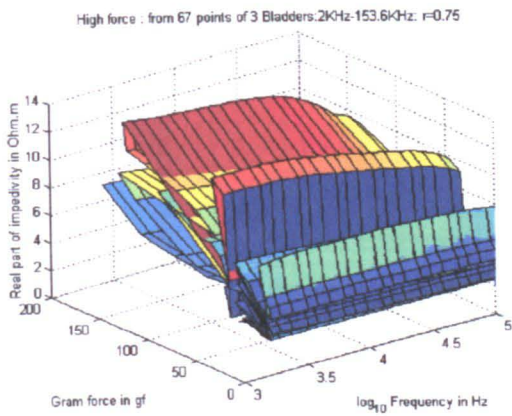
1SEM

**Figure 6.4b** The reproducibility of the measurements resultant from the 6 resected bladders with pressure (each point is the average of 3 different measurements from that point). The calculated coefficient of variation ( $Var = \frac{SD}{Mean}$ ) for these plots are:  $Var\ 7 = 0.26$ ,  $Var\ 8 = 0.44$ ,  $Var\ 9 = 0.21$ ,  $Var\ 10 = 0.52$ . (Left hand side: using large probe, Right hand side: using small probe)

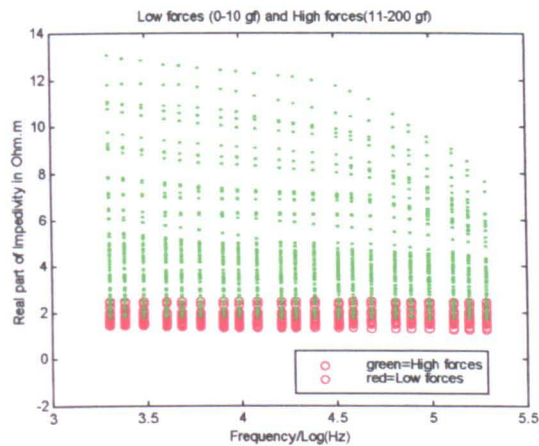
In Figure 6.4a and b, the mean value of the measured data was plotted against the frequency with related error bars using both small and large probes with different applied forces. According to this figure, the error for the reproducibility of the large probe application is about 3%-8% but for the small probe applications it will be about 6%-19% over all of the frequencies. Thus, the large probe is more reproducible than small one. Following this, the effect of different applied forces on the measured data is presented here. Three patients' resected bladders were chosen in this study. Initially, three points of the bladder 1 were chosen accurately and then 7 measurements were performed per point using 7 different applied forces (Table 6.1). Then, the applied forces were divided into two low (0-10 gf) and high forces (11-200 gf). There is a 3-D plot of the applied low and high forces effects on the measured impedances in Figure 6.5.



a



b



c

**Figure 6.5** Effect of applied pressure on the electrical impedance using small probe: a) Low force: 0-10 gf b) High force: 11-200 gf c) All forces

For every case, an error bar plot is presented to show the mean value of the impedance on the low and high forces including 1SEM (standard error of mean) at the right-hand side of Figures 6.5a and b. Following this, all the measured impedance (89 measurements) representing the effect of applied force on the measured impedance are shown in the above-mentioned groups (Figure 6.5c). Figure 6.6 show the effect of different pressure groups (Table 6.1b) using small probe on the measured data.

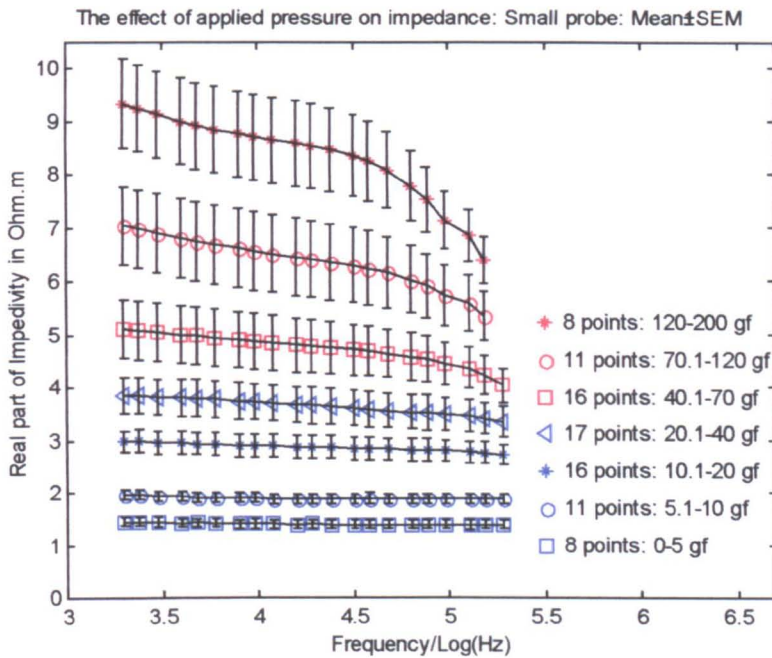


**Figure 6.6 Effect of applied pressure on the electrical impedance using small probe: All forces**

Therefore, it is clear from the graphs that there is a stepwise increase of the impedance at all of the frequencies from one force group to the next. In addition, the impedance in the highest force group is about 7 times bigger than the impedance of the lowest force group. There is about 5% variation of measured impedance in the lowest force groups (0-5 gf and 5.1-10 gf) that can cause the first visible indentation.

The low force group (0-10gf) is compared with the high force group (11-200gf) in Figure 6.7.

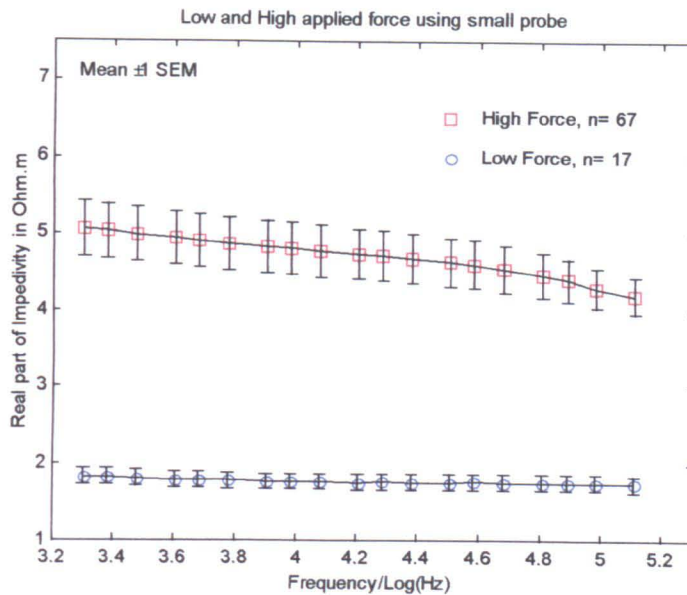
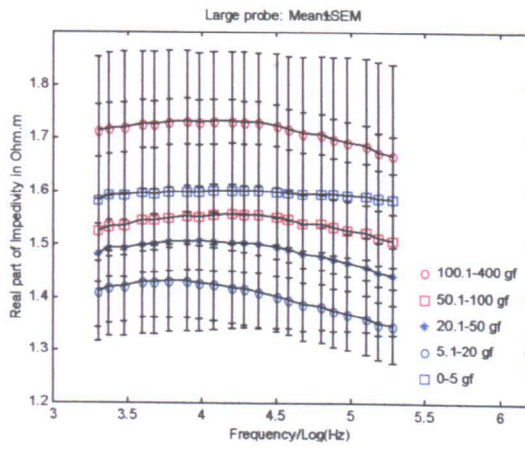
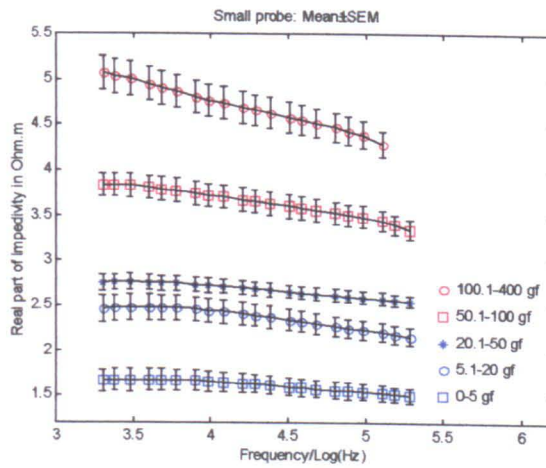


**Figure 6.7 Effect of applied pressure (Low: 0-10gf and High: 11-200gf) on the electrical impedance using small probe**

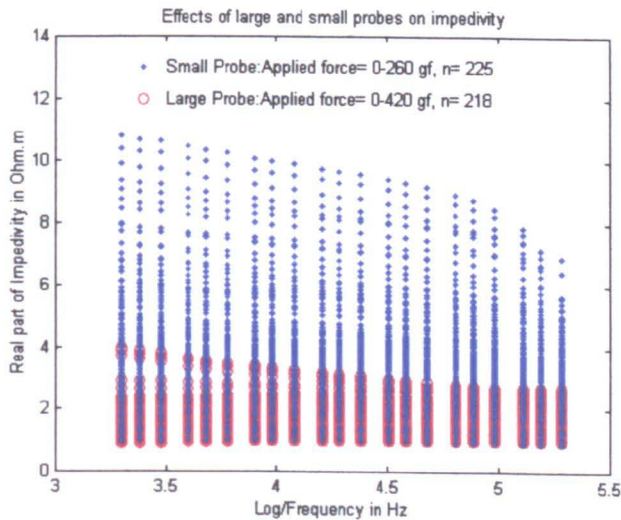
To eliminate or minimise the effect of pressure on measured impedance, the effect of the large size of the probe is considered. Thus, in this part of the work, bladder sample impedances have been measured both with a probe without a white plastic disc (radius, 1mm) and with a probe with a white plastic disc (radius, 5mm). Then, the measured data compared to consider the effect of probe size on the measurement process. For this purpose, there were used 2 resected bladder samples and the author chose a total of 10 points for assessment. The measurements were taken over a range of applied pressures (at 7 different pressures) and at first with the probe alone (small probe) and then repeated using the white disc (large probe). Three measurements were taken from each of 10 points because of reproducibility. The effect of the large probe on the measured impedance of the bladder tissue is presented in Figure 6.8. The plotted results (from about 420 separate readings) show that the measured impedivities using large and small probes were significantly different ( $p < 0.001$ ).



**a**



**b**



**c**

**Figure 6.8** Effect of applied pressure on the electrical impedance using small (1mm radius) and large (5mm radius) probes over the resected bladders 1 and 2 in different forces: **a)** Large probe **b)** Small probe **c)** All of the measured points

## 6.2.4 Conclusion

The reproducibility of the impedance measurements using the urinary bladder tissue was evaluated and because of the variation of measured impedance from the defined points of the bladder tissue the effect of applied force on the probe was considered. The results of different experiments in this section that were demonstrated graphically showed that the increasing the applied force over the probe caused significant increases of the bladder tissue impedances. Also, the optimum force that can be applied to the bladder was found to be less than 10 gf and thus this first visible indentation was used as an indicator for taking impedance readings. At this applied force, the variance in the impedance readings is less than 5%. Finally, the effect of the probe contact area using a large probe was important because of the significant decrease of the impedance changes due to the applied force.

## 6.3 The effect of bladder volume changes on the measured results

### 6.3.1 Introduction

The aim of this section is to find the effect of volume changes on the measured data. When the bladder volume changes, the bladder wall thickness also changes and this may alter the electrical impedance of the bladder. For example, as the bladder distends, its thickness decreases and the superficial cells are flattened (Figure 1.2). The penetration depth, ( $\cong 500\mu m$ ) of the applied current remains constant and therefore the current could pass through the underlying tissue. Therefore, the structure of the underlying tissue may have an effect on the measured data. The path length of the current also depends on frequency. At lower frequencies, stretching of the bladder increases the path length of the current through the epithelial tissue but at higher frequencies the path length is decreased as the epithelial layer is thinner. The influence of the underlying tissue will therefore depend both on degree of stretch and frequency. Therefore, a number of impedance measurements have been done to show the effect of bladder distension on impedance using different volumes of glycine solution in the bladder. Glycine was selected in this study because it is an electrical insulator and commonly used during electro-surgery inside the bladder. Finally, three porcine bladder samples (*ex vivo*) and five human bladders (*in vivo*) were used in this study to assess this effect on the measured data.

### 6.3.2 Measurement method for *ex vivo* study

This experiment was carried out using a training box that was described by Radley et al in 2000 (Radley, Chapple et al. 2000). The porcine bladders were brought from the abattoir with a delay of about 3 hours and were then mounted in the training box. The shape of this box including a porcine bladder is demonstrated in Figure 6.9. To see inside the bladder and take impedance data, a compact endoscopic system was used (STORZ). In this procedure, a pin was used as a marker (to find the exact measurement point) and then impedance readings taken about 1 cm away from this pin.

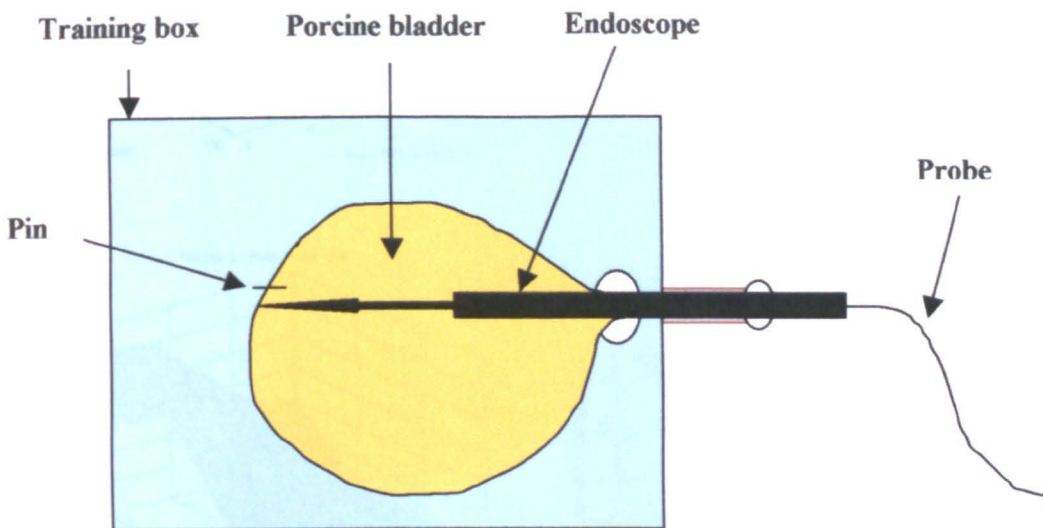


**Figure 6.9** The *ex vivo* training box to assess the effect of porcine bladder volume changes on the resulting impedance using a defined glycine solution.

In this study, three porcine bladders were filled with a defined glycine solution to increase the volume, thus distending the bladder wall. 100 ml of glycine was inserted into bladder 1 and then 3 independent impedance spectra were taken separately (probe removed and then procedure repeated) using the small sized probe to assess the reproducibility. After that, the volume of glycine was increased to 150 ml and then 3 more measurements were taken. This procedure was continued up to 350 ml (the maximum capacity of this bladder) and then 3 measurements were taken for each new case as usual. Finally, the impedance was measured by removing glycine solution from the bladder in increments of 50 ml up to 100 ml. This procedure was carried out for bladders 2 and 3 as well as for bladder 1 but only for increasing volume. The maximum volume of glycine inside these bladders varied with each bladder (for the bladders 1 and 2 it was 350 ml and for bladder 3, 600 ml). Electrical impedance was measured for every point (10 points of bladder 1, 6 points of bladder 2 and 6 points of bladder 3).

### 6.3.3 Results and discussion

Results are shown in Figure 6.10.

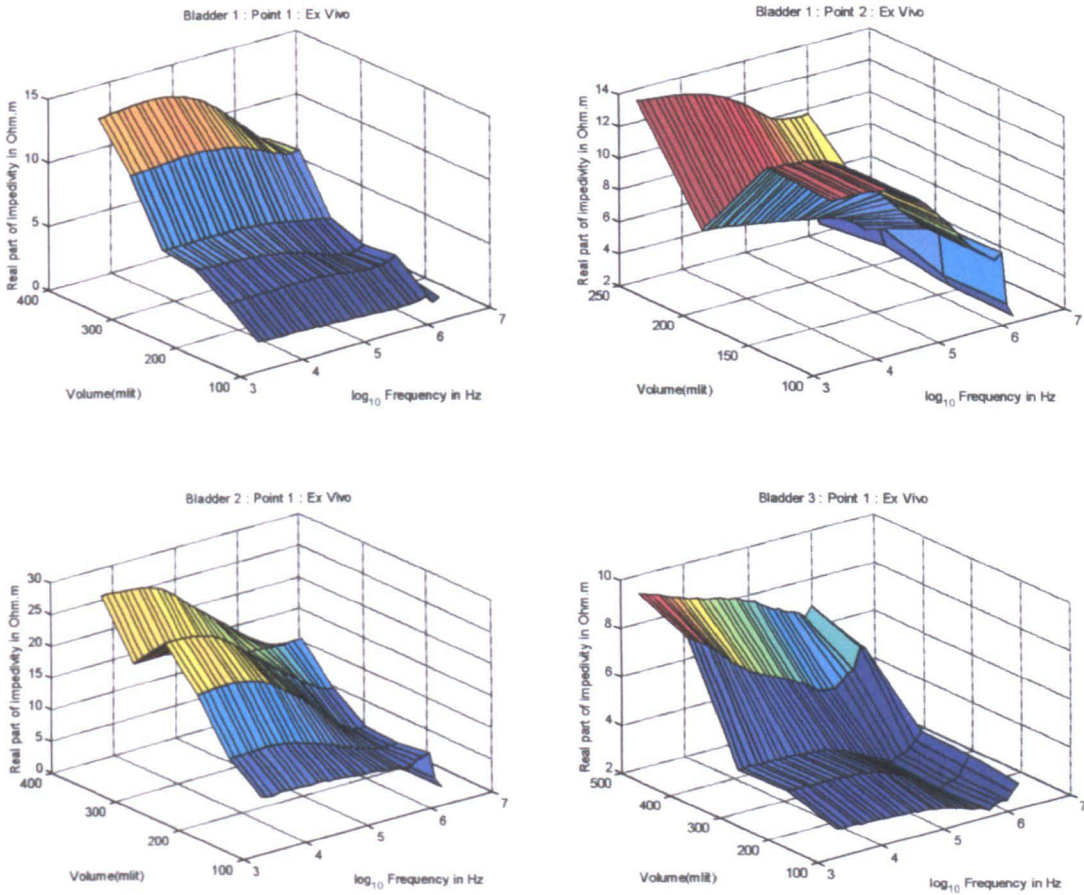


**Figure 6.10 Effect of volume changes of porcine urinary bladder on the measured impedance (*ex vivo*). There are three separated resected bladders.**

All of the measured points of three bladders are plotted in Figure 6.11 to assess the above-mentioned effect. Because the readings are not normally distributed, the Kolmogorov-Smirnov 2sample test was used as a statistical method to analyse the effect of volume changes on the measured data. There was no significant difference between the volumes of 100-150 ml, 150-200 ml, 200-250 ml, 250-300 ml and 300-350 ml. Although these figures do not show a significant difference between different volume changes in terms of electrical impedance, it is shown that the measured impedance will increase in general if the bladder volume increases. The path length at low frequencies was predicted to increase with bladder volume, which is consistent with the results. A smaller increase in impedance was seen at high frequencies, which may be due to

increased influence of the underlying tissue. The excised bladder was not constrained by the surrounding tissue, as it would be *in vivo*, and it was therefore difficult to apply a consistent force to the probe, which may have resulted in a high variability in the measurements.

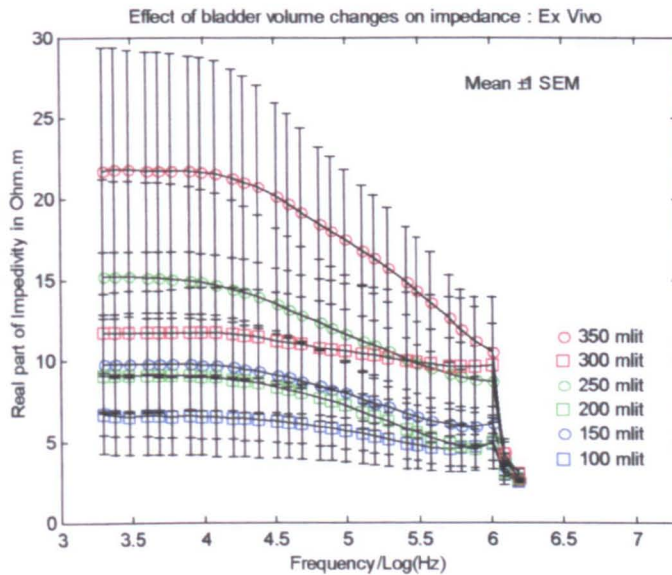


**Figure 6.11** Effect of volume changes of the porcine urinary bladder on the measured impedance (*ex vivo*) at 30 frequencies for the total number of points of three separated bladders.

### 6.3.4 Measurement method for *in vivo* study

There were five patients' bladders assessed in this experiment to evaluate the effect of bladder distension on the resulting impedance of the urothelium (*in vivo*). All of the patients were under anaesthesia. First of all, each measured point of the bladder was marked using indigo carmine as described in Chapter 4 to take the impedance reading about 2 mm away from this point. After that, each bladder was filled with a defined volume of glycine solution and an electrical impedance reading was immediately taken from that point. The maximum volume for each bladder varied from patient to patient, and is the volume at which all of the mucosal folds are flattened. Thus, different volumes of bladders were assessed to measure their impedance as shown in Table 6.4.

Patient		V1	V2	V3	V4	V5	V6	V7	V8
		(ml)							
Patient 1	Point1	230	330	430	530				
	Point2	530	430	330	230	130	30		
Patient 2	Point1	210	310	410	510				
	Point2	510	410	310	210	110	10		
Patient 3	Point1	150	250	350	450				
	Point2	-	-	-	-				
Patient 4	Point1	200	300	400	500				
	Point2	-	-	-	-				
Patient 5	Point1	200	260	320	380	440	740	720	200
	Point2	200	260	320	380	440	740	720	200

**Table 6.4 The different values of glycine solution inside the five bladders (*in vivo*) at different points. The initial volume for minimum distension is the range 150-230 ml and the final volume for maximum distension will be about 450-740 ml.**

Then, we changed the glycine solution volume and made repeated readings for different volumes shown in Table 6.4. This process was carried out for all of the patients' bladders.

### **6.3.5 Results and discussion**

The impedivity was plotted against frequency for the five patients' bladders that were used in this study (Figure 6.12). These plots demonstrate no significant relation between the urothelium impedance and the degree of the bladder extension using the glycine solution. Finally, the graph (scatter plot) in Figure 6.13 shows that the impedance in general decreases with an increase in the bladder volume at 2 KHz.

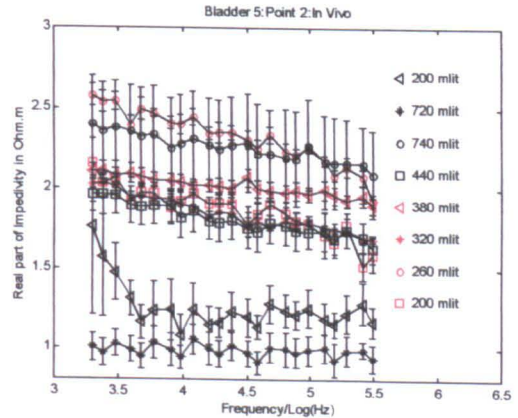
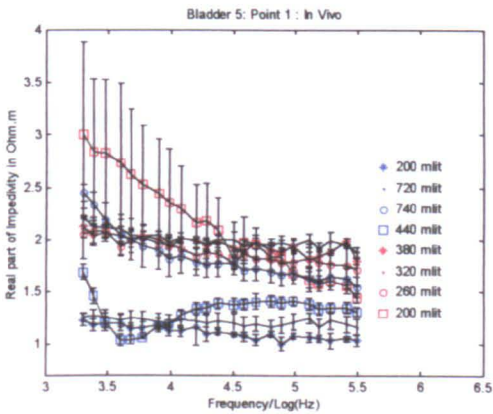
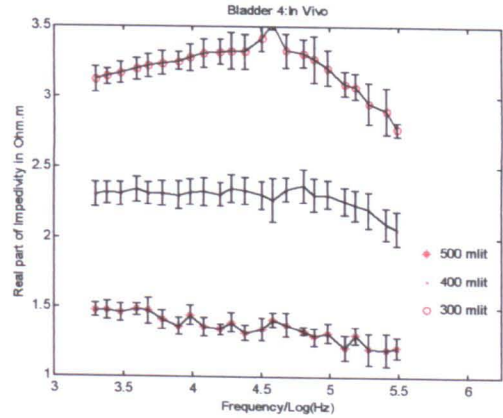
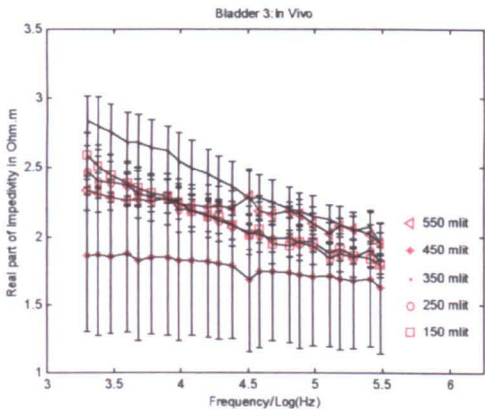
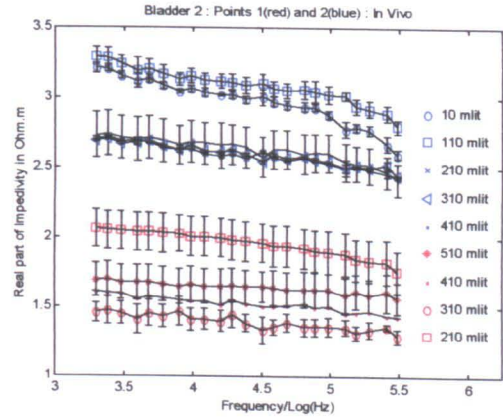
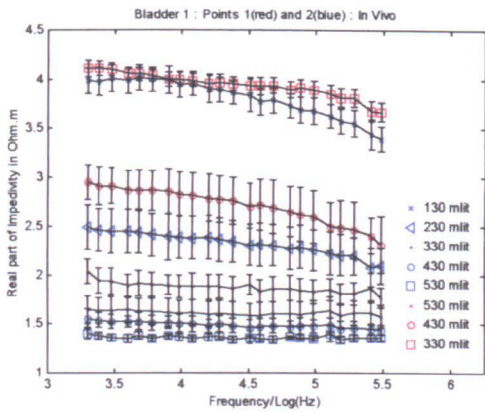


**Figure 6.12** Effect of volume changes of human urinary bladders on the measured impedance (*in vivo*) for all of five human patient's bladders.

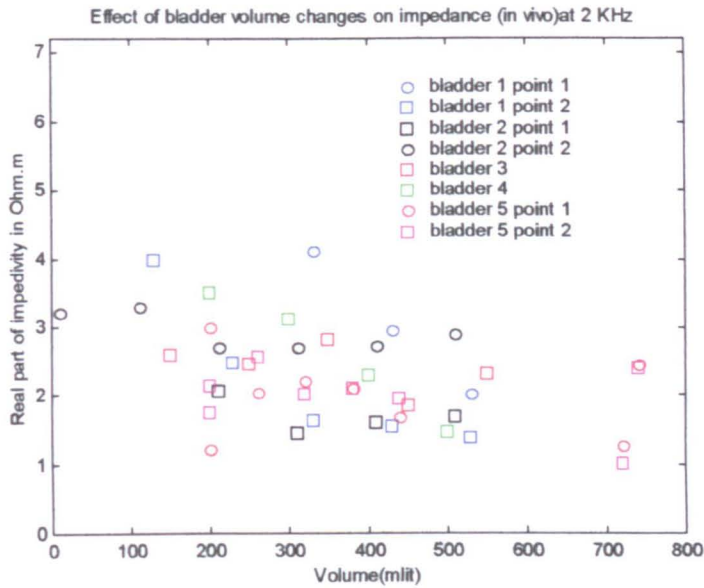


**Figure 6.13** Effect of the bladder volume changes on the measured electrical impedance (*in vivo*) in the forms of impedivity against increased volume with glycine solution.

### 6.3.6 Conclusion

The figures in this section show that if the bladder were stretched using glycine, the measured impedance usually decreased (but not significantly). In practice, for the *in vivo* measurements, the bladder was filled until folds in the mucosal surface were removed i.e. minimum tension was applied to the bladder wall, rather than filling the bladder to a constant volume and therefore creating a varying degree of tension in the wall.

## **6.4 The effect of different surface fluids on the electrical impedance of the bladder**

### **6.4.1 Introduction**

The effect of surface fluids (mucus) on the impedance spectrum on the surface of cervical epithelium was studied using a finite element model by Walker et al in 2002 (Walker, Brown et al. 2002). They found that there is an apparent change of tissue impedance depending on the type and thickness of the surface fluid. Jones et al in 2003 modelled the effect of conductive surface fluid on the apparent tissue impedance (Jones, Smallwood et al. 2003). Because of the common application of some surface fluids during bladder surgery the *in vivo* impedance readings were taken under this condition. Two fluids (normal saline solution and glycine solution) are commonly used to distend the human urinary bladder epithelium to allow adequate visualisation of the bladder mucosa in theatre using the endoscopic procedure. Glycine solution (1.5 %) is usually used as an insulator when diathermy is required but saline solution (0.9 %) is used if a diagnostic procedure such as cystoscopy does not require electro surgery. The first fluid has high and the later fluid has low impedance and thus can affect the real impedance measured in this study. Therefore, the author carried out an experiment to search for the possible effects of these fluids on the impedance measurements of the bladder tissue in benign and malignant cases. This study is expected to evaluate the appropriate fluid that could be used to characterise the bladder urothelium significantly.

### **6.4.2 Methods**

#### **6.4.2.1 *Ex vivo* study**

The effect of some common surface fluids and air were studied in this section using three resected human bladders (*ex vivo*). These bladders were moved from theatre to the histopathology department immediately after excision and then were opened and pinned to a corkboard to take the impedance readings using the Mk3.5 Sheffield System. Before any reading, the bladder samples were marked at ten areas using sutures. Following this, the bladder and corkboard were completely submerged in saline solution and then the readings were taken about 1 cm from the sutures. This procedure was repeated with the bladder submerged in glycine and then air respectively. Both glycine and saline solutions were usually at 37°C, the normal human body temperature. A total of 30 points (26 benign and 4 malignant points) were assessed in this work. In

addition, a biopsy was taken from the same measured point in order to compare the malignant and non-malignant tissue response in the presence of these materials and to gain information about their effect on impedance. Three readings per point were taken from 30 points of the bladder when it was covered by saline, glycine and air respectively.

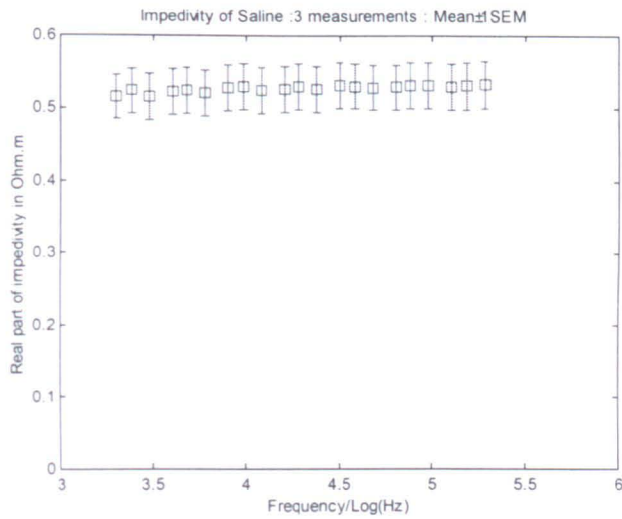
#### **6.4.2.2 *In vivo* study**

In this study, a total of six points of three bladders were assessed using saline solution and glycine separately. These fluids were inserted in the bladder to distend its mucosa. In each case, a mark was made on the bladder urothelium using indigo carmine as mentioned in chapter 4 (section 4.5). Then the impedance readings were taken from two points (1 cm either side of this mark) using Mk3.5 Sheffield System. After the impedance measurements, the bladder was emptied and the amount of liquid measured to use in further evaluation of the impedance readings. This procedure was repeated for both saline and glycine solutions at the same points.

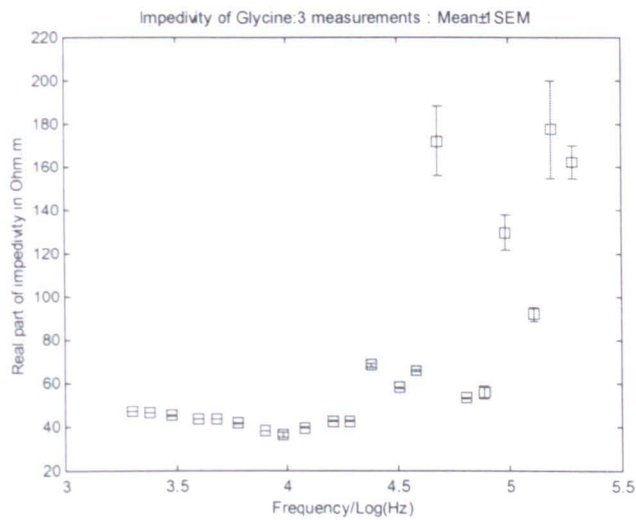
### **6.4.3 Results and discussions**

#### **6.4.3.1 *Ex vivo***

First of all, the impedivity of the surface fluids was measured three times and then averaged using the Mk3.5 Sheffield system (Figure 6.14). The volume of these fluids was about 100 ml at body temperature. The figure demonstrates that the impedance of glycine ( $\cong 50\Omega m$ ) is about 100 times larger than that of saline ( $\cong 0.5\Omega m$ ). Then, three human bladders were submerged in different surface fluids and the impedance of malignant (3 points of bladder 1 and 1 point of bladder 3) and benign (7 points of bladder 1, 10 points of bladder 2 and 9 points of bladder 3) points were measured. Each measured point includes 3 separated impedance readings because of reproducibility. Thus the total number of measured malignant points was  $4 \times 3 = 12$  and for non-malignant was  $26 \times 3 = 78$ . As Figure 6.15 shows, there are three plots of the bladder submerged in air (Figure 6.15a), saline (Figure 6.15b) and glycine (Figure 6.15c).



**a) Impedivity of saline solution**



**b) Impedivity of glycine**

**Figure 6.14 Impedivity of saline and glycine solutions at 21 frequencies (2-192 KHz)** The volume of these liquids was about 100 ml. Note that the system failed to obtain several readings at certain frequencies because these points are out of probe calibration range (see Figure 4.3). The data represent the mean of 3 readings per point for reason of reproducibility.

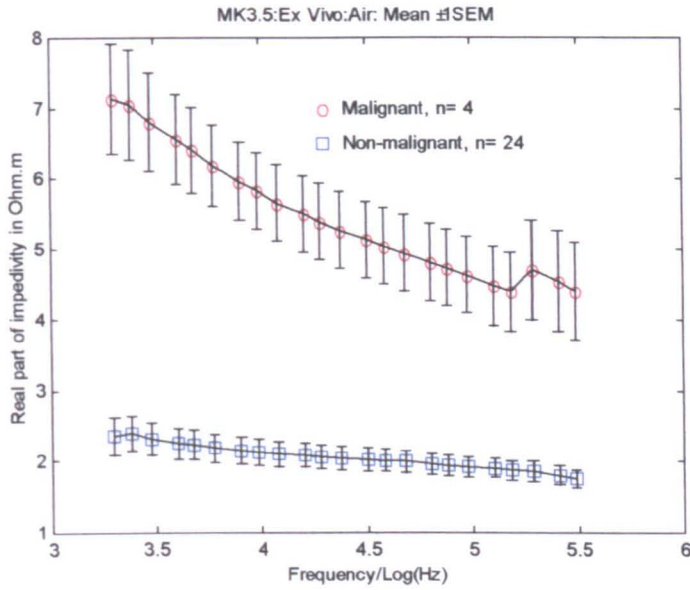


**Figure 6.15a Comparison of Malignant (n=4) and Non-malignant (n=26) points in air**

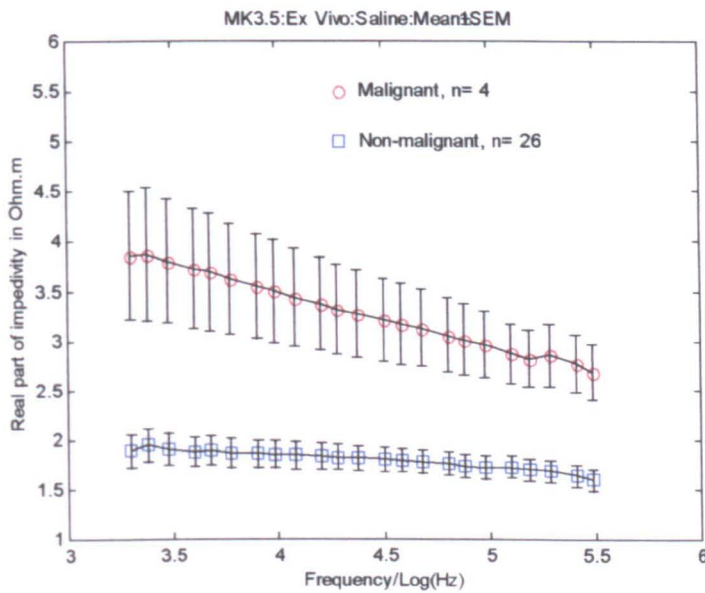


**Figure 6.15b Comparison of Malignant (n=4) and Non-malignant (n=26) points in saline solution (0.9 %)**

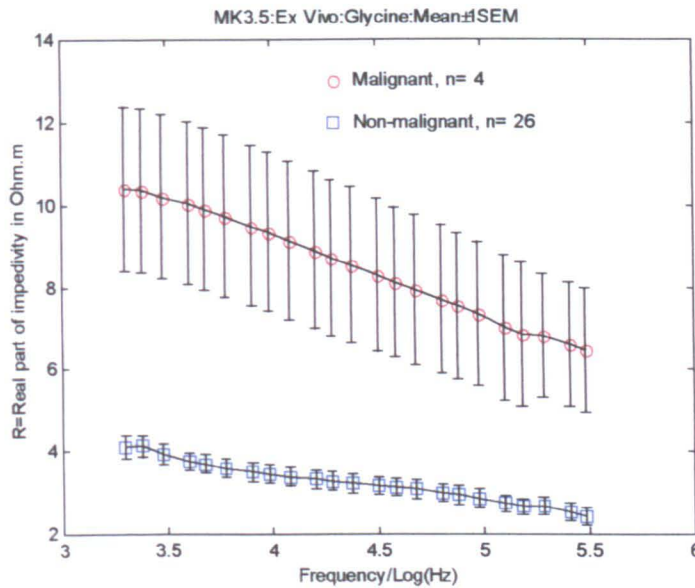


**Figure 6.15c Comparison of Malignant (n=4) and Non-malignant (n=26) points in glycine (1.5 %)**

The Kolmogorov-Smirnov 2 sample test was used at each frequency because the data distribution was not normal. There was a significant difference between the impedance of malignant and non-malignant points using air ( $p < 0.0001$ ), saline solution ( $p < 0.001$ ) and glycine solution ( $p < 0.001$ ).

These 3 plots show a significant separation of malignant and non-malignant groups from each other. These plots also show that the measured data for the bladder with glycine has higher impedance than the bladder with air. So, the electrical impedance of the bladder filled with air is more than the bladder filled with saline solution at all frequencies and in both malignant and non-malignant states. Another plot compares the measured data of malignant and non-malignant groups in the presence of various materials (Figure 6.16).

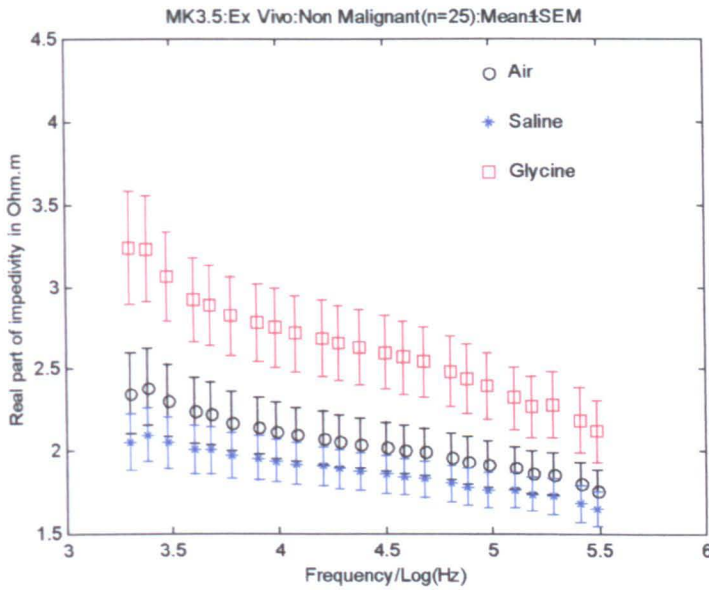


**Figure 6.16a Comparison of non-malignant points (n=25) in air, saline (0.9 %) and glycine (1.5 %) (each point is the average of 3 separated readings because of reproducibility)**

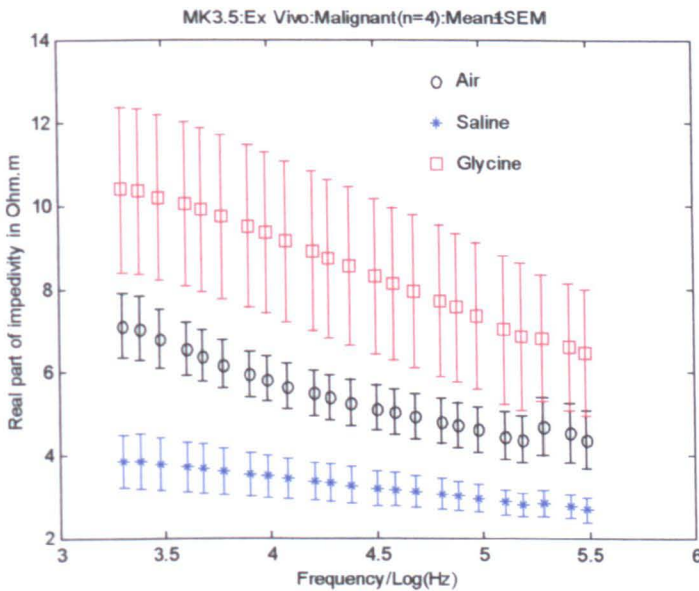


**Figure 6.16b Comparison of malignant points (n=4) in air, saline (0.9 %) and glycine (1.5 %) (each point is the average of 3 separated readings because of reproducibility).**

From these figures it is clear that there is a difference of the electrical impedance for malignant and non-malignant points. However, in all cases, for glycine the impedance is more than air and for air it is more than saline. The Kolmogorov-Smirnov 2 sample test was used at each frequency because the data distribution was not normal. There was

no significant difference between measured data of non-malignant points using air-saline, air-glycine but there is a significant difference between saline-glycine ( $p < 0.02$ ). Also, for malignant cases, there was no significant difference between air-saline, air-glycine but there is a significant difference between saline-glycine ( $p < 0.03$ ).

If we use glycine or saline in our measurements, the measurement will be dominated by its high and low impedivity respectively rather than the tissue impedivity. Thus, the possible reason that the results in Figure 6.16a and b are different for malignant and non-malignant groups may be due to fluid between probe and tissue. It is clear that the type of surface fluid has a significant effect on the measured data. Generally, the impedance taken in glycine is of the order of 1.3-2 fold greater than readings taken in air (especially at lower frequencies) and in saline this ratio will be 20 % lower than in air.

#### **6.4.3.2 *In vivo***

As mentioned above, a total of six points (all benign) from three bladders were compared in resultant impedance using saline and glycine fluids separately (Figure 6.17). Each measured point included 3 separated impedance readings. This figure shows that the mean value of impedance when we used glycine was higher than when saline was used (approximately 3 fold increase). There is a significant difference in measured impedance between the six points of the bladder urothelium when the bladder included saline and then glycine ( $p < 0.03$ ). Although the measured impedance using glycine is significantly more than the impedance using saline solution (*in vivo*) and the mean value of impedance in saline cases seems to be the same as *ex vivo* results, the mean value of impedance for glycine cases for *in vivo* and *ex vivo* cases is different (compare Figures 6.16a and 6.17 for saline and glycine results). This difference may be due to the small number (6) of measurements for *in vivo* study.

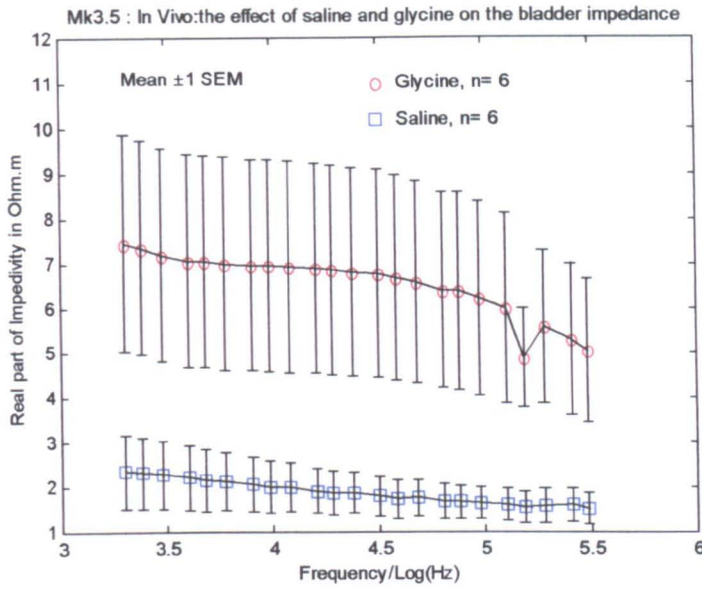


**Figure 6.17 Comparison of the benign bladder impedance when it is submerged in saline and then glycine (*in vivo*)**

#### 6.4.4 Conclusion

It was expected that the surface fluid on the bladder epithelium would affect the measured transfer impedance. The measurements in this section show that the impedance of bladder tissue using surface fluids such as air, saline and glycine is different, and the impedance will be 1.3-2 folds greater when we take the readings in glycine than in air. Also, this measurement for saline is about 20% lower than in air. However, the measured impedance is usually between the impedance of saline ( $0.5\Omega m$ ) and glycine ( $50\Omega m$ ). This impedance is the highest when we are using glycine and the lowest if the saline solution is used as the surface fluid. The folds of the bladder will disappear as the bladder is distended, and readings should be taken at the minimum filling which removes folds. Finally, the best fluid between air, glycine and saline to measure the impedance of the urinary bladder can be air ( $p < 0.0001$ ) because of the greater separation of malignant and benign points when using this fluid inside the bladder. For consistency, it is essential to always use the glycine in the bladder during impedance measurements (*in vivo*). This would allow diathermy to be used in the surgery procedure and would save time and cost as fluid would not have to be changed for the tumour resection.

# **Chapter 7**

## **Comparison of experimental and computational modelling results**

### **7.1 Introduction and background**

#### **7.1.1 Introduction**

In the Department of Medical Physics, a number of electrical impedance measurements have been carried out on the cervix, the oesophagus and the urinary bladder. The effect of abnormal tissue changes on the electrical impedance has been investigated, which has prompted mathematical models of these organs. Computational modelling of the electrical impedance technique may be able to produce an insight into the use of this method as a diagnostic technique. An important problem in modelling is obtaining quantitative information about the organs; their type and structure of tissues; the size of the cells, the ability of cells to contract or distend; and in response to physiological changes the changes in tissue and cell structure in pathologic situations because the measured impedance strongly depends on these factors. Unlike normal oesophagus and cervix, the urinary bladder tissue is distensible and lined with transitional epithelium (cell shape changes from cuboidal to squamous) depending on the state of contraction or distension. Changes in cell shapes and arrangements due to distension are expected to influence the electrical properties of the tissue. A numerical technique, finite element analysis (FEA) was used to model the electrical properties of bladder tissue in order to predict the impedance spectrum of normal and malignant areas of this organ. The modelled data will be compared with the experimental results in this study.

#### **7.1.2 Background**

Miller et al reviewed the application of finite element methods to the modelling of bioelectric phenomena (Miller and Henriquez 1990). They formulated the governing equations for these models and then derived the finite element equations for the generalized bioelectric problem. The finite element method has previously been applied to oesophagus and cervical tissues (Walker 2001; Jones 2003). Before the normal oesophagus changes to cancerous oesophagus, the tissue undergoes metaplasia from normal stratified squamous to a columnar epithelium. However, in the case of the cervix, the stratified tissue exhibits changes during a pre-cancerous development called

cervical intraepithelial neoplasia (CIN) which includes an increased nuclear-cytoplasmic ratio, losing flattened cell layers close to the surface of the tissue and increasing the volume of extra-cellular space (Sorensen, Bichel et al. 1991). Differences in the electrical impedance spectra of the tissues appear to be explained by changes in cell arrangements and in the extra-cellular space. This suggests that an indication of tissue structure may be able to be derived from electrical impedance spectral measurements.

### 7.1.2.1 The impedance measurements and modelling of cervical tissue

Brown et al (2000) measured the impedance of cervix tissue. According to their work, the measured electrical impedance made on normal squamous tissues was well separated from that made on pre-cancerous tissues. (Brown, Tidy et al. 2000; Walker, Brown et al. 2002). It was hypothesized that the characterisation of the electrical impedance spectrum of cervical tissue is related to cellular arrangements of the tissue and the nuclear to cytoplasmic ratio. Walker et al. modelled the electrical impedivity of normal and pre-malignant cervical tissue using finite element analysis (Walker, Brown et al. 2000; Walker, Brown et al. 2002). They used data published in the literature, and a survey of histological sections to obtain cell and nuclear size parameters used to construct finite element models of individual cells. These parameters were published in Walker et al. 2003 (Walker, Brown et al. 2002; Walker, Brown et al. 2003). Table 7.1 summarises some of their results.

Layer no.	Cell dimensions ( $\mu\text{m}$ )			N:C ratio	ECS width ( $\mu\text{m}$ )
	X	Y	Z		
<b>1. Superficial</b>	65	65	15	0.01	0.05
<b>2. Intermediate</b>	50	50	15	0.01	0.1
<b>3. Parabasal</b>	30	30	15	0.05	0.2
<b>4. Basal</b>	15	15	15	0.2	0.4

**Table 7.1 Dimensions of cellular compartments used in model construction (N:C=nuclear – cytoplasmic ratio, ECS=extra-cellular space).(Walker, Brown et al. 2002)**

Electrical properties calculated from the cellular level model were then used in a tissue level model and currents applied using a similar arrangement to that used in the *in vivo* probe. This allowed the calculation of a potential distribution in the tissue model, and hence a transfer impedance could be calculated. This was compared to the measured results.

The effect of basement membrane properties, the depth of surface mucus layer, and epithelial thickness, on the real component of impedivity for modelled impedance spectrum, was investigated, and the results compared to measured data. They indicated that a value of 10  $\mu\text{m}$  surface mucous layer gave the best fit to experimental data. They concluded that this model can predict differences in electrical transfer impedance between normal and cancerous tissues as well as real measurements and could aid the improvement in the design of the measurement system for early cervical pre-cancer detection.

#### **7.1.2.2 The impedance measurements and modelling of oesophagus (columnar) tissue**

Gonzalez-Correa et al (1999) measured the electrical impedance of the oesophagus. They showed that the squamous and columnar tissues of the oesophagus could be separated by electrical impedance spectroscopy. They expected that it is possible to separate these tissue types using a data modelling process (Gonzales-Correa, Brown et al. 1999). Therefore, electrical impedance measurement may detect pre-malignant changes in the oesophageal tissue.

Also, in the department of medical physics, Dr. D. M. Jones used finite element modelling to model the electrical properties of normal and pre-cancerous oesophageal tissue (Jones 2003). He hypothesised that the measured data was very sensitive to the surface environment. Thus, he decided to assess the performance of the measurement system using finite element analysis. He developed a computational model of the tissues using finite element analysis, and applied this method to the gastric epithelium, in particular a section of gastric crypt. This long and narrow section is an important feature of gastric epithelium.

In addition, this modelling method was used to model the electrical properties of squamous and glandular columnar epithelia of the gastrointestinal tract in order to characterise the electrical properties of these tissues. The properties used for modelling of a section of a gastric crypt are shown in Table 7.2. A 3-D model of a whole section of mucosa, including glands, was produced using the electrical properties of a small section of gland (Figure 7.1).

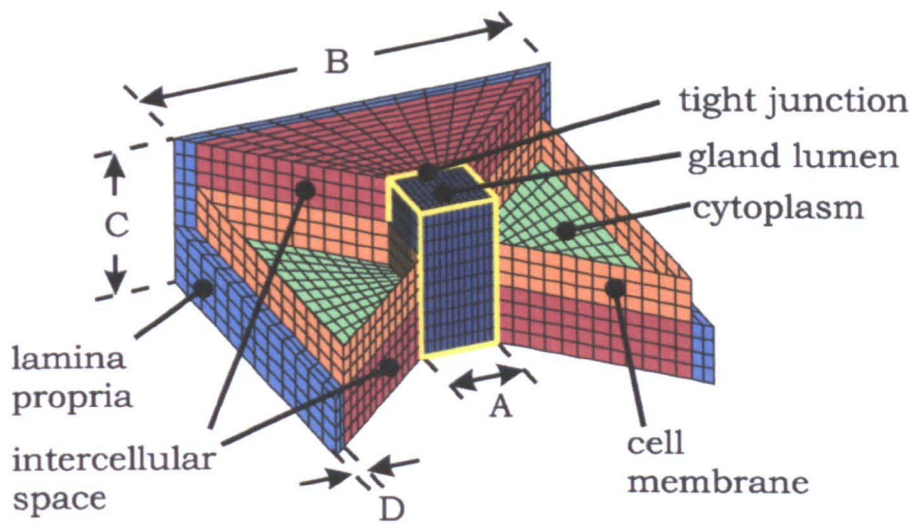


**Figure 7.1 Three dimensional diagram of gland section finite element model. Dimensions A, B, C and D are given in Table 7.2 (Jones 2003)**

The output from this model was compared with the measured impedance spectra. According to the comparison of experimental and modelling results, the modelling confirmed the difference between the impedance of columnar and squamous tissues but the modelled impedance varied significantly depending on the amount of surface fluid present (Jones 2003).

Property	Value
Side of gland lumen (A)	10 $\mu\text{m}$
Thickness of lateral intercellular space	0.5 $\mu\text{m}$
Side of the whole of the model (B)	50 $\mu\text{m}$
Height of columnar cells along gland lumen (C)	20 $\mu\text{m}$
Half-thickness of lamina propria section of model (D)	2 or 4 $\mu\text{m}$
Conductivity of contents of gland lumen	1 $\text{Sm}^{-1}$
Conductivity of cell cytoplasm	1 $\text{Sm}^{-1}$
Conductivity of lamina propria	1 $\text{Sm}^{-1}$
Cell membrane capacitance per unit area	0.01 $\text{Fm}^{-2}$
Cell membrane conductance per unit area	1 $\text{Sm}^{-2}$

**Table 7.2 Properties used in modelling procedure (Jones, Smallwood et al. 2003)**

The impedance measurements of the human urinary bladder tissue were carried out by the author of this thesis. Then, the computational modelling approach was extended to the bladder in a combined study by Dr. D. C. Walker and the author. As was mentioned before, there is a need for more accurate, non-invasive, cheaper and faster methods of

bladder cancer diagnosis. In the light of work on cervical and oesophageal epithelia, it is expected that the electrical impedance measurement of the bladder tissue, combined with the modelling of this tissue, may offer an alternative method to diagnosing the bladder epithelium as either normal or pathological. Bladder modelling is further complicated because this organ, unlike the cervix, is a very distensible and thus its shape changes with filling or emptying in both normal and abnormal states. Also, the bladder tissue is different from the cervical tissue because the epithelial tissue of the bladder is usually variable in appearance and transitional. The superficial shape changes from cuboidal to squamous depend on the degree of the bladder wall distension.

Thus, the modelling can be expected to be difficult and should incorporate the minimum and maximum changes of the urinary bladder tissues. This depends on the extension and contraction of this organ, which determines cell sizes, shapes, intracellular and extracellular spaces which are required as parameters in the modelling process. As before, finite element analysis was used to model the electrical properties of this tissue. The values of cell sizes were obtained from both the literature and the analysis of the tissue sections of the measurement site. The measurements were made on the resected specimens of the human urothelium obtained immediately after resection surgery. It is believed that the image analysis of tissue sections may be useful in understanding the shape and cell arrangements, which can aid accurate modelling and ultimately can predict the actual electrical impedance of tissue.

## **7.2 Finite element modelling of the electrical properties of urothelium**

Accuracy and computability are two important considerations when one creates any mathematical model of a physical system or living organ. Either analytical or numerical methods can be used in this procedure. The first method provides an exact solution (direct solution of mathematical equations) and hence is the most accurate method to predict the behaviour of a system, but it is usually applied to isotropic and homogenous volumes. Living tissue is inhomogeneous in structure and therefore in terms of electrical properties and numerical techniques is therefore essential. The human urothelium is constructed of transitional epithelium and has a highly anisotropic nature. Numerical methods are used to model complex structures and calculate the best fit solution to the

problem based on the minimisation of an error term. This technique divides the volume into a many smaller volumes, named '*elements*' that are connected at '*nodes*', hence the name 'finite element' modelling.

Finite element analysis is a numerical technique routinely used in the solution of physics and engineering field problems. In the case of electrical problems, it is used to calculate an approximate solution for the potential distribution within a volume partitioned into elements. The theory of this technique and examples of applications to electrical biomedical problems can be found in (Miller C E 1990). If the electrical properties of the various materials in our cell or tissue model are known or assumed, for any given set of applied currents, the resulting potential at any point on the model boundary and hence the transfer impedance, can be calculated. As the number of nodes is increased, the solution approaches that of a continuous distribution. This method has been extended to model the transitional epithelium of the bladder. Model meshes were generated in the ANSYS software package (Ansys Inc., Pennsylvania), and models solved using in-house software written in Matlab.

We cannot model the dimensions of tissue 'seen' by our impedance measurement system with cellular level detail due to computing resource limitations, so we used a hierarchical method of modelling. Initially, finite element models of cells with dimensions typical of different depths in normal and malignant bladder epithelium were constructed, and the electrical transfer properties calculated from these models were then used as material properties in our macroscopic tissue level model.

## 7.3 Modelling methods

### 7.3.1 Cellular level finite element models

For the purpose of modelling tissue structure, it is easier if cells are modelled as simple geometric shapes. An example of a simple cell shape used in the cellular level model is shown in Figure 7.2. Geometrical and physical parameters of the urothelium were used in this study to construct a high-resolution model of the cell. Geometric parameters, such as cell size were obtained from both literature and observation of histology sections. According to a study in 1959 by Walker, the transitional epithelium of the urinary bladder had generally been described as consisting of two cell types, surface and deep cells (there was no quantitative information). It was shown that the deep cells can be subdivided into cells of an intermediate layer and cells of a basal layer (Walker 1959). One of the original papers (Ward, Stewart et al. 1986) demonstrated that the small cells (cuboidal-rounded) occupy the basal layer, the pyramidal cells (elongated cells) are intermediate layers, and the giant cells (large single cells) lie in the superficial layer of the normal human urothelium.

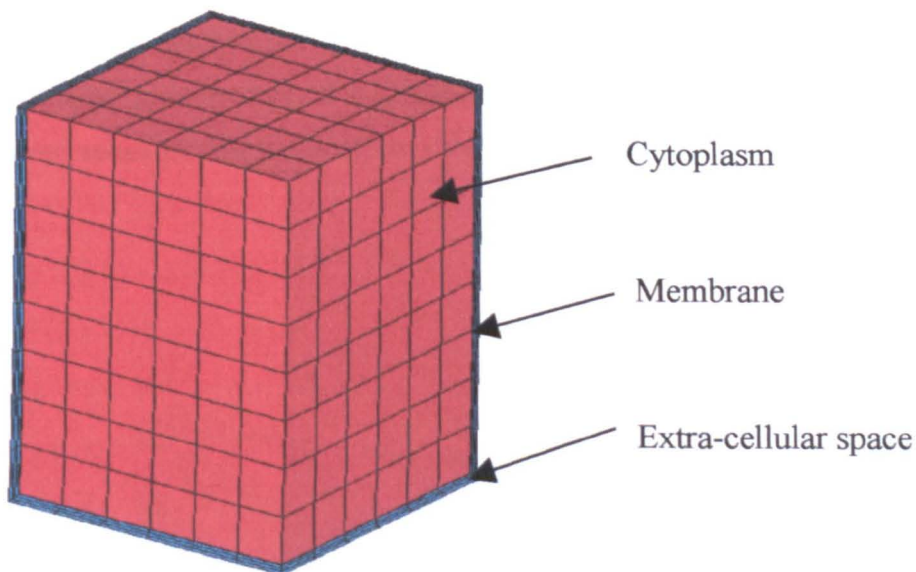


**Figure 7.2 Finite element mesh of part of a single cell**

There are original studies that include photographs of cells in these three layers for stretched tissue of the normal rabbit bladder tissue (Lewis and Hanrahan 1990; Lewis 2000). Values estimated from these photographs are shown in Table 7.3:

Layer	Cell size ( $\mu\text{m}$ ) (Lewis 2000)	Cell size ( $\mu\text{m}$ ) (Lewis and Hanrahan 1990)
Superficial	50-120	60-120 in length and 5-10 in height
Intermediate	20	30
Basal	5-10	15

**Table 7.3 The cellular morphological parameters of the normal rabbit urinary bladder obtained from literature (Lewis and Hanrahan 1990; Lewis 2000).**

The normal and malignant cellular morphological parameters of the human urinary bladder were obtained from analysis of digital images of bladder histology sections in this study by the author. To produce this quantitative information, initially 10 digital images of histological sections of normal, and 6 sections from malignant areas of the human urinary bladder, were chosen randomly (All sections were related to the *ex vivo* measurement study). One of these images is shown in Figure 7.3. Sections of epithelium were selected at random from each classified image and divided into superficial, intermediate and basal regions. Ten cells were selected from each region and Photoimpact SE version 3.02 used to calculate parameters such as the length and width of cells (parallel and perpendicular to the epithelial surface) and the thickness of the epithelium. Digital photographs of a graticule taken on the same magnification were used to convert measurements in pixels to values in micrometers.

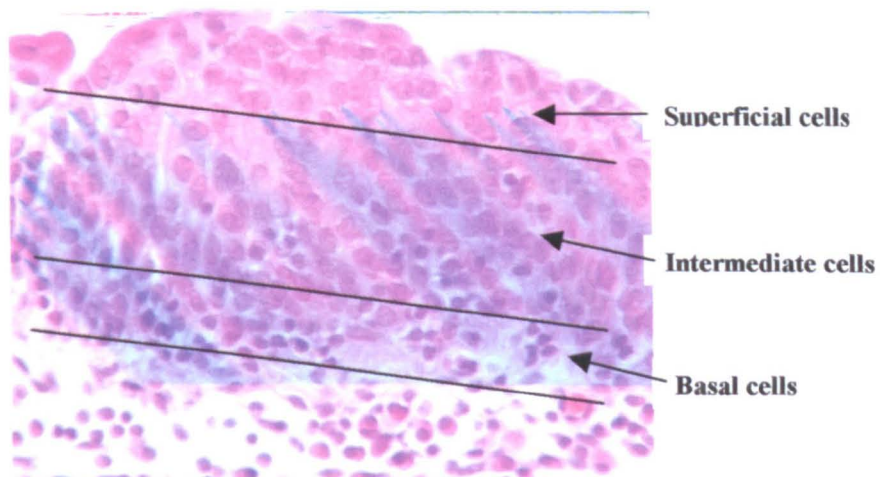


**Figure 7.3 A digital image of benign section of the urinary bladder (this image was stained by haematoxylin and eosin, H+E).**

Finally, the mean value of each area for the cell size (length and width) from 6 sections was considered for malignant and 10 sections for benign areas (Appendix 12). In every section, the length and width of 10 cells were measured randomly and then averaged. The mean value of cell sizes resulting from three areas (superficial, intermediate and basal cells) for malignant and benign groups was calculated. Table 7.4 shows the final values which were then used as parameters to create finite element models of normal and malignant epithelium.

Tissue type	Layer	Cell dimensions ( $\mu\text{m}$ )		Epithelium thickness ( $\mu\text{m}$ )
		Length (Mean $\pm$ SD)	Width (Mean $\pm$ SD)	
Normal	1. Superficial	14.84 $\pm$ 02.83	11.26 $\pm$ 01.27	60.80 $\pm$ 19.58
	2. Intermediate	10.91 $\pm$ 01.63	12.78 $\pm$ 02.36	
	3. Basal	08.87 $\pm$ 02.01	09.22 $\pm$ 01.72	
Malignant	1. Superficial	14.94 $\pm$ 02.29	09.81 $\pm$ 2.59	68.69 $\pm$ 18.91
	2. Intermediate	16.00 $\pm$ 04.25	16.41 $\pm$ 03.46	
	3. Basal	10.62 $\pm$ 1.45	13.98 $\pm$ 01.90	

**Table 7.4 The mean values of the cellular morphological parameters of the human urinary bladder obtained from analysis of the both malignant and normal bladder histology sections by the author**

The average cell dimensions obtained from the literature (Table 7.3, using the reference (Lewis 2000)) and the bladder histology sections (Table 7.4) were adjusted to allow for 20% shrinkage during the fixation process. It was necessary to round the values slightly for meshing purposes, but the aspect ratios of cell were not significantly altered. High-resolution digital micrographs were not available, so it was not possible to obtain values of extra-cellular space for bladder tissue. Instead, approximate values obtained from the literature for cervical and other squamous epithelia were used (Walker 2001). Nuclei were not included in the model, as modelled impedance spectra have already been shown to be relatively insensitive to increases in nuclear to cytoplasmic ratio (Walker 2001). Extra-cellular space was modelled as a continuous layer around the outer surface of each individual cell. In the case of the normal superficial cells, tight junctions were modelled by fusing adjacent cell membranes at one edge, thus eliminating all extra-cellular space. Superficial bladder cells are also known to contain plaques, which allow

the surface area of the membrane to be dramatically increased when the bladder is stretched by filling. These structures were not incorporated into the model as they are very small (approximately  $0.5 \mu\text{m}$  in diameter and  $12 \text{ nm}$  in thickness (Lewis 2000)), and when the bladder is relaxed, simply form vesicles within the cytoplasm. It was not thought appropriate to include these structures into this cellular level model of urothelium, but it may be possible to include plaques in future, higher resolution models. Finally, dimensions of the cellular compartments used in constructing the cellular level models of related urothelium are given in Table 7.5.

Tissue type	Layer	Cell dimensions ( $\mu\text{m}$ )			ECS width ( $\mu\text{m}$ )
		X	Y	Z	
Normal	1. Superficial	18	18	12	0.05
	2. Intermediate	12	12	16	0.2
	3. Basal	12	12	12	0.4
Malignant	1. Superficial	18	18	12	0.4
	2. Intermediate	20	20	20	0.6
	3. Basal	12	12	16	0.8

**Table 7.5 Dimensions of cellular compartments of the human urinary bladder used in model construction (ECS=extra-cellular space). These data obtained from analysis of the both malignant and benign bladder histology sections by the author**

Electrical properties assigned to each cellular compartment (i.e. cytoplasmic membrane, intra-and extra-cellular space) were based on averages of values published in the literature, and are given in Tables 7.6 and 7.7.

Cellular compartment	Conductivity, $\sigma$ (S/m)	Relative Permittivity, $\epsilon_r$
Extra-cellular space	1.1	72
Cytoplasm	0.6	86

**Table 7.6 Electrical properties used to model cellular compartments, derived from the average values published in literature (Geddes and Baker 1967; Huang, Wang et al. 1995)**

	Thickness (nm)	Capacitance $\mu\text{F}/\text{m}$	Conductivity $\mu\text{S}/\text{m}$
Cytoplasmic membrane	8.0	0.01	0.1

**Table 7.7 Electrical properties used to model membranes, derived from the average values published in the literature (Cole 1972; Pethig and Kell 1987)**

Each element in the model is assigned both a conductivity and permittivity and therefore has complex electrical properties, so current flow will be frequency dependent. Single cells were meshed together to form the ‘bricked’ pattern observed in normal epithelium. Currents in the frequency range 100 Hz-10 MHz were applied at the boundaries of the model in the x and z planes (i.e. parallel and perpendicular to the long axis of the cell, which is usually aligned parallel to the epithelial surface). The resulting potentials on the appropriate boundary planes were obtained, as shown in Figure 7.4, and hence the electrical transfer impedance,  $Z$ , and conductivity,  $\sigma$  calculated using:

$$Z = \frac{V_a}{I_A} \quad (7.1)$$

$$\sigma = \frac{l}{Z.A} \quad (7.2)$$

Where  $l$  is the length of the volume modelled, and  $A$  is the cross sectional area. The models are identical in all respects in the x and y planes, and hence the properties in these two directions will also be identical.

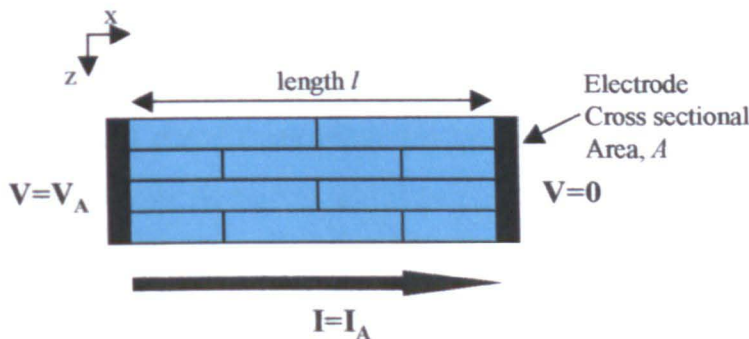


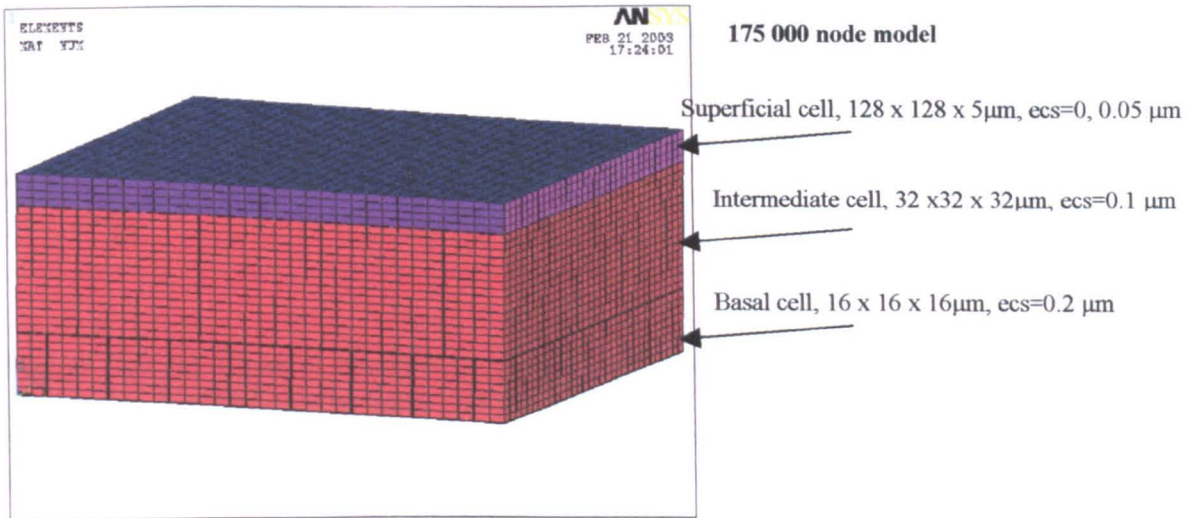
**Figure 7.4 Method of obtaining electrical transfer properties from cellular level finite element models (Applied voltage are  $V_A$  and  $V = 0$  and the calculated current is  $I_A$ ).**

### **7.3.2 Macroscopic tissue level finite element models**

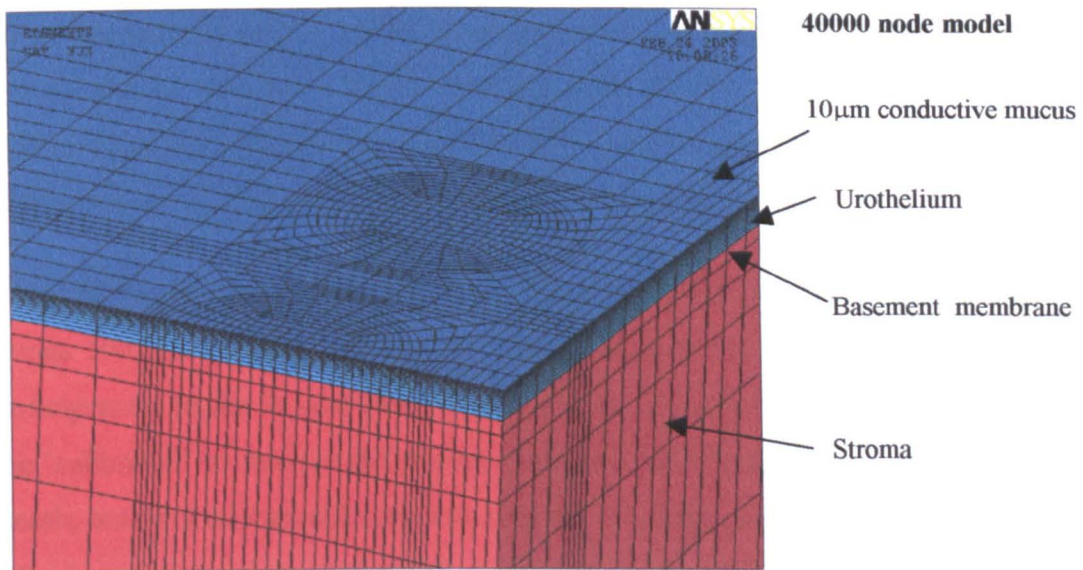
Electrical transfer conductivities obtained from the cellular level models were assigned as material properties to epithelial layers in the macroscopic tissue model. This model consisted of three epithelial layers representing superficial, intermediate and basal cell types, underlying layers representing the basement membrane and connective tissue, and a surface layer of variable thickness, representing a thin layer of mucus or surface fluid. The latter was included as previous modelling work has shown models without a surface conductive layer to be unstable (Walker 2001). It is also a realistic assumption that as the electrodes cannot be exactly flush with the end of the probe, that there will be at least a few microns depth of fluid between the electrodes and the high resistance superficial cell membranes. The macroscopic model based on the cellular dimensions extracted from the literature review (Table 7.3) for stretched rabbit urothelium is shown in Figure 7.5.

The macroscopic tissue model was constructed using the experimental morphological parameters for human bladder samples. Therefore, the thickness of normal and malignant urothelium was measured from a number of digital micrographs of histology slides, as described for obtaining cell sizes in the previous section. The mean depth for normal urothelium was 73  $\mu\text{m}$  whilst malignant urothelium was found to have a slightly greater thickness of 83  $\mu\text{m}$  (Table 7.4). These values are adjusted for an estimated 20% shrinkage during the fixation process.

There is no published data for the electrical properties of basement membrane, so models were solved using the published conductivity and permittivity values for the tendon (Gabriel, Lau et al. 1996). The conductivity of the underlying connective tissue was based on conductivity values previously measured from unfixed healthy cervical stroma (Walker 2001) and permittivity published in the literature for uterus (Gabriel, Lau et al. 1996). The mucus layer was assigned similar properties to those used for extra-cellular fluid. Circular areas at the surface of this model were designated as electrodes. The radius of each area was 0.26 mm, and separation between the edges was 0.2 mm. These parameters were average values of electrode radius and edge separation measured from the probes used to collect data, using a travelling microscope. The macroscopic model mesh, with the electrode areas highlighted, is shown in Figure 7.6.



**a**



**b**

**Figure 7.5** Macroscopic tissue model constructed from the literature using the morphological parameters of rabbit urothelium ( $\text{ecs}$ =extracellular space)

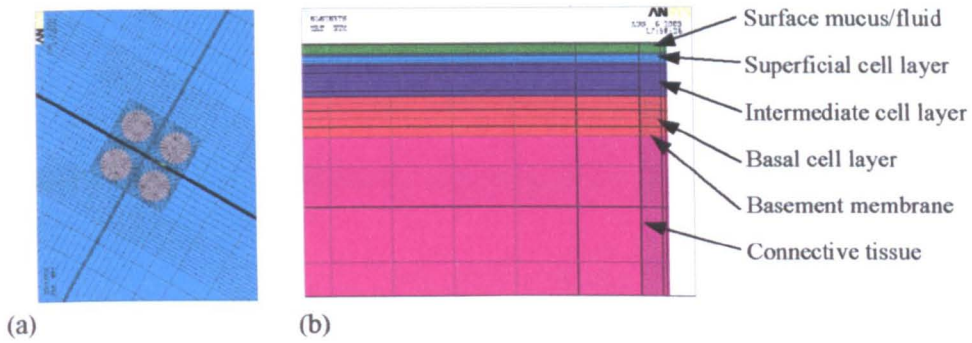


**Figure 7.6 (a) Central surface (x-y plane) of macroscopic tissue model showing electrodes highlighted in grey (b) Layering in macroscopic model (x-z plane). Mesh densities used in the model solution were approximately twice those illustrated above**

The mesh density in this figure has been reduced for reasons of clarity. In the models solved a variable mesh density was used, with increased element numbers close to the electrodes to eliminate instabilities associated with high field gradients. Standard checks were carried out on the model mesh to ensure that instabilities did not arise due to poorly shaped elements. Checks were also made that the volume of tissue modelled was sufficient so that current was not artificially confined by the model boundaries. A total tissue volume of 1.5 cm x 1.5 cm x 0.3 cm was modelled.

Current was applied to the drive electrodes in the macroscopic model in the frequency range 100 Hz- 10 MHz, and voltages calculated at the receiver electrodes in an identical arrangement to the *in vivo* tissue measurements. These modelled impedance spectra can be ‘calibrated’ to remove the effects of the electrode geometry by solving for the same mesh, but with all material conductivities set to a frequency-independent value of 1 S/m. The impedance value obtained is equivalent to a calibration factor, by which all raw modelled impedances can be divided to obtain impedivities in  $\Omega m$ . It is therefore possible to directly compare plots of transfer impedivity against frequency (i.e. the impedance spectra) obtained from the model with those obtained experimentally.

The current flowing through every node located on the boundary midway between the two drive electrodes can also be calculated and then integrated to give the total current flowing through each layer. This information can provide an indication of the current distribution *in vivo*, and hence the depth sensitivity of the probe. Various model parameters can be altered at either the cellular or the macroscopic stage of the modelling process in order to assess the effect on the impedance spectrum or the current

distribution. Models were solved with mucus layer thicknesses in the range 5  $\mu\text{m}$ -100  $\mu\text{m}$ .

## 7.4 Results and discussions: Comparison of modelling and the experimental results

The real part of the complex modelled impedance spectrum for stretched normal rabbit urothelium from the literature is demonstrated in Figure 7.7. This figure shows the effect of different thickness of the surface conductive layers (in micrometers) on the bladder tissue impedance. Thus, it is clear that any increase in thickness of the surface layer will decrease the modelled impedance.

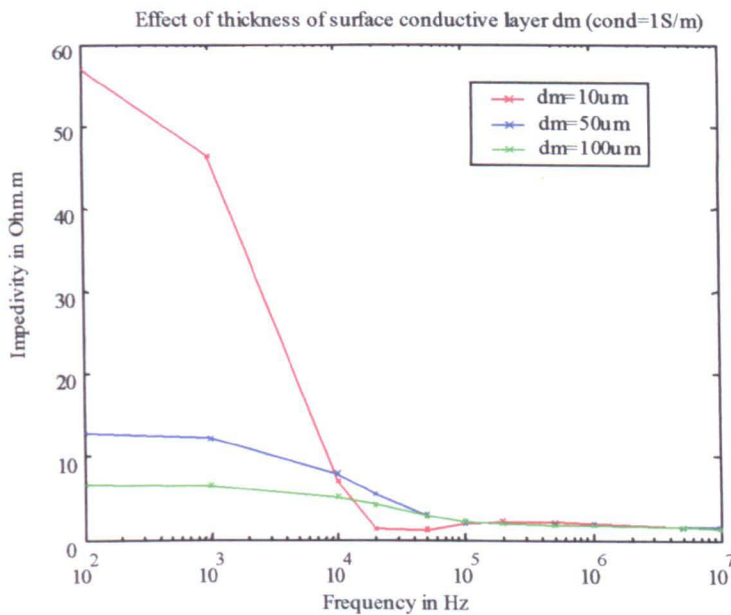
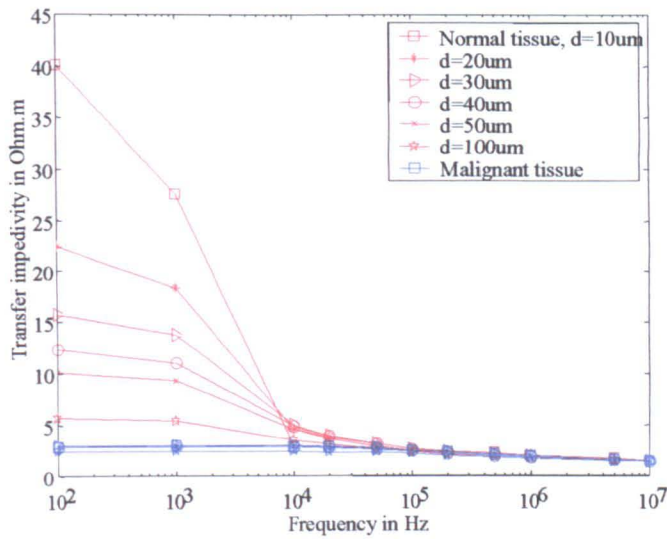


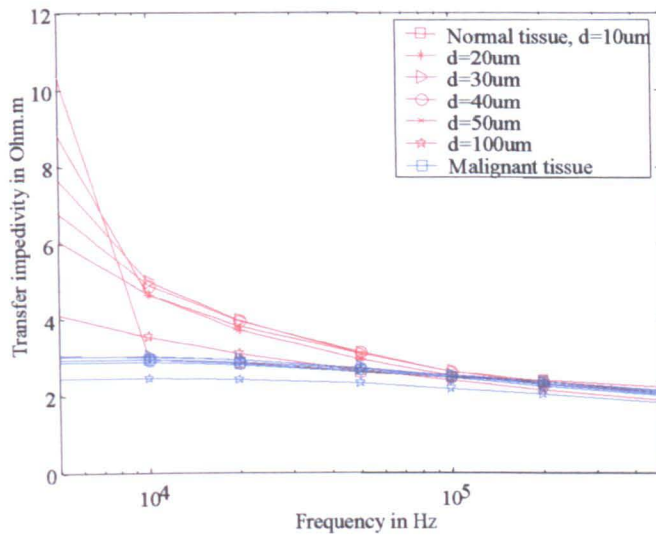
**Figure 7.7** The real part of the complex modelled impedance spectra for normal rabbit bladder tissue using the literature review

In addition, the real part of the complex impedance spectra modelled using parameters obtained for relaxed benign and malignant cells parameters measured from histology sections are shown in Figure 7.8a. The effect of different mucosal layer thickness (in micrometers) on the normal impedance is also shown in this figure.

Figure 7.8b shows the same spectra, but in this case within the frequency range of the impedance measurement system.



a



b

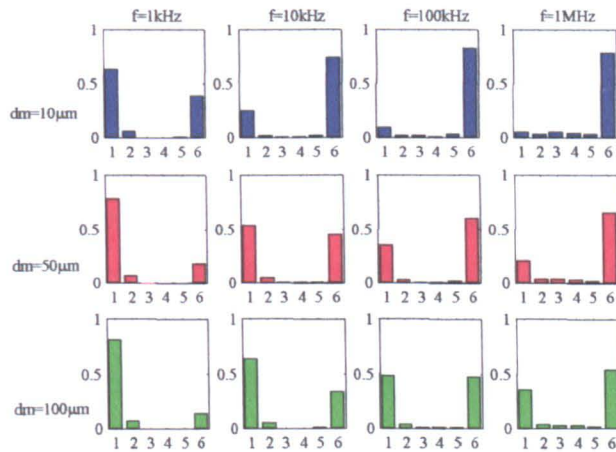
**Figure 7.8 The real part of the complex modelled impedance spectra for normal and malignant urothelial tissue**

It can be seen that the model predicts impedance spectra that are within the same magnitude range as the data collected *in vivo* and *ex vivo*. However, the model predicts that at frequencies less than 100 kHz, impedances measured from benign tissue should be higher than those measured from abnormal or malignant tissue. This is the opposite situation to that suggested by the measured data, where higher impedances are measured from abnormal tissue (see Figure 5.7). The model results also suggest that impedance spectra associated with normal tissue structure are sensitive to the thickness of the mucus or fluid layer at the tissue surface, whereas those associated with abnormal tissue are not. We can gain a greater understanding of this behaviour by examining the current

distribution in the normal and malignant models. Figure 7.9a shows the proportion of the total current flowing through each of the macroscopic model layers – surface fluid, superficial urothelium, intermediate urothelium, basal urothelium, basement membrane and connective tissue respectively, in the normal tissue model. Data is shown for a number of frequencies and for three thicknesses of surface fluid. Figure 7.9b shows similar data for the malignant tissue model. It is immediately apparent that very little of the current actually flows through the urothelium itself (layer 2-4), but is divided between the surface fluid and underlying connective tissue at a ratio which depends on current frequency, depth of surface fluid and urothelial pathology. In the case of normal tissue, the presence of tight junctions and narrow intercellular spaces forms a very high impedance barrier, and at low frequencies in particular, current is confined to the surface fluid. As the frequency is increased, the capacitive nature of cell membranes allows current flow into the surface cells, effectively ‘short-circuiting’ the tight junctions and allowing current to penetrate beneath the epithelium and into the relatively high conductivity connective tissue beneath, thus causing the characteristic drop in tissue impedance with increasing frequency. However, our malignant superficial cell models do not include tight junctions, and the extra-cellular space is also wider (see Table 7.5), so the barrier to current flow is greatly reduced, even at low frequencies. Figure 7.9b shows that at least 50% of the injected current flows beneath transformed urothelium across the frequency range modelled.

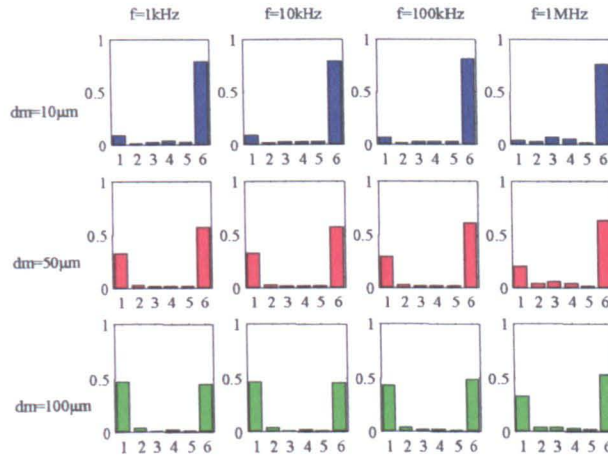
The results of the models do not explain the measurements recorded *in vivo* and *ex vivo*, where higher impedances were measured from tissue independently diagnosed as malignant, but are in agreement with measurements and models of other squamous epithelia, where malignancy results in a reduction in electrical impedance, Gonzalez-Correa et al. (2003), (Brown, Tidy et al. 2000), (Walker D C 2002). However, in constructing the computational models of normal and malignant urothelium, due to the limited availability of data, we have had to make a number of assumptions about tissue structure and electrical properties. For example, no information was available concerning the distribution of extra-cellular space in normal and abnormal urothelium, so we used those that had previously been used for models of normal and CIN cervical epithelium. These values were based on measurements on high magnification micrographs published in the literature for squamous epithelia, and may not be relevant to transitional bladder epithelium. Surface plaques are not included in his model, and

though these structures are extremely small, it is possible that they might influence the electrical properties of the tissue in a non-intuitive way.



(a)

Layer no:



(b)

**Figure 7.9 Modelled current – depth distribution midway between drive electrodes for (a) normal tissue model, (b) Malignant tissue model at different frequencies and surface layer thicknesses (dm) Layer no. key: 1 – surface fluid, 2-superficial urothelium, 3-intermediate urothelium, 4-basal urothelium, 5- basement membrane, 6- connective tissue**

The model results, Figure 7.9, show that much of the injected current flows through the connective tissue beneath the urothelium. Again, there is no data available for the electrical properties of this layer, so data measured from the cervical stroma was used in this model, but may not be applicable to the bladder tissue, which contains a higher density of muscle than the cervical tissue. Also, modelling of other squamous epithelia (e.g. cervix) has shown that the changes in the impedance spectrum associated with neoplasia are primarily due to the increase in the volume of extra-cellular space and

breakdown of surface tight junctions that are known to be associated with precancerous changes. The fact that the measurements on bladder tissue yield the opposite results to those on cervix i.e. an increase in low frequency impedance for CIS compared to normal tissue suggest that: There is a reduction in the volume of ECS associated with CIS of the bladder, or the structure of bladder tissue is significantly different to cervix in other respects, leading to a completely different distribution of current flow. Also, it is much more difficult to obtain good quality, histological sections of bladder epithelium, and in particular, there is little quantitative data available on the morphology of stretched bladder tissue. It is virtually impossible to find information on the distribution of ECS in normal and CIS bladder, so it may be possible that the assumption that ECS increases with CIS, which was made when constructing the computational models, may be incorrect, and hence at least partially explain the different results. Bladder urothelium is also much thinner than cervical epithelium (approximately 80 $\mu$ m compared to 300-400 $\mu$ m), which suggests that current flow in the lamina propria may be even more important than the current flow in cervical stroma. The modelling presented here focussed on changes within the urothelium only, assuming that the properties of the underlying tissue remain unchanged and therefore could not predict this result.

## **7.5 Conclusions**

Computational modelling is a technique that allows us to improve our understanding of current flow in tissues, and hence electrical impedance methods as potential diagnostic techniques. Finite element analysis is a numerical method that is useful in solving complex physics and engineering problems. Finite element models were constructed according to data obtained from literature and measurements of histological sections of normal and malignant areas of the urothelium. Then, the real part of the complex modelled impedance spectrum based on models of rabbit (normal stretched) and human (normal and abnormal relaxed) urothelium was calculated. The results of the models do not explain the measurements recorded *in vivo* and *ex vivo*. In conclusion, there are many factors, which may account for discrepancies between the measured and modelled data, and access to more comprehensive data on normal and transformed urothelial structure in the future may allow more accurate models to be developed. It is anticipated that computational models may still play an important role in elucidating the differences in the measured electrical properties of normal and malignant bladder tissue.

# Chapter 8

## Conclusions and recommendations for future work

### 8.1 Conclusions

The aim of this thesis was to measure and assess the ability of electrical impedance spectroscopy to characterise human urothelium. This minimally invasive technique has been used to differentiate various pathological changes in the cervix, which led to a trial of the method in the bladder. In developed countries, most bladder cancers are transitional cell carcinomas and it is one of the most common cancers, with approximately 13,000 new cases and 5400 deaths per year in the UK (Black et al 1977). *Carcinoma in situ* (CIS) of the bladder is an aggressive form of bladder cancer, manifested as flat and disordered proliferation of urothelial cells. It may be an early phase in the evolution of an invasive cancer that tends to persist and may progress over time and is not predictable. CIS requires aggressive treatment and surveillance after detection.

Various investigations are currently available to help with the diagnosis of bladder cancer such as cystoscopy, urine cytology, urine markers, the CT-Scan and MRI but cystoscopy is the most common urological procedure in the investigation of bladder pathology. At present, definitive diagnosis can be made by biopsy only, usually under general anaesthesia, with resultant patient discomfort and morbidity, relatively high cost, and needs a few days to process the pathological results. The biopsies are usually taken from limited points of the bladder and information related to small parts of the area suspected of disease. On the other hand, an area of CIS is flat and these lesions cannot be differentiated from other benign flat areas using cystoscopy because they look macroscopically normal. This means that this area cannot be distinguished from other red patches or benign areas of the urothelium and the only recourse is to use random biopsies. However, if we use random bladder biopsies in patients in whom the disease is suspected, it is possible no lesion may be found. Because of these difficulties, the search for other detection methods continues. This is the rationale for developing an alternative technique to scan the whole of the bladder rapidly and gain useful diagnostic information as soon as possible. There are methods that use light scattering to detect abnormalities in the bladder and other organs (Backman, Wallace et al. 2000). This is a new optical-probe technique based on light-scattering spectroscopy that is able to detect

pre-cancerous and early cancerous changes in cell-rich epithelia. This technique has been used to diagnose dysplasia and '*Carcinoma in situ*' in four different human organs: Columnar epithelia of the colon and Barrett's oesophagus, transitional epithelium of the urinary bladder and stratified squamous epithelium of the oral cavity. This thesis investigates the potential of another novel minimally invasive technique, electrical impedance spectroscopy, for use as a new diagnostic method to detect bladder abnormalities. The electrical impedance technique has been tested in the human oesophagus (to separate columnar from squamous epithelium) (Gonzales-Correa, Brown et al. 1999) and also, in the human cervix (to identify cervical intraepithelial neoplasia from the normal cervical tissue)(Brown, Tidy et al. 1998). Furthermore, bio-impedance measurements have previously shown that cancerous tissues in many cases have impedivities that are different to normal tissues (Blad and Baldetorp 1996);(Blad, Wendel et al. 1999); (Brown, Tidy et al. 2000); (Chauveau, Hamzaoui et al. 1999); (da Silva, de Sa et al. 2000); (Boston 1999); (Gonzales-Correa, Brown et al. 1999); (Heinitz and Minet 1995); (Jossinet and Lavandier 1998); (Morimoto, Kinouchi et al. 1990); (Zarowitz and Pilla 1989).

The author has investigated the application of bio-impedance measurements to the bladder as a novel and non-invasive technique to distinguish between normal and abnormal tissues. Patient feedback about this technique was not negative and the process added little extra time to the normal operating procedure. We have used two measurement systems, the Mk3.a and Mk3.5 Sheffield System and made measurements both *ex vivo* and *in vivo*. The histopathology of biopsies was compared to electrical impedance measurements from 35 bladders (*ex vivo*) and 74 bladders (*in vivo*). According to the analysed measured data and the results shown in the figures related to *ex vivo* and *in vivo*, the impedivity of malignant bladder tissue is significantly higher than the impedivity of benign tissue in every case when tested as a group (Figure 5.12, Figure 5.26). This is in contrast to measurements made by Gonzales et al. and Brown et al, who found that normal tissue had a higher impedivity than malignant tissue in oesophagus and cervix, particularly at lower frequencies (Gonzales-Correa, Brown et al. 1999); (Brown, Tidy et al. 2000). These results on squamous epithelia may demonstrate the effect of tight junctions on tissue electrical impedances (there is a lack of tight junctions in malignant tissue). However, tight junctions are also very common among epithelial cells lining the urinary bladder. These junctions in the urinary bladder do not permit fluid leakage into the body by passing between cells. The epithelial tissue of this

organ consists of closely packed cells with little extra-cellular material between adjacent cells. Tight junctions prevent ion movement through the extra-cellular space, thus causing high impedance at low frequencies for both normal and malignant tissues. Current cannot pass through the cell membrane at lower frequencies resulting in higher impedance than at higher frequencies. We hypothesized that the impedivity of normal bladder tissue at lower frequencies would be also higher than that of malignant tissue but our lower frequency study (62.5 Hz-1.5 MHz) in section 5.2.3 showed that the malignant areas always have higher impedance than benign areas. The explanation may lie in the detailed structure of the epithelial tissue and the underlying bladder wall, but insufficient structural data is available at present to test this hypothesis. This study was carried out in both *ex vivo* and *in vivo* states using both spectroscopy systems. The measured impedance was usually lower *ex vivo* than *in vivo*. This is probably due to the effect of bladder sample handling during transport from theatre to the histopathology department for the *ex vivo* study and also, because of the time delay after the bladder excision in this study. Handling of the tissue causes inflammation in the tissue and hence increased impedance. Also, the blood supply to the bladder tissue is terminated after the bladder excision and thus the impedance of tissue will decrease depending on the time passed after tissue resection due to ischaemic changes (Konishi, Morimoto et al. 1995). The resistivity of tissue is essentially constant during the first hour after removal from the body (Crile, Hosmer et al. 1922). Finally, the glycine inside of the bladder in *in vivo* study can increase the measured impedance in this case.

Malignancy is usually accompanied by variable degrees of inflammation, which can cause an increased cellular infiltrate in the lamina propria and hence increase the impedance of the tissue. This process can be correlated with a significant increase in impedivity at all frequencies ( $p < 0.005$ ) for *ex vivo* study. The mathematical modelling demonstrates that a significant proportion of the current flows in the lamina propria, therefore, it might be expected that the changes in the lamina propria be reflected in the measured electrical impedances of the bladder tissue. The results from Chapter 5 confirm that CIS can not be distinguished from inflammation with higher degrees (Figures 5.17). The epithelial structural changes associated with CIS alone may not be enough to explain the resulting impedance of the urothelium, if we compare the impedance of CIS with a severely inflamed area.

Oedema results in an increase of fluid in the extra-cellular space due to widening of the gaps between cells, which allows more current to pass this space and decreases the impedivity at lower frequencies. The effect of probe size (area) is very important in electrical impedance measurement of the urinary bladder because if more pressure is applied with the probe, the measured impedivity of the tissue will be increased and pressure dependent artefacts will be introduced in the results. If a large probe is used then the variation of the applied pressure will have less effect on the impedivity but this is not practicable for *in vivo* measurement. The calculated results show that the impedivity measured using big and small probes was significantly different ( $p < 0.02$ ). This is likely to be the result of removing liquids from the extra-cellular area and thus increasing the measured impedance. It may be predicted that the variability of our measurements on normal and malignant tissues will differ according to the size of the probes used.

Another factor affecting impedance measurement of the bladder is the volume changes of this organ. The figures in Section 6.3 show that if the bladder were stretched using glycine, the measured impedance usually would be decreased. In practice, the bladder should be filled to the stage at which folds in the mucosa are just removed, when there will be no impedance changes as a result of stretching the epithelium.

The effect of surface liquids such as saline and glycine on the impedance results is important because of their presence inside of the bladder during measurement process. Therefore, the bladder was alternately filled with air, saline solution and glycine in order to assess their effect on the bladder impedance measurements, both *in vivo* and *ex vivo*. The impedance readings in this study demonstrated a significant difference of impedance if these surface liquids are used. There is also a complementary study to determine whether the effect of surface fluid on the measured results at several frequencies can be reduced (Jones 2003; Jones, Smallwood et al. 2003). In this work, they used different conductivities of 50  $\mu\text{m}$  thick surface fluids to show the effect on impedance using different electrode configurations. The results of their study have shown that any conductive surface fluid may cause a decrease in impedance. If we fill the bladder with glycine, the measured impedivity of the bladder in malignant and non-malignant cases will be more than if we fill it with air or saline solution (with greater differences at lower frequencies). But if we use the saline solution to fill in the bladder, the measured impedance will be smaller than if we fill it with glycine or air and the

separation of malignant and non-malignant area of the bladder will be better than with other surface fluids (Figures 6.15 and 6.16). Glycine is usually used inside of the bladder during bladder cancer operations because of its insulating effect when diathermy is applied to cut tumours, and the saline is used for washing inside of the bladder. In practice, the same fluid should be used for filling the bladder so that the effect of different conductivity fluid is removed. The *in vivo* results for the low frequency system suggest that it is possible to diagnose patients with malignancy using electrical impedance spectroscopy and this method maybe a useful screening test. A positive predictive value of 100% with a negative predictive value of 70% (on a small sample) suggests that, even without further refinement, the technique would be a useful screening test. This is based on 1) the need to identify early all cases of malignancy and 2) the possibility of excluding 70% of patients from the need to have general anaesthetic and bladder biopsy, which is not entirely risk free.

Finally, to improve our understanding of the current flow in urothelium, the finite element method was applied to model the electrical properties of normal and malignant bladder tissue in both cellular and macroscopic tissue levels. Finite element models were constructed according to data obtained from literature and histological sections. The real part of complex impedance spectra was calculated using the model for normal and malignant tissue structures, and then compared with the experimental impedance readings. The results of the modelling were unable to explain the impedance measurements resulting from *ex vivo* and *in vivo* studies. However, it is anticipated that computational models may still play an important role in elucidating the differences in the measured electrical properties of normal and malignant bladder tissue.

## **8.2 Recommendations for future work**

Recommendations for future work which need to be addressed most urgently can be prioritised. Top priority is clinical trial (and it can be done with existing equipment). 2nd is understanding, which is a major research project. 3rd is improving equipment, which is incremental. Therefore, there are three main areas in which more work is required: Initially, an enlarged clinical trial using the modified Mk3.5 Sheffield System is essential and an extensive clinical trial to determine whether the promise shown by the final series of *in vivo* measurements leads to a robust and powerful screening technique. In addition, understanding of the relationship between bladder pathology and impedance spectra is important. The modelling results suggest that the main determinant

of the impedance spectrum is likely to be the underlying tissue rather than the epithelial tissue in itself. Reducing the electrode dimensions in order to confine current flow to the epithelium is unlikely to be successful, due to the increased electrode impedance. There is a singular lack of structural information to inform computational models of current flow in the bladder wall, and understanding of the relationship between pathology and impedance spectra is dependent this information. It would be difficult to obtain structural information down to the level of the dimensions of the extra-cellular space from normal human bladders (though it might be possible to obtain small numbers of normal bladders post-mortem), so it would be necessary to set up an animal model. The most promising candidate is the pig. This would be a major undertaking. If the primary requirement is a diagnostic indicator, it might be difficult to justify such a fundamental study.

Then, improving the technical aspects of the measurements is needed. Some aspects of improving the user interface (for cervical measurement) are being pursued by Brown with a NEAT grant (Department of Health Programme): disposable electrodes and a wire-less probe with push-button data collection. Of more importance in this context is standardisation of the measurement procedure, the most important aspect of which is ensuring that the force applied to the probe tip is constant. A simple and commonly used technique is to have a sliding part controlled by a spring which is long compared to the travel of the sliding part. Exploration of this technique suggested that it would not be reliable at the low force (10 gf) required, and that an active servo device might be necessary. Given the small dimensions, and the need for a flexible device to pass down a cystoscope, this is quite challenging, but a possible approach would be to explore a micro-electro-mechanical device.

Finally, because of the small number of patients (18) in the final study, it is not possible to calculate Positive and Negative Prediction Values per patient, though this has been done for individual biopsies with promising results. An enlarged clinical trial is essential if the predictive value of the technique is to be determined. If the area under the ROC curve remains constant at 0.91 with increasing numbers of patients, a decision would have to be made as to whether the additional time and expense of performing a test with 30% false positives was justified by the reduced morbidity and patient anxiety of deciding that 70% of patients with benign changes did not need to return for biopsy.

# References

- Ackerman, L. V. (1981). Ackerman's surgical pathology. London, Mosby.
- Ackmann, J. J. and M. A. Seitz (1984). "Methods of complex impedance measurements in biologic tissue." Crit Rev Biomed Eng 11(4): 281-311.
- Anderstrom, C., S. Johansson, et al. (1980). "The significance of lamina propria invasion on the prognosis of patients with bladder tumors." J Urol 124(1): 23-6.
- Avis, N. J., S. W. Lindow, et al. (1996). "In Vitro multi frequency electrical impedance measurements and modelling of the cervix in late pregnancy." Physiol Meas 17: A97-A103.
- Backman, V., M. B. Wallace, et al. (2000). "Detection of preinvasive cancer cells." Nature 406(6791): 35-6.
- Badalament, R. A., V. Ortolano, et al. (1992). "Recurrent or aggressive bladder cancer. Indications for adjuvant intravesical therapy." Urol Clin North Am 19(3): 485-98.
- Bailey, F. R. (1984). Bailey's textbook of microscopic anatomy, Williams & Wilkins.
- Bertemes-Filho, P. (2002). Tissue characterisation using an impedance spectroscopic probe. Medical Physics and Clinical Engineering Dep. Sheffield, PhD thesis, Sheffield University.
- Bertemes-Filho, P., B. H. Brown, et al. (2000). "A comparison of modified Howland circuits as current generators with current mirror type circuits." Physiol Meas 21(1): 1-6.
- Black, R. J., F. Bray, et al. (1997). "Cancer incidence and mortality in the European Union: cancer registry data and estimates of national incidence for 1990." Eur J Cancer 33(7): 1075-107.
- Blad, B. and B. Baldetorp (1996). "Impedance spectra of tumour tissue in comparison with normal tissue; a possible clinical application for electrical impedance tomography." Physiol Meas 17 Suppl 4A: A105-15.
- Blad, B., P. Wendel, et al. (1999). "An electrical impedance index to distinguish between normal and cancerous tissues." J Med Eng Technol 23(2): 57-62.
- Blair, A., S. H. Zahm, et al. (1999). "Occupational cancer among women: research status and methodologic considerations." Am J Ind Med 36(1): 6-17.
- Boone, K. G. and D. S. Holder (1996). "Current approaches to analogue instrumentation design in electrical impedance tomography." Physiol Meas 17(4): 229-47.

**Boston, K. J. (1999). Impedance Spectroscopy of Human Cervical Tissue. University of Sheffield; MPhil thesis.**

**Brown, B. H., A. D. Leathard, et al. (1995). "Measured and expected Cole parameters from electrical impedance tomographic spectroscopy images of the human thorax." Physiol Meas 16(3 Suppl A): A57-67.**

**Brown, B. H., R. H. Smallwood, et al. (1999). Medical Physics and Biomedical Engineering. London, IOP.**

**Brown, B. H., J. A. Tidy, et al. (1998). Tetrapolar measurement of cervical tissue structure using impedance spectroscopy. IEEE Conference on Biomedical Engineering, Hong Kong.**

**Brown, B. H., J. A. Tidy, et al. (2000). "Relation between tissue structure and imposed electrical current flow in cervical neoplasia." Lancet 355(9207): 892-5.**

**Brown, B. H., J. A. Tidy, et al. (2000). "Relation between tissue structure and imposed electrical current flow in cervical neoplasia." Lancet 355(9207): 892-5.**

**Brown, B. H., A. J. Wilson, et al. (2000). "Bipolar and tetrapolar transfer impedance measurements from volume conductor." Electronics Letters 36(25): 2060-2062.**

**Caiazzo, F., P. Canonico, et al. (1996). "Electrode discharge for plasma surface treatment of polymeric materials." Journal of Materials Technology 58(1): 96-9.**

**Campbell, J. H., N. D. Harris, et al. (1994). "Clinical applications of electrical impedance tomography in the monitoring of changes in intrathoracic fluid volumes." Physiol Meas 15 Suppl 2a: A217-22.**

**Chauveau, N., L. Hamzaoui, et al. (1999). "Ex vivo discrimination between normal and pathological tissues in human breast surgical biopsies using bioimpedance spectroscopy." Ann N Y Acad Sci 873: 42-50.**

**Clausen, C. (1989). "Impedance analysis in tight epithelia." Methods Enzymol 171: 628-42.**

**Cole, K. S. (1972). Ions and Impulses. Berkeley, University of California Press.**

**Cole, K. S. and R. H. Cole (1941). "Dispersion and absorption on dielectrics. I. Alternating current characteristics." J Chem Phys 9: 341-51.**

**Cole, K. S. and R. H. Cole (1942). "Dispersion and absorption on dielectrics. I. Direct current characteristics." J Chem Phys 10: 98.**

**Crile, G. W., H. R. Hosmer, et al. (1922). "The electrical conductivity of animal tissues under normal and pathological conditions." Am. J. Physiol. 60: 59-106.**

**da Silva, J. E., J. P. de Sa, et al. (2000). "Classification of breast tissue by electrical impedance spectroscopy." Med Biol Eng Comput 38(1): 26-30.**

Da Silva, J. E., J. P. M. Desa, et al. (2000). "Classification of breast tissue by electrical impedance spectroscopy." Med Biol Eng Comput 38: 26-30.

Damjanov, I. and J. Linder (1996). Anderson's Pathology, Mosby-year book.

Denyer, C. W., F. J. Lidgley, et al. (1994). "A high output impedance current source." Physiol Meas 15 Suppl 2a: A79-82.

Eroschenko, V. P. (2000). Di Fiore's Atlas of Histology with functional correlations. Philadelphia; London, Lippincott Williams & Wilkins.

Farrow, G. M. (1992). "Pathology of carcinoma in situ of the urinary bladder and related lesions." J Cell Biochem Suppl 16I: 39-43.

Farrow, G. M. and D. C. Utz (1982). "Observations on Microinvasive Transitional Cell Carcinoma of the Urinary Bladder." Clinics in Oncology 1(2).

Farrow, G. M., D. C. Utz, et al. (1976). "Morphological and clinical observations of patients with early bladder cancer treated with total cystectomy." Cancer Res 36(7 PT 2): 2495-501.

Fleshner, N. E., H. W. Herr, et al. (1996). "The national cancer data report on bladder carcinoma." Cancer 77: 1505-13.

Foresman, W. H. and E. M. Messing (1997). "Bladder cancer: natural history, tumor markers, and early detection strategies." Seminars in Surgical Oncology 13(5): 299-306.

Foster, K. R. and H. P. Schwan (1989). "Dielectric properties of tissues and biological materials: a critical review." Crit Rev Biomed Eng 17(1): 25-104.

Foster, K. R. and H. P. Schwan (1989). "Dielectric properties of tissues and biological materials: a critical review." Critical Reviews in Biomedical Engineering 17(1): 25-104.

Fricke, H. and S. Morse (1926). "The electricity capacity of tumors of the breast." Journal of Cancer Research 15: 340-376.

Gabriel, C., S. Gabriel, et al. (1996). "The dielectric properties of biological tissues: I. Literature survey." Physics in Medicine & Biology 41(11): 2231-49.

Gabriel, S., R. W. Lau, et al. (1996). "The dielectric properties of biological tissues: II. Measurements in the frequency range 10 Hz to 20 GHz." Phys Med Biol 41(11): 2251-69.

Gabriel, S., R. W. Lau, et al. (1996). "The dielectric properties of biological tissues: III. Parametric models for the dielectric spectrum of tissues." Phys Med Biol 41(11): 2271-93.

Geddes, L. A. (1972). Electrodes and the Measurement of Bioelectric Events. New York, Wiley.

Geddes, L. A. and L. E. Baker (1967). "The specific resistance of biological material—a compendium of data for the biomedical engineer and physiologist." Med Biol Eng 5(3): 271-93.

Geddes, L. A. and L. E. Baker (1989). Principles of Applied Biomedical Instrumentation, Chapters 1, 2 and 11, Wiley.

Gonzales-Correa, C. A. (2000). Endoscopic measurement of electrical impedance spectra and their dependence on tissue properties in barrett's oesophagus. Department of Medical Physics and Clinical Engineering. Sheffield, PhD thesis, Sheffield University.

Gonzales-Correa, C. A., B. H. Brown, et al. (2003). "Low frequency electrical bioimpedance for the detection of inflammation and dysplasia in Barrett's oesophagus." Physiol.Meas. 24: 291-296.

Gonzales-Correa, C. A., B. H. Brown, et al. (1999). "Virtual Biopsies in Barrett's Esophagus using an Impedance probe." Annals New York Academy of Sciences 873: 313-321.

Gray, H. (1995). Gray's anatomy : the anatomical basis of medicine and surgery. New York; Edinburgh : Churchill Livingstone,.

Hanley, J. A. and B. J. McNeil (1982). "The meaning and use of the area under a receiver operating characteristic (ROC) curve." Radiology 143(1): 29-36.

Heinitz, J. and O. Minet (1995). Dielectric properties of female breast tumours. 9th Int. Conf. Electrical Bioimpedance, University of Heidelberg, University of Heidelberg Press.

Huang, Y., X. B. Wang, et al. (1995). "Electrorotational studies of the cytoplasmic dielectric properties of Friend murine erythroleukaemia cells." Phys Med Biol 40(11): 1789-806.

Jequier, S. and O. Rousseau (1987). "Sonographic measurements of the normal bladder wall in children." AJR Am J Roentgenol 149(3): 563-6.

Jones, D. M. (2003). Measurement and Modelling of the Electrical Properties of Normal and Pre-cancerous Oesophageal Tissue. Department of Medical Physics and Engineering. Sheffield, PhD thesis, Sheffield University: 286.

Jones, D. M., R. H. Smallwood, et al. (2003). "Modelling of epithelial tissue impedance measured using three different designs of probe." Physiol Meas 24(2): 605-23.

Jossinet, J. (1998). "The impedivity of freshly excised human breast tissue." Physiol Meas 19(1): 61-75.

Jossinet, J. and B. Lavandier (1998). "The discrimination of excised cancerous breast tissue samples using impedance spectroscopy." Bioelectrochem Bioenerg 45: 161-167.

- Keshtkar, A., R. H. Smallwood, et al. (2001). Virtual bladder biopsy by bioimpedance measurements. XI International Conference On Electrical Bio-Impedance, Oslo, Norway, Oslo University.
- Konishi, Y., T. Morimoto, et al. (1995). "Electrical properties of extracted rat liver tissue." Res Exp Med (Berl) 195(4): 183-92.
- Lamm, D. L. and R. F. Gittes (1977). "Inflammatory carcinoma of the bladder and interstitial cystitis." J Urol 117(1): 49-51.
- Lapham, R. L., J. Y. Ro, et al. (1997). "Pathology of transitional cell carcinoma of the bladder and its clinical implications." Seminars in Surgical Oncology 13(5): 307-18.
- Lavelle, J. P., S. A. Meyers, et al. (2000). "Urothelial pathophysiological changes in feline interstitial cystitis: a human model." Am J Physiol Renal Physiol 278(4): F540-53.
- Lee, B. R., W. W. Roberts, et al. (1999). "Bioimpedance: novel use of a minimally invasive technique for cancer localization in the intact prostate." Prostate 39(3): 213-8.
- Lewis, S. A. (2000). "Everything you wanted to know about the bladder epithelium but were afraid to ask." Am J Physiol Renal Physiol 278(6): F867-74.
- Lewis, S. A. and J. M. Diamond (1976). "Na<sup>+</sup> transport by rabbit urinary bladder, a tight epithelium." J Membr Biol 28(1): 1-40.
- Lewis, S. A. and J. W. Hanrahan (1990). "Physiological approaches for studying mammalian urinary bladder epithelium." Methods Enzymol 192: 632-50.
- Lionheart, W. R., J. Kaipio, et al. (2001). "Generalized optimal current patterns and electrical safety in EIT." Physiol Meas 22(1): 85-90.
- Lu, L., B. H. Brown, et al. (1995). "A fast parametric modelling algorithm with the Powell method." Physiol Meas 16(3 Suppl A): A39-47.
- Lu, L., L. Hamzaoui, et al. (1996). "Parametric modelling for electrical impedance spectroscopy system." Med Biol Eng Comput 34(2): 122-6.
- Marieb, E. N. (1998). Human Anatomy & Physiology. Menlo Park, Calif., Harlow, Benjamin Cummings.
- Martin, B. F. (1972). "Cell replacement and differentiation in transitional epithelium: a histological and autoradiographic study of the guinea-pig bladder and ureter." J Anat 112(3): 433-55.
- McAdams, E. T. and J. Jossinet (1995). "Tissue impedance: a historical overview." Physiol Meas 16(3 Suppl A): A1-13.

- Melicow, M. (1952). "Histological study of vesical urothelium investigating between gross neoplasms in total cystoscopy." J.Urol. 68: 261.
- Memmler, R. L., B. J. Cohen, et al. (1996). Structure & Function of the Human Body; Chapter 19; The Urinary system and body fluids, Lippincott-Raven Publishers.
- Metherall, P. (1998). Three Dimensional Electrical Impedance Tomography of the Human Thorax. Department of Medical Physics and Clinical Engineering. Sheffield, University of Sheffield.
- Miller C E, H., C S (1990). "Finite Element Analysis of bioelectric phenomena." Critical Reviews in Biomedical Engineering 18(3): 207-233.
- Miller, C. E. and C. S. Henriquez (1990). "Finite element analysis of bioelectric phenomena." Crit Rev Biomed Eng 18(3): 207-33.
- Minsky, B. D. and F. J. Chlapowski (1978). "Morphometric analysis of the translocation of luminal membrane between cytoplasm and cell surface of transitional epithelial cells during the expansion-contraction cycles of mammalian urinary bladder." J Cell Biol 77(3): 685-97.
- Morimoto, T., Y. Kinouchi, et al. (1990). "Measurement of the electrical bio-impedance of breast tumors." Eur Surg Res 22(2): 86-92.
- Pethig, R. (1984). "Dielectric properties of biological materials: Biophysical and medical applications." IEEE Trans.Elec.Insul EI-19: 453-74.
- Pethig, R. (1987). "Dielectric properties of body tissues." Clin Phys Physiol Meas 8 Suppl A: 5-12.
- Pethig, R. and D. B. Kell (1987). "The passive electrical properties of biological systems: their significance in physiology, biophysics and biotechnology." Phys Med Biol 32(8): 933-70.
- Philippson, M. (1921). "Les lois de la resistance electrique des tissue vivants." Bull. dela classe des sciences, Acad. Roy.de Belg. 6: 387-403.
- Powell, H. M., D. C. Barber, et al. (1987). "Impedance imaging using linear electrode arrays." Clin Phys Physiol Meas 8 Suppl A: 109-18.
- Press, W. H., S. A. Teukolsky, et al. (1992). Numerical recipes in FORTRAN : the art of scientific computing, Cambridge University Press.
- Prout, G. R., Jr., W. W. Koontz, Jr., et al. (1983). "Long-term fate of 90 patients with superficial bladder cancer randomly assigned to receive or not to receive thiotepa." J Urol 130(4): 677-80.
- Radley, S. C., C. R. Chapple, et al. (2000). "Transurethral implantation of silicone polymer for stress incontinence: evaluation of a porcine model and mechanism of action in vivo." BJU Int 85(6): 646-50.

Reuter, V. E. (1992). 'Urinary Bladder and Urethra', in Histology for Pathologists. New York, Raven Press.

Ro, J. Y., G. A. Staerckel, et al. (1992). "Cytologic and histologic features of superficial bladder cancer." Urol Clin North Am 19(3): 435-53.

Schwan, H. P. (1955). "Electrical properties of body tissues and impedance plethysmography." IEEE Trans. Bio-Med. Electron. BME 3: 32-46.

Schwan, H. P. (1957). Electrical Properties of tissue and cell suspensions, A advances in Biological and Medical Physics. New York, Academic Press.

Schwan, H. P. and C. F. Kay (1957). "Capacitive properties of body tissues." Circ.Res. 5: 493-443.

Schwan, H. P. and C. F. Kay (1957). The conductivity of living tissues. Ann. NY Acad.Sci.

Seeley, R. R., T. D. Stephens, et al. (2000). Anatomy & Physiology, McGraw-Hill.

Sharkey, F. E. and M. F. Sarosdy (1997). "The significance of central pathology review in clinical studies of transitional cell carcinoma in situ." Journal of Urology 157(1): 68-70; discussion 70-1.

Siegel, S. (1988). Nonparametric statistics for the behavioral sciences. New York; London, McGraw-Hill.

Silverberg, S. G. (1988). Principles and practice of surgical pathology: Chapter 36: The Renal Pelvis, Ureter, Urinary Bladder, and Urethra. Washington, D.C., Churchill livingstone.

Silverman, D. T., L. I. Levin, et al. (1989). "Occupational risks of bladder cancer in the United States: I. White men." J Natl Cancer Inst 81(19): 1472-80.

Silverman, D. T., N. Rothman, et al. (1999). Epidemiology of bladder cancer: Biology, Diagnosis and management. Oxford, Oxford University Press.

Singh, B., C. W. Smith, et al. (1979). "In vivo dielectric spectrometer." Med Biol Eng Comput 17(1): 45-60.

Smallwood, R. H., A. Keshtkar, et al. (2002). "Electrical impedance spectroscopy (EIS) in the urinary bladder: the effect of inflammation and edema on identification of malignancy." IEEE Trans Med Imaging 21(6): 708-10.

Sonny, L. J. and M. C. Samuel (1996). Anderson's pathology, St. Louis; London : Mosby.

Sorensen, F. B., P. Bichel, et al. (1991). "Stereological estimates of nuclear volume in squamous cell carcinoma of the uterine cervix and its precursors." Virchows Arch A Pathol Anat Histopathol 418(3): 225-33.

Sugar, F. (1968). "An electron microscopic study of early invasive growth in human skin tumours and laryngeal carcinoma." Eur J Cancer 4(1): 33-8.

Syrigos, K. N. and D. G. Skinner (1999). Bladder Cancer (Biology, Diagnosis and Management). Chapter 12, Oxford University Press.

Tearney, G. J., M. E. Brezinski, et al. (1997). "Optical biopsy in human urologic tissue using optical coherence tomography." J Urol 157(5): 1915-9.

Tortora, G. J. and S. R. Grabowski (2000). Principles of anatomy and physiology. New York; Chichester, Wiley.

UICC (1987). :Staging of urinary bladder cancer. In: TNM classification of malignant tumours, (ed.Hermanek P, Sobin LH).Springer-Verlag, Berlin,1987, pp. 118-123.

UICC (1997). :Staging of urinary bladder cancer. In: TNM classification of malignant tumours, (ed.Sobin LH, Wittekind C).John Wiley and sons, New York,1997, pp. 201-213.

Underwood, J. C. E. (2000). General and systematic pathology. Edinburgh, Churchill Livingstone.

Utz, D. C. and G. M. Farrow (1984). "Carcinoma in situ of the urinary tract." Urol Clin North Am 11(4): 735-40.

van der Meijden, A., W. Oosterlinck, et al. (1999). "Significance of bladder biopsies in Ta,T1 bladder tumors: a report from the EORTC Genito-Urinary Tract Cancer Cooperative Group. EORTC-GU Group Superficial Bladder Committee." Eur Urol 35(4): 267-71.

Walker, B. E. (1959). "Electron microscopical observations on Transitional Epithelium of the mouse urinary bladder." J. Ultrastructure Res, 3: 345-361.

Walker D C, B. B. H., Smallwood R H, Hose D R, Jones D M (2002). "Modelled current distribution in cervical squamous tissue." Physiological Measurement 23(1): 159-168.

Walker, D. C. (2001). Modelling the Electrical Properties of Cervical Epithelium. Department of Medical Physics and Engineering, PhD thesis, University of Sheffield, U. K.

Walker, D. C. (2001). Modelling the electrical properties of cervical epithelium. Department of Medical physics and clinical engineering. Sheffield, PhD thesis Sheffield University: Chapter 6.

Walker, D. C., B. H. Brown, et al. (2003). "A study of the morphological parameters of cervical squamous epithelium." Physiol Meas 24(1): 121-35.

Walker, D. C., B. H. Brown, et al. (2000). "Modelling the electrical impedivity of normal and premalignant cervical tissue." Electronics Letters 36(19): 1603-1604.

- Walker, D. C., B. H. Brown, et al. (2002). "Modelled current distribution in cervical squamous tissue." Physiol Meas 23(1): 159-68.
- Ward, G. K., S. S. Stewart, et al. (1986). "Cellular heterogeneity in normal human urothelium: an analysis of optical properties and lectin binding." J Histochem Cytochem 34(7): 841-6.
- Waterworth, A. R. (2000). Data analysis techniques of measured biological impedance. PhD Thesis. University of Sheffield.
- Weiss, M. A. and M. Stacey (1989). Atlas of genitourinary tract disorders, Neoplasms of the urinary tract.
- White, F. H. and K. Gohari (1984). "Alterations in the volume of the intercellular space between epithelial cells of the hamster cheek-pouch: quantitative studies of normal and carcinogen-treated tissues." J Oral Pathol 13(3): 244-54.
- Wilkinson, B. A., R. H. Smallwood, et al. (2002). "Electrical impedance spectroscopy and the diagnosis of bladder pathology: a pilot study." J Urol 168(4 Pt 1): 1563-7.
- Wilson, A. J., P. Milnes, et al. (2001). "Mk3.5: a modular, multi-frequency successor to the Mk3a EIS/EIT system." Physiol Meas 22(1): 49-54.
- Wilson, B. (1981). A low-distortion bipolar feedback current amplifier technique.
- Young, B. (2000). Wheater's Functional histology: a text and colour atlas. Edinburgh, Churchill Livingstone.
- Zarowitz, B. J. and A. M. Pilla (1989). "Bioelectrical impedance in clinical practice." Dicp 23(7-8): 548-55.
- Zhu, Q. S., C. N. McLeod, et al. (1994). "Development of a real-time adaptive current tomograph." Physiol Meas 15 Suppl 2a: A37-43.

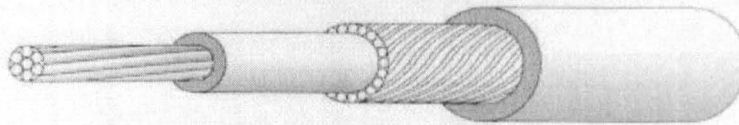
# Appendices

## Appendix (1): The dimensions of cable parts, structure and its electrical characteristics

Technical data sheet

### SINGLE PICO-COAX®

## PCX 38 K 10



Inner Conductor: SP Copper alloy      Dielectric: FEP      Served Shield: TPC      Jacket: Polyester (\*)

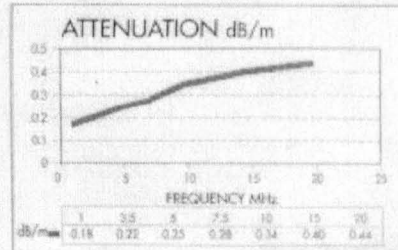
(\*) 8 colours : black / red / orange / yellow / green / blue / white / purple or brown

### DIMENSIONS

INNER CONDUCTOR			DIELECTRIC	SERVED SHIELD	JACKET
AWG	COMPOSITION	Ø (mm)	Ø (mm)	Ø (mm)	Ø (mm)
38	7 x 0.04	0.120	0.35	0.45	0.51

### ELECTRICAL CHARACTERISTICS

- Nom. resistance (Ω/m) : 2.40
- Nom. resistance (shield/conductor) (Ω/m) : 2.75
- Nom. capacitance (pF/m) : 100
- Nom. impedance (Ω) : 50



### AXON® REFERENCE

**PCX 38 K 10**

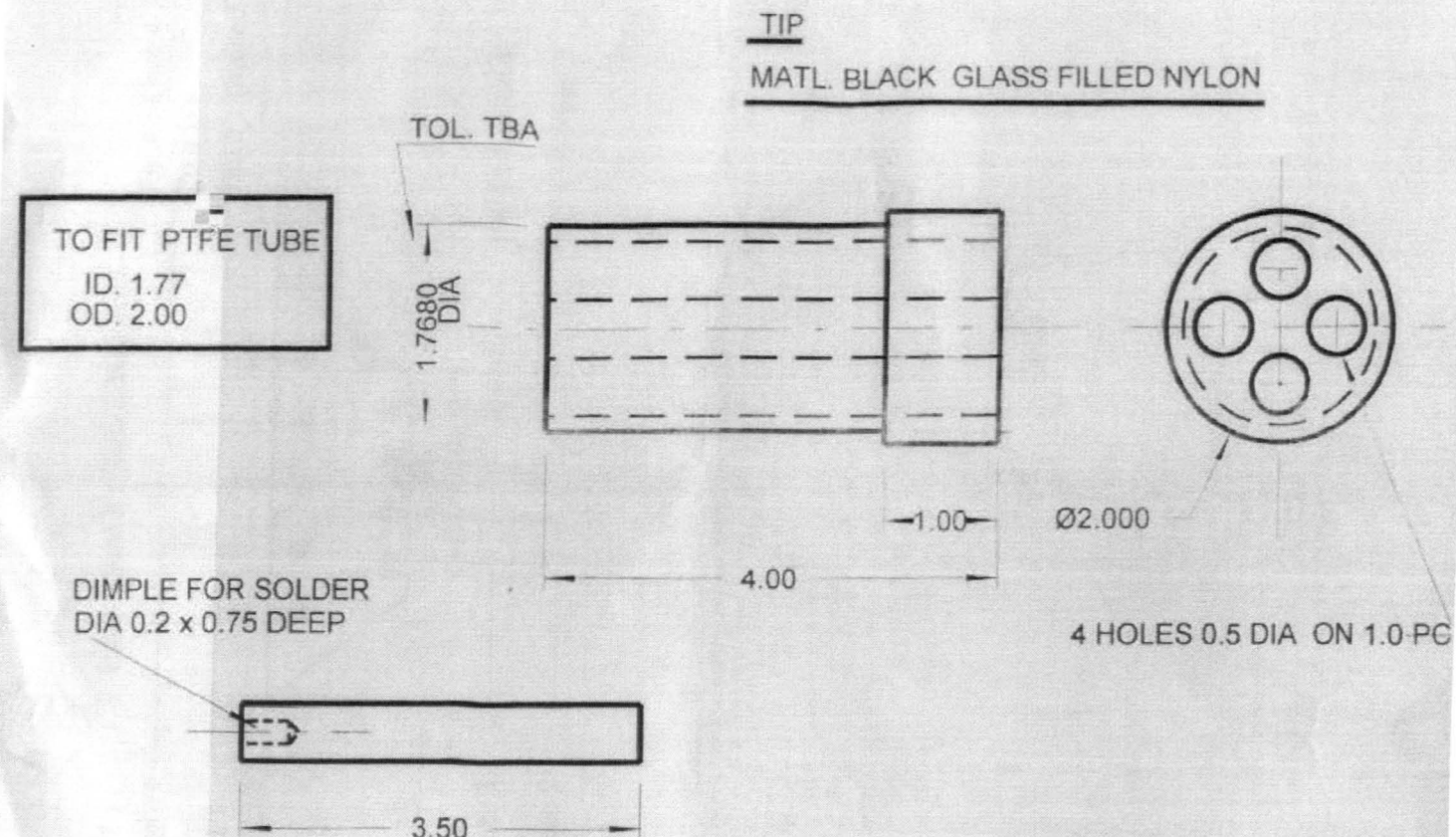
Capacity / 10  
Dielectric : K = FEP  
Gauge of the inner conductor  
PICO-COAX®

AXON® reserves the right to change this specification without prior notice.



cable and interconnect systems for advanced technologies

LOGICAM® REGISTERED TRADEMARK OF AXON® CABLE  
PICO-COAX® CABLE® REGISTERED TRADEMARK OF AXON® CABLE



TO FIT PTFE TUBE  
ID. 1.77  
OD. 2.00

TIP  
MATL. BLACK GLASS FILLED NYLON

DIMPLE FOR SOLDER  
DIA 0.2 x 0.75 DEEP

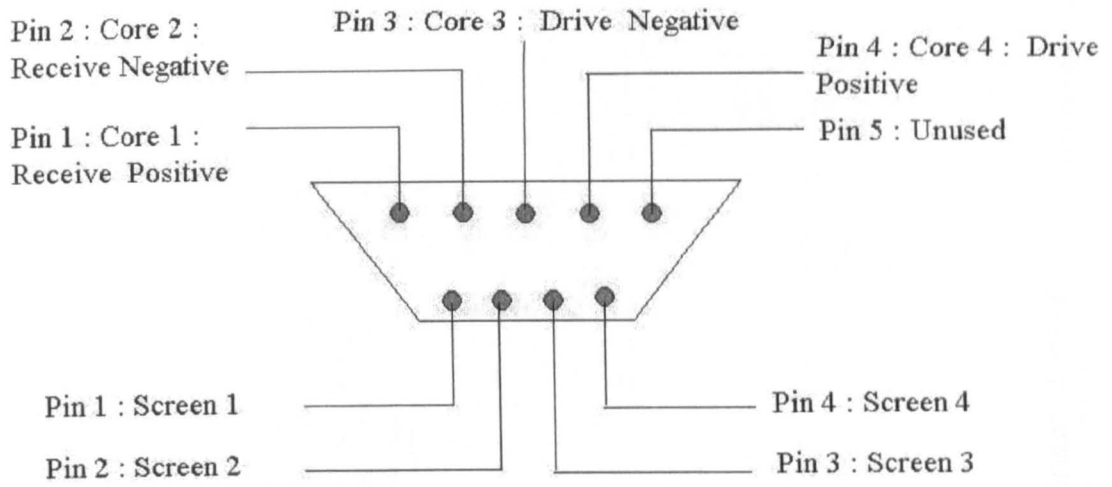
GOLD RODS DIA 0.5

GOLD SUPPLIED BY P.A. JEWELERY

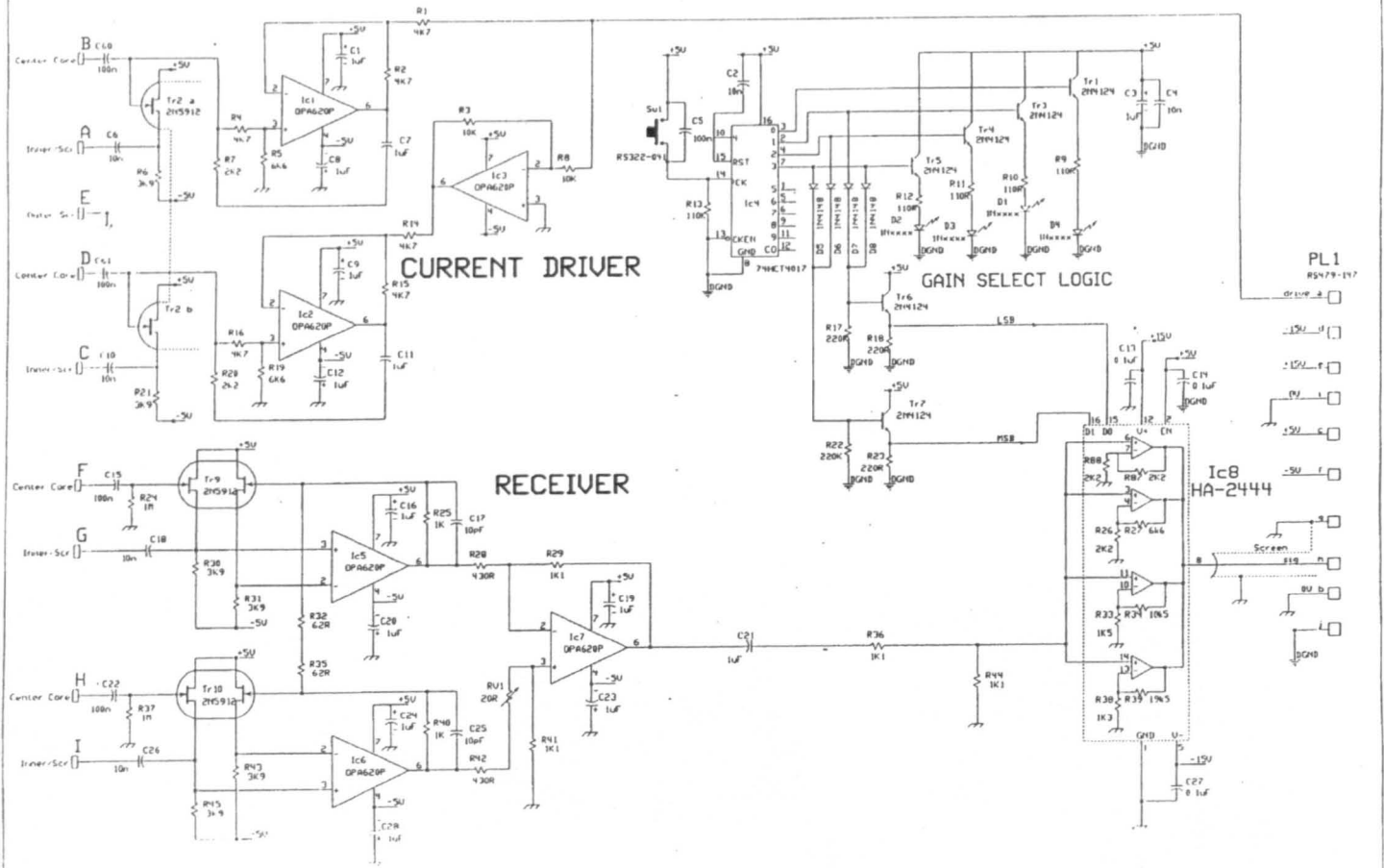
FOR AHMED JOB NO/ 473

Medical Workshop	Scale	Drawn	Date	ISS	Revision	Date
Dept. of Medical Physics and Clinical Engineering		RS	22/11/99			
© Copyright 1999	Title			DRG. No.		
	BLADDER IMPEDANCE PROBE			BIP 0047:		
	Sheet			of		

### Appendix (3): Probe-Cable 9way Connector



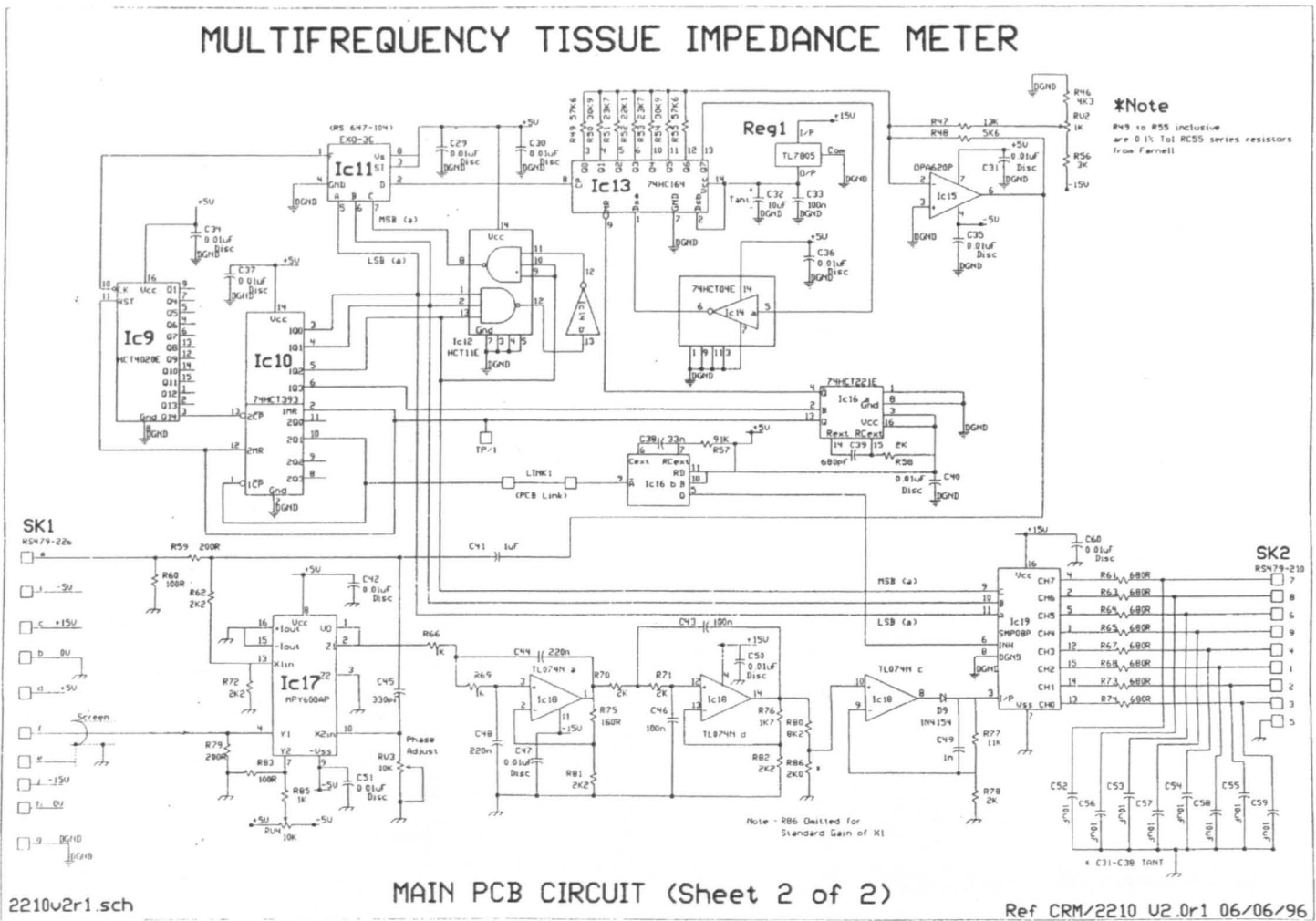
# MULTIFREQUENCY TISSUE IMPEDANCE METER

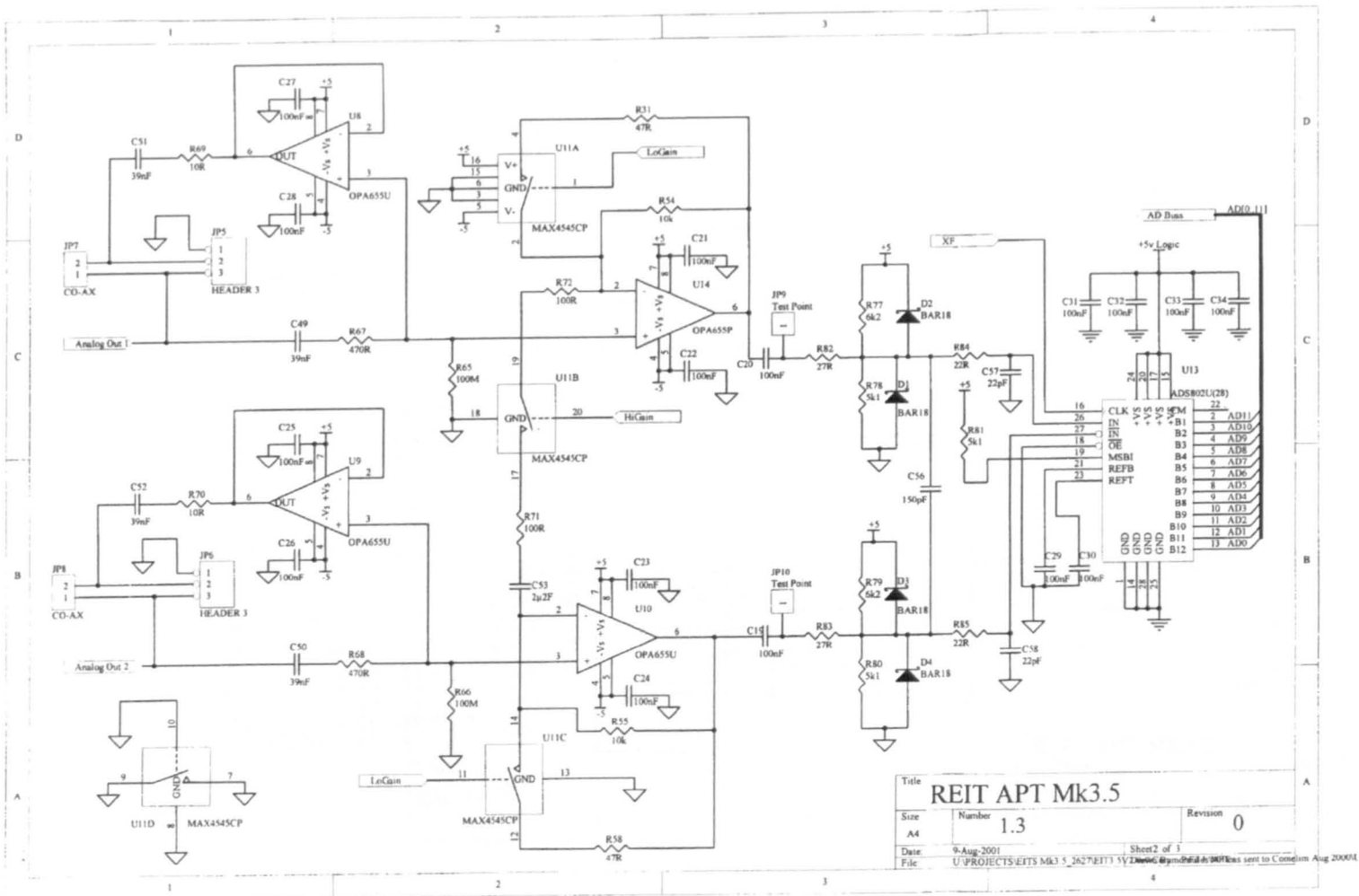


PROBE PCB CIRCUIT (Sheet 1 of 2)

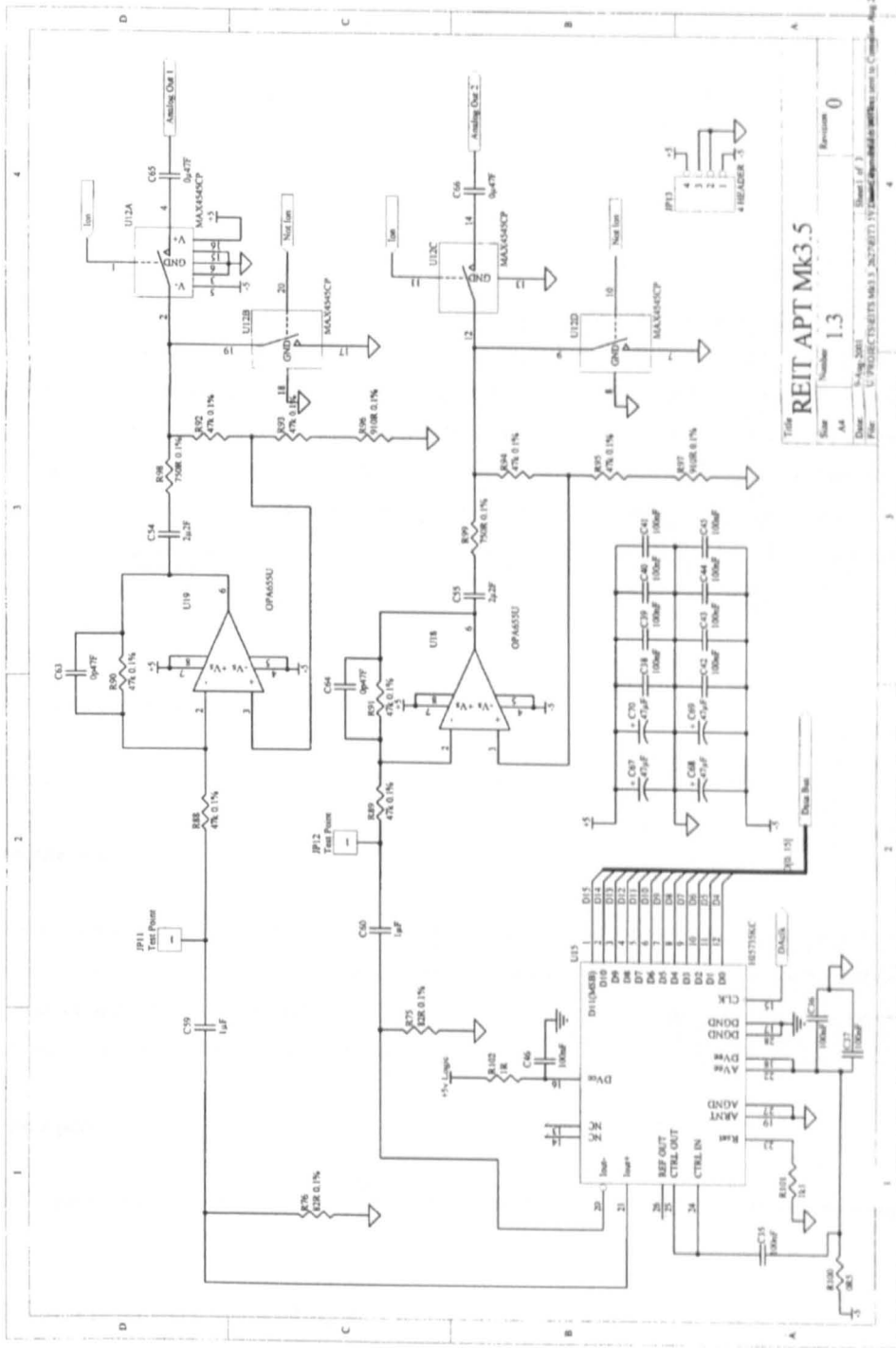
2211v2r0.sch

(REF CRM2211 V2\_0r0\_12/02/96)





# Appendix (7): Mk3.5: (Sheet 2 of 2)



## **Appendix(8): Patient's consent form to sign: Electrical measurements of the bladder lining**

You are being invited to take part in a research study. Before you decide it is important for you to understand why the research is being done and what it will involve. Please take time to read the following information carefully and discuss it with friends, relatives and your GP if you wish. Ask us if there is anything that is not clear or if you would like more information. Take time to decide whether or not you wish to take part.

### **Introduction:**

Red patches in the bladder are common. There are many causes of a red patches, but we cannot tell its exact nature just by looking it. In order to find out more about the problem you would normally be asked to come back to hospital for a General Anaesthetic and a sample is taken of the red area. This is then examined under the microscope to determine what has caused it. We can then decide what, if any, treatment is needed. Tests on the oesophagus (gullet) and cervix have shown that an electrical instrument placed on the surface can tell the nature of the problem by measuring the way a very weak electrical current is conducted through the abnormal patch. We want to test this method in the bladder, and compare the results with the examination under the microscope to see if it can tell us what has caused the red patch. This study is for two years, and 40 patients will be needed. If the experiment measurements match the sample, it means that in the future patients may not require a sample of tissue to be taken away to decide their treatment.

### **Why have I been chosen for the study?**

You have been chosen because you have a red patch in your bladder, which we have seen today.

### **What if I enter the study?**

Before we take the biopsies of the red patch we will put the instrument on to its surface. The instrument is small and fits down the inside of the camera we use to look inside the bladder. This will pass a tiny current through the lining of the bladder and take some electrical measurements. The instrument is safe and has been used in this hospital for 15 years without any known side effects. We will then take the biopsies in the usual way.

### **Do I have to take part?**

No, you do not have to take part. Any decisions you make will not affect the standard of care or treatment you receive.

### **Will the information in the study be confidential?**

No names will be mentioned in any reports of the study. With your agreement we will inform your family doctor that you are helping with the study.

### **What happens if I am harmed by the study?**

The instruments that take the electrical measurements have been used safely in this hospital for 15 years. There are no known side effects. However, if you are harmed due to someone's negligence, then you may have grounds for a legal action.

## Appendix(9): Patient information and impedance measurement form

### 1. Electrical Impedance Measurements By MK3.a Sheffield System

**Name:** \_\_\_\_\_ **File name:** \_\_\_\_\_

**Date:** \_\_\_\_\_ **Probe No:** \_\_\_\_\_

**In Vivo:** \_\_\_\_\_ **Ex Vivo:** \_\_\_\_\_

Biopsy No:	Meas. No:	Gain	Total Points

---

### 2. Electrical Impedance Measurements By MK3.5 Sheffield System

**Name:** \_\_\_\_\_ **File name:** \_\_\_\_\_

**Date:** \_\_\_\_\_ **Probe No:** \_\_\_\_\_

**In Vivo:** \_\_\_\_\_ **Ex Vivo:** \_\_\_\_\_

Biopsy No:	Meas. No:	Total Points

## Appendix (10): Instructions in Matlab programme to build the data base files

```
» Subject(1).number=[]
```

```
Subject =
```

```
    number: []
```

```
» Subject(1).name=[]
```

```
Subject =
```

```
    number: []
```

```
    name: []
```

```
» Subject(1).date=[]
```

```
Subject =
```

```
    number: []
```

```
    name: []
```

```
    date: []
```

```
» Subject(1).histology_reference=[]
```

```
Subject =
```

```
    number: []
```

```
    name: []
```

```
    date: []
```

```
    histology_reference: []
```

```
» Subject(1).data=struct('spectrum',[],'nest',struct('histology_report',[]))
```

```
Subject =
```

```
    number: []
```

```
    patient_reference: []
```

```
    name: []
```

```

        date: []

        histology_reference: []

        data: [1x1 struct]

save Bladder_Data_MK3a_Ex_vivo

```

---

## Appendix (11): AppendRecord m.file

```
% The mean of 3 measurements per biopsy point
```

```
function []=AppendRecord3(InputFileName,OutputFileName,new_data)
```

```
dynamicname=['\My_Matlab\data\bladder\ahmad\' InputFileName];
```

```
eval(['load ' dynamicname])
```

```
% get number of subjects
```

```
[rows,NumberOfSubjects]=size(Subject);
```

```
Subject(NumberOfSubjects+1).number=NumberOfSubjects+1;
```

```
% get patient name
```

```
Subject(NumberOfSubjects+1).name=input('Enter patient name ','s');
```

```
% get test date
```

```
Subject(NumberOfSubjects+1).date=input('Enter test date ','s');
```

```
% enter number of biopsies
```

```
numberofbiopsies=input('Enter number of biopsies ');
```

```
for m=1:numberofbiopsies
```

```
    Subject(NumberOfSubjects+1).data(m).nest.histology_report=...
```

```
        input('Enter histology report ','s');
```

```
    Subject(NumberOfSubjects+1).data(m).nest.histology_proportion=input('hi
stology_proportion','s');
```

```

% get inflammation

Subject (NumberOfSubjects+1) .data (m) .nest .histology_inflammation=input ('
histology_inflammation', 's');

% get oedema

Subject (NumberOfSubjects+1) .data (m) .nest .histology_oedema=input ('histol
ogy_oedema', 's');

% get comment

Subject (NumberOfSubjects+1) .data (m) .nest .histology_Comment=input ('histo
logy_Comment', 's');

end

% mean value of 3 measurements per biopsy point

for m=1:numberofbiopsies;

    biopsydata (1, :) =real (new_data (m*3-2) .calib);

    biopsydata (2, :) =real (new_data (m*3-1) .calib);

    biopsydata (3, :) =real (new_data (m*3) .calib);

    AverageSpectrum=mean (biopsydata);

    Subject (NumberOfSubjects+1) .data (m) .spectrum=AverageSpectrum;

end

% save database

dynamicname=['\My_Matlab\data\bladder\ahmad\' OutputFileName];

eval(['save ' dynamicname ' Subject'])

```

**Appendix (12): The cellular morphological parameters of the human urinary bladder**

Non-malignant Sections	Length ( $\mu m$ ) (Mean $\pm$ SD)	Width ( $\mu m$ ) (Mean $\pm$ SD)	Epithelium thickness ( $\mu m$ ) (Mean $\pm$ SD)
1	16.25 $\pm$ 3.35	11.28 $\pm$ 1.53	50.53 $\pm$ 11.11
2	13.33 $\pm$ 3.54	10.71 $\pm$ 4.33	35.34 $\pm$ 3.91
3	13.84 $\pm$ 3.27	13.26 $\pm$ 2.85	101.27 $\pm$ 14.98
4	11.71 $\pm$ 3.20	9.21 $\pm$ 2.01	42.23 $\pm$ 6.38
5	12.37 $\pm$ 3.50	10.86 $\pm$ 4.18	65.50 $\pm$ 11.64
6	14.66 $\pm$ 3.49	11.28 $\pm$ 2.89	64.36 $\pm$ 11.41
7	16.00 $\pm$ 2.60	13.26 $\pm$ 3.88	82.99 $\pm$ 14.32
8	16.14 $\pm$ 2.64	10.69 $\pm$ 4.31	51.96 $\pm$ 4.81
9	21.41 $\pm$ 6.26	11.89 $\pm$ 2.83	63.19 $\pm$ 6.56
10	12.64 $\pm$ 2.37	10.18 $\pm$ 2.75	50.58 $\pm$ 6.98
<b>Average</b>	14.84 $\pm$ 2.83	11.26 $\pm$ 1.27	60.80 $\pm$ 19.58

**Table A1 The cellular morphological parameters of the human urinary bladder obtained from analysis of the normal bladder histology sections (Superficial cell size) by the author (SD = Standard deviation)**

Non-malignant Sections	Length ( $\mu m$ ) (Mean $\pm$ SD)	Width ( $\mu m$ ) (Mean $\pm$ SD)	Epithelium thickness ( $\mu m$ ) (Mean $\pm$ SD)
1	10.13 $\pm$ 1.77	13.64 $\pm$ 2.98	
2	9.96 $\pm$ 3.55	10.38 $\pm$ 1.72	
3	12.07 $\pm$ 2.09	13.64 $\pm$ 2.59	
4	9.39 $\pm$ 1.77	8.20 $\pm$ 1.25	
5	9.87 $\pm$ 0.63	14.16 $\pm$ 2.14	
6	8.41 $\pm$ 1.22	16.39 $\pm$ 2.29	
7	12.77 $\pm$ 2.33	13.86 $\pm$ 2.54	
8	12.00 $\pm$ 2.75	12.99 $\pm$ 1.43	
9	13.56 $\pm$ 3.64	13.93 $\pm$ 1.21	
10	10.96 $\pm$ 1.58	10.57 $\pm$ 2.28	
<b>Average</b>	10.91 $\pm$ 1.63	12.78 $\pm$ 2.36	

**Table A2 The cellular morphological parameters of the human urinary bladder obtained from analysis of the normal bladder histology sections (Intermediate cell size) by the author (SD = Standard deviation)**

<b>Non-malignant</b>	<b>Length ( <math>\mu m</math> )</b>	<b>Width ( <math>\mu m</math> )</b>	<b>Epithelium thickness ( <math>\mu m</math> )</b>
<b>Sections</b>	<b>(Mean <math>\pm</math> SD)</b>	<b>(Mean <math>\pm</math> SD)</b>	<b>(Mean <math>\pm</math> SD)</b>
<b>1</b>	6.87 $\pm$ 1.40	7.88 $\pm$ 0.71	
<b>2</b>	5.75 $\pm$ 0.77	5.67 $\pm$ 0.70	
<b>3</b>	7.86 $\pm$ 0.90	8.65 $\pm$ 1.20	
<b>4</b>	8.20 $\pm$ 0.98	7.80 $\pm$ 1.37	
<b>5</b>	8.62 $\pm$ 1.55	10.83 $\pm$ 1.99	
<b>6</b>	9.66 $\pm$ 2.62	10.96 $\pm$ 2.64	
<b>7</b>	9.31 $\pm$ 1.29	9.74 $\pm$ 1.99	
<b>8</b>	10.74 $\pm$ 1.50	9.77 $\pm$ 1.47	
<b>9</b>	12.97 $\pm$ 1.83	11.17 $\pm$ 2.38	
<b>10</b>	8.70 $\pm$ 0.83	9.66 $\pm$ 1.40	
<b>Average</b>	8.87 $\pm$ 2.01	9.22 $\pm$ 1.72	

**Table A3 The cellular morphological parameters of the human urinary bladder obtained from analysis of the normal bladder histology sections (Basal cell size) by the author (SD = Standard deviation)**

<b>Malignant</b>	<b>Length ( <math>\mu m</math> )</b>	<b>Width ( <math>\mu m</math> )</b>	<b>Epithelium thickness ( <math>\mu m</math> )</b>
<b>Sections</b>	<b>(Mean <math>\pm</math> SD)</b>	<b>(Mean <math>\pm</math> SD)</b>	<b>(Mean <math>\pm</math> SD)</b>
<b>1</b>	14.81 $\pm$ 2.29	8.78 $\pm$ 1.40	55.21 $\pm$ 8.78
<b>2</b>	17.70 $\pm$ 4.41	14.80 $\pm$ 4.11	75.40 $\pm$ 7.75
<b>3</b>	12.83 $\pm$ 1.86	8.76 $\pm$ 2.12	55.56 $\pm$ 6.87
<b>4</b>	14.16 $\pm$ 2.31	7.28 $\pm$ 1.42	46.48 $\pm$ 6.95
<b>5</b>	17.64 $\pm$ 2.70	9.67 $\pm$ 1.78	87.67 $\pm$ 15.03
<b>6</b>	12.45 $\pm$ 1.85	9.55 $\pm$ 1.80	91.82 $\pm$ 11.83
<b>Average</b>	14.94 $\pm$ 2.29	9.81 $\pm$ 2.59	68.69 $\pm$ 18.91

**Table A4 The cellular morphological parameters of the human urinary bladder obtained from analysis of the malignant bladder histology sections (Superficial cell size) by the author (SD = Standard deviation)**

<b>Malignant</b>	<b>Length ( <math>\mu m</math> )</b>	<b>Width ( <math>\mu m</math> )</b>	<b>Epithelium thickness ( <math>\mu m</math> )</b>
<b>Sections</b>	<b>(Mean <math>\pm</math> SD)</b>	<b>(Mean <math>\pm</math> SD)</b>	<b>(Mean <math>\pm</math> SD)</b>
1	10.00 $\pm$ 5.16	13.23 $\pm$ 3.41	
2	17.05 $\pm$ 3.06	22.38 $\pm$ 6.07	
3	10.87 $\pm$ 2.20	15.29 $\pm$ 2.96	
4	12.79 $\pm$ 2.75	13.04 $\pm$ 3.16	
5	22.29 $\pm$ 9.05	16.96 $\pm$ 6.51	
6	13.96 $\pm$ 2.53	17.58 $\pm$ 2.86	
<b>Average</b>	<b>16.00 <math>\pm</math> 4.25</b>	<b>16.41 <math>\pm</math> 3.46</b>	

**Table A5 The cellular morphological parameters of the human urinary bladder obtained from analysis of the malignant bladder histology sections (Intermediate cell size) by the author (SD = Standard deviation)**

<b>Malignant</b>	<b>Length ( <math>\mu m</math> )</b>	<b>Width ( <math>\mu m</math> )</b>	<b>Epithelium thickness ( <math>\mu m</math> )</b>
<b>Sections</b>	<b>(Mean <math>\pm</math> SD)</b>	<b>(Mean <math>\pm</math> SD)</b>	<b>(Mean <math>\pm</math> SD)</b>
1	10.25 $\pm$ 1.31	12.32 $\pm$ 3.20	
2	10.19 $\pm$ 2.57	12.67 $\pm$ 2.68	
3	9.22 $\pm$ 1.73	14.33 $\pm$ 1.75	
4	9.74 $\pm$ 3.50	12.90 $\pm$ 2.71	
5	13.34 $\pm$ 1.01	14.16 $\pm$ 4.13	
6	11.02 $\pm$ 0.93	17.47 $\pm$ 1.72	
<b>Average</b>	<b>10.62 <math>\pm</math> 1.45</b>	<b>13.98 <math>\pm</math> 1.90</b>	

**Table A6 The cellular morphological parameters of the human urinary bladder obtained from analysis of the malignant bladder histology sections (Basal cell size) by the author (SD = Standard deviation)**

## **Publications**

Keshtkar, A., F. C. Hamdy, et al. (2001). Virtual bladder biopsy by bioimpedance measurements. XI International Conference On Electrical Bio-Impedance, Oslo, Norway, Oslo University.

Smallwood, R. H., A. Keshtkar, et al. (2002). "Electrical impedance spectroscopy (EIS) in the urinary bladder: the effect of inflammation and edema on identification of malignancy." IEEE Trans Med Imaging 21(6): 708-10.

Wilkinson, B. A., R. H. Smallwood, et al. (2002). "Electrical impedance spectroscopy and the diagnosis of bladder pathology: a pilot study." J Urol 168(4 Pt 1): 1563-7.



**PROCEEDINGS  
OF THE  
XI INTERNATIONAL CONFERENCE  
ON  
ELECTRICAL BIO-IMPEDANCE**

**JUNE 17-21, 2001**

**OSLO, NORWAY**

**EDITORS:**

**SVERRE GRIMNES  
ØRJAN G. MARTINSEN  
HEIDI BRUVOLL**

**Published in cooperation with unipub forlag  
ISBN: 82-91853-05-3**

## VIRTUAL BLADDER BIOPSY BY BIOIMPEDANCE MEASUREMENTS

Ahmad Keshtkar<sup>1,4</sup>, Freddie C. Hamdy<sup>2</sup>, Beverley Wilkinson<sup>2</sup>, John A. Lee<sup>3</sup> & Rod Smallwood<sup>1</sup>

<sup>1</sup>Department of Medical Physics and Clinical Engineering, University of Sheffield, Sheffield, UK; <sup>2</sup>Section of Urology, Division of Clinical Sciences; University of Sheffield, UK;

<sup>3</sup>Department of Pathology, Division of Genomic Medicine, University of Sheffield, S10 2JF, UK; <sup>4</sup>Medical Physics Department, Tabriz University of Medical Sciences, Tabriz, Iran

*Correspondence should be addressed to A.Keshtkar : email: mpp98ak @sheffield.ac.uk*

**Abstract.** Cystoscopy is a common urological procedure in the investigation of bladder pathology. Erythematous areas of urothelium are frequently observed, but these abnormal areas can represent significantly different conditions, ranging from simple inflammation to flat carcinoma-in-situ (CIS). At present, definitive diagnosis can be made by biopsy only, usually under general anaesthesia, with resultant patient discomfort and morbidity, and relatively high cost. In addition, selection of biopsy sites currently depends on simple visual inspection. In order to improve the cystoscopic detection and assessment of bladder lesions, we have assessed the feasibility of detecting epithelial abnormalities in the bladder using electrical impedance spectroscopy (EIS). In freshly excised human bladder tissue we observed a clear separation between normal and inflamed tissue and CIS. CIS has a significantly higher impedivity at all 7 measurement frequencies between 9.6 kHz and 614 kHz ( $p < 0.02$  at all frequencies), whereas direct current measurements of trans-epithelial resistance have shown that the low frequency resistivity of normal epithelium is very high. The impedance spectrum of CIS is significantly different from the impedance spectrum of both normal ( $p < 0.002$ ) and inflamed tissue ( $p < 0.02$ ). These results demonstrate the potential of EIS for developing a novel and minimally invasive tool for the identification, selection for sampling and possible diagnosis of flat bladder lesions.

### 1. INTRODUCTION

In developed countries, most bladder cancers are transitional cell carcinomas (TCC). TCC is one of the commonest cancers, with approximately 13,000 new cases and 5400 deaths per year in the UK (Black et al 1977). The majority of patients present with haematuria and superficial papillary tumours, and although recurrence is common (50-70%), the disease can usually be controlled by local treatment. Nevertheless, 10-15% of patients with superficial TCC eventually progress to muscle-invasive and metastatic disease (Silverman et al 1999).

We have investigated whether it is possible to diagnostically classify bladder mucosa using the minimally invasive technique of electrical impedance spectroscopy (EIS), which was developed initially to screen for cervical cancer (Brown et al 2000), and has subsequently been used in the assessment of Barrett's esophagus (Gonzalez-Correa et al 1999). The morphology of urothelium, and the natural history of pre-cancerous changes in urothelium, are significantly different from that found in the cervix and esophagus.

## 2. METHODS

The electrical transfer impedance of the mucosa was measured in 17 freshly excised human bladders using a specially designed probe. Four 0.5 mm diameter gold electrodes were equally spaced on a 1.0 mm diameter circle at the end of the probe and could be closely approximated to the mucosa. The electrodes were soldered to sub-miniature coaxial cables (Axon Mini Coaxial Cable), PCX 36 K 08 O/D 0.5mm, which are inserted into a medical grade Polytetrafluoroethylene (PTFE) tube with an outer diameter of 2mm. The PTFE tube gives maximum flexibility; the ability to be wiped clean; and allows the probe to be passed through the biopsy channel of a cystoscope into the bladder. In the process of fitting cables into the tube, we used the Vacuum Plasma Method to remove fluorine atoms, which gives good adhesion between the dental composite around the electrode connections and the cables at the end of the probe. This process is very important for protection against penetration or leakage of liquids from both sides of the tip

The system is calibrated by measuring the transfer impedance of saline of known resistivity, which enables the transfer impedance measurements to be converted to the equivalent resistivity of a uniform isotropic medium, which is independent of electrode configuration. Measurements were made at seven frequencies from 9.6 kHz to 614 kHz, drive current 10  $\mu$ A, with a depth sensitivity of approximately 0.5 mm. Following the electrical measurements, punch biopsies were taken from the electrically sampled areas for correlation with the microscopical appearances.

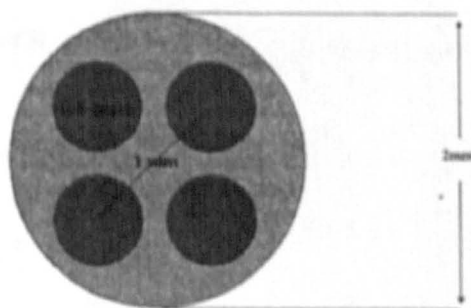


Figure 1 : Probe Structure including 4 gold electrodes

Measurements were performed at 7 different frequencies from 9.6 KHz to 614.4 KHz. Every measurement consists of the mean of 50 spectral measurements. Three measurements were made at every biopsy site to show the reproducibility of the impedance measurements. We have performed a calibration process for electrodes with different saline solution conductivities from 0.16-6.00 mS  $\text{cm}^{-1}$ . Measurements were made on bladders excised from 17 patients. Biopsy samples from the measurement sites were independently classified by the histologist as CIS, tumour, inflammation and normal tissue areas.

The simple and commonly used model, which is a physical representation of the Cole equation (Cole and Cole 1940), treats the data as resulting from the impedance of the extracellular space in parallel with a series combination of a membrane capacitance and the intracellular impedance. The membrane capacitance is usually assumed to be frequency-dependent. A complex non-linear least-squares procedure is used to fit the model to the data (Lu et al 1995, Waterworth et al 2000), resulting in three parameters which describe the shape of the impedance spectrum. These are: R, the extra-cellular impedivity; S, the intra-cellular impedivity and C, the membrane capacity. The Kolmogrov-Smirnov Two Sample Test was used to analyse the results.



grouped data does not imply perfect categorisation of individual measurements, as can be seen from figure 3. The two principal groups which need to be separated are CIS and inflammation. Examination of figure 3 shows that 5 of the 9 CIS measurements are clearly separated from the inflammation measurements, 1 is equivocal, and 3 lie within the inflammation group. The percentile plots of the impedance spectra in figure 2 show the overlap between the groups that gives rise to this misclassification. Further examination of figure 2 suggests two reasons for this. Firstly, measurements of trans-epithelial resistance at zero frequency in vitro have been used to assess the tightness of the urothelium. For urothelium with normal differentiation, the trans-epithelial resistance is very high (e.g.  $4 \cdot 10^3 \Omega$  across  $1 \text{ cm}^2$  in cat, equivalent to a resistivity  $> 400 \Omega\text{m}$ ) (Lavelle et al 2000). We therefore predict that the impedivity of normal tissue at low frequencies will be one to two orders of magnitude greater than the impedivity measured at our lowest frequency of 9.6 kHz, as a result of the greater tightness of the normal urothelium. We also predict that the impedivity of CIS at low frequencies will be in the range that is found in cervical tissue (5 – 15  $\Omega\text{m}$ ), due to the reduced number of tight junctions. Secondly, the Cole equation, used for the modelling of the data, gives rise to a curve which has zero slope at both low and high frequencies, with a negative slope in the  $\beta$  dispersion region around 10 – 100 kHz. It is clear from figure 2 that our measurements cover only the negative slope region, with the result that the data fitting process is not optimal. These preliminary results demonstrate the need to extend the measurement range towards lower frequencies (from 9.6 kHz down to ~ 100 Hz). This should lead to improved classification as a result of the predicted high impedivity of normal urothelium at low frequencies, and the predicted difference in the shape of the impedance spectra

## ACKNOWLEDGEMENTS

This conference would not be possible without the support of the members of the International Committee for the Promotion of Research in Bio-Impedance (ICPRBI).

## REFERENCES

- Black RJ, Bray F, Ferlay J et al Cancer incidence and mortality in the European Union: cancer registry data and estimates of national incidence for 1990. *Eur J Cancer* 1997, 33, 1075 – 1107.
- Brown B H, Tidy J A, Boston K, Blackett A D, Smallwood R H and Sharp S (2000) The relationship between tissue structure and imposed electrical current flow in cervical neoplasia. *Lancet* 355 892-895
- Cole K S and Cole R H (1940) *J Chem Phys* 9 341-351
- Gonzalez-Correa C A, Brown B H, Smallwood R H, Kalia K, Stoddard C J, Stephenson T J, Haggie S J, Slater D N and Bardhan K D (1999) Virtual biopsies in Barrett's Esophagus using an impedance probe. *Annals New York Academy of Science* 873 313-321
- Lavelle J P, Meyers S A, Ruiz W G, Buffington C A T, Zeidel M L and Apodaca G, Urothelial pathophysiological changes in feline interstitial cystitis: a human model. *Am J Physiol Renal Physiol* 278 F450-F553 2000
- Lu L, Brown B H, Barber D C and Leathard A D (1995) A fast parametric modelling algorithm with the Powell method. *Physiol Meas* 16 (3A) A39-A48
- Silverman DT, Rothman N & Devesa SS Epidemiology of bladder cancer, in Syrigos KN & Skinner DG, Eds., *Bladder cancer: biology, diagnosis and management*, Oxford University Press, 1999, pp 12 – 55.
- Waterworth A R, Milnes P, Smallwood R H and Brown B H (2000) Cole equation modelling to measurements made using an impulse driven transfer impedance system. *Physiol Meas* 21 137-144

# Correspondence

## Electrical Impedance Spectroscopy (EIS) in the Urinary Bladder: The Effect of Inflammation and Edema on Identification of Malignancy

R. H. Smallwood\*, A. Keshtkar, B. A. Wilkinson, J. A. Lee, and F. C. Hamdy

**Abstract**—Previous studies have shown that tetrapolar electrical impedance spectroscopy measurements can identify cervical interstitial neoplasia with the same sensitivity and specificity as cervical smears. In the urinary bladder, the same technique yields significant differences ( $p < 0.05$  at seven frequencies between 9.6 and 614 kHz) between normal and malignant urothelium, but is unable to classify individual measurements. Detailed histological examination demonstrates that inflammation and edema—both of which are common in abnormal urothelium—alter the impedance spectrum significantly in opposing directions. Consideration of morphological changes in abnormal urothelium suggests alternative measurement strategies.

**Index Terms**—Bladder, cancer, electrical impedance spectroscopy, urothelium.

### I. INTRODUCTION

In developed countries, most bladder cancers are transitional cell carcinomas (TCC). TCC is one of the most common cancers, with approximately 13 000 new cases and 5400 deaths per year in the United Kingdom [1]. The majority of patients present with haematuria and superficial papillary tumours, and although recurrence is common (50%–70%), the disease can usually be controlled by local treatment. Nevertheless, 10%–15% of patients with superficial TCC eventually progress to muscle-invasive and metastatic disease [2]. At present, the accepted treatment strategy for patients presenting with superficial disease is transurethral resection, followed by adjuvant intravesical chemotherapy to combat recurrence. Patients are followed-up with regular check cystoscopies, placing a high load on clinical resources.

Approximately 20% of patients have tumours which are muscle-invasive at presentation. These tumours are thought to develop from carcinoma *in situ* (CIS), have a poor prognosis (less than 40% five-year survival compared with 80%–90% for superficial disease) and require radical treatment. Cystourethroscopy remains the gold-standard for investigating these patients. The erythematous areas seen at cystoscopy can represent several different pathologies from simple inflammation through to flat CIS, and significant pathology may be present in areas with no obvious visible abnormality.

Manuscript received August 28, 2001; revised February 14, 2002. *Asterisk indicates corresponding author.*

\*R. H. Smallwood is with Medical Physics and Engineering, University of Sheffield, Royal Hallamshire Hospital, Sheffield S10 2JF, U.K. (e-mail: r.smallwood@shef.ac.uk).

A. Keshtkar is with Medical Physics and Engineering, University of Sheffield, Royal Hallamshire Hospital, Sheffield S10 2JF, U.K., on study leave from the Medical Physics Department, Tabriz University of Medical Sciences, Tabriz, Iran.

B. A. Wilkinson and F. C. Hamdy are with the Department of Urology, University of Sheffield, Royal Hallamshire Hospital, Sheffield S10 2JF, U.K.

J. A. Lee is with the Department of Pathology, University of Sheffield, Royal Hallamshire Hospital, Sheffield S10 2JF, U.K.

Publisher Item Identifier 10.1109/TMI.2002.800608.

We have investigated whether it is possible to diagnostically classify bladder mucosa using the minimally invasive technique of electrical impedance spectroscopy (EIS), which we developed initially to screen for cervical cancer [3], and have subsequently used in the assessment of Barrett's esophagus [4]. The morphology of urothelium, and the natural history of precancerous changes in urothelium, are significantly different from that found in the cervix and esophagus.

The impedance spectrum generated by EIS is a function of the detailed structure of the tissue at the cellular level. Normal human urothelial mucosa consists of an epithelial layer 3–6 cells thick, a lamina propria of loose connective tissue, and a variable discontinuous band of submucosal muscle. Occasionally white blood cells are often present. The superficial epithelial cells are specialized. Known as "umbrella" cells, they have abundant eosinophilic cytoplasm and may contain and secrete mucin. In CIS, the umbrella cells usually disappear and are replaced by undifferentiated cells. Urothelial CIS is characterized by flat, disordered proliferation of urothelial cells with marked cytological abnormalities including; nucleomegaly (increased nuclear size), nucleolomegaly (increased nucleoli size), pleomorphism (abnormally shaped cells), loss of cellular polarity, and mitoses. The normal lamina propria can be divided into an inner and outer zone by a prominent collection of arteries and veins [5]. In inflammatory conditions, the white cells, small vessels, and fibrous tissue components of the lamina propria may all increase, sometimes dramatically.

The aim of this paper is to demonstrate the relationship between histology and impedance spectrum in excised human bladder.

### II. MATERIALS AND METHODS

The electrical transfer impedance of the mucosa was measured in 23 freshly excised human bladders using a specially designed pencil probe, with four gold wire electrodes 0.5 mm in diameter spaced equally on a 1.6-mm-diameter circle, flush with the face of the probe. A current of 10  $\mu$ A peak-to-peak was passed between an adjacent pair of electrodes and the real part of the resulting potential was measured between the two remaining electrodes. The ratio of the measured potential to the amplitude of the imposed current determines a transfer impedance. Measurement constraints are discussed elsewhere [6]. Measurements were made at seven frequencies by doubling the frequency in steps between 9.6 and 614 kHz. Measurements were made serially at 67 frames/s and input to a computer. In nearly all cases, two separate sets of data (each of 50 measurements) were recorded in succession in order to check reproducibility of the measurements. Calibration was performed by placing the probe in saline of known electrical conductivity. A four-electrode measurement of the transfer impedance spectrum is essentially independent of the contact impedance between electrode and tissue (which is of the order of 1 k $\Omega$  compared with the transfer impedance of 100  $\Omega$ ). Following the electrical measurements, punch biopsies were taken from the electrically sampled areas for correlation with the microscopic appearances.

Measurements were made on 23 human cystectomy specimens, with a total of 138 readings and biopsies. Thirteen of these specimens had invasive TCC, eight had invasive TCC with CIS, one had been resected for interstitial cystitis, and one for a chronic pyocystis. After surgical removal from the body, the bladder was immediately transferred to an adjacent pathology laboratory, opened by a single cut along the mid-line, and pinned to a cork board. Measurements were made at room temperature within 30 min. of excision. Measurements were made on each

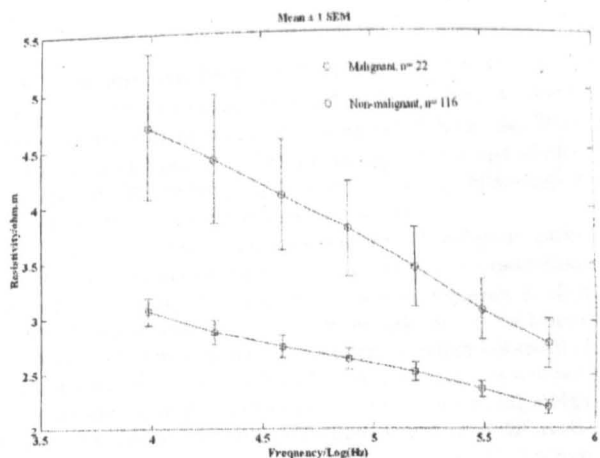


Fig. 1. Plot of resistivity versus frequency for normal and malignant tissue.

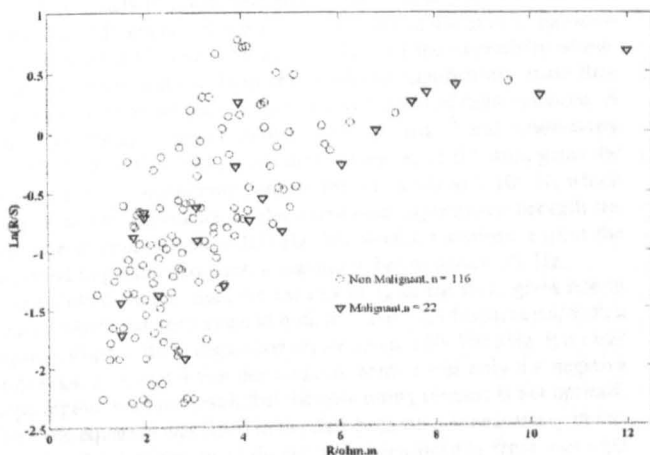


Fig. 2. Scatter plot of parameters  $R$  and  $S$  resulting from fitting a Cole equation to normal and malignant frequency spectra.

specimen in areas that looked macroscopically different, particularly areas of erythema. Three measurements were taken at each point. A biopsy was then immediately taken where the probe had made an indentation on the mucosa. The biopsies were then put in separate containers in formalin, and sent for histopathological analysis.

A simple and commonly used model, which is a physical representation of the Cole equation [7], treats the data as resulting from the impedance of the extracellular space in parallel with a series combination of a membrane capacitance and the intracellular impedance. The membrane capacitance is usually assumed to be frequency dependent. A complex nonlinear least-squares procedure is used to fit the model to the data [8], [9], resulting in three parameters which describe the shape of the impedance spectrum. These are:  $R$ , the extracellular impedivity;  $S$ , the intracellular impedivity, and  $C$ , the membrane capacity. Fig. 1 shows the relationship between resistivity and frequency for normal and pathological tissue and Fig. 2 shows a scatter plot of  $(R/S)$  versus  $R$  (note that  $R$  and  $S$  are independent variables).

The Kolmogorov-Smirnov 2-sample test was used to determine the significance of the results [10].

### III. RESULTS

Over the measured frequency range the impedivity of malignant areas was significantly higher than that of normal areas at all frequencies ( $p < 0.05$  for all frequencies). Determination of extracellular

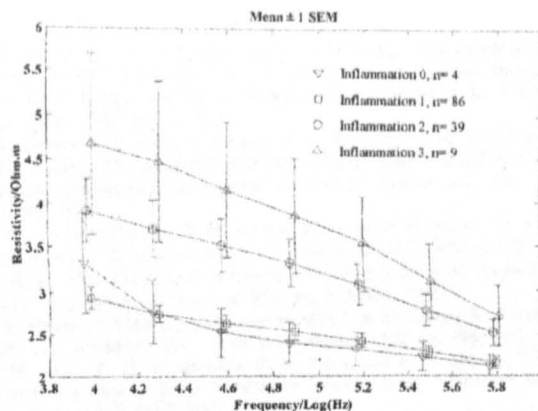


Fig. 3. Plot of resistivity versus frequency for different degrees of inflammation (0—no inflammation, 4—extensive inflammation). Error bars are displaced for clarity.

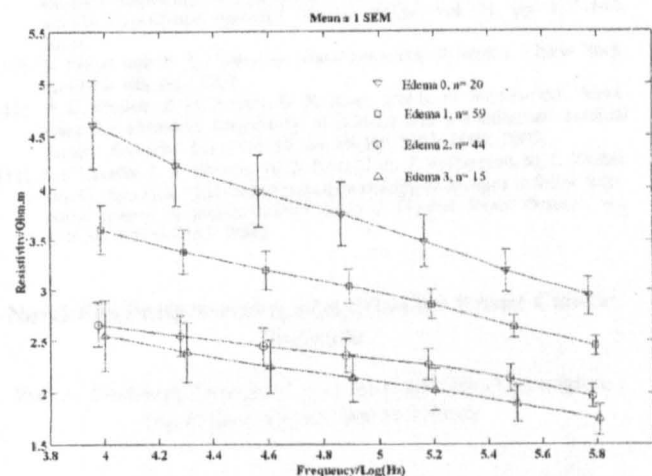


Fig. 4. Plot of resistivity versus frequency for different degrees of edema (0—no edema, 4—extensive edema). Error bars are displaced for clarity.

impedivity  $R$  from the Cole model gives a significant separation between the impedance spectra for malignant and normal mucosa ( $p < 0.05$ ). This separation of grouped data does not imply perfect categorization of individual measurements.

Examination of Fig. 2 shows that six of the 22 measurements on malignant tissue are clearly separated from the nonmalignant measurements, and two of the nonmalignant measurements lie within the malignant group.

Having established that the variability in the frequency spectra for bladder epithelium was much greater than for cervical epithelium, we re-examined the histological sections. The majority of the sections that showed abnormalities also showed, to some extent, either inflammation, or edema, or both. Inflammation and edema were separately classified on a scale of 0 (not present) to 4 (extensive). Fig. 3 shows the change in the impedance spectrum with inflammation for all samples, and Fig. 4 shows the change with edema.

### IV. DISCUSSION

Edema results in an increase in fluid in the extracellular space and, thus, reduces the low-frequency resistivity of the tissue. The presence of edema results in a significant reduction in the resistivity at all frequencies, with the magnitude of the reduction increasing with increasing level of edema. In inflammatory conditions there are changes

in the lamina propria underlying the epithelium. Cellular-level modeling has shown that, contrary to the situation in a uniform medium, the majority of the current penetrates the epithelial layer and flows through the lamina propria [11]. The increasing cellular and fibrous tissue content of the lamina propria with increasing inflammation results in a progressive increase in tissue resistivity.

Fig. 1 shows that the low-frequency impedance of malignant tissue is higher than that for normal tissue. This is contrary to expectation. Measurements of trans-epithelial resistance at zero frequency *in vitro* have been used to assess the tightness of the urothelium, i.e., the barrier preventing water movement through the epithelium, which is a result of tight junctions between the umbrella cells. The tight junctions will prevent ion movement through the extracellular space, thus giving a high impedance at low frequencies. For urothelium with normal differentiation, the trans-epithelial resistance is very high (e.g.,  $4 \cdot 10^3 \Omega$  across  $1 \text{ cm}^2$  in cat, equivalent to a resistivity  $>400 \Omega\text{m}$ ) [12]. We, therefore, predict that the impedivity of normal tissue at low frequencies will be one to two orders of magnitude greater than the impedivity measured at our lowest frequency of 9.6 kHz, as a result of the greater tightness of the normal urothelium. We also predict that the impedivity of malignant urothelium at low frequencies will be significantly lower than for normal urothelium, due to the reduced number of tight junctions. A typical membrane capacitance of  $1 \cdot 4 \cdot 10^{-14} \text{ F}\mu\text{m}^{-2}$  and conductivity of  $1 \cdot 10^{-11} \text{ S}\mu\text{m}^{-2}$ , and an electrode diameter of 0.5 mm, gives the resistance of the membrane beneath the electrode as  $5 \cdot 10^5 \Omega$ , which is equal to the impedance of the membrane capacitance beneath the electrode at approximately 100 Hz. We would, therefore, expect the measured impedance to reach a maximum below about 100 Hz.

The Cole equation, used for the modeling of the data, gives rise to a curve which has zero slope at both low and high frequencies, with a negative slope in the  $\beta$  dispersion region around 10–100 kHz. It is clear from Figs. 1, 3, and 4 that our measurements cover only the negative slope region, with the result that the data fitting process is not optimal. The Cole equation was fitted to the data because it is customary in this field, but the data presented do not differ significantly from a straight line (a  $\chi^2$  test of each of the curves presented in Figs. 1, 3, and 4 against a fitted straight line shows that the curves do not differ from a straight line at the  $p < 0.0001$  level of confidence). A scatter plot of slope  $v$  intersect for straight lines fitted to individual curves (i.e.,  $a$  versus  $b$  for a line  $y = ax + b$ ) gives a separation similar to that in Fig. 2. *A priori* considerations suggest that measurement at lower frequencies should lead to improved classification as a result of the predicted high impedivity of normal urothelium at low frequencies, and the predicted difference in the shape of the impedance spectra. Measurement at higher frequencies is constrained by the finite output impedance of the current source relative to the impedance of the very small electrodes, and would be unlikely to yield useful information, as the high-frequency impedance of all tissues is very similar.

In summary, we have demonstrated that electrical impedance measurement of human bladder urothelium, taken immediately after excision, has the ability to differentiate between normal and malignant groups, but the effect of inflammation and edema on the measurements is of the same order (in the measurement range) as the effect of malignancy. Classification of individuals is not possible. Consideration of the effect of malignancy on urothelial morphology suggests that measurements at lower frequencies offer the potential to develop a novel minimally invasive technique to diagnose bladder pathology, and warrants further clinical testing.

## REFERENCES

- [1] R. J. Black, F. Bray, and J. Ferlay *et al.*, "Cancer incidence and mortality in the European union: Cancer registry data and estimates of national incidence for 1990," *Eur. J. Cancer*, vol. 33, pp. 1075–1107, 1997.

- [2] D. T. Silverman, N. Rothman, and S. S. Devesa, "Epidemiology of bladder cancer," in *Bladder Cancer: Biology, Diagnosis and Management*, K. N. Syrigos and D. G. Skinner, Eds. Oxford, U.K.: Oxford Univ. Press, 1999, pp. 12–55.
- [3] B. H. Brown, J. A. Tidy, K. Boston, A. D. Blackett, R. H. Smallwood, and F. Sharp, "The relationship between tissue structure and imposed electrical current flow in cervical neoplasia," *Lancet*, vol. 355, pp. 892–895, 2000.
- [4] C. A. Gonzalez-Correa, B. H. Brown, R. H. Smallwood, K. Kalia, C. J. Stoddard, T. J. Stephenson, S. J. Haggie, D. N. Slater, and K. D. Bardhan, "Virtual biopsies in barrett's esophagus using an impedance probe," *Ann. NY Acad. Sci.*, vol. 873, pp. 313–321, 1999.
- [5] V. E. Reuter, "Urinary bladder and urethra," in *Histology for Pathologists*, S. S. Sternberg, Ed. New York: Raven, 1992, pp. 709–720.
- [6] D. M. Jones, R. H. Smallwood, D. R. Hose, and B. H. Brown, "Constraints on tetrapolar tissue impedance measurements," *Electron. Lett.*, vol. 37, pp. 1515–1517, 2001.
- [7] K. S. Cole and R. H. Cole, *J. Chem. Phys.*, vol. 9, pp. 341–351, 1940.
- [8] L. Lu, B. H. Brown, D. C. Barber, and A. D. Leathard, "A fast parametric modeling algorithm with the powell method," *Physiol. Meas.*, vol. 16, no. 3A, pp. A39–A48, 1995.
- [9] A. R. Waterworth, P. Milnes, R. H. Smallwood, and B. H. Brown, "Cole equation modeling to measurements made using an impulse driven transfer impedance system," *Physiol. Meas.*, vol. 21, pp. 137–144, 2000.
- [10] S. Siegel and N. J. Castellan, *Non-Parametric Statistics*. New York: McGraw-Hill Int., 1988.
- [11] D. C. Walker, B. H. Brown, D. R. Hose, and R. H. Smallwood, "Modeling the electrical impedivity of normal and premalignant cervical tissue," *Electron. Lett.*, vol. 36, no. 19, pp. 1603–1604, 2000.
- [12] J. P. Lavelle, S. A. Meyers, W. G. Ruiz, C. A. T. Buffington, M. L. Zeidel, and G. Apodaca, "Urothelial pathophysiological changes in feline interstitial cystitis: A human model," *Amer. J. Physiol. Renal Physiol.*, vol. 278, pp. F450–F553, 2000.

## Novel EIS Postprocessing Algorithm for Breast Cancer Diagnosis

Yaël A. Glickman, Orna Filo\*, Udi Nachaliel, Sarah Lenington, Sigal Amin-Spector, and Ron Ginor

**Abstract**—A new postprocessing algorithm was developed for the diagnosis of breast cancer using electrical impedance scanning. This algorithm automatically recognizes bright focal spots in the conductivity map of the breast. Moreover, this algorithm discriminates between malignant and benign/normal tissues using two main predictors: phase at 5 kHz and crossover frequency, the frequency at which the imaginary part of the admittance is at its maximum. The thresholds for these predictors were adjusted using a learning group consisting of 83 carcinomas and 378 benign cases. In addition, the algorithm was verified on an independent test group including 87 carcinomas, 153 benign cases and 356 asymptomatic cases. Biopsy was used as gold standard for determining pathology in the symptomatic cases. A sensitivity of 84% and a specificity of 52% were obtained for the test group.

**Index Terms**—Breast cancer, electrical impedance scanning, medical diagnosis, postprocessing algorithm.

## I. INTRODUCTION

Electrical impedance scanning (EIS) was demonstrated to be a valuable noninvasive adjunctive technology for breast cancer diagnosis

Manuscript received October 15, 2001; revised April 26, 2002. Asterisk indicates corresponding author.

Y. A. Glickman, U. Nachaliel, S. Lenington, S. Amin-Spector, and R. Ginor are with TransScan Medical Ltd., 10550 Migdal Ha'Emek, Israel. (e-mail: orna@transscan.co.il).

\*O. Filo is with TransScan Medical Ltd., P. O. Box 786, 10550 Migdal Ha'Emek, Israel (e-mail: orna@transscan.co.il).

Publisher Item Identifier 10.1109/TMI.2002.800605.

## ELECTRICAL IMPEDANCE SPECTROSCOPY AND THE DIAGNOSIS OF BLADDER PATHOLOGY: A PILOT STUDY

B. A. WILKINSON, R. H. SMALLWOOD, A. KESHTAR, J. A. LEE AND F. C. HAMDY

*From the Academic Urology and Pathology Units, and Department of Medical Physics and Engineering, University of Sheffield, Royal Hallamshire Hospital, Sheffield, United Kingdom*

### ABSTRACT

**Purpose:** Carcinoma in situ is an aggressive form of bladder cancer with a high propensity for invasion if left untreated. On cystoscopy these flat lesions cannot be differentiated from other erythematous, potentially benign areas and they require biopsy for definitive diagnosis. Other methods of detecting carcinoma in situ remain experimental. We assessed the effectiveness of electrical impedance spectroscopy, a method that measures the variation of electrical current flow with frequency through the mucosa, for differentiating various pathological changes in the urothelium.

**Materials and Methods:** We obtained 250 impedance measurements immediately after resection in 35 cystectomy specimens using a custom designed probe. Three consecutive readings were recorded per point to assess reproducibility and punch biopsy was done at the measurement site.

**Results:** Changes in the urothelium were classified histologically into 7 subgroups according to the degree of edema and inflammation. Electrical impedance spectroscopy measurements were able to separate benign and malignant changes when tested as a group ( $p < 0.001$ ), although some individual points overlapped. Edema also had a significant effect on tissue impedance ( $p < 0.001$ ).

**Conclusions:** Using measurements we established patterns of electrical impedance in the human bladder. Early results suggest that this minimally invasive technique is able to differentiate benign and malignant bladder pathologies. However, it requires further refinement and evaluation at lower frequencies, where the greatest impedance difference in benign and malignant tissues is expected.

**KEY WORDS:** bladder, spectrum analysis, electric impedance, bladder neoplasms, carcinoma in situ

In the United States it was estimated that 54,200 new patients would be diagnosed with bladder cancer in 1999 with 12,100 projected deaths from the disease.<sup>1</sup> In developed countries transitional cell carcinoma accounts for approximately 90% of cases. Carcinoma in situ is a high grade and aggressive manifestation of transitional cell carcinoma with a highly variable course. Carcinoma in situ is commonly seen in patients with a current or previous tumor, that is secondary carcinoma in situ.<sup>2</sup> Estimates of the incidence of carcinoma in situ adjacent to papillary tumors are 10% to 40%<sup>3</sup> and up to 75% adjacent to invasive lesions.<sup>4</sup> In a review of 14 series with a followup of 1 to 16 years the average incidence of subsequent invasive disease was 54%.<sup>5</sup>

The typical cystoscopic appearance of carcinoma in situ is an erythematous patch of mucosa that bleeds easily on contact. There may be several areas that become confluent, giving the appearance of more generalized cystitis. However, these lesions may be inflammatory or benign and a definitive diagnosis is made by histopathological analysis of biopsies. Conversely cystoscopy may not reveal a discernible abnormality in the presence of carcinoma in situ, emphasizing the importance of random bladder biopsies in patients in whom the disease is suspected. Because of the difficulty of diagnosing flat lesions within the bladder, the search for in vivo detection methods continues.

Intravesical administration of methylene blue was abandoned because of the high false-negative results of 70% to 85%.<sup>6</sup> A more promising development in this area is fluores-

cence detection of tumors after intravesical administration of aminolevulinic acid. It is not a sensitizer but it is converted intracellularly into the photoactive compound protoporphyrin IX. Protoporphyrin IX appears to localize in malignant and premalignant tissue up to 20-fold compared with in healthy urothelium in rats.<sup>7</sup> This technique has an average sensitivity and specificity of 97% and 65%, respectively.<sup>8</sup>

It is apparent that 2 problems exist with our present diagnostic techniques. 1) We cannot determine the nature of an erythematous area within the bladder without definitive histology. 2) We do not have an optimal technique to allow guided rather than random biopsies.

Electrical impedance spectroscopy is an innovative technique that has been used to demonstrate premalignant changes in the epithelium of the human cervix and esophagus.<sup>9,10</sup> Little information is available regarding the use of electrical impedance spectroscopy in the human bladder. The majority of studies have investigated the function and capacity of the bladder<sup>11</sup> rather than assessed morphological changes.

The frequency spectrum generated by electrical impedance spectroscopy is a function of the detailed structure of tissue at a cellular level. Theoretically it should be able to differentiate malignant and nonmalignant tissue due to changes at this level. Urothelial carcinoma in situ is characterized by a flat, disordered proliferation of urothelial cells with marked cytological abnormalities. The urothelium may be 1 to 20 cells thick. Abnormalities that may be observed include nucleomegaly, nucleolomegaly, hyperchromatism, pleomorphism, loss of cellular polarity and mitoses. In inflammatory conditions the macrophages, mast cells and small vessels of the lamina propria may increase. With increased vascular

Accepted for publication April 5, 2002.  
Supported by British Urological Foundation/Merck Sharp & Dohme, Royal College of Surgeons of Edinburgh, Sheffield University Hospitals, and Engineering and Physical Sciences Research Council in the United Kingdom EPSRC GR/R42320/01.

permeability there is an increase in fluid exudates within the tissues.

Ohm's law states that the resistance of a substance is proportional to the voltage drop of an applied electrical current as it passes through the resistive substance. All substances offer resistance to the flow of an electrical current according to the formula,  $r = E/I$ , where  $r$  is resistance in  $\omega$ ,  $E$  is applied voltage in V. and  $I$  is current in A. Strictly speaking it applies only to direct current, that is current that does not vary with time. For time varying currents, that is alternating current, the measured property is impedance ( $Z$ ) according to the formula,  $Z = E/I$ .

Measured impedance varies with frequency (hence, the impedance spectrum) in a manner characteristic of the material. Tissues can be considered electrically as an organization of cells in an extracellular fluid. Cell membranes behave as capacitors when exposed to electrical current. At low frequencies current flows by ion-free movement in the extracellular space and, therefore, measured impedance is a function of the spatial arrangement of this space. Free ions do not cross the cell membrane in bulk and, thus, the membrane acts as a barrier to current flow at low frequencies. In contrast, at high frequencies bound charges in the cell membrane, which give rise to the capacitance of the membrane, facilitate current flow within the cell in addition to the extracellular space current flow. As a result, the measured high frequency impedance is always less than the low frequency impedance.

We hypothesized that at low frequencies the normal and inflamed epithelium with its tight junctions would have higher impedance than carcinoma in situ. At higher frequencies carcinoma in situ with its larger abnormal shaped cells and nuclei should have higher impedance than normal tissue. The results and their implications are presented and discussed.

#### MATERIALS AND METHODS

**Patients.** We evaluated 28 male and 7 female patients who underwent cystectomy for benign (5) and malignant (30) conditions. Median patient age at cystectomy was 65 years (range 37 to 79). Malignant bladders were resected due to grade 3 stage pT2 disease in 19 cases, refractory carcinoma in situ/grade 3 stage pT1 disease in 3 and grade 3 stage T2/3 disease with carcinoma in situ in 8. Cystectomy for benign disease involved a chronically painful bladder, interstitial cystitis and chronic pyocystitis in 1 case each.

**Materials.** An impedance probe was designed specifically with 4, 0.5 mm. diameter gold electrodes equally spaced on a 1.6 mm. diameter circle. It could be closely approximated to the mucosa. Measurements were obtained at 7 frequencies from 9.6 to 614 kHz. with the frequency doubled at each increment. A drive current of 10  $\mu$ A. peak to peak was passed between an adjacent pair of electrodes and the voltage drop was measured between the 2 remaining electrodes. Measurements were made serially at 67 spectra per second and input into a computer. The system was calibrated using saline solutions of known conductivity. Therefore, calibrated results are expressed in terms of the impedivity (the inverse of conductivity) of a saline solution that would give the same impedance reading as the measurement on the tissue.

**Methods.** Bladders were assessed immediately after excision in areas that appeared macroscopically different, particularly areas of erythema. At each point 3 readings were done by removing the probe completely from the mucosa and then reapplying it to assess the reproducibility of the system. The probe was mounted in a clamp to avoid movement during measurements and allowing exact repeat measurements. Punch biopsies were done at electrically sampled areas and fixed separately in formalin solution for standard histopathological examination. Changes in the urothelium were classi-

fied histologically into 7 subgroups according to the degree of edema and inflammation. Histopathological assessment included the first 500  $\mu$ m. from the mucosal surface, representing the depth of the electrical impedance spectroscopy measurement.

The groups were intact epithelium, ragged epithelium, denuded epithelium, denuded epithelium with residual von Brunn's nests, partial coverage carcinoma in situ, full coverage carcinoma in situ and exophytic carcinoma. A more detailed classification of the tissue assigned each sample a separate score according to the degree of edema and inflammation, namely 0—no edema and/or inflammation, 1—mild, 2—moderate and 3—severe edema and/or inflammation. It was believed that considering the degree of edema and inflammation was necessary in view of their potential effects on measurements.

**Analysis.** A simple and commonly used model that is a physical representation of the Cole equation<sup>12</sup> treats the data as resulting from the impedance of the extracellular space in parallel with a series combination of membrane capacitance and intracellular impedance. A complex nonlinear least squares procedure was used to fit the model to the data. The resulting parameters extracellular space, membrane capacitance and intracellular impedance characterized the tissue. The Kolmogorov-Smirnov 2-sample test was used to determine the significance of the results.

#### RESULTS

A total of 250 points were demonstrated on 35 human cystectomy specimens. The effect of malignancy, and degree of edema and inflammation in the tissues were considered.

**Malignant versus nonmalignant.** Using grouped data the impedivity of malignant points was higher than that of normal points at all frequencies ( $p < 0.001$ , fig. 1). However, on an individual point basis benign and malignant points overlapped (fig. 2).

**Effects of edema.** The severity of edema had a marked effect on tissue impedivity. With an increase in edema from grades 0 to 3 there was a gradual decrease in tissue impedivity (fig. 3). There was complete separation of edema grades 0 and 1 ( $p < 0.002$ ), and 1 and 2 ( $p < 0.001$ ). These results were significant at all 7 measured frequencies.

**Effects of inflammation.** Conversely inflammation had an opposite effect on tissue impedivity with an increase in inflammation resulting in an increase in impedivity (fig. 4). However, the impedivity difference was not significant in consecutive grades. Analysis of the data in the 2 largest groups, namely 145 and 18 samples with grades 1 and 3 inflammation, respectively, showed a significant difference at all frequencies ( $p < 0.005$ ).

**Carcinoma in situ versus inflammation.** There was a significant difference in electrical impedance spectroscopy measurements in areas of urothelium with no or mild inflammation (grades 0 to 1) and areas with carcinoma in situ ( $p = 0.01$ ). However, as the degree of inflammation increased, becoming moderate to severe (grades 2 to 3), the difference versus carcinoma in situ was no longer significant.

#### DISCUSSION

We assessed the effectiveness of electrical impedance spectroscopy, a method that measures the resistivity of the mucosa, for differentiating various pathological changes in the urothelium *ex vivo*. In a review of this technique Foster and Swann analyzed several studies that had compared *ex vivo* and *in vivo* electrical measurements in animal models.<sup>13</sup> They concluded that electrical impedance spectroscopy readings obtained immediately and up to several hours after the tissue was excised still agree with those obtained *in vivo*.

We correlated biopsy histopathology with electrical impedance measurements in 250 samples from 35 bladders excised

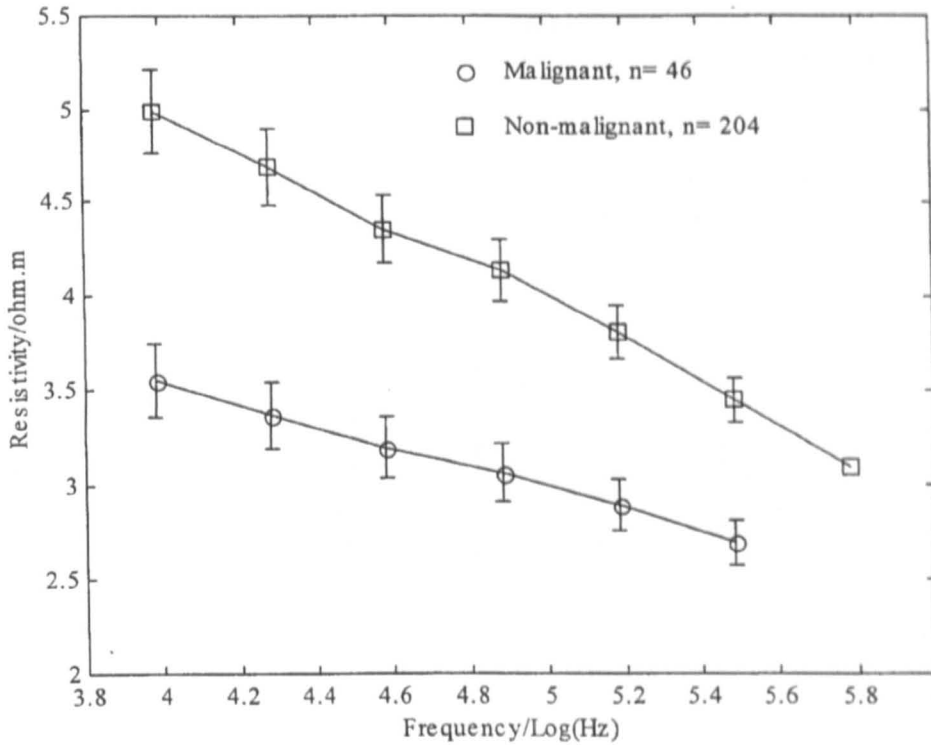


FIG. 1. Plot of resistivity versus frequency in normal and malignant tissue

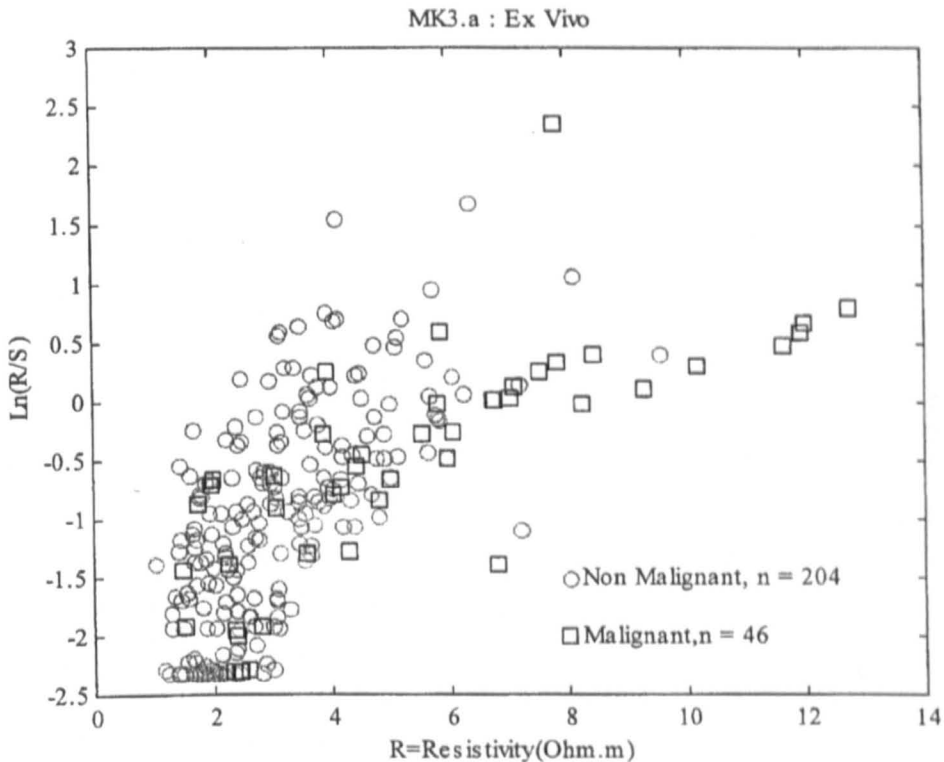


FIG. 2. Scatterplot of independent variables resistivity ( $R$ ) versus intracellular impedance ( $S$ )

due to various benign and malignant conditions. Tissue inflammation resulted in an increased cellular infiltrate in the lamina propria. This increased number of cells correlated with a significant increase in impedivity at all frequencies ( $p < 0.005$ ). Cellular level modeling has demonstrated that in

contrast to the situation in a uniform medium, most of the current penetrates the epithelial layer and flows through the lamina propria. Therefore, we would expect changes in the lamina propria to be reflected in the results.

The edema that often accompanies inflammation, resulting

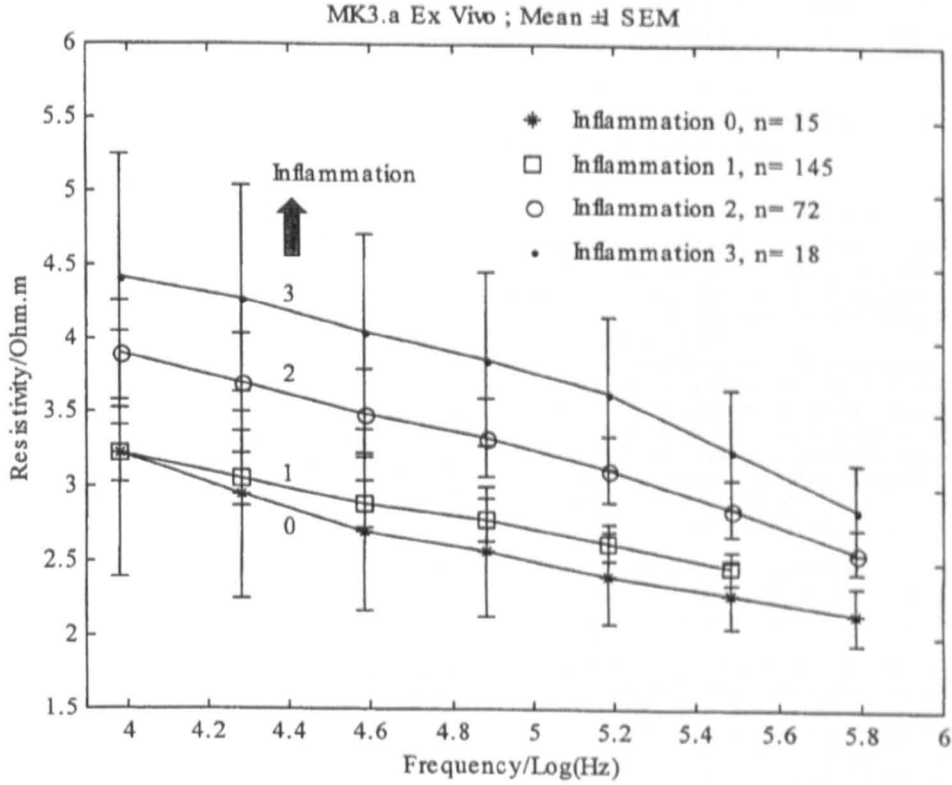


FIG. 3. Plot of resistivity versus frequency for different degrees of inflammation, namely 0—no inflammation to 4—severe inflammation

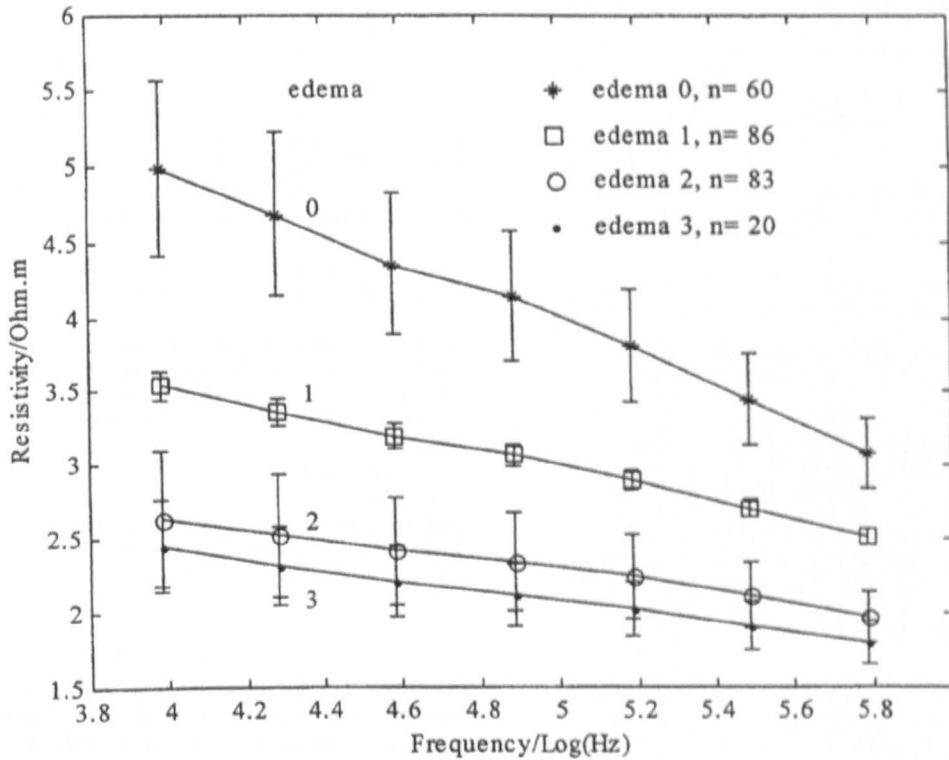


FIG. 4. Plot of resistivity versus frequency for different degrees of edema, namely 0—no edema to 4—severe edema

in an increase of fluid in the extracellular space, allows current to flow more readily in this space and significantly decreased the resistivity at all frequencies. A similar effect

was noted in human cervical tissue, in which the increase in edema associated with pregnancy significantly decreased tissue impedivity ( $p = 0.001$ ).<sup>14</sup>

This technique was not able to separate points with moderate and severe inflammation from carcinoma *in situ*. During cystectomy we would expect bladder handling to make inflammation more severe and, thus, this variable would be difficult to measure. In addition, the severe degree of inflammation in the *ex vivo* group due to bladder handling, may not be representative of the degree of inflammation observed in an *in vivo* situation. Also, we predicted that the impedivity of normal tissues at low frequencies would be higher than that of malignant tissue but were unable to demonstrate it in our findings (fig. 1).

Measurements of trans-epithelial resistance at zero frequency *in vitro* have been used to assess the tightness of the epithelium. For urothelium with normal differentiation trans-epithelial resistance is high (for example 0.4100  $\Omega$  across 1 cm.<sup>2</sup> in cats, equivalent to a resistivity of greater than 400  $\Omega$ m).<sup>15</sup> Therefore, we believe that if measurements are made at a lower frequency than 9.6 kHz. (the lowest frequency used in this study), results may demonstrate an increase in impedivity that is a consequence of the tight junctions. Conversely there should be a decrease in the impedivity of malignant tissue due to the lack of tight junctions.

A further limitation is that the Cole equation used for modeling the data gives rise to a curve with zero slope at high and low frequencies, and a negative slope in the region of 10 to 100 kHz. (the region in which this occurs is known as the  $\beta$  dispersion region). Figures 1, 3 and 4 show that our readings cover the negative slope region with the result that the data fitting process may not have been optimal. It should be achieved by additional readings at lower frequencies, leading to improved classification.

Electrical measurements *in vivo* agreed with readings made up to several hours after excision.<sup>13</sup> However, dramatic changes begin to occur as tissues are excised or deprived of a blood supply.<sup>16</sup> Therefore, the *ex vivo* results presented may not apply completely to the *in vivo* situation. Such studies are currently being performed to analyze this technique further.

Paradoxically patients with the most aggressive carcinoma *in situ* may present with denuded epithelium as a result of epithelium lifting off of the underlying lamina propria. These cases pose a difficult problem for the pathologist. Sometimes a diagnosis is made or suspicion is raised from a few abnormal cells seen at the edge of a denuded biopsy specimen. It is unlikely that our electrical impedance spectroscopy method would be sufficiently sensitive to detect changes in a few cells. It would require a field change of the epithelium to detect differences.

Despite these limitations we believe that there is scope to develop an electrical impedance spectroscopy method that would assist the urologist to detect appropriate sites for biopsy because current methods are far from ideal and random biopsies can be negative in up to 90% of cases.<sup>17</sup> Therefore, this method should be considered an adjunct to biopsy and histopathological evaluation rather than a method to replace it. Experiments at lower frequencies may demonstrate greater separation, which would warrant larger studies *in vivo* to assess the sensitivity and specificity of this novel technique.

#### CONCLUSIONS

Using *ex vivo* measurements we established patterns of electrical impedance in the human bladder. Early results suggest that this minimally invasive technique is able to differentiate benign and malignant bladder pathologies but

currently classifying individuals is not possible. The technique requires further refinement and evaluation at lower frequencies *ex vivo* and *in vivo*, where the greatest impedance difference in benign and malignant tissues is expected.

J. B. Anderson, A. G. Bryden, C. R. Chapple and D. Rosario provided material for study.

#### REFERENCES

- Landis, S. H., Murray, T., Bolden, S. and Wingo, P. A.: Cancer statistics, 1999. *CA Cancer J Clin*, **49**: 8, 1999
- Lum, B. L. and Torti, F. M.: Therapeutic approaches including interferon to carcinoma *in situ* of the bladder. *Cancer Treat Rev*, **12**: 45, 1985
- Utz, D. C. and Farrow, G. M.: Carcinoma *in situ* of the urinary tract. *Urol Clin North Am*, **11**: 735, 1984
- Prout, G. R., Jr., Koontz, W. W., Jr., Coombs, L. J., Hawkins, I. R. and Friedell, G. H.: Long-term fate of 90 patients with superficial bladder cancer randomly assigned to receive or not to receive thiotepa. *National Bladder Cancer Collaborative Group A J Urol*, **130**: 677, 1983
- Lamm, D. L.: Carcinoma *in situ*. *Urol Clin North Am*, **10**: 499, 1992
- Vicente, J., Chechile, G. and Algaba, F.: Value of *in vivo* mucosa-staining test with methylene blue in the diagnosis of pretumoral and tumoral lesions of the bladder. *Eur Urol*, **13**: 15, 1987
- Baumgartner, R., Kriegmair, M. and Stepp, H.: Photodynamic diagnosis following intravesical instillation of aminolevulinic acid (ALA)—first clinical experiences in urology. *Optical Meth Tumour Treatment Detection SPIE*, **1881**: 20, 1993
- Filbeck, T., Roessler, W., Knuedel, R., Straub, M., Kiel, H. J. and Wieland, W. F.: Clinical results of the transurethral resection and evaluation of superficial bladder carcinomas by means of fluorescence diagnosis after intravesical instillation of 5-aminolevulinic acid. *J Endourol*, **13**: 117, 1999
- Gonzalez-Correa, C. A., Brown, B. H., Smallwood, R. H., Kalia, N., Stoddard, C. J., Stephenson, T. J. et al: Virtual biopsies in Barrett's esophagus using an impedance probe. *Ann NY Acad Sci*, **873**: 313, 1999
- Brown, B. H., Tidy, J. A., Boston, K., Blackett, A. D., Smallwood, R. H. and Sharp, F.: Relation between tissue structure and imposed electrical current flow in cervical neoplasia. *Lancet*, **355**: 892, 2000
- Kim, C. T., Linsenmeyer, T. A., Kim, H. and Yoon, H.: Bladder volume measurement with electrical impedance analysis in spinal cord-injured patients. *Am J Phys Med Rehabil*, **77**: 498, 1998
- Cole, K. S. and Cole, R. H.: Dispersion and absorption dielectrics. I. Alternating current characteristics. *J Chem Physics*, **9**: 341, 1941
- Foster, K. R. and Schwan, H. P.: Dielectric properties of tissues and biological materials: a critical review. *Crit Rev Biomed Eng*, **17**: 25, 1989
- O'Connell, M. P., Tidy, J., Wisher, S. J., Avis, N. J., Brown, B. H. and Lindow, S. W.: An *in vivo* comparative study of the pregnant and nonpregnant cervix using electrical impedance measurements. *BJOG*, **107**: 1040, 2000
- Lavelle, J. P., Meyers, S. A., Ruiz, W. G., Buffington, C. A., Zeidel, M. L. and Apodaca, G.: Urothelial pathophysiological changes in feline interstitial cystitis: a human model. *Am J Physiol Renal Physiol*, **278**: F540, 2000
- Konishi, Y., Morimoto, T., Kinouchi, Y., Iritani, T. and Monden, Y.: Electrical properties of extracted rat liver tissue. *Res Exp Med*, **195**: 183, 1995
- van der Meijden, A., Oosterlinck, W., Brausi, M., Kurth, K. H., Sylvester, R. and de Balincourt, C.: Significance of bladder biopsies in T<sub>a</sub>, T<sub>1</sub> bladder tumors: a report from the EORTC Genito-Urinary Tract Cancer Cooperative Group EORTC-GU Group Superficial Bladder Committee. *Eur Urol*, **35**: 267, 1999